AD_____

Award Number: W81XWH-04-1-0891

TITLE: XIAP as a molecular target for therapeutic intervention in prostate cancer

PRINCIPAL INVESTIGATOR: Colin S. Duckett, Ph.D.

CONTRACTING ORGANIZATION: Regents of the University of Michigan
Ann Arbor, MI 48109-1274

REPORT DATE: October 2007

TYPE OF REPORT: Final

PREPARED FOR: U.S. Army Medical Research and Materiel Command
Fort Detrick, Maryland 21702-5012

REPORT DOCUMENTATION PAGE

Form Approved
OMB No. 0704-0188

1. REPORT DATE *(DD-MM-YYYY)*	2. REPORT TYPE	3. DATES COVERED *(From - To)*
01/10/07	Final	23 Sep 2004 – 22 Sep 2007

4. TITLE AND SUBTITLE

XIAP as a molecular target for therapeutic intervention in prostate cancer

5a. CONTRACT NUMBER

5b. GRANT NUMBER
W81XWH-04-1-0891

5c. PROGRAM ELEMENT NUMBER

6. AUTHOR(S)
Colin S. Duckett, Ph.D.

E-Mail: colind@umich.edu

5d. PROJECT NUMBER

5e. TASK NUMBER

5f. WORK UNIT NUMBER

7. PERFORMING ORGANIZATION NAME(S) AND ADDRESS(ES)

Regents of the University of Michigan
Ann Arbor, MI 48109-1274

8. PERFORMING ORGANIZATION REPORT NUMBER

9. SPONSORING / MONITORING AGENCY NAME(S) AND ADDRESS(ES)
U.S. Army Medical Research and Materiel Command
Fort Detrick, Maryland 21702-5012

10. SPONSOR/MONITOR'S ACRONYM(S)

11. SPONSOR/MONITOR'S REPORT NUMBER(S)

12. DISTRIBUTION / AVAILABILITY STATEMENT
Approved for Public Release; Distribution Unlimited

13. SUPPLEMENTARY NOTES

14. ABSTRACT:
This is the final report of our CDMRP-funded research grant. Our study comprised of two research aims to validate and examine the therapeutic potential of targeting XIAP for the treatment of prostate cancer. In the first of the two Aims, we generated cell lines in which XIAP was suppressed, using lentiviral-based RNA interference delivery system. Additionally, we reconstituted these lines with a panel of XIAP variants lacking either the caspase inhibitory or the E3 ubiquitin ligase properties of this molecule. In functionall studies, we have obtained important We have made very significant progress towards the completion of the goals proposed in this award. In the first of the two Aims, we experimental data concerning the relative contribution of these different aspects of XIAP to the cytoprotective effects of this protein, although for technical reasons the use of these lines in xenograft studies generated excessive variation. In the second Aim, we have examined XIAP expression in the TRAMP transgenic murine model of prostate cancer. These studies have revealed an interesting trend towards Xiap-deficient animals being more susceptible to tumors, which correlates with some recent clinical data on XIAP expression in prosate cancer patients. Thus, these data have significant implications for the clinical use of XIAP antagonists as anti-cancer agents. Finally, the data described above are included in three manuscripts are currently in review.

15. SUBJECT TERMS
Prostate Cancer; X-linked Inhibitor of Apoptosis; TRAMP; Xenograft

16. SECURITY CLASSIFICATION OF:			17. LIMITATION OF ABSTRACT	18. NUMBER OF PAGES	19a. NAME OF RESPONSIBLE PERSON
a. REPORT	b. ABSTRACT	c. THIS PAGE			USAMRMC
U	U	U	UU	76	19b. TELEPHONE NUMBER *(include area code)*

Table of Contents

Introduction

This is the final report of a three-year IDEA development award entitled "XIAP as a molecular target for therapeutic intervention in prostate cancer." The primary goal of this project was to investigate the contribution played by the X-linked inhibitor of apoptosis (XIAP) protein in the development and establishment of prostate cancer. The impetus behind these experiments came from a number of earlier studies indicating that XIAP was overexpressed, at least at the level of mRNA, in prostatic tumors, both in humans and in mice. The question raised by these earlier studies, however, was whether the described overexpression of XIAP necessarily makes it a suitable therapeutic target in prostate cancer, or whether this enhanced expression is simply an epiphenomenon unrelated itself to tumor development. Prior to our studies, the general concensus in the field was that XIAP would be likely to play a crucial role in tumorigenesis, and that this role would be related to its described ability to suppress apoptotic cell death through the inhibition of caspases, which are the principal effectors of the apoptotic or programmed cell death cascade. However, we and others have shown that XIAP is involved in many other cellular processes unrelated to caspase inhibition, and so a second part of our project was to dissect the various physiological properties of XIAP to evaluate which cellular activities are required for its tumor-enhancing effects. As described below, most of our original goals were achieved, and the questions posed were, to a large extent, addressed, with an exception of an experiment which, for technical reasons, led to a less conclusive endpoint than we had hoped for.

Body

The proposed experiments were separated into two Aims, which are detailed below. These Aims were related in terms of the scope of the questions being posed, but were not reliant on each other. Since to date the research supported by this IDEA has yielded seven publications in peer-reviewed journals, we have chosen to utilize the guidelines provided to us, regarding the inclusion of data, and will refer to specific manuscripts and figures depicted therein. We hope that this will provide a clearer picture of the studies we have performed, and will also help to keep this report as concise as possible, instead of additionally including redundant figures.

SPECIFIC AIM 1. To dissect and evaluate the contributions of the distinct caspase inhibitory and signaling functions of XIAP in the development of prostate cancer.

Much of Aim 1 was completed within the first two years of the funding period, and consequently some of the summary below is taken from the annual report form year 2.

In this aim we proposed to use lentiviral-mediated RNA interference to generate clones of prostate cancer lines lacking XIAP. We proposed to subsequently reintroduce mutants of XIAP variously lacking either the caspase-inhibitory or E3 ubiquitin ligase activity of XIAP. We have made very significant progress in this area. As outlined in our previous report, we have concentrated on the PC-3 cell as a model to test our reagents and the experimental model, and we have effectively ablated XIAP with these mutants. We have now had the opportunity to extensively analyze these lines, as well as 'rescue' lines in which the XIAP mutants have been reintroduced, in xenografts. We did find a modest suppression of tumorigenicity in cells lacking XIAP, the suppression observed is only slightly that observed in control lines transduced with an irrelevant RNAi cassette. Both groups of transduced lines appear to form tumors at a time following injection which is significantly delayed relatively to parental, untransduced cells, and

this gives us cause for concern, since it raises the possibility that an immune response is being generated against these lentivirally modified tumor lines which would hamper subsequent analysis of 'rescue' lines and prevent us from establishing an experimental window to conclusively gauge our results. Additionally, the experimental variation in these lines is very significant. One possible explanation for this would be a relatively non-specific interferon response, perhaps initiated by the expression of the dsRNA hairpin. While we cannot conclusively exclude this possibility, we have tested for the expression of interferon-responsive genes by real-time quantitivative RT-PCR, and have not observed any significant differences in the various cell lines. However, we note now that relatively few examples have been described in the literature of this approach being taken, although at the time of proposing and first performing our studies the technique of RNA interference was so novel that no data had been presented for or against it being successful in xenograft studies.

As described above, we were very successful at incorporating the lentiviral system for both RNA interference and ectopic expression into our laboratory, which were new experimental systems for us at the beginning of this project, and effectively suppressing/overexpressing XIAP and its variants. From this perspective the studies can be considered a success. However, our data examining the combination of lentivirally delivered shRNAs and subsequent analysis of growth kinetics by xenograft implantation was less clear-cut. There are a number of future directions to take, capitalizing on both our initial experiences and reports that have been published since our original proposal was submitted. The most significant of these would be to examine the sensitivity of our generated cell lines in similar xenograft studies to the ones we have already performed, but additionally examining their sensitivity to apoptosis-inducing agonists, such as TRAIL. Both published and our own unpublished data strongly suggest that while suppression of XIAP, either by RNA interference or by another other approach, greatly sensitizes prostate cancer cells to TRAIL, as well as other receptor-dependent apoptotic agonists, even while the reduction of XIAP alone may have little or no effect on the growth characteristics of the cell line or xenograft. Thus, a regulated loss of XIAP may serve to modulate the apoptotic sensitivity of the tumor cell to a pro-apoptotic signal, rather than providing the apoptotic signal itself.

While these experiments were underway, our studies also provided insights into other physiological roles of XIAP. While a number of these studies were not directly described in our proposal, they were related to the IDEA award in various ways: for example, XIAP-related reagents, such as expression vectors, antibodies, shRNA vectors, which were generated or obtained specifically under the auspices of Aim 1 of this award, were also used for other studies within the laboratory. Consequently, we have published six of papers, which are appended to this final report, in which we have cited and acknowledged this IDEA award, even though the studies may not appear to be obviously included in the specific aims and statement of work of the award. In particularly, our studies on the signaling and caspase-independent properties of XIAP led us to identify a novel family of XIAP-associated proteins now known as the COMMDs (Burstein et al,, manuscript 1, J. Biol. Chem). Stemming from these studies, we also found that XIAP plays an entirely unanticipated role in copper homeostasis (Mufti et al, manuscript 3, Molecular Cell), and that it interacts in a non-apoptotic scenario with AIF (Apoptosis Inducing Factor; Wilkinson et al, manuscript 6, Mol. Cell Biol). These papers are attached to this report; as noted in an earlier annual report, several of these inadvertently cited the proposal log number (PC040215) instead of the award number (W8AXWH-04-1-0891); unfortunately we were not aware of this convention until after the studies were published..

SPECIFIC AIM 2. To validate XIAP as a novel target for the treatment of prostate cancer, using established transgenic and conditionally targeted murine models.

The experiments proposed in Aim 2 were designed to understand the in vivo role of XIAP in tumorigenesis, and to evaluate the therapeutic potential of targeting XIAP in animals using an antisense approach. Rather than examining these questions in a xenograft system, which necessitates the use of immunodeficient animals, we turned to a well-described immunocompetent model of prostate cancer, the TRAMP model. The first sub-aim in this section was highly informative, and had led to a recent publication in *Cell Death and Differentiation* (Hwang et al; manuscript 7 in the reportable outcomes section). The second sub-aim was not so successful, because we found a non-specific antitumor effect with control antisense compounds, as described below.

2.1 Analysis of the rate of tumor progression in *Xiap*-deficient mice.

a) Examination of Xiap expression profiles in TRAMP and Pten conditionally deficient mice. In this sub-aim, we proposed firstly to confirm a previous report that Xiap expression is enhanced in prostate cancer. For the TRAMP model of prostate cancer, this section was completed and much of the data are described in manuscript 7 (Hwang et al; Cell Death Diff, Figures 4, 5 and Table 1). Within the funding period we did not reach a point where we could draw inferences from Pten conditionally deficient mice.

b) Evaluation of the contribution to tumorigenesis of XIAP using *Xiap*-targeted mice. The second goal of this sub-aim was to breed our Xiap-deficient mice to TRAMP (and ultimately Pten-conditional) mice, and examine tumor burden. For the case of the TRAMP model, this section of work has been completed, and have been described in detail in manuscript 7 (Hwang et al; Cell Death Diff). To our initial surprise, if anything these mice demonstrated a trend towards developing more aggressive tumors. Despite observing this trend, however, our study showed statistically significant differences between Xiap-deficient mice and littermate controls, in terms of tumor onset, animal survival and general pathology. Again, within the funding period for this Award we did not reach a point where we could make any conclusions from Pten conditionally deficient mice.

Finally, for future experiments our data strongly suggest that an acute ablation of XIAP have a much more dramatic effect on a tumor cell than allowing it to evolve in the absence of XIAP. Furthermore, to address these issues in the future,, based on our experiences and conclusions from both of the Aims of this award, we would add an additional arm to these studies using a chemotherapeutic drug (e.g. taxotere,TRAIL), to determine whether there are any combined effects of XIAP deficiency and therapy.

2.2 Use of murine models of prostate cancer to evaluate the effectiveness of XIAP-specific antisense strategies.

For these studies we used stabilized antisense oligonucleotides designed and validated specifically to target murine Xiap, in a study to examine their effects on tumor development in TRAMP and Pten-conditional murine prostate cancer models. The dosage regimen for this reagent (in parallel with a scrambled control oligonucleotide) was studied in detail using TRAMP transgenic mice. We have found good evidence that adminstration of Xiap-specific antisense elicits an anti-tumor response. However, we also observed a number of non-specific effects that are deleterious to the mice using the scrambled non-specific control. It has been technically challenge to titrate the levels of antisense used for these experiments to obtain a therapeutic window in which off-target effects were not seen, and these experiments have therefore been less fruitful. However, an approach to this problem that does not rely on an antisense strategy has recently been developed, employing small molecule antagonists of IAP

that trigger their degradation by activating the autoubiquitination of these molecules. Therefore, in future studies we plan to use these so-called Smac mimetic IAP antagonists to examine their therapeutic potential in prostate cancer, especially in combination with additional therapeutics, especially TRAIL and taxotere.

Key Research Accomplishments

- Generated a large panel of cell lines lacking XIAP, and reconstituted these lines with XIAP mutants lacking various functional aspects of the protein.
- Examined these lines in xenografts and in cell culture systems.
- Tested the cells lines described above for apoptotic sensitivities to a range of stimuli.
- Completed the breedings of XIAP-deficient mice to TRAMP mice.
- Completed the experiments describing the onset and mortality of TRAMP mice in a wild type and XIAP-null background.
- Characterized the anti-tumor and pro-apoptotic effects of small molecule IAP antagonists.

Reportable Outcomes

The following manuscripts have been published to date citing this award:

1. Burstein, E., Hoberg, J.E., Wilkinson, A.S., Rumble, J.M., Csomos, R.A., Komarck, C.M., Maine, G.N., Wilkinson, J.C., Mayo, M.W. and **Duckett, C.S.** COMMD proteins: a novel family of structural and functional homologs of MURR1. *J Biol. Chem.* **280:**22222-22232 (2005).

2. Wright, C.W. and **Duckett, C.S.** Re-awakening the cellular death program in neoplasia through the therapeutic blockade of IAP function. *J. Clin. Invest.* **115:**2673-2678 (2005).

3. Mufti, A.R., Burstein, E., Csomos, R.A., Graf, P.C.F., Wilkinson, J.C., Dick, R.D., Challa., M., Son, J.-K., Bratton, S.B., Su, G.L., Brewer, G.J., Jakob., U. and **Duckett, C.S.** XIAP is a copper binding protein deregulated in Wilson's Disease and other copper toxicosis disorders. *Mol. Cell* **21**:775-785 (2006).

4. Xia, Y., Novak, Lewis, J., **Duckett, C.S.** and Phillips, A.C. Xaf1 can cooperate with TNF-a in the induction of apoptosis, independently of interaction with XIAP. *Mol. Cell. Biochem.* **286:**67-76 (2006).

5. Hwang, C., Giri, V.N., Wilkinson, J.C., Wright, C.W., Wilkinson, A.S., Cooney, K.A. and **Duckett, C.S.** EZH2 regulates the transcription of estrogen-responsive genes through association with REA, and estrogen receptor corepressor. *Breast Canc* Res Treat **107**:235-242 (2008).

6. Wilkinson, J.C., Wilkinson, A.S., Csomos, R.A., Galban, S. and **Duckett, C.S.** AIF is a target for ubiquitination through interaction with XIAP. *Mol. Cell. Biol* **28**:237-247 (2008).

7. Hwang, C., Oetjen, K.A., Kosoff, D, Wojno, K.J., Albertelli, M.A., Robins, D.M., Cooney, K.A. and **Duckett, C.S.** X-linked inhibitor of apoptosis deficiency in the TRAMP mouse prostate cancer model. *Cell Death Diff* 208:1-10.

Conclusions

The two experimental Aims that we originally proposed in our application have been completed and, to a very large extent, have been successful. In Aim 1, we established an experimentally tractable system that allowed us to directly examine the various functional properties of XIAP, and to evaluate the contribution of these properties to the control of the apoptotic threshold. Although we learnt that the use of lentivirally manipulated cell lines in xenograft studies results in excessive variation, the lines generated have turned out to extremely helpful not only in dissecting these functional aspects of XIAP, but also in understanding in mechanistic terms the efficacy of pharmacologic XIAP antagonists which became available to us during the course of the study. Aim 2 was also highly successful, and especially interesting to us was the observed trend that XIAP-deficient mice may be more susceptible to tumors than their littermate counterparts, and these studies were described in detail in a recent publication (manuscript 7). The final subsection of Aim 2 was less successful, due to off-target effects of the antisense reagents being used, but this approach could now be superceded by the use of small-molecule synthetic IAP antagonists, to which we have access. Future studies will address the question of whether a combined treatment of standard chemotherapeutics and XIAP-deficiency, either in these murine knockout systems or with synthetic XIAP antagonists, may function cooperatively.

Appendix

1. Burstein, E., Hoberg, J.E., Wilkinson, A.S., Rumble, J.M., Csomos, R.A., Komarck, C.M., Maine, G.N., Wilkinson, J.C., Mayo, M.W. and **Duckett, C.S.** COMMD proteins: a novel family of structural and functional homologs of MURR1. *J Biol. Chem.* **280:**22222-22232 (2005).

2. Wright, C.W. and **Duckett, C.S.** Re-awakening the cellular death program in neoplasia through the therapeutic blockade of IAP function. *J. Clin. Invest.* **115:**2673-2678 (2005).

3. Mufti, A.R., Burstein, E., Csomos, R.A., Graf, P.C.F., Wilkinson, J.C., Dick, R.D., Challa., M., Son, J.-K., Bratton, S.B., Su, G.L., Brewer, G.J., Jakob., U. and **Duckett, C.S.** XIAP is a copper binding protein deregulated in Wilson's Disease and other copper toxicosis disorders. *Mol. Cell* **21**:775-785 (2006).

4. Xia, Y., Novak, Lewis, J., **Duckett, C.S.** and Phillips, A.C. Xaf1 can cooperate with TNF-a in the induction of apoptosis, independently of interaction with XIAP. *Mol. Cell. Biochem.* **286:**67-76 (2006).

5. Hwang, C., Giri, V.N., Wilkinson, J.C., Wright, C.W., Wilkinson, A.S., Cooney, K.A. and **Duckett, C.S.** EZH2 regulates the transcription of estrogen-responsive genes through association with REA, and estrogen receptor corepressor. *Breast Canc* Res Treat **107**:235-242 (2008).

6. Wilkinson, J.C., Wilkinson, A.S., Csomos, R.A., Galban, S. and **Duckett, C.S.** AIF is a target for ubiquitination through interaction with XIAP. *Mol. Cell. Biol* **28**:237-247 (2008).

7. Hwang, C., Oetjen, K.A., Kosoff, D, Wojno, K.J., Albertelli, M.A., Robins, D.M., Cooney, K.A. and **Duckett, C.S.** X-linked inhibitor of apoptosis deficiency in the TRAMP mouse prostate cancer model. *Cell Death Diff* 208:1-10.

THE JOURNAL OF BIOLOGICAL CHEMISTRY Vol. 280, No. 23, Issue of June 10, pp. 22222–22232, 2005
Printed in U.S.A.

COMMD Proteins, a Novel Family of Structural and Functional Homologs of MURR1*[S]

Received for publication, February 22, 2005, and in revised form, March 11, 2005
Published, JBC Papers in Press, March 30, 2005, DOI 10.1074/jbc.M501928200

Ezra Burstein‡§, Jamie E. Hoberg¶, Amanda S. Wilkinson‖, Julie M. Rumble‖, Rebecca A. Csomos‖, Christine M. Komarck‡, Gabriel N. Maine‡, John C. Wilkinson‖, Marty W. Mayo‖, and Colin S. Duckett‡‖**

From the Departments of ‡Internal Medicine and ‖Pathology, University of Michigan Medical School, Ann Arbor, Michigan 48109-0602, ¶Department of Biochemistry and Molecular Genetics, University of Virginia, Charlottesville, Virginia 22908, and §Gastroenterology Section at the Ann Arbor Veterans Affairs Medical Center, Ann Arbor, Michigan 48105

MURR1 is a multifunctional protein that inhibits nuclear factor κB (NF-κB), a transcription factor with pleiotropic functions affecting innate and adaptive immunity, apoptosis, cell cycle regulation, and oncogenesis. Here we report the discovery of a new family of proteins with homology to MURR1. These proteins form multimeric complexes and were identified in a biochemical screen for MURR1-associated factors. The family is defined by the presence of a conserved and unique motif termed the COMM (copper metabolism gene MURR1) domain, which functions as an interface for protein-protein interactions. Like MURR1, several of these factors also associate with and inhibit NF-κB. The proteins designated as COMMD or COMM domain containing 1–10 are extensively conserved in multicellular eukaryotic organisms and define a novel family of structural and functional homologs of MURR1. The prototype of this family, MURR1/COMMD1, suppresses NF-κB not by affecting nuclear translocation or binding of NF-κB to cognate motifs; rather, it functions in the nucleus by affecting the association of NF-κB with chromatin.

NF-κB is a dimeric complex formed by members of a highly conserved family of proteins that share a defining motif designated the Rel homology domain (RHD).[1] Through transcriptional regulation of many gene products, NF-κB participates in a number of biological processes including innate and adaptive immune responses, programmed cell death, cell cycle progression, and oncogenesis (1–6). Additionally, by its ability to regulate transcription of various viral genomes including human immunodeficiency virus-1 (HIV-1) (7–10), NF-κB also participates in viral cycle progression.

Studies into the regulation of NF-κB activation have largely focused on the role of cytoplasmic sequestration of the NF-κB complex as a mainstay level of control. In most cells NF-κB is localized in the cytoplasm through the interaction of the complex with members of the IκB family (11). These proteins contain ankyrin repeats that allow their interaction with NF-κB and mask the nuclear localization signal present in the RHD. Phosphorylation of IκB by a multimeric kinase known as the IκB kinase complex targets these proteins for ubiquitination and proteasomal degradation (3, 12). This allows the translocation of NF-κB to the nucleus where it binds to cognate DNA sequences present in an array of gene promoters.

MURR1 is a recently identified factor that has been shown to participate in two apparently distinct activities, regulation of the transcription factor NF-κB and control of copper metabolism (13). Mutations in *MURR1* are responsible for copper toxicosis in an inbred canine strain (Bedlington terriers) (14), and an interaction between MURR1 and the copper transporter ATP7B (15) has been recently reported.

In addition to its role in copper metabolism in mammals, more recent studies implicate MURR1 in the regulation of the transcription factor NF-κB (13, 16). MURR1 was found to be a broad inhibitor of NF-κB, affecting κB-responsive transcription from endogenous and viral promoters including the HIV-1 enhancer (16). Through this effect, MURR1 can function as a factor that limits HIV-1 replication in resting $CD4^+$ lymphocytes.

Here we report the discovery of a family of proteins structurally and functionally related to MURR1. These factors contain a unique and defining domain termed the COMM (copper metabolism gene MURR1) domain, and thus, these proteins have been named COMM domain-containing or COMMD proteins. Similar to MURR1/COMMD1, several of these factors associate with NF-κB and inhibit its transcriptional activity. In addition, we find that COMMD proteins form heteromeric complexes that are mediated by the COMM domain. The prototype of the family, MURR1/COMMD1, exerts its ability to inhibit κB-mediated transcription without affecting nuclear translocation but through nuclear regulation of NF-κB. We show here that MURR1/COMMD1 is recruited to chromatin of a κB-responsive promoter upon NF-κB activation and negatively regulates the association of RelA to chromatin. Therefore, this work identifies a novel family of factors that regulate NF-κB-mediated transcription by controlling the occupancy of NF-κB on chromatin.

* This work was supported in part by the University of Michigan Biological Scholars Program, Department of Defense Idea Award PC040215 and National Institutes of Health Grant GM067827 (to C. S. D.), by an American Gastroenterological Association Research Scholar Award, a Merit Review Entry Program Award, and a Veterans Education and Research Association of Michigan Award (to E. B.), by NCI, National Institutes of Health Grants K01CA78595, R01CA104397, and R01CA095644 (to M. W. M.), and by T32 CA09676 (to J. C. W.). The costs of publication of this article were defrayed in part by the payment of page charges. This article must therefore be hereby marked "*advertisement*" in accordance with 18 U.S.C. Section 1734 solely to indicate this fact.

[S] The on-line version of this article (available at http://www.jbc.org) contains a supplemental figure and table.

** To whom correspondence should be addressed: Med. Sci. I, Rm. 5315, 1301 Catherine, Ann Arbor, MI 48109-0602. Tel.: 734-615-6414; Fax: 734-615-7012; E-mail: colind@umich.edu.

[1] The abbreviations used are: RHD, Rel homology domain; EGFP, enhanced green fluorescence protein (GFP); TAP, tandem affinity purification; GST, glutathione *S*-transferase; TNF, tumor necrosis factor; MS, mass spectroscopy; RT, reverse transcription; EMSA, electrophoretic mobility shift assay; ChIP, chromatin immunoprecipitation; RNAi, RNA interference; siRNA, small interfering RNA; HIV-1, human immunodeficiency virus-1.

EXPERIMENTAL PROCEDURES

Plasmids—The plasmids pEBB, pEBG, pEBB-MURR1-Flag and pEBB-MURR1-GST, pEBB-T7-IκB-αS.D., 2κB-luc, and EGFP-p65 (kindly provided by Dr. Rainer de Martin) have been described previously (17–22). pEBB-COMMD1-GST vectors expressing exon 1, exon 2-3, and exon 1-3 were generated by PCR amplification using pEBB-MURR1-Flag as template with the boundaries outlined in Fig. 3*C*. pEBB-MURR1-TAP was constructed by subcloning MURR1 into pEBB-TAP, which was generated by PCR amplification of the coding sequence for the tandem affinity purification (TAP) tag using pBS1539 as template (23). Expression vectors for COMMD proteins in fusion with Flag and glutathione *S*-transferase (GST) (pEBB-COMMD-Flag or pEBB-COMMD-GST) were generated by PCR amplification of the coding sequences for each of these proteins. To that effect the following full-length IMAGE clones were used as templates to amplify COMMD2 through COMMD10, respectively: 4443942, 3531636, 5743903, 6644608, 1692591, 5275167, 4051246, 4333615, and 3683093. pEBG-RelA-(1–305), pEBG-RelA-(306–551), and pEBG-RelA-(1–180), pEBG-c-Rel-(1–180), pEBG-RelB-(97–267), and pEBG-p50-(1–233) and pEBG-p52-(1–212) were generated by PCR using the vectors RSV-RelA, RSV-c-Rel, RSV-RelB, RSV-p50, and RSV-p52 as templates, respectively (kindly provided by Dr. Neil Perkins) (24).

Cell Culture, Transfection, and Luciferase Assays—Human embryonic kidney 293 cells and prostate cancer and DU145 cells were obtained from ATCC. 293 cells were cultured in Dulbecco's modified Eagle's medium supplemented with 10% fetal bovine serum and L-glutamine, and DU145 cells were cultured in minimum Eagle's medium supplemented with 10% fetal bovine serum, L-glutamine, sodium bicarbonate, and pyruvate. A standard calcium phosphate transfection protocol (20) was used to transfect plasmids and siRNA oligonucleotides into 293 cells. Delivery of siRNA oligonucleotides into DU145 cells was performed using Oligofectamine (Invitrogen) as specified by the manufacturer. For luciferase reporter experiments, cells were seeded in 6-well plates and transfected with 4 μg of pEBB plasmid, and 25 ng of the reporter plasmid 2κB-luciferase. Luciferase assays were performed as described previously (25). TNF (Roche Applied Science) treatments consisted of 1000 units/ml for 12 h. For immunoprecipitation experiments cells were seeded in 10-cm plates and transfected with a total of 12 μg of plasmid. Finally, suppression of endogenous COMMD expression was achieved by transfection of 293 cells seeded in 6-well plates with 2 μg of the corresponding siRNA oligonucleotides (Qiagen).

TAP Screening—293 cells seeded in 15-cm plates were transiently transfected with pEBB-MURR1-TAP (15 μg of plasmid/plate) and 2 days later were lysed in Triton lysis buffer (25 mM HEPES, 100 mM NaCl, 1 mM EDTA, 10% glycerol, 1% Triton X-100, protease inhibitors). The lysate was supplemented with NaCl and Nonidet P-40 and applied to a chromatography column containing IgG-Sepharose beads (Amersham Biosciences). After 2 h of incubation at 4 °C the column was drained and washed with IPP150 buffer (10 mM Tris-HCl, pH^+ 8.0, 150 mM NaCl, 0.1% Nonidet P-40, protease inhibitors) and TEV cleavage buffer (10 mM Tris-HCl, pH^+ 8.0, 150 mM NaCl, 0.1% Nonidet P-40, 0.5 mM EDTA, 1 mM dithiothreitol, protease inhibitors). After incubation for 2 h at 16 °C in TEV cleavage buffer supplemented with TEV enzyme (Invitrogen), the eluate was collected and supplemented with $CaCl_2$ and IPP150 calmodulin binding buffer (10 mM Tris-HCl, pH^+ 8.0, 150 mM NaCl, 0.1% Nonidet P-40, 1 mM magnesium acetate, 1 mM imidazole, 2 mM $CaCl_2$, 10 mM β-mercaptoethanol). This was then applied to a chromatography column containing calmodulin 4B beads (Amersham Biosciences) and incubated at 4 °C for 1 h. The column was then drained and washed with IPP150 calmodulin binding buffer. After incubation at 4 °C with IPP150 calmodulin elution buffer (10 mM Tris-HCl, pH^+ 8.0, 150 mM NaCl, 0.1% Nonidet P-40, 1 mM magnesium acetate, 1 mM imidazole, 2 mM EGTA, 10 mM β-mercaptoethanol), a final eluate was collected. Proteins were precipitated by adding cold 10% trichloroacetic acid in acetone; after overnight incubation at −20 °C, the precipitate was collected by centrifugation at 4 °C (10,000 × *g* for 30 min), rinsed in 100% acetone, and allowed to air dry. These samples were then submitted to the Proteomics Centre at the University of Victoria for further processing, including tryptic digestion, high performance liquid chromatography separation, and tandem mass spectrometry (MS/MS) to determine peptide sequences.

RT-PCR and Expression Data—Total RNA was extracted from 293 cells using RNeasy (Qiagen) according to the manufacturer's instructions. Yield and purity was determined by measuring $A_{260/280}$ of RNA diluted in water. Oligonucleotides and internal probes for RT-PCR and quantitative RT-PCR of *COMMD* transcripts were designed with the use of the automated primer design tool, AutoPrime (www.autoprime.de). Detailed information about sequences and cycling parameters are available upon request. For non-quantitative RT-PCR, Titan One-Tube RT-PCR (Roche Applied Science) was used according to the manufacturer's instructions. For quantitative RT-PCR reactions, an RT reaction with 500 ng of total RNA in 25 μl was performed using random hexamers and Taqman reverse transcription reagents (Applied Biosystems). This was followed by quantitative PCR performed in the 7500 real time PCR system (Applied Biosystems). In all reactions, Taqman PCR Master Mix with the appropriate primers and probes was used. Primers and probe sets for *c-IAP2* (*BIRC3*) and *GAPDH* (glyceraldehyde-3-phosphate dehydrogenase) as an internal control were obtained from Applied Biosystems. Expression data in normal tissues were obtained from the Genomics Institute of the Novartis Research Foundation (26), downloaded, and further analyzed.

Immunoblotting and Immunoprecipitation—Cell lysates were prepared by adding Triton lysis buffer; immunoblotting and GSH precipitations were performed as previously described (19). A polyclonal COMMD1 antiserum was raised by immunizing New Zealand White rabbits. Recombinant protein, which was used as immunogen, was produced in *Escherichia coli* by expressing GST-COMMD1 using the pGEX-4T1 bacterial expression vector (Amersham Biosciences). GST-COMMD1 was purified over a glutathione-Sepharose chromatography column (Amersham Biosciences), and COMMD1 was generated by thrombin cleavage of the GST affinity tag according to the manufacturer's instructions. Antibodies against Flag (Sigma, A8592), RelA (BD Transduction Laboratories, 610868), c-Rel (Santa Cruz, sc-6955), RelB (Santa Cruz, sc-226), p50 (Upstate Biotechnology, 06–886), p52 (Upstate Biotechnology, 05–361), IκB-α (Upstate Biotechnology, 06–494), GST (Santa Cruz, sc-459), α-tubulin (Molecular Probes, A11126), and GCN5 (Santa Cruz, sc-20698) were used as indicated.

Confocal and Fluorescence Microscopy—293 cells were plated in chambered cover glass plates or 6-well plates and transfected with EGFP-p65 (25 or 50 ng/well, respectively). Morphological assays for nuclear translocation of EGFP-p65 were performed by observing cells with a Zeiss Axiovert 100 M confocal microscope before and after treatment with TNF. Representative images were obtained, and 250–400 cells were observed and scored accordingly.

Electrophoretic Mobility Shift Assay (EMSA)—293 cells were seeded in 10-cm dishes and transfected as indicated. TNF stimulation, when performed, consisted of treating cells with 1000 units/ml for 30 min before lysis. The preparation of nuclear extracts and EMSA have been described previously (24). For our studies, a double-stranded oligonucleotide encompassing a canonical κB sequence was used as probe (forward sequence, AGCTTACAAGGGACTTTCCGCTGGGGACTTTCCAGGG).

Cellular Fractionation—293 cells were plated in 10-cm plates 48 h before the procedure. Medium was aspirated, and the cells were rinsed in phosphate-buffered saline, scraped, and collected in a microcentrifuge tube. The cells were resuspended in 200 μl of buffer 1 (25 mM HEPES, 5 mM KCl, 0.5 mM $MgCl_2$, 1 mM phenylmethylsulfonyl fluoride, 1 mM dithiothreitol, and protease inhibitors). After that, 200 μl of buffer 2 were added (Buffer 1 with 1% Nonidet P-40), and the cells were incubated with constant rotation at 4 °C for 15 min. The samples were centrifuged for 1 min at 600 × *g*, and the supernatant, corresponding to the cytoplasmic fraction, was collected. The precipitated material was gently rinsed in 100 μl of buffer 3 (1:1 mixture of buffers 1 and 2). After centrifuging the samples again as before, the supernatant was collected as part of the cytoplasmic fraction. The remaining precipitated material was then treated by the addition of 500 μl of buffer 5 (25 mM HEPES, 10% sucrose, 350 mM NaCl, 1 mM phenylmethylsulfonyl fluoride, 1 mM dithiothreitol, 0.01% Nonidet P-40, protease inhibitors) and incubated with constant rotation at 4 °C for 60 min. After this, the samples were centrifuged for 10 min at 16,100 × *g*. The supernatant, corresponding to the nuclear fraction, was collected separately.

Chromatin Immunoprecipitation—Subconfluent DU145 cells were treated with TNF (1000 units/ml) before cross-linking for chromatin immunoprecipitation (ChIP) analysis. For attachment assays, 293 cells were re-plated in serum-free media on laminin-coated plates (Discovery Labware) as previously described (27). ChIP protocol and primers sequences have been previously described (28). Antibodies used in the ChIP studies include COMMD1 (described above), M2 Flag (Sigma, F3165), RNA polymerase II (Santa Cruz, SC-9001), and RelA (Upstate, 06-418).

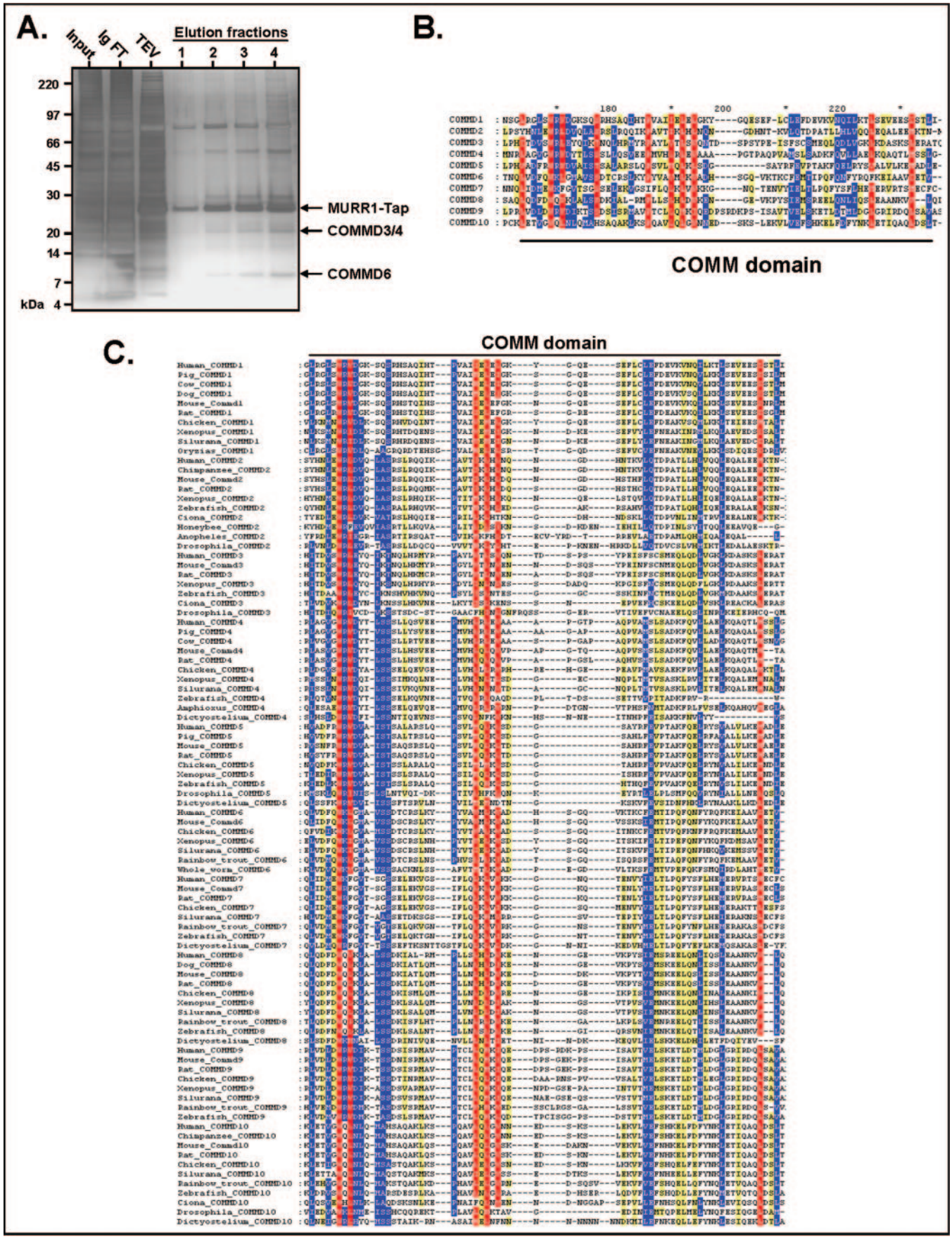

FIG. 1. *A*, identification of the COMMD protein family. Fractions obtained during TAP purification were separated by SDS-PAGE, and the gel was silver-stained. The lysate was subjected first to an immunoglobulin column, and the flow-through (*Ig FT*) and eluate (*TEV*) were collected. This eluate was further purified over a calmodulin column, and the eluates were collected in four fractions (*Elution fractions*). COMMD3, -4, and -6 were identified in the final eluate by liquid chromatography-MS/MS. *B*, human COMMD proteins. Analysis of the human protein databases using

RESULTS

Biochemical Screen for MURR1-associated Factors—To further understand the cellular activities of MURR1, a biochemical screen for associated proteins was performed based on the TAP scheme that has been previously described (23). Briefly, MURR1 in fusion with the TAP affinity tag was transiently expressed in 293 cells, and MURR1-TAP was subsequently purified from cells lysates using two sequential chromatography columns containing IgG and calmodulin beads, respectively (Fig. 1*A*). The material obtained was subjected to tryptic digestion, and the peptides generated were then identified by tandem mass spectrometry (MS/MS) after initial separation using liquid chromatography. A number of associated factors were identified, including three proteins that upon close inspection demonstrated the presence of a region with close homology to MURR1 in their carboxyl termini (Fig. 1, *A* and *B*). These factors were later designated as COMMD3, -4, and -6 (see below).

Identification of the COMMD Protein Family—After the identification of three MURR1 homologous factors in our biochemical screen, we performed an extensive search of the sequence databases for additional homologs. Through this approach we were able to identify 10 proteins in humans, including MURR1, that contain highly conserved carboxyl-terminal sequences (Fig. 1*B*). The majority of these genes were only known as open reading frames and had not been previously characterized.

Further analysis of orthologs present across multiple species demonstrated that the area of close homology in the carboxyl termini of these proteins represents a previously unrecognized, unique, and highly conserved motif (Fig. 1*C*). This leucine-rich, 70–85 amino acid long sequence is predicted to form a β-sheet. We have termed this region the copper metabolism gene MURR1 (COMM) domain.

The designation of homologs of MURR1 identified here required the generation of a new nomenclature. *Murr1* derived its name from its proximity to the *U2af1-rs1* locus in mice (mouse U2af1-rs1 region 1); however, this genomic organization is not observed in other organisms including humans. In addition, an unrelated gene that also lies in close proximity to *U2af1-rs1* has been designated *Murr2*, precluding the use of this name for MURR1 homologs (29). In consultation with the HUGO gene nomenclature committee, the term COMMD (COMM Domain containing) is proposed to designate these factors based on the shared structural domain that defines this family of proteins and has been adopted in NCBI public databases. The name COMMD1 is suggested for MURR1 as a means to standardize the nomenclature to designate this protein family and will be used hereafter.

With the exception of COMMD1, no other COMMDs have been previously described in any detail. *COMMD5* was identified as an open reading frame that is overexpressed in naturally hypertensive rats and suppressed in a number of primary tumors and cancer cell lines (30). The expressed protein localizes to the nucleus, although a direct role in transcription had not been previously demonstrated. *COMMD6* is orthologous to a mouse gene located in a region that is necessary for normal embryonic development, although it is unclear whether *COMMD6* itself is required for normal embryogenesis (31). Similarly, *COMMD3* was previously identified as a locus with close proximity to the Polycomb-group gene *Bmi-1* (32). Finally, an expressed sequence tag corresponding to *COMMD7* was found to be consistently repressed in an experimental system designed to screen for factors involved in leukemogenesis (33).

COMMD Genes Are Highly Conserved—We found that all 10 genes have been conserved throughout vertebrate evolution, as can be gleaned from orthologs found in *Silurana tropicalis, Xenopus laevis, Danio rerio*, *Oncorhynchus mykiss,* and *Oryzias latipes* (see the supplemental table). In general, mammalian sequences are about 90% conserved when compared with their human orthologs. Furthermore, lower metazoans, including insects, worms, and molds, also possess *COMMD* genes; however, none of these genes were identified in unicellular eukaryotic organisms or bacteria. Five of these genes were found in *Drosophila melanogaster* (*COMMD2*, *-3*, *-4*, *-5*, and *-10*) and *Dictyostelium discoideum* (*COMMD4*, *-5*, *-7*, *-8*, and *-10*). Overall, eight of the *COMMD* genes can be found in lower metazoans, with *COMMD1* and *COMMD9* orthologs being restricted to vertebrate species (see the supplemental figure).

Despite the presence of a conserved and defining motif in all these proteins, a significant proportion of the sequence of each COMMD protein is composed of unique regions that are divergent across members of the family. For example, human and zebrafish COMMD1 are 72% conserved, whereas human COMMD1 and COMMD10 are only 34% conserved when regions outside the COMM domain are included in the comparison (data not shown).

COMMD Genes Are Widely Expressed—Given that COMMD proteins were initially identified as COMMD1-associated factors in 293 cells, we first investigated the pattern of expression of human *COMMD* genes in this cell line. To this end, we designed primers for RT-PCR of each one of these genes including in each case one primer that was selected at an exon-exon junction. This strategy minimizes the possibility of spurious amplification from contaminating genomic DNA because such junctions are generated only after splicing. In addition, the potential for mispriming against the intronic boundary was taken into account in the design. With this algorithm we identified primers for all 10 human *COMMD* genes, with the amplicon size and position of exon-exon primers indicated in Fig. 2*A*. Using these primers and total RNA extracted from 293 cells we were able to amplify the appropriate size products for each of the *COMMD* genes (Fig. 2*B*). Template-lacking negative controls did not amplify these products (data not shown). This indicated that 293 cells express all *COMMD* genes, a fact that was also confirmed by publicly available expression data (not shown here).

Next, the level of *COMMD* expression in multiple tissues was analyzed using data available from the Genomics Institute of the Novartis Research Foundation. Utilizing oligonucleotide arrays, expression levels for more than 44,000 mRNA transcripts across 79 human tissues were determined (26). This raw data were downloaded, and the corresponding probes for most *COMMD* genes (with the exception of *COMMD6*) were identified. Expression levels in 13 selected tissues were further analyzed and are presented in Fig. 2*C*. As shown, *COMMDs* are

BLAST allowed for the identification of six additional proteins with sequence homology to MURR1. A partial alignment of all 10 human COMMD proteins is shown, demonstrating a region of higher conservation (COMM domain). The accession numbers for the 10 human mRNA sequences are NM_152516, AY542158, AY542159, AY542160, NM_014066, AY542161, AY542162, AY542163, AY542164, and AY542165, corresponding to COMMD1–10, respectively. The degree of conservation of each amino acid residue among these sequences is indicated based on Dayhoff PAM 250 scoring matrices (*red*, 90% conserved; *blue*, 70% conserved; *yellow*, 50% conserved). *C*, alignment of 91 COMMD proteins from multiple species across the COMM domain. All protein sequences spanning through the COMM domain were aligned using the ClustalV algorithm, and this alignment was then refined using the SAM program. The resulting alignment was then annotated using the GeneDoc program. The degree of conservation of each amino acid residue among these sequences is indicated based on Dayhoff PAM 250 scoring matrices as before.

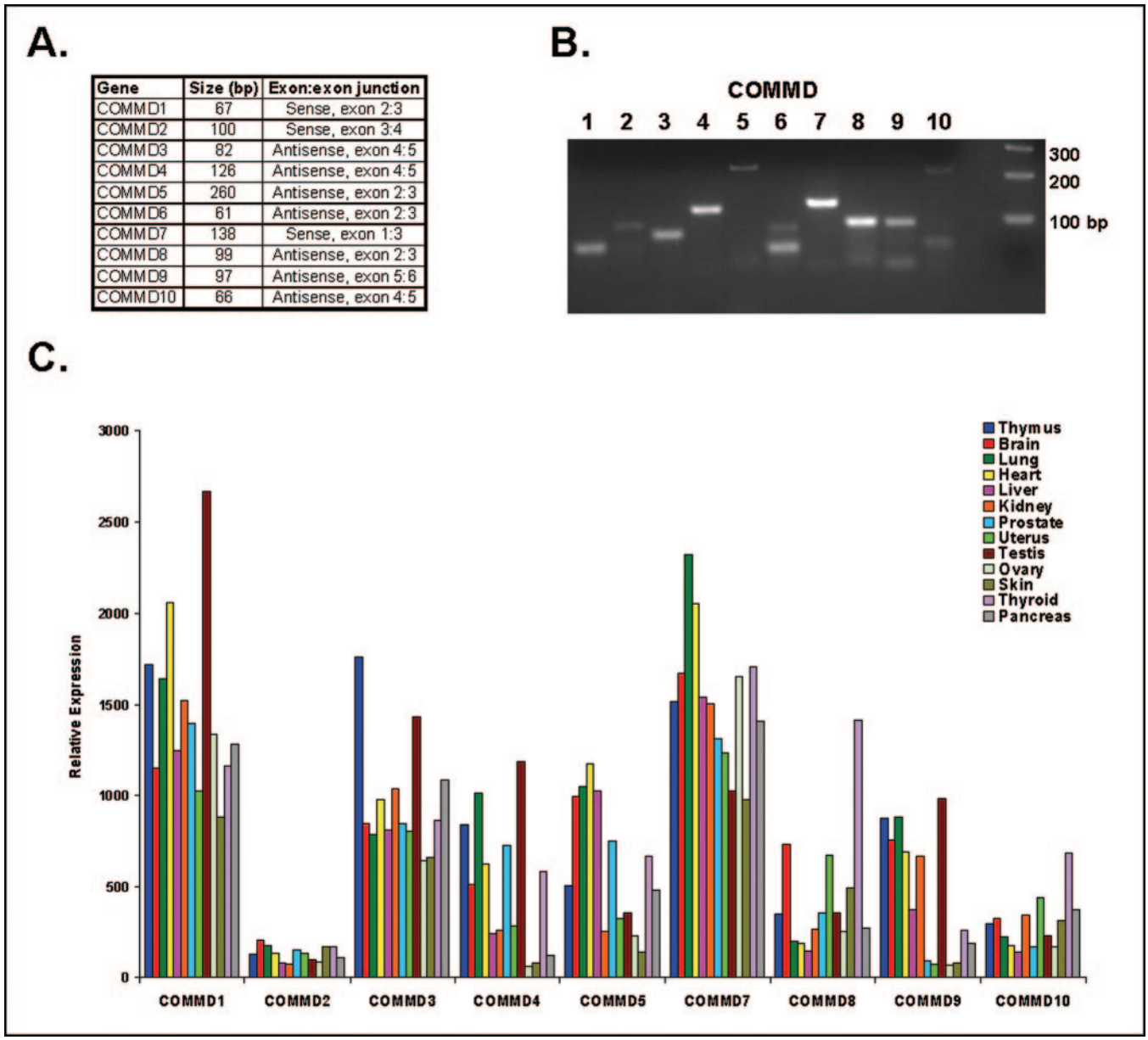

Gene	Size (bp)	Exon:exon junction
COMMD1	67	Sense, exon 2:3
COMMD2	100	Sense, exon 3:4
COMMD3	82	Antisense, exon 4:5
COMMD4	126	Antisense, exon 4:5
COMMD5	260	Antisense, exon 2:3
COMMD6	61	Antisense, exon 2:3
COMMD7	138	Sense, exon 1:3
COMMD8	99	Antisense, exon 2:3
COMMD9	97	Antisense, exon 5:6
COMMD10	66	Antisense, exon 4:5

FIG. 2. *A*, amplicon size and position of mRNA-specific primers utilized for RT-PCR. *B*, *COMMD* genes are expressed in 293 cells. Using the primer sets described, RT-PCR was performed with total RNA extracted from 293 cells serving as template. The presence of amplified products of the proper sizes was determined by agarose gel electrophoresis as shown here. *C*, expression of *COMMD* genes in 13 normal tissues. Levels of mRNA expression were determined using oligonucleotide microarrays.

widely expressed in human tissues, but the relative abundance of any given *COMMD* mRNA is different across the samples. For example, whereas *COMMD1* expression is highest in the testis, *COMMD3* is the highest expressed in the thymus, *COMMD7* in the lung, and *COMMD8* in the thyroid. Conversely, any given tissue has a complement of *COMMD* genes that demonstrate highest expression, and these subsets are not identical in each case (data not shown).

COMMD1 Can Associate with Other COMMD Proteins—COMMD3, -4, and -6 were initially identified biochemically by their ability to interact with COMMD1. Therefore, the ability of all the members of the family to interact with COMMD1 was evaluated. Each of the 10 COMMD proteins was fused to GST and expressed in 293 cells. COMMD-GST fusion proteins were then precipitated from cell lysates with glutathione-Sepharose beads, and the recovered material was immunoblotted for endogenous COMMD1 (Fig. 3*A*). COMMD1–8 and COMMD10 could readily precipitate endogenous COMMD1; COMMD9 also co-associates with COMMD1 but to a lesser extent (not shown here). These experiments demonstrated that COMMD1 can interact with itself and with all other COMMD proteins, consistent with the interactions detected in the initial TAP screen.

COMMD-COMMD Protein Interactions Are Mediated by the COMM Domain—To define the domain(s) required for COMMD multimer formation, a variety of deletion constructs of COMMD1 were tested for their ability to bind COMMD1 and COMMD3. The coding regions corresponding to each exon of COMMD1 were used as boundaries in constructs expressing fusion proteins with GST (Fig. 3*B*). The hereditary canine copper toxicosis mutation described previously consists of a genomic deletion encompassing exon 2 of *COMMD1* such that the expressed open reading frame lacks 94 amino acid residues (14). This protein product was also expressed in fusion with GST and similarly tested for its ability to bind COMMD1 and COMMD3.

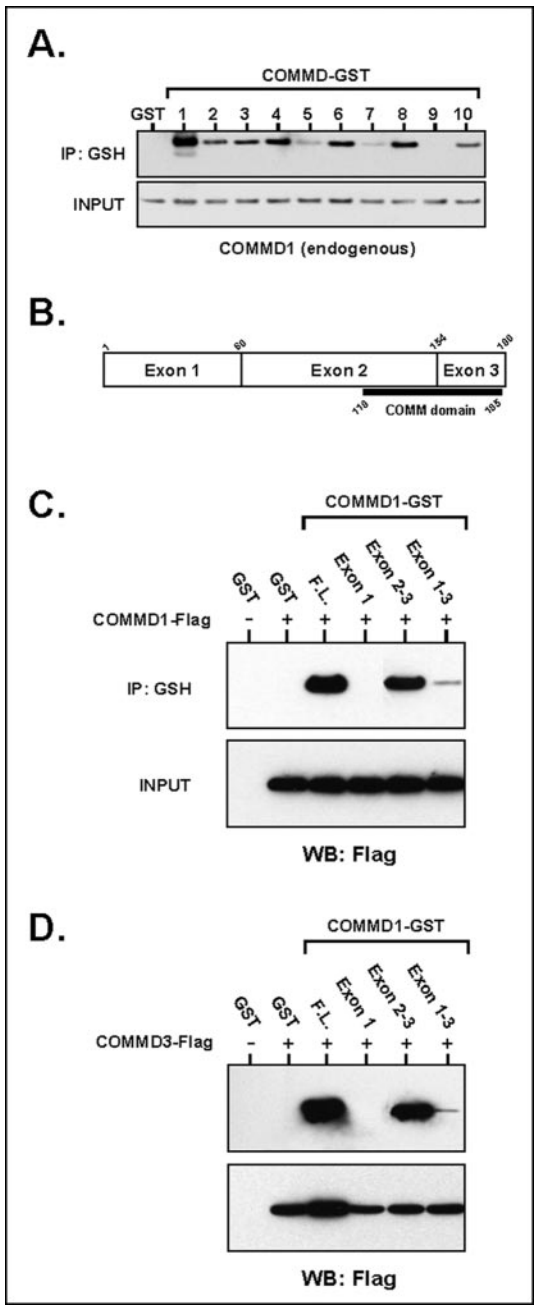

FIG. 3. *A*, COMMD-COMMD interactions. Each of the 10 COMMD proteins was expressed in 293 cells in fusion with GST and precipitated (*IP*) from cell lysates by glutathione-Sepharose beads. The presence of endogenous COMMD1 in the precipitates was determined by immunoblotting. *B*, schematic representation of COMMD1 and the amino acid residues that are the boundaries for interaction mapping experiments. *C* and *D*, the COMM domain is required for the association of COMMD proteins. COMMD1-Flag (*C*) or COMMD3-FLAG (*D*) were expressed in 293 cells along with various regions of COMMD1 in fusion with GST as indicated. COMMD1-GST was precipitated from cell lysates by glutathione-Sepharose beads and the presence of COMMD1 or -3 in the precipitates was determined by immunoblotting (*WB*) with a Flag antibody.

These fusion proteins were expressed in 293 cells and precipitated with glutathione-Sepharose beads. The ability of these fragments to support an interaction was determined by the presence of COMMD1 or COMMD3 in the precipitate (Fig. 3, *C* and *D*). The carboxyl terminus of COMMD1 (exon 2-3), which contains the COMM domain, was found to be sufficient for interactions with COMMD1 and COMMD3. The lack of the COMM domain in the exon 1-GST fusion protein abrogated binding in both cases. Furthermore, the exon 1-3 product, replicating the protein product in dogs with copper toxicosis and lacking part of the COMM domain, had a significant impairment in binding. These data demonstrated that the COMM domain that defines this protein family serves as an interface for COMMD-COMMD interactions.

Several COMMD Proteins Suppress κB-mediated Transcription—MURR1/COMMD1, the prototype member of the family, was recently reported to inhibit κB-mediated transcription from endogenous and viral promoters (16). Therefore, the ability of other COMMD proteins to inhibit NF-κB was investigated. Cells were transfected with a κB-responsive reporter plasmid (2κB-luc) along with each of the COMMD proteins, and the response to TNF stimulation was subsequently evaluated. As shown in Fig. 4*A*, COMMD1, -2, -4, -7, -9, and -10 were capable of strongly inhibiting TNF-mediated NF-κB activation, whereas COMMD3 and -8 inhibited NF-κB weakly in this assay. Similarly, most COMMD proteins also inhibited basal levels of κB-mediated transcription.

Next, the ability of these proteins to control transcription of an endogenous κB-responsive gene was evaluated. Expression levels of endogenous *COMMD1*, *-4,* and *-6* were decreased by the use of RNA interference (RNAi), and the induction of *c-IAP2* mRNA levels in response to TNF was evaluated (Fig. 4, *B* and *C*). The effectiveness of RNAi against *COMMD1*, *-4*, and *-6* was confirmed by quantitative RT-PCR (Fig. 4*C*). When compared with mRNA levels present in control samples, transfection with siRNA oligonucleotides against *COMMD1*, *-4,* and *-6* resulted in a 75–95% suppression of mRNA expression, consistent with efficient RNAi of these transcripts. Next, the effect of reduced COMMD expression on *cIAP-2* transcription was evaluated (Fig. 4*B*). In cells transfected with oligonucleotides against an irrelevant target (GFP), treatment with TNF resulted in a 9-fold increase in *c-IAP2* mRNA levels, as measured by quantitative RT-PCR, a fold increase that is identical to that observed in untransfected cells (data not shown). Decreased *COMMD* levels resulted in heightened expression of *c-IAP2* after TNF treatment, with this effect being most notable after *COMMD6* RNAi. Therefore, these factors not only share a common domain but have similar functional properties in the regulation of NF-κB transcriptional activity.

COMMD Proteins Associate with the NF-κB Complex—The ability of COMMD1 to inhibit κB-mediated transcription was previously found to depend on its association with the NF-κB complex (16). Indeed, precipitation of endogenous COMMD1 with the use of rabbit polyclonal sera against COMMD1 resulted in the co-precipitation of endogenous RelA and c-Rel (Fig. 5*A*).

The possibility that other COMMD proteins can interact with the NF-κB complex was evaluated using fusion proteins with GST expressed in 293 cells. Precipitations with glutathione-Sepharose beads were performed followed by immunoblotting for detection of endogenous NF-κB subunits RelA, c-Rel, RelB, NF-κB1/p105, and NF-κB2/p100. As was the case for COMMD1, most COMMD proteins were also capable of precipitating NF-κB complexes (Fig. 5*B*). Although the intensity of recovery of NF-κB subunits correlated with the level of expression of the COMMD-GST proteins themselves (data not shown), the pattern of association with NF-κB subunits was different between the various COMMDs. Some COMMD proteins favor complexes containing RelB and NF-κB1/p105 (as in the case of COMMD3 and 9), whereas others seem to interact preferentially with RelA-containing complexes (as in the case of COMMD6 and -7). COMMD1, -2, -4, -5, -8, and -10 could associate more broadly with NF-κB subunits, although pattern differences were still evident. COMMD1 could asso-

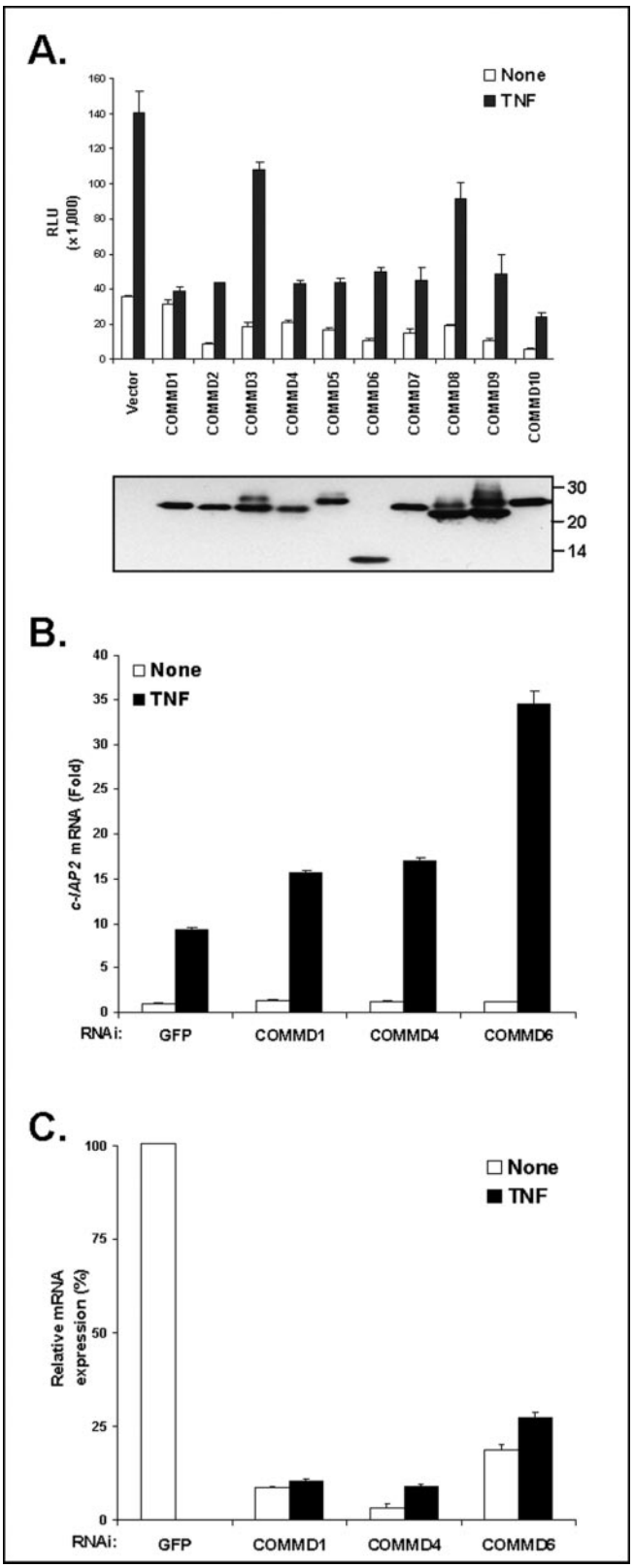

FIG. 4. *A*, COMMD proteins suppress κB-mediated transcription. Cells were transfected with the 2κB-luciferase reporter and COMMD proteins and were treated with TNF (1000 units/ml) for 12 h. Transcriptional activation of NF-κB was determined by luciferase assay (*top panel*), and expression of COMMD proteins in these lysates was determined by Flag immunoblotting (*bottom panel*). *RLU*, relative luminescence units. *B*, effect of COMMDs on *c-IAP2* expression. Endogenous levels of COMMD1, -4, and -6 were decreased with the use of siRNA oligonucleotides. The effects of TNF treatment on the expression levels of *c-IAP2*, a known NF-κB responsive gene, were evaluated by quantitative RT-PCR. *C*, efficiency of *COMMD* RNAi. Levels of expression of *COMMD1*, *-4,* and *-6* were determined by quantitative RT-PCR and compared with the corresponding control samples transfected with the GFP siRNA oligonucleotide. The data are presented as a percentage of the control samples, which was standardized to 100%.

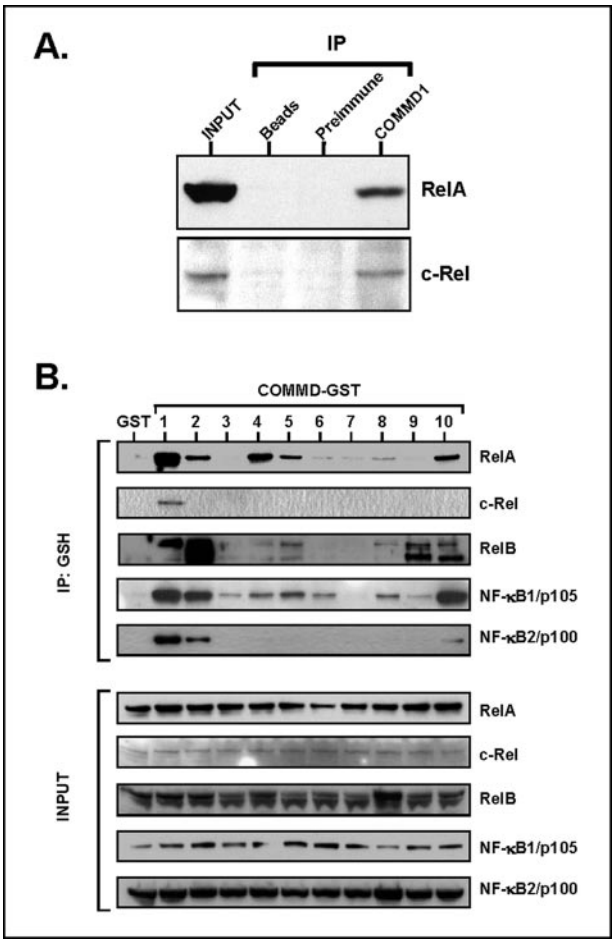

FIG. 5. *A*, COMMD1 associates with endogenous NF-κB subunits. Endogenous COMMD1 was immunoprecipitated (*IP*) from cell lysates prepared from 293 cells. This material was immunoblotted for endogenous RelA (*top panel*) and c-Rel (*bottom panel*). *B*, other COMMDs also associate with NF-κB. GST fusions with all COMMD proteins were expressed in 293 cells and precipitated from cell lysates by glutathione-Sepharose beads, and the presence in the precipitates of endogenous RelA, c-Rel, RelB, NF-κB1/p105, and NF-κB/p100 was determined by immunoblotting.

ciate with all five subunits and was the only COMMD able to precipitate c-Rel, whereasCOMMD2 also associated broadly with NF-κB subunits but interacted more strongly with RelB-containing complexes.

COMMD1-NF-κB Interactions Can Be Mapped to Distinct Domains—The ability of various regions of COMMD1 to sustain an interaction with endogenous RelA was evaluated next. In these experiments GST fusions of various domains of COMMD1, as depicted in Fig. 3*B*, were used for co-precipitation experiments. Unlike COMMD1-COMMD interactions that seem to require only the COMM domain (Fig. 3, *C* and *D*), COMMD1-RelA interactions are only detectable with full-length COMMD1 (Fig. 6*A*). Therefore, the interaction between COMMD1 and RelA relies on the presence of elements other than the COMM domain.

Next, the interaction between COMMD1 and RelA was evaluated further by determining the domains in RelA that are required for this interaction (Fig. 6*B*). Different domains of RelA in fusion with GST were expressed in 293 cells and

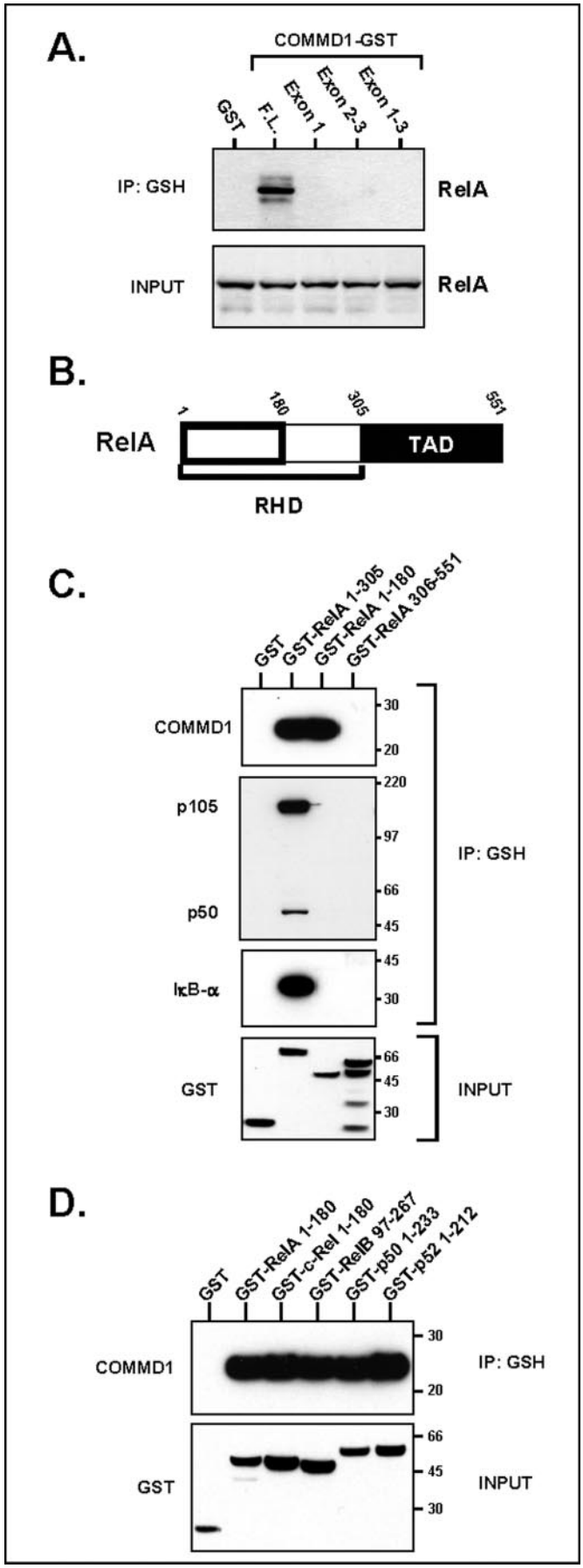

FIG. 6. *A*, domains involved in the interaction between COMMD1 and RelA. Deletion constructs of COMMD1 in fusion with GST corresponding to the boundaries described in Fig. 3*B* were utilized for co-precipitation experiments. The presence of endogenous RelA in the precipitate was determined by immunoblotting. *B*, shown is a schematic depicting the boundaries of the RHD and transactivation domain (*TAD*) of RelA. *C*, the ability of COMMD1 to bind to different regions of RelA was evaluated. Different domains of RelA were expressed in fusion with GST in 293 cells. These fusion proteins were precipitated from cell lysates by glutathione-Sepharose beads, and the presence of COMMD1, p50/p105, and IκB-α was determined by immunoblotting. Input levels for COMMD1, p50, p105, and IκB-α were identical in all samples (data not shown). *D*, regions derived from other NF-κB subunits that are homologous to RelA-(1–180) were expressed in fusion with GST and precipitated from cell lysates with glutathione-Sepharose beads. The presence of COMMD1 in the precipitate was determined by immunoblotting. Input levels for COMMD1 were identical in all samples (data not shown). *IP*, immunopreipitate.

precipitated with glutathione-Sepharose beads; the presence of COMMD1, p50 or its precursor p105, and IκB-α in the precipitates was determined by immunoblotting. As shown in Fig. 6*C*, the RHD of RelA was sufficient for binding to COMMD1, p50 or p105, and IκB-α. The carboxyl-terminal 246 amino acids of RelA (306–551), which correspond to the transactivation domain of the molecule (TAD), did not bind any of these molecules. Within the RHD, the first 180 amino acids comprise the DNA binding domain, whereas the remainder of the RHD (181–305) contains residues involved in IκB binding and dimerization with other subunits and the nuclear localization signal. Interestingly, the first 180 amino acids of RelA were capable of binding COMMD1 but not p50/p105 or IκB-α, probably because of the absence of the dimerization sequences. Reciprocal experiments, in which precipitation of COMMD1-GST was performed to determine its ability to bind to different domains of RelA, also supported these results (data not shown).

The RHD is highly conserved in all five NF-κB subunits (34). Therefore, the possibility that COMMD1 could also bind to similar sequences present in the RHD of other NF-κB subunits was similarly evaluated. Sequences contained in c-Rel-(1–180), RelB-(97–267), p50-(1–233), and p52-(1–212) were found to be homologous to RelA-(1–180) by aligning all five subunits using the ClustalV algorithm (data not shown). Each one of these regions in fusion with GST was expressed in 293 cells and precipitated from cell lysates with glutathione-Sepharose beads, and the presence of COMMD1 was determined by immunoblotting. As shown in Fig. 6*D*, these homologous regions, present in the RHD of all five NF-κB subunits, were capable of binding to COMMD1.

COMMD1 Does Not Affect Nuclear Translocation of NF-κB—In most cells NF-κB is ordinarily localized in the cytoplasm through interactions with members of the IκB family, which results in masking of the nuclear localization signal and cytoplasmic sequestration of the complex (11). Because the translocation of NF-κB from the cytosol to the nucleus is a well characterized regulatory step in the activation of κB-dependent transcription, the ability of COMMD1 to affect this process was investigated.

First, cellular localization of a fusion protein between RelA and EGFP was assessed by fluorescence microscopy before and after TNF treatment. TNF stimulation resulted in nuclear translocation of EGFP-RelA, a process that was inhibited in cells cotransfected with a superdominant form of IκB-α (Fig. 7, *A* and *B*). In contrast, the distribution of EGFP-RelA was unchanged by COMMD1 transfection, suggesting that unlike IκB-α, COMMD1 does not suppress the nuclear translocation of the NF-κB complex.

The translocation of NF-κB complexes into the nucleus and their DNA binding capacity was also evaluated by EMSA. Cells transfected with a control vector and subsequently treated with TNF demonstrated increased κB binding activity in nuclear extracts (Fig. 7*C*). As a control, this induction was blocked by

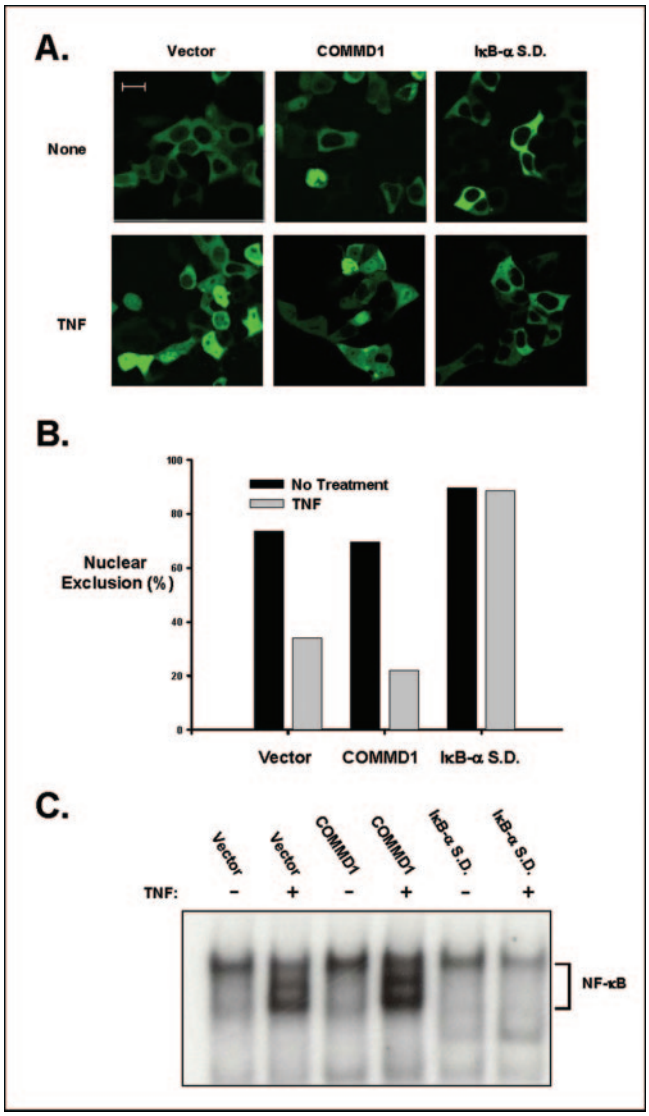

FIG. 7. *A*, COMMD1 does not prevent nuclear translocation of NF-κB. 293 cells were plated in cover glass-chambered slides and transfected with a vector encoding for RelA in fusion with EGFP and with COMMD1, IκB-αS.D. or a vector control (pEBB). Twenty-four hours after transfection cells were treated with TNF for 1 h. Representative images are shown (magnification bar corresponds to 18 μm). *B*, quantification of nuclear translocation. 293 cells were plated 6-well dishes, transfected as described in *A* and treated with TNF for 1 h. Before and after treatment, 250–400 cells in each group were counted under the microscope and rated for the presence or absence of appreciable nuclear signal from RelA, the absence of which was recorded as nuclear exclusion. The data are presented as a percentage of the total number of cells counted in each group. *C*, nuclear translocation was also evaluated by EMSA. 293 cells plated in 10-cm plates were transfected with the constructs indicated in the figure. TNF stimulation was performed 30 min before extraction of nuclear proteins, which were used for EMSA.

transfection of superdominant IκB-α. However, COMMD1 transfection had no appreciable effects on the induction of κB binding activity in nuclear extracts after TNF treatment. In addition, whereas RNAi of COMMD1 led to transcriptional activation of NF-κB, this did not lead to induction of κB binding by EMSA (data not shown).

COMMD1 Binds to κB-responsive Promoter Regions and Affects NF-κB Binding to Chromatin—Although COMMD proteins can interact with the NF-κB complex, the ability of COMMD1 to inhibit transcriptional activation is independent of the nuclear translocation of NF-κB. This suggested that the activity of NF-κB complexes in the nucleus was compromised by COMMD1. To investigate this possibility, the presence of nuclear

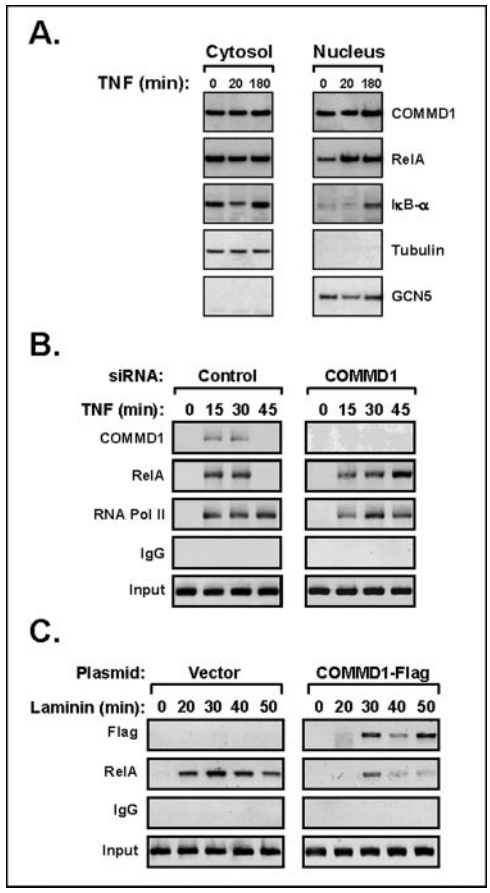

FIG. 8. *A*, presence of a nuclear pool of COMMD1. Cell lysates were fractionated to obtain nuclear and cytosolic fractions during timed stimulation with TNF. These fractions were used for immunoblotting to determine the cellular localization of endogenous COMMD1. As a control for the of TNF stimulation, the effects on RelA and IκB-α levels were also determined by immunoblotting. Tubulin and GCN5 served as cytosolic and nuclear markers, respectively. *B* and *C*, COMMD1 inhibits its chromatin occupancy by NF-κB. ChIP analysis on the *cIAP-2* promoter after TNF stimulation was performed on DU145 cells transfected with siRNA oligonucleotides to COMMD1 or GFP (control). (*B*). ChIP analysis was performed on the *cIAP-2* gene using 293 cells expressing either Flag-tagged COMMD1 or empty vector control. Cell adhesion to a laminin-coated plate was used as the NF-κB activating stimulus. *Pol*, polymerase.

COMMD1 was first established. Subcellular fractions were prepared from 293 cells during timed stimulation with TNF (including an early and late time point). As shown in Fig. 8*A*, COMMD1 was present in both nuclear and cytosolic fractions, and its quantity seemed slightly increased in the late time point (180 min). As expected, TNF stimulation also resulted in nuclear translocation of RelA and early degradation of IκB-α with late accumulation of this protein in the nuclear fraction. The purity of the fractions was determined by immunoblotting for tubulin (cytosolic marker) and GCN5 (nuclear marker).

Based on the above findings, the effects of COMMD1 on NF-κB nuclear function were investigated by examining the recruitment of RelA to chromatin. Utilizing ChIP, the effects of COMMD1 levels on the recruitment of RelA to the κB-responsive *c-IAP2* promoter were determined. The effects of stimulation with TNF were compared after transfection of control and COMMD1 siRNA oligonucleotides (Fig. 8*B*). Decreases in endogenous COMMD1 levels resulted in prolongation of the occupancy time of RelA on the *c-IAP2* promoter. In addition, COMMD1 itself was found to be recruited to this κB-responsive site after TNF stimulation. A complementary set of experiments was also performed to determine if increases in

COMMD1 protein levels would have the converse effect on RelA recruitment to chromatin. In this case, cell adhesion to laminin was used as the stimulus for NF-κB activation, as this results in robust and sustained recruitment of RelA to the *c-IAP2* promoter site. As shown in Fig. 8*C*, overexpression of COMMD1 resulted in a marked decrease in the duration of RelA association with chromatin after NF-κB activation; again, COMMD1 recruitment to chromatin in response to stimulation was also detected.

Taken together, these data indicate that COMMD1 affects the half-life of the RelA-chromatin complex that is recruited in response to NF-κB-activating stimuli. Because COMMD1 itself is recruited to chromatin and remains associated even after NF-κB has been displaced, this suggests that COMMD1 either alone or through the recruitment of other factors can affect the affinity of NF-κB for chromatin.

DISCUSSION

In this report we describe the identification of a novel and conserved family of homologs of MURR1. These factors are defined by the presence of a unique carboxyl-terminal motif termed the COMM domain. The existence of this protein family and any insights into the cellular functions of these factors were largely unknown up to this point.

We show here that all COMMD proteins can interact with MURR1/COMMD1. Interestingly, whereas all 10 factors are expressed in 293 cells, only COMMD3, -4, and -6 were identified as COMMD1-associated factors in our TAP screen, suggesting that certain associations might be preferentially present in cells. In addition, other COMMD-COMMD complexes that do not include COMMD1 are likely to occur, and indeed, our search of the *Drosophila* protein interaction map recently published (35) predicts an interaction between *Drosophila* COMMD2 and COMMD3. Therefore, once antibodies to all 10 proteins are available, the composition of physiologic COMMD-COMMD complexes would be able to be identified. We also show that interactions between COMMD proteins are mediated by the COMM domain.

Several COMMD proteins are functionally similar to the prototype member of the family, MURR1/COMMD1, and bind to and suppress NF-κB. We studied in further detail the binding mechanism by which COMMD1 interacts with RelA and demonstrate that this is distinct from dimerization to other NF-κB subunits or binding to IκB-α (Fig. 6*C*), indicating that these two events are not required for the interaction of COMMD1 with NF-κB. This is similarly supported by the observation that COMMDs can also associate with RelB (Fig. 5*B*), an NF-κB subunit that does not associate with IκB-α (36). These findings suggest that the prior identification of an association between IκB-α and COMMD1 that requires the ankyrin repeats of IκB-α could be potentially explained as a tertiary complex, since the ankyrin repeats are required for IκB-α binding to the NF-κB subunits (16).

Unlike the association between COMMD1 and itself or COMMD3, COMMD1-RelA interactions are not supported by the COMM domain alone (Figs. 3, *C* and *D*, and 6*A*), indicating that the association of COMMDs to NF-κB complexes is likely mediated by a mechanism distinct from COMMD-COMMD interaction. Similarly, the pattern of COMMD association to NF-κB could not be simply explained by COMMD multimer formation. Despite the demonstrated interaction between COMMD1 and COMMD3, only COMMD1 could precipitate RelA. In addition, COMMD9 could readily precipitate RelB, whereas COMMD6 did not despite the stronger COMMD6-COMMD1 interaction (Figs. 3*A* and 5*B*).

NF-κB-mediated transcription is largely controlled by the cytoplasmic sequestration of NF-κB complexes through the binding to ankyrin repeat-containing inhibitory molecules such as the IκBs (11, 37). Activation of the IκB kinase complex in response to a variety of extracellular signals initiates a cascade of events leading to IκB degradation and nuclear translocation on NF-κB. Whereas a role for MURR1/COMMD1 in the regulation of IκB-α degradation has been demonstrated (16), our findings here suggest that this effect is not sufficient to explain its ability to inhibit NF-κB-mediated transcription, since nuclear translocation of NF-κB subunits is unaffected by COMMD1. Rather, we find that COMMD1 can regulate the nuclear function of NF-κB through its recruitment to κB-responsive promoters where it affects the duration of RelA binding to chromatin.

Once activated, NF-κB can mediate expression of multiple gene targets. However, the observed responses are often specific to the cell type and stimulus in question. For example, NF-κB has been reported to be able to activate transcription of both pro- and anti-apoptotic factors in various settings (5, 6). The regulation of NF-κB solely by IκB-mediated sequestration of the complex is unlikely to account for these differences in gene expression. In this regard, post-translational modifications of NF-κB (38) and preferential promoter binding by different subunits have been shown to participate in the regulation of certain promoters in response to specific stimuli (36, 39). However, additional layers of regulation that could account for the tissue- and promoter-specific nature of the response are likely at play. The identification here of the COMMD family reveals an additional regulatory level that might be important in this regard. The conservation of all 10 *COMMD* genes through vertebrate evolution and the differential pattern of association to NF-κB complexes suggest that despite their similarities, COMMD proteins probably serve unique and non-redundant functions. A thorough understanding of the mode of action of these factors in different cell types may help to account for the precision and selectivity by which expression of the multitude of NF-κB-responsive genes can be orchestrated in response to a diverse range of stimuli.

Unlike other nuclear regulators of NF-κB such as histone acetylases and deacetylases, the COMMDs themselves possess no apparent intrinsic enzymatic activity. The transcriptional inhibitory functions of the COMMDs must in turn be regulated in response to certain stimuli, possibly by post-translational modifications. XIAP, a stress responsive pro-survival factor (40), can ubiquitinate COMMD1, resulting in its degradation (19), suggesting that the regulation of COMMD proteins might be integrated into cellular stress responses that are known to activate NF-κB.

Acknowledgments—We are grateful to B. Balliu for valuable technical assistance. We thank Dr. Neil Perkins for insightful suggestions and for generously providing several expression plasmids used in our studies. We are also indebted to Dr. Ranier de Martin who provided us with EGFP-p65.

REFERENCES

1. Ghosh, S., May, M. J., and Kopp, E. B. (1998) *Annu. Rev. Immunol.* **16,** 225–260
2. Silverman, N., and Maniatis, T. (2001) *Genes Dev.* **15,** 2321–2342
3. Karin, M., Yamamoto, Y., and Wang, Q. M. (2004) *Nat. Rev. Drug Discov.* **3,** 17–26
4. Joyce, D., Albanese, C., Steer, J., Fu, M., Bouzahzah, B., and Pestell, R. G. (2001) *Cytokine Growth Factor Rev.* **12,** 73–90
5. Karin, M., and Lin, A. (2002) *Nat. Immunol.* **3,** 221–227
6. Baldwin, A. S. (2001) *J. Clin. Investig.* **107,** 241–246
7. Perkins, N. D., Edwards, N. L., Duckett, C. S., Agranoff, A. B., Schmid, R. M., and Nabel, G. J. (1993) *EMBO J.* **12,** 3551–3558
8. Alcami, J., Lain de Lera, T., Folgueira, L., Pedraza, M. A., Jacque, J. M., Bachelerie, F., Noriega, A. R., Hay, R. T., Harrich, D., and Gaynor, R. B. (1995) *EMBO J.* **14,** 1552–1560
9. Nabel, G. J., and Baltimore, D. (1987) *Nature* **326,** 711–713
10. Bohnlein, E., Lowenthal, J. W., Siekevitz, M., Ballard, D. W., Franza, B. R., and Greene, W. C. (1988) *Cell* **53,** 827–836
11. Baldwin, A. S. (1996) *Annu. Rev. Immunol.* **14,** 649–681

12. Chen, Z., Hagler, J., Palombella, V. J., Melandri, F., Scherer, D., Ballard, D., and Maniatis, T. (1995) *Genes Dev.* **9,** 1586–1597
13. Greene, W. C. (2004) *Nat. Immunol.* **5,** 18–19
14. van De Sluis, B., Rothuizen, J., Pearson, P. L., van Oost, B. A., and Wijmenga, C. (2002) *Hum. Mol. Genet.* **11,** 165–173
15. Tao, T. Y., Liu, F., Klomp, L., Wijmenga, C., and Gitlin, J. D. (2003) *J. Biol. Chem.* **278,** 41593–41596
16. Ganesh, L., Burstein, E., Guha-Niyogi, A., Louder, M. K., Mascola, J. R., Klomp, L. W., Wijmenga, C., Duckett, C. S., and Nabel, G. J. (2003) *Nature* **426,** 853–857
17. Duckett, C. S., Li, F., Wang, Y., Tomaselli, K. J., Thompson, C. B., and Armstrong, R. C. (1998) *Mol. Cell. Biol.* **18,** 608–615
18. Richter, B. W. M., Mir, S. S., Eiben, L. J., Lewis, J., Reffey, S. B., Frattini, A., Tian, L., Frank, S., Youle, R. J., Nelson, D. L., Notarangelo, L. D., Vezzoni, P., Fearnhead, H. O., and Duckett, C. S. (2001) *Mol. Cell. Biol.* **21,** 4292–4301
19. Burstein, E., Ganesh, L., Dick, R. D., van De Sluis, B., Wilkinson, J. C., Lewis, J., Klomp, L. W. J., Wijmenga, C., Brewer, G. J., Nabel, G. J., and Duckett, C. S. (2004) *EMBO J.* **23,** 244–254
20. Duckett, C. S., Gedrich, R. W., Gilfillan, M. C., and Thompson, C. B. (1997) *Mol. Cell. Biol.* **17,** 1535–1542
21. Schmid, J. A., Birbach, A., Hofer-Warbinek, R., Pengg, M., Burner, U., Furtmuller, P. G., Binder, B. R., and de Martin, R. (2000) *J. Biol. Chem.* **275,** 17035–17042
22. Mir, S. S., Richter, B. W. M., and Duckett, C. S. (2000) *Blood* **15,** 4307–4312
23. Puig, O., Caspary, F., Rigaut, G., Rutz, B., Bouveret, E., Bragado-Nilsson, E., Wilm, M., and Seraphin, B. (2001) *Methods* **24,** 218–229
24. Duckett, C. S., Perkins, N. D., Kowalik, T. F., Schmid, R. M., Huang, E. S., Baldwin, A. S., Jr., and Nabel, G. J. (1993) *Mol. Cell. Biol.* **13,** 1315–1322
25. Birkey Reffey, S., Wurthner, J. U., Parks, W. T., Roberts, A. B., and Duckett, C. S. (2001) *J. Biol. Chem.* **276,** 26542–26549
26. Su, A. I., Wiltshire, T., Batalov, S., Lapp, H., Ching, K. A., Block, D., Zhang, J., Soden, R., Hayakawa, M., Kreiman, G., Cooke, M. P., Walker, J. R., and Hogenesch, J. B. (2004) *Proc. Natl. Acad. Sci. U. S. A.* **101,** 6062–6067
27. Hoberg, J. E., Yeung, F., and Mayo, M. W. (2004) *Mol. Cell* **16,** 245–255
28. Yeung, F., Hoberg, J. E., Ramsey, C. S., Keller, M. D., Jones, D. R., Frye, R. A., and Mayo, M. W. (2004) *EMBO J.* **23,** 2369–2380
29. Nabetani, A., Hatada, I., Morisaki, H., Oshimura, M., and Mukai, T. (1997) *Mol. Cell. Biol.* **17,** 789–798
30. Solban, N., Jia, H. P., Richard, S., Tremblay, S., Devlin, A. M., Peng, J., Gossard, F., Guo, D. F., Morel, G., Hamet, P., Lewanczuk, R., and Tremblay, J. (2000) *J. Biol. Chem.* **275,** 32234–32243
31. Semenova, E., Wang, X., Jablonski, M. M., Levorse, J., and Tilghman, S. M. (2003) *Hum. Mol. Genet.* **12,** 1301–1312
32. Haupt, Y., Barri, G., and Adams, J. M. (1992) *Mol. Biol. Rep.* **17,** 17–20
33. Roperch, J. P., Lethrone, F., Prieur, S., Piouffre, L., Israeli, D., Tuynder, M., Nemani, M., Pasturaud, P., Gendron, M. C., Dausset, J., Oren, M., Amson, R. B., and Telerman, A. (1999) *Proc. Natl. Acad. Sci. U. S. A.* **96,** 8070–8073
34. Chen, F. E., Huang, D. B., Chen, Y. Q., and Ghosh, G. (1998) *Nature* **391,** 410–413
35. Giot, L., Bader, J. S., Brouwer, C., Chaudhuri, A., Kuang, B., Li, Y., Hao, Y. L., Ooi, C. E., Godwin, B., Vitols, E., Vijayadamodar, G., Pochart, P., Machineni, H., Welsh, M., Kong, Y., Zerhusen, B., Malcolm, R., Varrone, Z., Collis, A., Minto, M., Burgess, S., McDaniel, L., Stimpson, E., Spriggs, F., Williams, J., Neurath, K., Ioime, N., Agee, M., Voss, E., Furtak, K., Renzulli, R., Aanensen, N., Carrolla, S., Bickelhaupt, E., Lazovatsky, Y., DaSilva, A., Zhong, J., Stanyon, C. A., Finley, R. L., Jr., White, K. P., Braverman, M., Jarvie, T., Gold, S., Leach, M., Knight, J., Shimkets, R. A., McKenna, M. P., Chant, J., and Rothberg, J. M. (2003) *Science* **302,** 1727–1736
36. Saccani, S., Pantano, S., and Natoli, G. (2003) *Mol. Cell* **11,** 1563–1574
37. Henkel, T., Machleidt, T., Alkalay, I., Krönke, M., Ben-Neriah, Y., and Baeuerle, P. A. (1993) *Nature* **365,** 182–185
38. Vermeulen, L., De Wilde, G., Notebaert, S., Vanden Berghe, W., and Haegeman, G. (2002) *Biochem. Pharmacol.* **64,** 963–970
39. Bonizzi, G., Bebien, M., Otero, D. C., Johnson-Vroom, K. E., Cao, Y., Vu, D., Jegga, A. G., Aronow, B. J., Ghosh, G., Rickert, R. C., and Karin, M. (2004) *EMBO J.* **23,** 4202–4210
40. Holcik, M., and Korneluk, R. G. (2001) *Nat. Rev. Mol. Cell Biol.* **2,** 550–556

Reawakening the cellular death program in neoplasia through the therapeutic blockade of IAP function

Casey W. Wright[1] and Colin S. Duckett[1,2]

[1]Department of Pathology, and [2]Department of Internal Medicine, University of Michigan, Ann Arbor, Michigan, USA.

Recent studies have shown that members of the inhibitor of apoptosis (IAP) protein family are highly expressed in several classes of cancer. The primary implication of these findings is that the elevated expression of IAPs is not coincidental but actually participates in oncogenesis by helping to allow the malignant cell to avoid apoptotic cell death. This concept, together with the discovery of several IAP-regulatory proteins that use a conserved mode of action, has stimulated a major effort by many research groups to devise IAP-targeting strategies as a means of developing novel antineoplastic drugs. In this Review, we consider the evidence both for and against the IAPs being valid therapeutic targets, and we describe the types of strategies being used to neutralize their functions.

IAPs: structure and function

Inhibitor of apoptosis (*iap*) genes were first described in insect viruses through a genetic screen to identify compensatory replacements for the loss of the baculoviral antiapoptotic p35 protein, which functions to block baculovirus-induced apoptosis during infection (1–3). Since the initial identification in baculoviruses, *iap* homologs have been identified across phyla from *Caenorhabditis elegans* and yeast to insects and mammals. As many as 8 human *iap* gene products have been identified (reviewed in ref. 4), XIAP (hILP/MIHA/BIRC4), hILP-2 (TS-IAP), cellular IAP1 (c-IAP1/HIAP2/MIHB/BIRC2), cellular IAP2 (c-IAP2/HIAP1/MIHC/BIRC3), melanoma-associated IAP (ML-IAP/Livin/KIAP1/BIRC7), neuronal apoptosis–inhibitory protein (NAIP/BIRC1), survivin (TIAP1/BIRC5), and Apollon (BRUCE/BIRC6) (Figure 1A). These IAP proteins have been shown to play, for the most part, nonredundant cellular roles that range from apoptotic inhibition to the formation of the mitotic spindle during cytokinesis. For this reason, the term "IAP" is somewhat misleading, and these factors are often referred to as BIR-containing proteins, or BIRPs (5), a term derived from the presence of what has become the defining motif of this family, an approximately 65-residue domain rich in histidines and cysteines known as the baculovirus *iap* repeat (BIR). BIRPs contain 1–3 imperfectly repeated BIRs (Figure 1). Most of the IAP family members also harbor a RING domain at the carboxy terminus. The RING functions as an E3 ubiquitin ligase, which is preceded by ubiquitin-activating enzymes (E1) and ubiquitin-conjugating enzymes (E2) in the cascade of protein ubiquitination (6–9). E3 ubiquitin ligases provide specificity for the transfer of ubiquitin moieties onto the target protein. Therefore, IAP-mediated protein ubiquitination has a pivotal role in the regulation of apoptosis, allowing the IAP to control stability of itself and other proteins (10).

Survivin is a small (17 kDa) protein composed of a single BIR motif and is similar in structure to the IAPs/BIRPs of yeasts and nematodes (11). Targeted deletion of the murine *survivin* gene revealed a critical role for this protein in the cell cycle through regulation of the spindle formation during mitosis (12, 13), a role that is similar to that found in yeasts and the nematode *C. elegans* (14, 15). Additionally, a number of reports have also implicated survivin in apoptotic inhibition, although the details of this role are not entirely clear (16). Nevertheless, *survivin* is highly expressed in dividing cells and cancer-derived cell lines and has become a valid target for anticancer drugs, including those that use antisense approaches.

In addition to survivin, much attention has been focused on XIAP, in large part because its antiapoptotic properties have been best demonstrated (17). XIAP is a ubiquitously expressed 56-kDa protein that contains 3 BIRs, as well as a RING domain at the carboxy terminus that has been shown to exhibit E3 ubiquitin ligase activity (9, 18). A number of reviews have examined the clinical utility of survivin in more detail (19); therefore, this Review will focus on XIAP.

Ectopic expression of XIAP has been shown to confer protection from a wide range of apoptotic stimuli, and this protection is presumed to be largely mediated by the ability of XIAP to directly bind and enzymatically inhibit key components of the apoptotic machinery, the caspases (20, 21). This group of cysteine proteases with a specificity for aspartate residues (reviewed in this issue of the *JCI*, ref. 22) play essential roles in apoptotic cell death. They are initially produced as inactive zymogens, which are typically activated in a hierarchical sequence in which initiator caspases, such as caspase-8, are activated following, for example, engagement of a death receptor signal. Processed initiator caspases subsequently activate, through cleavage, downstream or effector caspases, such as caspase-3, which then disassemble the cell through the orchestrated proteolysis of essential cellular proteins. XIAP has been shown to directly bind and inhibit caspase-3, caspase-7, and caspase-9, which are important mediators of the apoptotic program (20, 23). c-IAP1 and c-IAP2 can also block caspase activity; however, they inhibit caspases 100- to 1,000-fold less efficiently than XIAP (24).

IAPs in cancer

Many studies have revealed a circumstantial association of IAPs and neoplasia (25). For example, XIAP levels are elevated in many

Nonstandard abbreviations used: ASO, antisense oligonucleotide; BIR, baculovirus *iap* repeat; BIRP, BIR-containing protein; c-IAP, cellular IAP; Hid, head involution defective; IAP, inhibitor of apoptosis; IBM, IAP-binding motif; ML-IAP, melanoma-associated IAP; Rpr, reaper; Smac/DIABLO, second mitochondria-derived activator of caspase/direct IAP-binding protein with low pI; TRAIL, TNF-related apoptosis-inducing ligand.

Conflict of interest: The authors have declared that no conflict of interest exists.

Citation for this article: *J. Clin. Invest.* **115**:2673–2678 (2005). doi:10.1172/JCI26251.

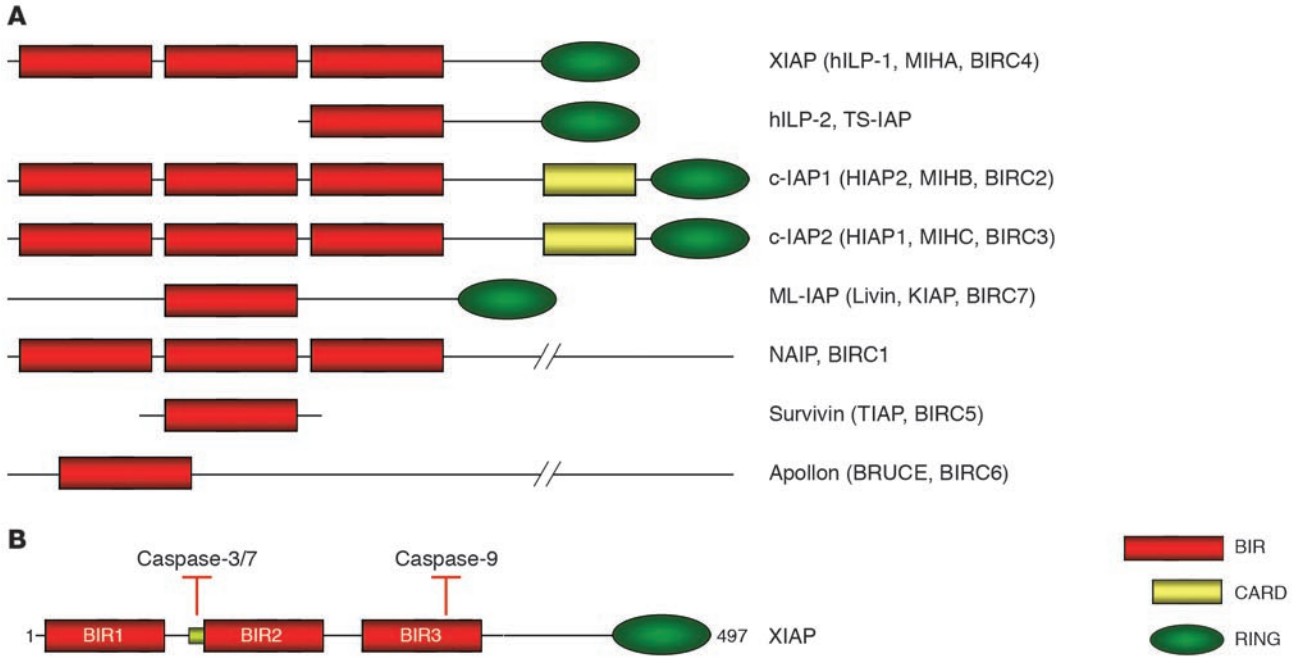

Figure 1
The IAP family members. (**A**) All IAP members contain 1 or more imperfect baculovirus *iap* repeats (BIRs), the defining motif of the IAP family. Many of the IAP proteins also posses an E3 ubiquitin ligase RING domain at the carboxy terminus. (**B**) XIAP can bind and enzymatically inhibit caspase-3, caspase-7, and caspase-9. XIAP binds caspase-3 and caspase-7 at a sequence directly upstream of BIR2, while it binds caspase-9 in a region of BIR3. CARD, caspase recruitment domain.

cancer cell lines, and several reports have shown that suppression of XIAP protein levels can sensitize cancer cells to chemotherapeutic drugs (26–29). IAP proteins appear to regulate the transcriptional activator NF-κB family, which itself has been associated with malignancy (30–32). NF-κB activation in turn upregulates expression of c-IAP2, providing a positive feedback loop for cell survival that may be important in the development of some cancers (32). Also, the presence of increased levels of c-IAP2 protein is correlated with carcinogenesis and chemotherapeutic resistance in malignant pleural mesothelioma, a tumor that attacks the pleura of the lung (33). Survivin expression is normally limited to cells of the developing fetus and is not expressed in differentiated adult tissue (11). However, aberrant expression of *survivin* has been detected in a number of different cancers and lymphomas (11), and expression of a dominant-negative form of *survivin* induced apoptosis in cancer but not normal cell lines (27). Furthermore, ML-IAP was identified as an IAP that is highly expressed in the majority of melanoma cell lines tested, but undetectable in primary melanocytes (34).

Although heightened expression of IAPs has been reported in and may contribute to the progression of many cancers, it is important to caution that many of these results are correlative in nature. For example, to our knowledge, no solid evidence has been reported to show that XIAP is itself an oncogene, or specifically that mutations, translocations, or amplifications at the XIAP locus have ever been found in natural tumors. This is true for all of the IAP/BIRP family, with the single exception of c-IAP2, which has been found to be translocated in mucosal-associated lymphoid tissue (MALT) lymphoma, where a RING-deleted form of c-IAP2 is fused to the MALT1 protein (35, 36). Furthermore, while elevated expression of IAPs has been reported in many cancers, it has also been shown that IAP levels are not always correlated with disease progression or prognosis (37–39). However, this does not invalidate the targeting of, for example, XIAP, for therapeutic intervention, but it does emphasize that the relevance of XIAP as an anticancer target should be scrutinized more rigorously than that of a typical oncogene. It is quite possible that future studies will identify alterations in IAPs as a major causative genetic lesion in specific malignancies, and indeed a recent study reported the presence of the closely linked c-IAP1 and c-IAP2 genes in an amplicon associated with esophageal squamous cell carcinoma (40). Nevertheless, the current model of targeting IAPs, particularly XIAP, relies exclusively on expression differences between malignant and normal cells and presumes that tumor cells have selected for enhanced expression levels in the absence of apparent genetic alterations at the XIAP locus.

Two pathways of caspase activation regulated by the IAP proteins

Two major apoptotic signaling cascades have been described and are generally referred to as the extrinsic (or receptor-mediated) and intrinsic (or mitochondrial) pathways (41) (Figure 2). The extrinsic pathway transduces an intracellular signal into an apoptotic response and is exemplified by proapoptotic members of the TNF receptor superfamily, such as the TNF-related apoptosis-inducing ligand (TRAIL) receptor and the Fas receptor. Ligand-mediated activation of these receptors results in the binding of adaptor molecules that subsequently recruit and promote the activation of procaspase-8 (42–44). In this scheme, activated caspase-8 is thought to function as an initiator caspase, leading to the subsequent cleavage and activation of effector caspases, such as caspase-3, and thus leading to cell death (Figure 2).

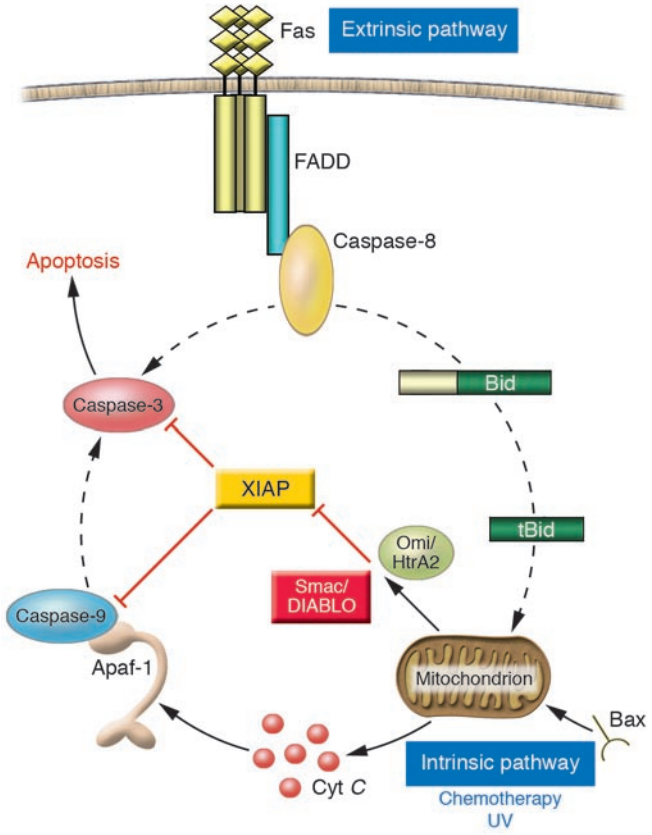

Figure 2
XIAP in apoptosis regulation. Following an apoptotic stimulus, enzymes known as caspases are activated and initiate a cascade leading to the destruction of the cell. The caspases are activated via 2 main avenues, by the stimulation of death receptors (the extrinsic pathway) and by the release of apoptogenic factors from the mitochondria (the intrinsic pathway). XIAP regulates both the extrinsic and the intrinsic apoptotic pathways through direct inhibition of caspase-3 and caspase-9.

The intrinsic pathway is activated by a range of apoptotic stimuli, including DNA damage, treatment of cells with chemotherapeutic agents, and growth factor withdrawal. The mitochondria serve as the control point for this pathway (45). A pivotal step in this process is the release of cytochrome *c* from the mitochondria into the cytosol (46). The Bcl-2 family of proteins very carefully regulates this release.

Once released into the cytosol, cytochrome *c* binds directly to a key cellular component of the apoptotic cascade, apoptotic protease–activating factor-1 (Apaf-1), which subsequently oligomerizes to form a high–molecular weight structure designated the apoptosome (47). This complex is able to recruit and activate caspase-9, which is the key initiator caspase in the intrinsic pathway. Apoptosome-activated caspase-9 is subsequently able to act on downstream effector caspases, such as caspase-3 and caspase-7, to generate the apoptotic signal (Figure 2).

Signaling crosstalk exists between the intrinsic and extrinsic cell death pathways. For example, the proapoptotic Bcl-2–related protein Bid can be cleaved by caspase-8 to produce an active form, known as tBid, which can subsequently translocate to mitochondria and lead to the induction of the intrinsic pathway (48, 49). Thus, in certain situations, the intrinsic pathway is required for the full induction of receptor-mediated apoptosis and is thought to exert these effects through an amplification loop.

Numerous studies of XIAP have revealed its ability to directly bind to caspase-3, caspase-7, and caspase-9 (50). Consequently, in the scheme of apoptosis shown in Figure 2, XIAP can function directly at the most downstream effector caspase (caspase-3 or caspase-7) in the extrinsic pathway and can block cell death at 2 distinct points (caspase-9 and caspase-3) in the intrinsic pathway. Indeed, biochemical studies have shown that XIAP can be found in the apoptosome (51), presumably in complex with caspase-9, and a number of elegant structural studies have revealed the presence of 2 distinct domains of XIAP that interact with caspase-3 and caspase-7, and with caspase-9 (52). The caspase-3/caspase-7–binding domain is located directly aminoterminal to the second BIR within XIAP, while the caspase-9–binding domain is contained within the third (most carboxyterminal) BIR (Figure 1B).

IAP antagonists

After the realization that XIAP can directly bind caspases, the crucial discovery that enforced the concept that XIAP is an attractive therapeutic target came from studies that identified endogenous regulators of its activity. The first, and best, characterized of these is second mitochondria-derived activator of caspase/direct IAP-binding protein with low pI (Smac/DIABLO), a nuclear-encoded protein that in healthy cells is localized to the mitochondria in a mature form lacking the aminoterminal 55 residues, which are removed during mitochondrial translocation (53, 54). Smac/DIABLO is a functional homolog of 3 proapoptotic factors in *Drosophila*, namely *reaper* (*rpr*), *head involution defective* (*hid*), and *grim* (55, 56). The main functional motif of these IAP antagonists is at the extreme amino terminus of Rpr, Hid, and Grim, and the mature form of Smac/DIABLO. Thus, this sequence has been termed the Rpr/Hid/Grim (RHG) motif, or IAP-binding motif (IBM) as a more general term (57). With kinetics that appear to be identical to those of cytochrome *c*, Smac/DIABLO is released from the mitochondria into the cytosol, where it can bind XIAP. Importantly, Smac/DIABLO has been shown to bind precisely into the same 2 grooves within XIAP that can be occupied by caspase-3 and -7 or caspase-9 (Figure 3), and this leads to an attractive model in which Smac/DIABLO can act as a proapoptotic molecule that functions through the displacement of XIAP from caspases (23).

Subsequent studies in mammalian cells have revealed the existence of additional molecules that target IAPs in a manner akin to that of Smac/DIABLO. Specifically, 2 factors have been described, designated Omi/HtrA2 (58–62) and GSPT1/eRF3 (63), that share with Smac/DIABLO the properties of mitochondrial localization and cytoplasmic release, as well as the presence of an IBM at the amino terminus of the mature protein. Beyond the tetrapeptide sequence, however, there is virtually no similarity between these proteins, and at least in the case of Omi/HtrA2, which appears to function as a chaperone and a regulator of oxidative stress (64), the primary physiological role appears to be very distinct from caspase/XIAP regulation.

Mimetics of IAP antagonists in cancer treatment

The development of small molecules that mimic Smac/DIABLO and therefore interfere with caspase-9 binding to XIAP is proving to be a promising avenue for the treatment of cancer (25, 65).

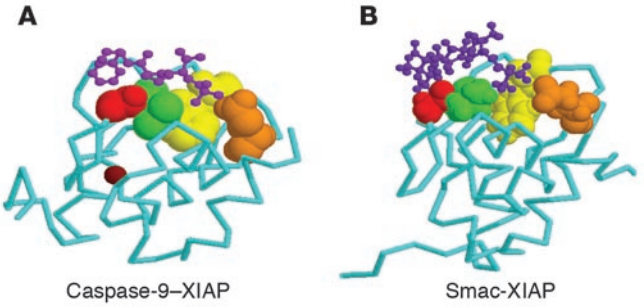

Figure 3
Smac/DIABLO displaces caspase-9 from BIR3 of XIAP. (**A**) Crystal structure of processed caspase-9 bound to BIR3 of XIAP. The purple peptide represents the first 4 amino acids that contact XIAP, with the amino terminus near the orange residue of XIAP. Coordinates were obtained from Brookhaven Protein Databank file 1NW9 (82). (**B**) NMR structure of the Smac/DIABLO IBM (purple peptide with the amino terminus near the orange residue of XIAP) bound to the same groove on BIR3 of XIAP that binds caspase-9, thus abrogating the ability of XIAP to block caspase-9 activity. Coordinates were obtained from Brookhaven Protein Databank file 1G3F (83). The 4 residues displayed in van der Waals radii spacefill on XIAP BIR3 are Gly306 (red), Leu307 (green), Trp310 (yellow), and Glu314 (orange). These 4 residues are critical in forming the Smac/DIABLO–binding groove on XIAP BIR3 (84). Images were created using Protein Explorer (85, 86).

Furthermore, since the extrinsic and intrinsic pathways are both regulated by XIAP at the step of caspase-3 activation, small molecules that interfere with this interaction are also being tested. Smac/DIABLO IBM peptides, when used in conjunction with TRAIL, proved to promote apoptosis in cancer cells through caspase-9 and resulted in complete tumor regression in a murine intracranial malignant glioma xenograft model (27, 66, 67). However, the use of peptides in therapy is not feasible, because of the proteolytic instability and low cellular permeability of the peptide. Thus, variations on the first 4 residues of Smac/DIABLO have been synthesized to make it a more stable moiety (68–70). These alterations have provided reagents with higher affinity for XIAP than Smac/DIABLO, and lower concentrations of the compounds were required for activity. One of these molecules bound to and antagonized c-IAP1 and c-IAP2, in addition to XIAP, and sensitized HeLa cells to TNF-induced apoptosis (71). This finding suggests that c-IAP1 and c-IAP2 are downstream of NF-κB activity and function to inhibit caspase-8 activation, allowing prosurvival signals to proceed. Thus Smac/DIABLO mimetics could also provide therapy for inflammation disorders that arise from increased TNF stimulation.

Continual efforts to increase the efficacy of Smac/DIABLO peptide agonists have led other groups to devise small-molecule nonpeptidic compounds that target BIR2 of XIAP, liberating caspase-3 (72, 73). There may be an advantage to pharmacological agents that antagonize XIAP to release caspase-3, since this caspase is at the convergence of both the extrinsic and the intrinsic pathway. The use of these compounds resulted in apoptosis in cancer cells without the requirement for concomitant chemotherapeutic treatment. Furthermore, targeting the release of caspase-3 would eliminate the requirement for mitochondria-mediated activation, which is blocked in many cancers by the deregulation of the Bcl-2 pathway (72).

IAP antisense technology in cancer treatment

Another approach to blocking IAP activity in order to promote caspase activation in cancer cells is to downregulate protein levels by delivering IAP antisense into the cell. Downregulation of XIAP protein levels by adenovirus-mediated introduction of antisense induced apoptosis in chemoresistant ovarian cancer cells (26). Furthermore, a similar antisense approach against c-IAP2 showed c-IAP2 to be a major contributor of chemotherapeutic resistance in pleural mesothelioma (33).

More recently, antisense oligonucleotides (ASOs) have been used in studies to reduce IAP protein levels. ASO technology uses approximately 20-bp oligonucleotide sequences targeted to the mRNA of the protein of interest; this interferes with expression of the transcript. Reduction of XIAP protein levels in bladder cancer using XIAP ASOs was reported to induce apoptosis and contribute to doxorubicin cytotoxicity (28). Combining ASOs targeted against XIAP and survivin with radiotherapy delayed tumor growth in a mouse lung cancer model and decreased the survival of H460 lung cancer cells (74).

In contrast, a recent study in which ASO technology was used to suppress XIAP levels in cells over time determined that not all chemotherapeutic drugs are effective in combination with decreased XIAP protein levels; this knowledge will prove beneficial in the development of treatment schemes for patients in clinical trials (29). A survivin ASO (ISIS 23722; Isis Pharmaceuticals Inc.) is in preclinical development, and ASOs that target XIAP are in phase I clinical trials (29).

Other functions of IAPs

It is widely assumed that the primary physiological role of XIAP is as an apoptotic suppressor, and XIAP is often referred to as the only known endogenous caspase inhibitor in mammals. The biochemical evidence for this is compelling, and the caspase-suppressing effects are so striking (with inhibitory constants in the nanomolar range) that the argument has been made that the XIAP-caspase interaction cannot be accidental. It is, however, worth bearing in mind that the biological evidence for XIAP being an essential endogenous inhibitor lags behind the in vitro data. For example, *Xiap*-deficient mice exhibit no overt apoptotic abnormalities that might be expected (75), although a sensitivity of sympathetic neurons following cytochrome *c* injection has been reported (76). This is not to say that *Xiap*-null mice are indistinguishable from control animals: recent reports have revealed alterations in intracellular copper levels (77), and in mammary gland development (78), but these phenotypic differences are unlikely to be caused by alterations in apoptotic sensitivity. The prevailing view is that *Xiap*-deficient mice survive through a degenerate mechanism, such as compensatory expression of other *Iap* family members, particularly of c-IAP1, which has been reported in embryonic fibroblasts derived from these animals (75). However, the caspase-inhibitory properties of the c-IAP proteins are much weaker than those of XIAP; this indicates nonredundant roles for these proteins. Other studies from several laboratories have implicated XIAP in a number of cellular functions unrelated to caspases, such as the activation of signal transduction cascades including JNK, NF-κB, TGF-β, and Akt (30, 31, 79, 80). To date, however, these studies have all relied on ectopic expression of XIAP, and to our knowledge no studies have been described to suggest alterations in these signaling pathways in Xiap-null animals. Thus, the evidence supporting a physiological role for XIAP as a signal transduction intermediate is no stronger than that suggest-

ing a function in apoptotic regulation. Recently, our laboratory has linked XIAP to copper homeostasis (77), through an interaction with MURR1, a mammalian factor whose gene was identified by positional cloning in an inbred canine strain affected by a non-Wilsonian inherited copper toxicosis disorder (81). MURR1 was found to be a target of ubiquitination by the RING-mediated E3 ubiquitin ligase activity of XIAP, and, consistent with a model in which XIAP can function to regulate MURR1 and copper, tissues from *Xiap*-null mice were found to contain at the same time higher levels of Murr1 and lower levels of intracellular copper, compared with control animals (77). Thus, clearly much work remains to elucidate the true physiological functions of XIAP. The concept that XIAP participates in oncogenesis and is an anticancer target remains valid if XIAP's participation is due not to caspase inhibition, but to an alternative regulatory function in, for example, intracellular signaling or copper metabolism. The possibility that XIAP is exerting noncaspase-regulatory properties may, however, affect the experimental approaches that need be taken to develop therapeutically effective antagonists of XIAP function.

Conclusions

The multifunctional IAP proteins are involved in apoptosis regulation, cell signaling, and cell division. Substantial progress has been made in identifying the IAP proteins as factors in cancer development, progression, and desensitization to a wide array of chemotherapeutic drugs. This knowledge should lead to pharmacological agents that antagonize or downregulate IAP proteins for the treatment of cancer in patients. However, because of the multifunctional nature of the IAP proteins, the consequences of affecting other nonapoptotic processes in the cell need to be considered in the design of preclinical agents for use in clinical trials. Nevertheless, the use of either Smac/DIABLO mimetics or IAP ASOs has resulted in tumor regression in mouse cancer models. Furthermore, ASO technology targeted against other apoptotic regulatory proteins besides IAP proteins has already proven to be a viable avenue of cancer treatment, making the promise of anticancer therapy by targeting of IAP proteins a reality.

Acknowledgments

We would like to express our gratitude to the Duckett laboratory for helpful discussions, and in particular to John Wilkinson for critical reading of the manuscript. We apologize to those researchers whose work we could not cite because of space constraints. This work was supported in part by NIH grant T32 HL07517 to C.W. Wright and by the University of Michigan Biological Scholars Program, Department of Defense Idea Award PC040215, and NIH grant GM067827 to C.S. Duckett.

Address correspondence to: Colin S. Duckett, Medical Science I, Room 5315, 1301 Catherine Street, Ann Arbor, Michigan 48109-0602, USA. Phone: (734) 615-6414; Fax: (734) 615-7012; E-mail: colind@umich.edu.

1. Crook, N.E., Clem, R.J., and Miller, L.K. 1993. An apoptosis-inhibiting baculovirus gene with a zinc finger-like motif. *J. Virol.* **67**:2168–2174.
2. Birnbaum, M.J., Clem, R.J., and Miller, L.K. 1994. An apoptosis-inhibiting gene from a nuclear polyhedrosis virus encoding a polypeptide with Cys/His sequence motifs. *J. Virol.* **68**:2521–2528.
3. Clem, R.J., Fechheimer, M., and Miller, L.K. 1991. Prevention of apoptosis by a baculovirus gene during infection of insect cells. *Science.* **254**:1388–1390.
4. Salvesen, G.S., and Duckett, C.S. 2002. IAP proteins: blocking the road to death's door [review]. *Nat. Rev. Mol. Cell Biol.* **3**:401–410.
5. Uren, A.G., Coulson, E.J., and Vaux, D.L. 1998. Conservation of baculovirus inhibitor of apoptosis repeat proteins (BIRPs) in viruses, nematodes, vertebrates and yeasts. *Trends Biochem. Sci.* **23**:159–162.
6. Huang, H.-K., et al. 2000. The inhibitor of apoptosis, cIAP2, functions as a ubiquitin-protein ligase and promotes in vitro monoubiquitination of caspases 3 and 7. *J. Biol. Chem.* **275**:26661–26664.
7. Olson, M.R., et al. 2003. A GH3-like domain in reaper is required for mitochondrial localization and induction of IAP degradation. *J. Biol. Chem.* **278**:44758–44768.
8. Suzuki, Y., Nakabayashi, Y., and Takahashi, R. 2001. Ubiquitin-protein ligase activity of X-linked inhibitor of apoptosis protein promotes proteasomal degradation of caspase-3 and enhances its anti-apoptotic effect in Fas-induced cell death. *Proc. Natl. Acad. Sci. U. S. A.* **98**:8662–8667.
9. Yang, Y., Fang, S., Jensen, J.P., Weissman, A.M., and Ashwell, J.D. 2000. Ubiquitin protein ligase activity of IAPs and their degradation in proteasomes in response to apoptotic stimuli. *Science.* **288**:874–877.
10. Jesenberger, V., and Jentsch, S. 2002. Deadly encounter: ubiquitin meets apoptosis. *Nat. Rev. Mol. Cell Biol.* **3**:112–121.
11. Ambrosini, G., Adida, C., and Altieri, D.C. 1997. A novel anti-apoptosis gene, *survivin*, expressed in cancer and lymphoma. *Nat. Med.* **3**:917–921.
12. Uren, A.G., et al. 2000. Survivin and the inner centromere protein INCENP show similar cell-cycle localization and gene knockout phenotype. *Curr. Biol.* **10**:1319–1328.
13. Okada, H., et al. 2004. Survivin loss in thymocytes triggers p53-mediated growth arrest and p53-independent cell death. *J. Exp. Med.* **199**:399–410.
14. Uren, A.G., et al. 1999. Role for yeast inhibitor of apoptosis (IAP)-like proteins in cell division. *Proc. Natl. Acad. Sci. U. S. A.* **96**:10170–10175.
15. Fraser, A.G., James, C., Evan, G.I., and Hengartner, M.O. 1999. Caenorhabditis elegans inhibitor of apoptosis protein (IAP) homologue BIR-1 plays a conserved role in cytokinesis. *Curr. Biol.* **9**:292–301.
16. Altieri, D.C. 2003. Survivin, versatile modulation of cell division and apoptosis in cancer. *Oncogene.* **22**:8581–8589.
17. Holcik, M., Gibson, H., and Korneluk, R.G. 2001. XIAP: apoptotic brake and promising therapeutic target. *Apoptosis.* **6**:253–261.
18. Li, X., Yang, Y., and Ashwell, J.D. 2002. TNF-RII and c-IAP1 mediate ubiquitination and degradation of TRAF2. *Nature.* **416**:345–347.
19. Altieri, D.C. 2004. Molecular circuits of apoptosis regulation and cell division control: the survivin paradigm. *J. Cell. Biochem.* **92**:656–663.
20. Deveraux, Q.L., Takahashi, R., Salvesen, G.S., and Reed, J.C. 1997. X-linked IAP is a direct inhibitor of cell-death proteases. *Nature.* **388**:300–304.
21. Shi, Y. 2004. Caspase activation, inhibition, and reactivation: a mechanistic view. *Protein Sci.* **13**:1979–1987.
22. Lavrik, I.N., Golks, A., and Krammer, P.H. 2005. Caspases: pharmacological manipulation of cell death. *J. Clin. Invest.* **115**:2665–2672. doi:10.1172/JCI26252.
23. Shiozaki, E.N., and Shi, Y. 2004. Caspases, IAPs and Smac/DIABLO: mechanisms from structural biology. *Trends Biochem. Sci.* **29**:486–494.
24. Roy, N., Deveraux, Q.L., Takahashi, R., Salvesen, G.S., and Reed, J.C. 1997. The c-IAP-1 and c-IAP-2 proteins are direct inhibitors of specific caspases. *EMBO J.* **16**:6914–6925.
25. Schimmer, A.D. 2004. Inhibitor of apoptosis proteins: translating basic knowledge into clinical practice. *Cancer Res.* **64**:7183–7190.
26. Sasaki, H., Sheng, Y., Kotsuji, F., and Tsang, B.K. 2000. Down-regulation of X-linked inhibitor of apoptosis protein induces apoptosis in chemoresistant human ovarian cancer cells. *Cancer Res.* **60**:5659–5666.
27. Yang, L., Cao, Z., Yan, H., and Wood, W.C. 2003. Coexistence of high levels of apoptotic signaling and inhibitor of apoptosis proteins in human tumor cells: implication for cancer specific therapy. *Cancer Res.* **63**:6815–6824.
28. Bilim, V., Kasahara, T., Hara, N., Takahashi, K., and Tomita, Y. 2003. Role of XIAP in the malignant phenotype of transitional cell cancer (TCC) and therapeutic activity of XIAP antisense oligonucleotides against multidrug-resistant TCC in vitro. *Int. J. Cancer.* **103**:29–37.
29. McManus, D.C., et al. 2004. Loss of XIAP protein expression by RNAi and antisense approaches sensitizes cancer cells to functionally diverse chemotherapeutics. *Oncogene.* **23**:8105–8117.
30. Hofer-Warbinek, R., et al. 2000. Activation of NF-κB by XIAP, the X chromosome-linked inhibitor of apoptosis, in endothelial cells involves TAK1. *J. Biol. Chem.* **275**:22064–22068.
31. Birkey Reffey, S., Wurthner, J.U., Parks, W.T., Roberts, A.B., and Duckett, C.S. 2001. X-linked inhibitor of apoptosis protein functions as a cofactor in transforming growth factor-β signaling. *J. Biol. Chem.* **276**:26542–26549.
32. Chu, Z.-L., et al. 1997. Suppression of tumor necrosis factor-induced cell death by inhibitor of apoptosis c-IAP2 is under NF-κB control. *Proc. Natl. Acad. Sci. U. S. A.* **94**:10057–10062.
33. Gordon, G.J., et al. 2002. Inhibitor of apoptosis protein-1 promotes tumor cell survival in mesothelioma. *Carcinogenesis.* **23**:1017–1024.
34. Vucic, D., Stennicke, H.R., Pisabarro, M.T., Salvesen, G.S., and Dixit, V.M. 2000. ML-IAP, a novel inhibitor of apoptosis that is preferentially expressed in human melanomas. *Curr. Biol.* **10**:1359–1366.

35. Dierlamm, J., et al. 1999. The apoptosis inhibitor gene *API2* and a novel 18q gene, *MLT*, are recurrently rearranged in the t(11;18)(q21;q21) associated with mucosa-associated lymphoid tissue lymphomas. *Blood.* **93**:3601–3609.
36. Uren, A.G., et al. 2000. Identification of paracaspases and metacaspases: two ancient families of caspase-like proteins, one of which plays a key role in MALT lymphoma. *Mol. Cell.* **6**:961–967.
37. Tamm, I., et al. 2000. Expression and prognostic significance of IAP-family genes in human cancers and myeloid leukemias. *Clin. Cancer Res.* **6**:1796–1803.
38. Ferreira, C.G., et al. 2001. Expression of X-linked inhibitor of apoptosis as a novel prognostic marker in radically resected non-small cell lung cancer patients. *Clin. Cancer Res.* **7**:2468–2474.
39. Carter, B.Z., et al. 2003. Caspase-independent cell death in AML: caspase inhibition in vitro with pancaspase inhibitors or in vivo by XIAP or Survivin does not affect cell survival or prognosis. *Blood.* **102**:4179–4186.
40. Imoto, I., et al. 2001. Identification of *cIAP1* as a candidate target gene within an amplicon at 11q22 in esophageal squamous cell carcinomas. *Cancer Res.* **61**:6629–6634.
41. Budihardjo, I., Oliver, H., Lutter, M., Luo, X., and Wang, X. 1999. Biochemical pathways of caspase activation during apoptosis. *Annu. Rev. Cell Dev. Biol.* **15**:269–290.
42. Hsu, H., Shu, H.-B., Pan, M.-G., and Goeddel, D.V. 1996. TRADD-TRAF2 and TRADD-FADD interactions define two distinct TNF receptor 1 signal transduction pathways. *Cell.* **84**:299–308.
43. Kischkel, F.C., et al. 1995. Cytotoxicity-dependent APO-1 (Fas/CD95)-associated proteins form a death-inducing signaling complex (DISC) with the receptor. *EMBO J.* **14**:5579–5588.
44. Boldin, M.P., Goncharov, T.M., Goltsev, Y.V., and Wallach, D. 1996. Involvement of MACH, a novel MORT1/FADD-interacting protease, in Fas/APO-1- and TNF receptor-induced death. *Cell.* **85**:803–815.
45. Desagher, S., and Martinou, J.C. 2000. Mitochondria as the central control point of apoptosis. *Trends Cell Biol.* **10**:369–377.
46. Li, P., et al. 1997. Cytochrome *c* and dATP-dependent formation of Apaf-1/caspase-9 complex initiates an apoptotic protease cascade. *Cell.* **91**:479–489.
47. Zou, H., Henzel, W.J., Liu, X., Lutschg, A., and Wang, X. 1997. Apaf-1, a human protein homologous to *C. elegans* CED-4, participates in cytochrome *c*-dependent activation of caspase-3. *Cell.* **90**:405–413.
48. Luo, X., Budihardjo, I., Zou, H., Slaughter, C., and Wang, X. 1998. Bid, a Bcl2 interacting protein, mediates cytochrome *c* release from mitochondria in response to activation of cell surface death receptors. *Cell.* **94**:481–490.
49. Li, H., Zhu, H., Xu, C.J., and Yuan, J. 1998. Cleavage of BID by caspase 8 mediates the mitochondrial damage in the Fas pathway of apoptosis. *Cell.* **94**:491–501.
50. Salvesen, G.S., and Abrams, J.M. 2004. Caspase activation: stepping on the gas or releasing the brakes? Lessons from humans and flies [review]. *Oncogene.* **23**:2774–2784.
51. Bratton, S.B., Lewis, J., Butterworth, M., Duckett, C.S., and Cohen, G.M. 2002. XIAP inhibition of caspase-3 preserves its association with the Apaf-1 apoptosome and prevents CD95- and Bax-induced apoptosis. *Cell Death Differ.* **9**:881–892.
52. Stennicke, H.R., Ryan, C.A., and Salvesen, G.S. 2002. Reprieval from execution: the molecular basis of caspase inhibition. *Trends Biochem. Sci.* **27**:94–101.
53. Verhagen, A.M., et al. 2000. Identification of DIABLO, a mammalian protein that promotes apoptosis by binding to and antagonizing IAP proteins. *Cell.* **102**:43–53.
54. Du, C., Fang, M., Li, Y., Li, L., and Wang, X. 2000. Smac, a mitochondrial protein that promotes cytochrome c-dependent caspase activation by eliminating IAP inhibition. *Cell.* **102**:33–42.
55. Wu, J.W., Cocina, A.E., Chai, J., Hay, B.A., and Shi, Y. 2001. Structural analysis of a functional DIAP1 fragment bound to grim and hid peptides. *Mol. Cell.* **8**:95–104.
56. Wright, C.W., and Clem, R.J. 2001. Sequence requirements for hid binding and apoptosis regulation in the anti-apoptotic baculovirus protein Op-IAP: hid binds Op-IAP in a manner similar to Smac binding of XIAP. *J. Biol. Chem.* **277**:2454–2462.
57. Shi, Y. 2002. A conserved tetrapeptide motif: potentiating apoptosis through IAP-binding. *Cell Death Differ.* **9**:93–95.
58. Hegde, R., et al. 2001. Identification of Omi/HtrA2 as a mitochondrial apoptotic serine protease that disrupts IAP-caspase interaction. *J. Biol. Chem.* **277**:432–438.
59. Martins, L.M., et al. 2001. The serine protease Omi/HtrA2 regulates apoptosis by binding XIAP through a Reaper-like motif. *J. Biol. Chem.* **277**:439–444.
60. Suzuki, Y., et al. 2001. A serine protease, HtrA2, is released from the mitochondria and interacts with XIAP, inducing cell death. *Mol. Cell.* **8**:613–621.
61. van Loo, G., et al. 2002. The serine protease Omi/HtrA2 is released from mitochondria during apoptosis. Omi interacts with caspase-inhibitor XIAP and induces enhanced caspase activity. *Cell Death Differ.* **9**:20–26.
62. Vaux, D.L., and Silke, J. 2003. Mammalian mitochondrial IAP binding proteins. *Biochem. Biophys. Res. Commun.* **304**:499–504.
63. Hegde, R., et al. 2003. The polypeptide chain-releasing factor GSPT1/eRF3 is proteolytically processed into an IAP-binding protein. *J. Biol. Chem.* **278**:38699–38706.
64. Martins, L.M., et al. 2004. Neuroprotective role of the reaper-related serine protease HtrA2/Omi revealed by targeted deletion in mice. *Mol. Cell. Biol.* **24**:9848–9862.
65. Huang, Y., Lu, M., and Wu, H. 2004. Antagonizing XIAP-mediated caspase-3 inhibition. Achilles' heel of cancers? [review]. *Cancer Cell.* **5**:1–2.
66. Fulda, S., Wick, W., Weller, M., and Debatin, K.M. 2002. Smac agonists sensitize for Apo2L/TRAIL- or anticancer drug-induced apoptosis and induce regression of malignant glioma in vivo. *Nat. Med.* **8**:808–815.
67. Arnt, C.R., Chiorean, M.V., Heldebrant, M.P., Gores, G.J., and Kaufmann, S.H. 2002. Synthetic Smac/DIABLO peptides enhance the effects of chemotherapeutic agents by binding XIAP and cIAP1 in situ. *J. Biol. Chem.* **277**:44236–44243.
68. Li, C.J., Friedman, D.J., Wang, C., Metelev, V., and Pardee, A.B. 1995. Induction of apoptosis in uninfected lymphocytes by HIV-1 Tat protein. *Science.* **268**:429–431.
69. Sun, H., et al. 2004. Structure-based design, synthesis, and evaluation of conformationally constrained mimetics of the second mitochondria-derived activator of caspase that target the X-linked inhibitor of apoptosis protein/caspase-9 interaction site. *J. Med. Chem.* **47**:4147–4150.
70. Oost, T.K., et al. 2004. Discovery of potent antagonists of the antiapoptotic protein XIAP for the treatment of cancer. *J. Med. Chem.* **47**:4417–4426.
71. Li, L., et al. 2004. A small molecule Smac mimic potentiates TRAIL- and TNFalpha-mediated cell death. *Science.* **305**:1471–1474.
72. Wu, T.Y., Wagner, K.W., Bursulaya, B., Schultz, P.G., and Deveraux, Q.L. 2003. Development and characterization of nonpeptidic small molecule inhibitors of the XIAP/caspase-3 interaction. *Chem. Biol.* **10**:759–767.
73. Schimmer, A.D., et al. 2004. Small-molecule antagonists of apoptosis suppressor XIAP exhibit broad antitumor activity. *Cancer Cell.* **5**:25–35.
74. Cao, C., Mu, Y., Hallahan, D.E., and Lu, B. 2004. XIAP and survivin as therapeutic targets for radiation sensitization in preclinical models of lung cancer. *Oncogene.* **23**:7047–7052.
75. Harlin, H., Reffey, S.B., Duckett, C.S., Lindsten, T., and Thompson, C.B. 2001. Characterization of XIAP-deficient mice. *Mol. Cell. Biol.* **21**:3604–3608.
76. Potts, P.R., Singh, S., Knezek, M., Thompson, C.B., and Deshmukh, M. 2003. Critical function of endogenous XIAP in regulating caspase activation during sympathetic neuronal apoptosis. *J. Cell Biol.* **163**:789–799.
77. Burstein, E., et al. 2004. A novel role for XIAP in copper homeostasis through regulation of MURR1. *EMBO J.* **23**:244–254.
78. Olayioye, M.A., et al. 2005. XIAP-deficiency leads to delayed lobuloalveolar development in the mammary gland. *Cell Death Differ.* **12**:87–90.
79. Sanna, M.G., Duckett, C.S., Richter, B.W.M., Thompson, C.B., and Ulevitch, R.J. 1998. Selective activation of JNK1 is necessary for the anti-apoptotic activity of hILP. *Proc. Natl. Acad. Sci. U. S. A.* **95**:6015–6020.
80. Asselin, E., Mills, G.B., and Tsang, B.K. 2001. XIAP regulates Akt activity and caspase-3-dependent cleavage during cisplatin-induced apoptosis in human ovarian epithelial cancer cells. *Cancer Res.* **61**:1862–1868.
81. van De Sluis, B., Rothuizen, J., Pearson, P.L., van Oost, B.A., and Wijmenga, C. 2002. Identification of a new copper metabolism gene by positional cloning in a purebred dog population. *Hum. Mol. Genet.* **11**:165–173.
82. Shiozaki, E.N., et al. 2003. Mechanism of XIAP-mediated inhibition of caspase-9. *Mol. Cell.* **11**:519–527.
83. Liu, Z., et al. 2000. Structural basis for binding of Smac/DIABLO to the XIAP BIR3 domain. *Nature.* **408**:1004–1008.
84. Wu, G., et al. 2000. Structural basis of IAP recognition by Smac/DIABLO. *Nature.* **408**:1008–1012.
85. Martz, E. 2002. Protein explorer: easy yet powerful macromolecular visualization. *Trends Biochem. Sci.* **27**:107–109.
86. Protein Explorer. http://proteinexplorer.org.

Molecular Cell *21*, 775–785, March 17, 2006 ©2006 Elsevier Inc. DOI 10.1016/j.molcel.2006.01.033

XIAP Is a Copper Binding Protein Deregulated in Wilson's Disease and Other Copper Toxicosis Disorders

Arjmand R. Mufti,[1,2,8] Ezra Burstein,[2,5,8] Rebecca A. Csomos,[1] Paul C.F. Graf,[4] John C. Wilkinson,[1] Robert D. Dick,[3] Madhavi Challa,[6] Jae-Kyoung Son,[7] Shawn B. Bratton,[6,7] Grace L. Su,[2,4] George J. Brewer,[2,3] Ursula Jakob,[4] and Colin S. Duckett[1,2,*]

[1] Department of Pathology
[2] Department of Internal Medicine
[3] Department of Human Genetics
[4] Department of Molecular, Cellular and Developmental Biology
University of Michigan Medical School
Ann Arbor, Michigan 48109
[5] Gastroenterology Section
The Ann Arbor VA Medical Center
Ann Arbor, Michigan 48105
[6] Division of Pharmacology and Toxicology
College of Pharmacology
[7] Institute for Cellular and Molecular Biology
University of Texas at Austin
Austin, Texas 78712

Summary

X-linked inhibitor of apoptosis (XIAP), known primarily for its caspase inhibitory properties, has recently been shown to interact with and regulate the levels of COMMD1, a protein associated with a form of canine copper toxicosis. Here, we describe a role for XIAP in copper metabolism. We find that XIAP levels are greatly reduced by intracellular copper accumulation in Wilson's disease and other copper toxicosis disorders and in cells cultured under high copper conditions. Elevated copper levels result in a profound, reversible conformational change in XIAP due to the direct binding of copper to XIAP, which accelerates its degradation and significantly decreases its ability to inhibit caspase-3. This results in a lowering of the apoptotic threshold, sensitizing the cell to apoptosis. These data provide an unsuspected link between copper homeostasis and the regulation of cell death through XIAP and may contribute to the pathophysiology of copper toxicosis disorders.

Introduction

Copper, an essential trace metal, is a catalytic cofactor for enzymes that play critical roles in a number of biological processes, including oxidative phosphorylation (e.g., cytochrome c oxidase) (Hamza and Gitlin, 2002) and oxidative stress protection (e.g., superoxide dismutase) (Torres et al., 2001). As copper is potentially toxic to cells, an intricate mechanism for handling intracellular copper ions has evolved, and free copper in the cell is almost undetectable (Rae et al., 1999).

*Correspondence: colind@umich.edu
[8] These authors contributed equally to this work.

Mutations in genes involved in copper homeostasis are responsible for disorders of copper metabolism in humans (Mercer, 2001). The best-described human copper toxicosis disorder, Wilson's disease (Llanos and Mercer, 2002), results from mutations in *ATP7B*, a gene encoding a P type ATPase. It is characterized by the pathologic accumulation of copper in the liver and brain (Brewer, 2000; Gitlin, 2003). A number of similar syndromes that are not due to mutations in *ATP7B* are collectively referred to as non-Wilsonian copper toxicosis. Recently, a mutation in the previously undescribed gene *COMMD1* (also known as *MURR1*; [Burstein et al., 2004]) was shown to be responsible for an autosomal recessive form of a non-Wilsonian copper toxicosis disorder affecting Bedlington terriers (Klomp et al., 2003; van De Sluis et al., 2002). COMMD1 has recently been reported to interact with ATP7B (Tao et al., 2003), although the functional role of this interaction remains to be elucidated.

We independently identified COMMD1 as a direct binding partner of the prosurvival protein XIAP (Burstein et al., 2004). XIAP is best known as a conserved metazoan protein (Duckett et al., 1996; Liston et al., 1996; Uren et al., 1996) that can suppress apoptosis by directly binding to and inhibiting the catalytic activity of several caspases (Chai et al., 2001; Deveraux and Reed, 1999; Riedl et al., 2001; Riedl and Shi, 2004; Shiozaki et al., 2003). Additionally, it has also been shown that XIAP regulates cellular levels of COMMD1 by functioning as an E3 ubiquitin ligase for this protein and promoting its proteasomal degradation (Burstein et al., 2004; Vaux and Silke, 2005; Yang et al., 2000). Consistent with this, changes in XIAP expression result in alterations of intracellular copper levels, and *Xiap*-deficient mice have copper deficiency in conjunction with increased COMMD1 levels (Burstein et al., 2004).

The identification of a role for XIAP in copper homeostasis prompted us to investigate the effects of copper on XIAP expression and function. In the course of these studies, we found that in situations associated with elevated copper, XIAP protein levels are greatly reduced and, when detectable, exhibit an altered electrophoretic mobility, which we show is indicative of a major conformational change in its structure. These alterations in XIAP levels and conformation are independent of COMMD1, because they are detected not only in affected Bedlington terriers but also in other canine and murine copper toxicosis diseases, as well as in biopsy material from patients affected with Wilson's disease. We report that the altered electrophoretic mobility of XIAP is due to a reversible conformational change in the protein induced by direct binding of copper to cysteine residues within the BIR and RING domains of XIAP. The copper bound form of XIAP in cells is significantly less stable than native XIAP and is greatly impaired in its ability to inhibit caspase-3, and cells expressing it are more susceptible to apoptosis. These findings suggest a model in which changes in intracellular copper levels can affect the apoptotic threshold by determining the level and activity of XIAP and provide an additional

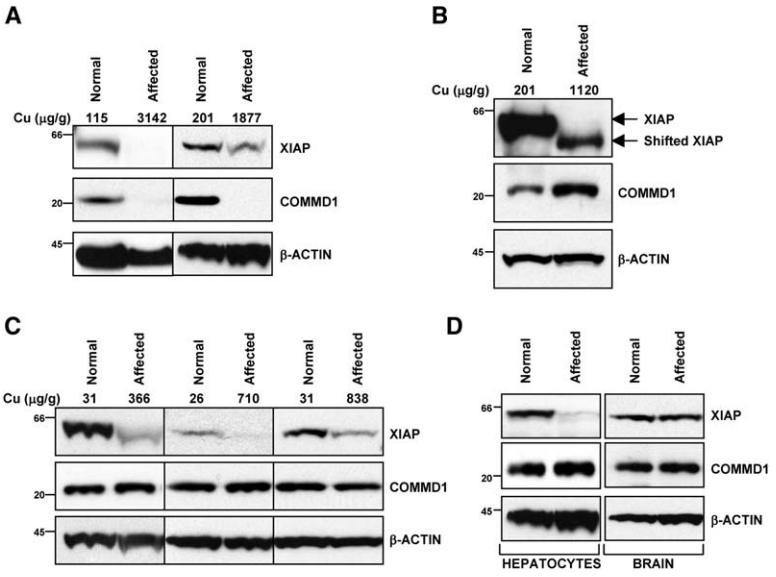

Figure 1. Altered Expression of XIAP in Copper Toxicosis Disorders

(A) Immunoblot analysis of liver tissue revealed decreased levels of XIAP in Bedlington terriers with inherited copper toxicosis (affected), compared to control animals (normal).

(B) Altered mobility of XIAP in a cocker spaniel with hepatic copper accumulation due to cholestasis. Hepatic tissues from an unaffected Bedlington terrier and an affected cocker spaniel were lysed and subsequently probed for XIAP, COMMD1, and β-actin.

(C) Decreased hepatic levels of XIAP in patients affected with Wilson's disease. Hepatic tissues from patients with Wilson's disease and normal controls were lysed and subsequently probed for XIAP, COMMD1, and β-actin.

(D) Decreased XIAP levels in hepatocytes, but not in brain tissue, from *Atp7b* mutant mice, the murine model of Wilson's disease. Purified hepatocytes and brain tissue from mutant or control animals were isolated, lysed, and subsequently probed for XIAP, COMMD1, and β-actin.

pathophysiological mechanism for the cellular damage observed in Wilson's disease and other copper toxicosis syndromes.

Results

Impaired Expression and Altered Mobility of XIAP in Disease States Associated with Copper Toxicosis

Genetic studies of Bedlington terriers affected with a hereditary, non-Wilsonian copper toxicosis disorder led to the discovery of the *COMMD1/MURR1* gene (van De Sluis et al., 2002). Because we had previously identified COMMD1 as an XIAP-interacting factor (Burstein et al., 2004), we used immunoblotting to compare the levels of canine XIAP protein in liver tissue samples from Bedlington terriers affected with copper toxicosis and normal control dogs. Interestingly, liver tissue from affected dogs expressed undetectable or greatly reduced XIAP levels compared to controls (Figure 1A). COMMD1 protein was undetectable in affected animals (Figure 1A, middle), confirming that the *COMMD1* locus is indeed targeted in these dogs.

The biopsy data from Bedlington terriers described above suggested that altered expression of XIAP might be due either to the elevated levels of copper in the liver of these animals or to the absence of COMMD1, perhaps through a regulatory feedback process. To discriminate between these two possibilities, we sought to examine pathophysiological situations involving elevations in levels of copper but in which COMMD1 is unaffected. Cholestasis is a condition in which bile excretion from the liver into the digestive tract is blocked, and because bile serves as the main excretory mechanism for copper (Gitlin, 2003), it also results in excessive copper accumulation in the liver. We therefore compared liver tissue from a dog with chronic cholestasis and high hepatic copper levels, but with a wild-type *COMMD1* gene, to a normal, unaffected animal. As shown in Figure 1B, XIAP in the affected animal was not only reduced in level when compared to a normal control but also additionally appeared as a faster-migrating species, under standard reducing and denaturing conditions used for polyacrylamide gel electrophoresis.

The data described above from canine biopsy samples raised the intriguing possibility that XIAP might be affected in human diseases of copper toxicosis. To explore this possibility, pairwise immunoblot analysis was used to compare biopsy samples from patients with Wilson's disease to normal individuals. Similar to the findings from dogs affected with copper toxicosis, liver tissue from patients with Wilson's disease contained lower levels of XIAP protein (Figure 1C), compared to normal, unaffected controls run in parallel. In at least one instance, this reduction was also accompanied by changes in the electrophoretic mobility of the protein (Figure 1C, left), similar to the effects displayed in the canine cholestatic model observed in Figure 1B. Taken together, these data suggested that copper accumulation is associated with reduced XIAP levels, together in some instances with an altered electrophoretic mobility of the protein.

The changes in the mobility and levels of XIAP could result from either direct copper accumulation in the tissue examined or from a generalized alteration of XIAP metabolism secondary to the disease state. To discriminate between these two possibilities, we examined a murine model for Wilson's disease that harbors a spontaneous mutation in the *Atp7b* locus, resulting in the massive accumulation of copper in the liver with only limited changes in brain copper levels (Buiakova et al., 1999; Fuentealba and Aburto, 2003). Similar to the data shown in Figures 1A–1C, hepatocytes from the affected animal contained markedly decreased levels of XIAP, whereas in the same animal, there were no changes in XIAP protein levels in brain tissue (Figure 1D). These findings suggest that the specific effect on XIAP observed in hepatocytes is the direct result of copper accumulation in these cells.

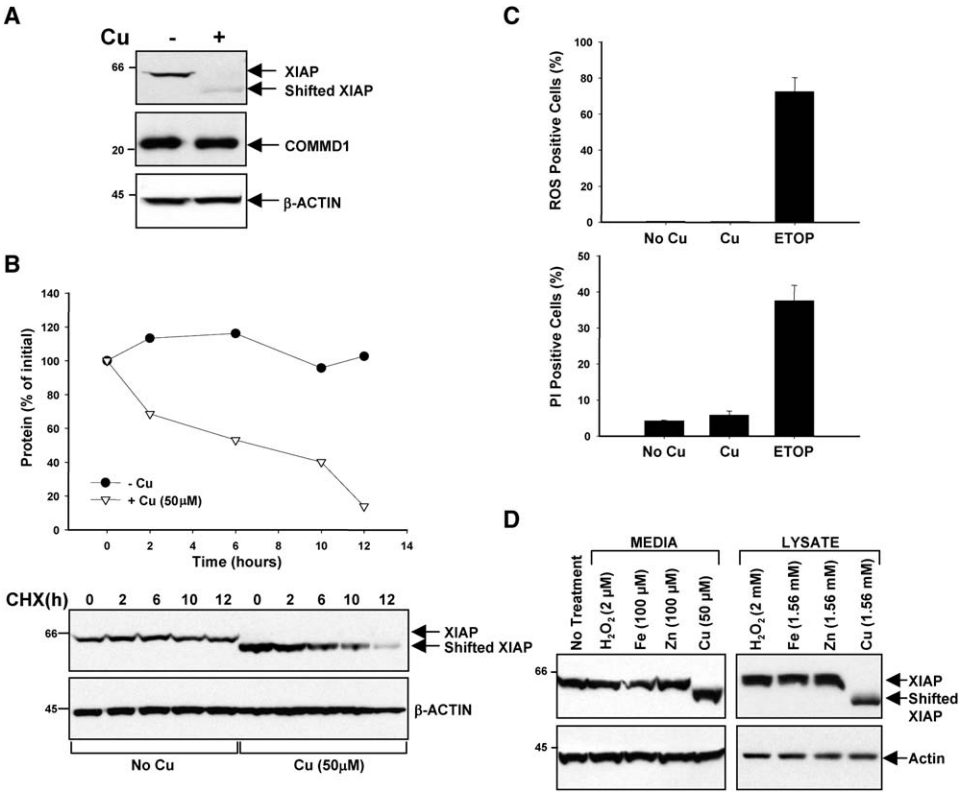

Figure 2. Copper Induces Altered Electrophoretic Mobility and Decreased Half-Life of XIAP

(A) HEK 293 cells were grown in the presence of additional copper sulfate (50 μM). These cells were lysed 48 hr after the addition of copper, and XIAP and β-actin were identified by immunoblotting.

(B) The copper bound form of XIAP has a shorter half-life than native XIAP. HEK 293 cells were grown in the presence or absence of copper sulfate (50 μM) for 48 hr. The cells were then lysed after being incubated with cycloheximide (CHX; 30 μg/ml) as indicated, and XIAP and β-actin were identified by immunoblotting.

(C) The addition of copper sulfate (50 μM) does not result in increased ROS production or cell death. HEK 293 cells were incubated with copper for 48 hr and subsequently probed for the generation of ROS or increased cell death by flow cytometry using CM-H_2DCFDA (1 μM) or propidium iodide, respectively. Etoposide (30 μg/ml) was used as a positive control in both experiments. The error bars represent the standard deviation of three independent samples.

(D) The mobility shift of XIAP is copper specific. HEK 293 cells were grown in the presence of additional copper, iron, zinc, and hydrogen peroxide as indicated. Copper, iron, zinc, and hydrogen peroxide were also added postlysis to untreated HEK 293 cell lysates as indicated. XIAP and β-actin were detected by immunoblotting.

Copper Accumulation Induces Instablility of XIAP Protein

Although the data presented above provided compelling evidence to suggest that XIAP may be altered in expression and mobility in disorders associated with copper toxicosis, these situations do not provide an experimentally tractable system to examine the relationship between XIAP and copper. We therefore tested the possibility that the addition of copper to cells in culture might be able to recapitulate the observations made in animals and patients. As shown in Figure 2A, we could mimic the observations made in biopsy samples by supplementing the media of human embryonic kidney 293 cells with low micromolar concentrations of excess copper, provided in the form of copper sulfate (Figure 2A). Added copper resulted in reduced XIAP levels and also induced a change in the electrophoretic mobility of XIAP resembling those observed in several of the biopsy samples examined in Figure 1. These results were reproduced by using copper chloride as an alternative source of supplemental copper, and similar results were also observed in HepG2 cells and CaCo2 cells (data not shown). The induction of the change in the electrophoretic mobility of XIAP was observed to be time dependent, appearing 24 hr after the addition of copper to culture medium (Figure S1A available in the Supplemental Data with this article online).

To assess whether the reduction in XIAP levels observed reflects changes in XIAP stability in the presence of copper, time decay experiments were performed. HEK 293 cells were cultured in growth media alone or supplemented with copper in order to induce the mobility shift of XIAP, and cycloheximide (CHX) was added to the media to block de novo protein synthesis. XIAP levels were examined by immunoblotting and densitometry after the addition of CHX (Figure 2B). Over a 12 hr period, the levels of XIAP in the control samples were essentially unchanged, indicating a half-life of XIAP significantly greater than 12 hr in the absence of copper. However, XIAP appeared greatly destabilized in the copper-treated cells, which exhibited the electrophoretically altered form of XIAP (Figure 2B). In this case, the half-life of XIAP induced to shift by the addition of copper was ~6 hr (Figure 2B). Quantitative real-time PCR

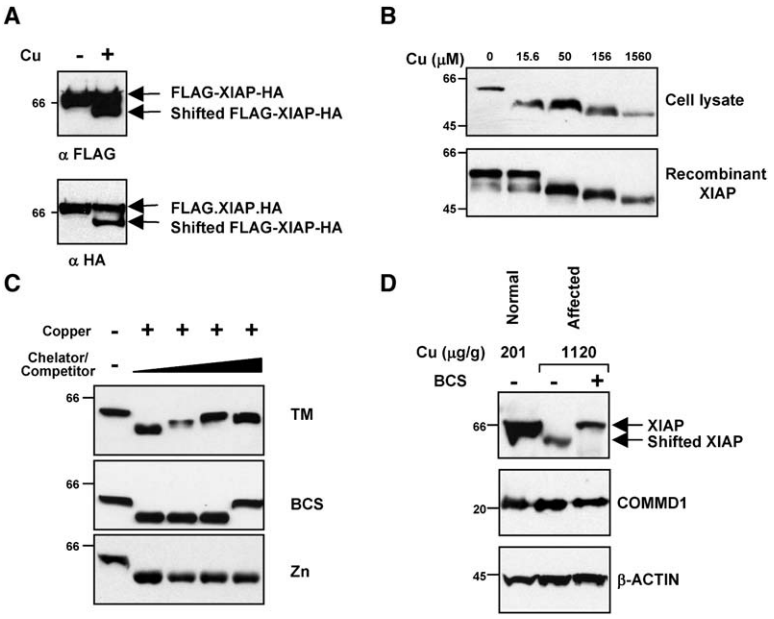

Figure 3. The XIAP Mobility Shift Is Not a Proteolytic Event and Is Reversible

(A) Doubly epitope-tagged XIAP containing an amino-terminal FLAG tag and a carboxy-terminal HA tag was expressed in HEK 293 cells. Copper sulfate (50 μM) was added to the media, and the cells were subsequently lysed. XIAP was detected by immunoblotting using FLAG and HA antibodies as indicated.

(B) The copper-induced mobility shift can be recapitulated in vitro. Increasing amounts of copper were added postlysis to untreated HEK 293 cell lysates and to recombinant XIAP prepared in *E. coli* as indicated. XIAP mobility was determined by immunoblotting.

(C) The copper-mediated mobility shift of XIAP is reversible. The XIAP shift was induced by the addition of copper sulfate (1.56 mM) to HEK 293 cell lysates after which increasing amounts (0, 0.156, 1.56, and 7.8 mM) of the copper chelators tetrathiomolybdate (TM) and bathocuproinedisulfonic acid (BCS) and zinc chloride were added. XIAP mobility was subsequently determined by immunoblotting.

(D) BCS (15.6 mM) was added to hepatic tissue lysate from an affected cocker spaniel and subsequently probed for XIAP, COMMD1, and β-actin.

analysis of XIAP showed no significant changes in XIAP mRNA expression levels (A. Wilkinson and C.S.D., unpublished data), indicating that the reduction in XIAP occurs posttranscriptionally.

Because copper is a strong oxidant, we sought to determine whether the concentration of copper used in our studies induced cellular oxidation or was otherwise toxic to the cell. As shown in Figure 2C, incubation with copper induced neither reactive oxygen species (ROS) formation nor cytoxicity (Figure 2C). Furthermore, changes in the mobility or levels of XIAP were not observed after the addition of other divalent metals such as zinc or iron, or hydrogen peroxide, a source of ROS (Figure 2D). These findings support the notion that copper induces alterations in XIAP of a highly specific nature.

The Mobility Shift of XIAP Can Be Recapitulated In Vitro and Is Reversible

One potential explanation to account for the copper-induced alteration in the electrophoretic mobility of XIAP is that copper might be inducing the proteolysis of one or both termini. To test this possibility, an expression vector was constructed encoding a doubly tagged XIAP modified to incorporate both an amino-terminal FLAG tag and a carboxy-terminal HA tag in the same protein. This plasmid was transfected into 293 cells, which were either left untreated or treated with copper, and samples were examined by immunoblot separately with anti-FLAG and anti-HA antibodies. In the lysates from cells incubated with copper (Figure 3A), the faster-migrating band was again observed, similar to that seen with endogenous XIAP, and furthermore, this altered mobility was detected with both FLAG- and HA-specific antibodies. These data indicate that neither terminus of the molecule undergoes proteolytic cleavage to produce the electrophoretically distinct form of XIAP observed after copper treatment.

The lack of a proteolytic event suggested that the mobility shift might represent a conformational change in the protein triggered by copper. Therefore, we tested whether the mobility shift could be recapitulated in vitro by incubating whole-cell lysates from HEK 293 cells with increasing amounts of copper. This resulted in a graded mobility shift of XIAP (Figure 3B, top) that resembled the phenomenon observed when incubating 293 cells in media supplemented with copper. This mobility shift has been observed in all cell lysates examined to date, tested from a wide range of cell types, including Jurkat, FL5.12, Ht29, Caco-2, and HeLa cell lines, suggesting that the conformational change in XIAP observed after copper treatment is a widely occurring phenomenon.

The observation that copper treatment was able to induce a mobility shift of XIAP in whole-cell lysates raised the question of whether this was an intrinsic property of XIAP or required other cellular factors. To explore this question in more detail, the ability of purified XIAP to undergo a mobility shift was tested. As shown in Figure 3B (bottom), recombinant bacterially expressed XIAP demonstrated a mobility shift that was essentially identical to that seen in whole-cell lysates after incubation with increasing concentrations of copper. These findings suggest that the mobility shift is intrinsic to XIAP and does not require other cellular cofactors.

Previous studies have described the ability of IAPs to bind zinc (Clem et al., 2001; Hinds et al., 1999; Miller, 1999; Sun et al., 1999), raising the possibility that like zinc, copper may also bind directly to XIAP. In that case, the mobility shift could potentially be reversed by copper chelation. In order to test this hypothesis, copper was added to whole-cell extracts to induce the mobility shift of XIAP (as in Figure 3B), and then increasing amounts of two different copper chelators, tetrathiomolybdate (TM) and bathocuproinedisulfonic acid (BCS), were added. Copper chelation restored the slower-migrating form of

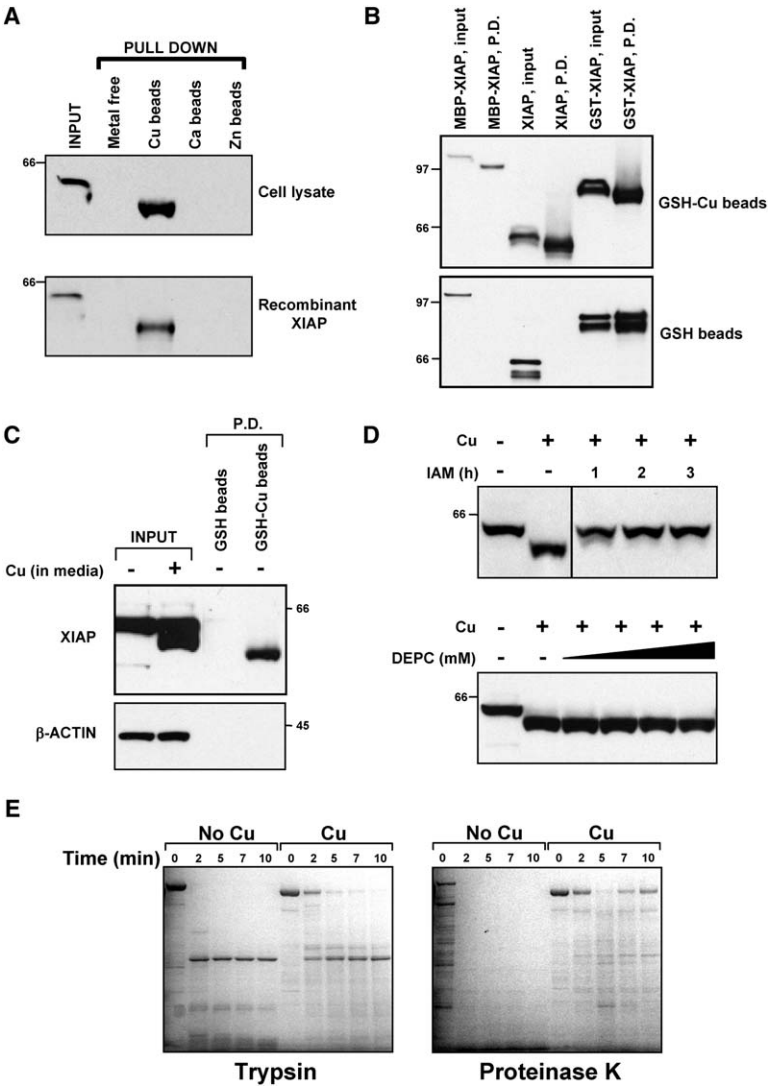

Figure 4. XIAP Binds Copper Directly and Undergoes a Conformational Change

(A) Metal-free and copper-, calcium-, and zinc-chelated beads were added to HEK 293 cell lysates and recombinant XIAP to ascertain which metals precipitate XIAP. Precipitated (pull-down) samples were subsequently probed for XIAP.

(B and C) Copper was loaded onto GSH beads and used to precipitate recombinant XIAP untagged and in fusion with MBP or GST (B) and similar precipitations were performed with cellular XIAP from HEK 293 cell lysates (C). XIAP and β-actin were detected by immunoblotting.

(D) Copper binds specifically to cysteine residues on XIAP. Copper binding to cellular XIAP (from HEK 293 lysates) was tested in the presence of iodocetamide (IAM) or diethyl pyrocarbonate (DEPC), which interfere with binding to cysteine and histidine residues, respectively. Protein was incubated on ice with IAM (31.2 mM) for 1, 2, or 3 hr (top) or with DEPC (0.5 mM, 1 mM, 2 mM, and 3 mM) for 3 hr. Copper sulfate (1.56 mM) was then added to induce the mobility shifted form of XIAP, which was detected by immunoblotting.

(E) Native and copper bound XIAP exhibit different patterns of digestion with trypsin and proteinase K. Native and copper bound XIAP were digested with trypsin and proteinase K for defined time points. The trypsin digests were then terminated by the addition of 5 mM phenylmethylsulfonyl fluoride (PMSF), and the proteinase K digests were terminated by boiling the samples in MBP elution buffer. The samples were then run on a denaturing polyacrylamide gel and the bands visualized with Coomassie staining technique.

XIAP (Figure 3C), indicating that the effect of copper on XIAP is a reversible change. In addition, increasing concentrations of zinc did not reverse the mobility shift, suggesting that there are distinct metal binding sites for copper and zinc. To investigate whether these results could be recapitulated in a cellular system, HEK 293 cells were cultured in media supplemented with copper, in the absence or presence of the cell-permeable copper chelator tetraethylenepentamine (TEPA). The presence of TEPA in the culture media similarly was sufficient to prevent the copper-induced mobility shift of XIAP (Figure S1B). Finally, the mobility shift observed in canine tissue described in Figure 1B was also reversed by the addition of copper chelators to the liver tissue lysate (Figure 3D). This finding strongly supports the idea that the altered mobility of XIAP as a consequence of copper overload in vivo is due to a similar process as that observed in cell culture.

Direct Binding of Copper to Cysteine Residues within XIAP Induces a Major Conformational Change in XIAP

The reversible nature of the mobility shift supported the notion that this event might be the result of direct copper binding by XIAP. To test this possibility, beads coupled with the metal chelator pentadentate (PDC) and in complex with various metals were used to precipitate protein from either whole-cell extracts or purified recombinant XIAP. As shown in Figure 4A, beads with immobilized copper, but not other metals, were found to efficiently precipitate recombinant XIAP (bottom) or endogenous XIAP from cell lysates (top). Interestingly, the precipitated XIAP migrated in the shifted position, consistent with the incorporation of copper into XIAP.

To independently confirm the observation that XIAP binds copper directly, we took advantage of the high affinity of glutathione (GSH) for copper. GSH Sepharose beads were either untreated or loaded with copper and then extensively washed to remove excess metal and subsequently tested for their ability to precipitate XIAP. Recombinant XIAP variants were used that were either untagged or contained amino-terminal affinity tags (maltose binding protein [MBP] or glutathione-S-transferase [GST]). As expected, native GSH Sepharose beads were only able to precipitate GST-XIAP, due to the high affinity of GST for GSH (Figure 4B, bottom). However, GSH beads in which copper had been adsorbed efficiently precipitated all recombinant proteins,

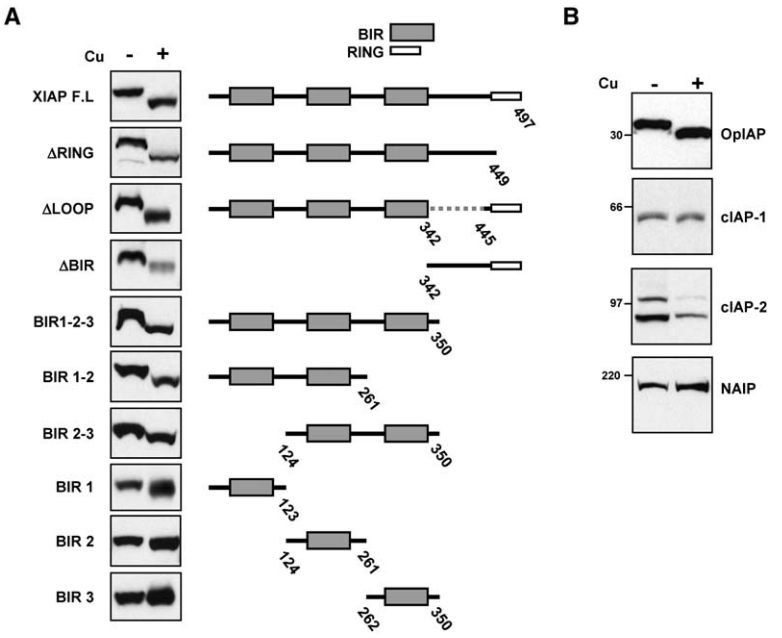

Figure 5. Copper Binding Is Mediated by Multiple Domains of XIAP and Is Shared by Other IAPs

(A) Multiple domains of XIAP can mediate the copper-induced shift. The indicated deletion mutants of XIAP were expressed in HEK 293 cells, which were subsequently lysed, and copper sulfate (1.56 mM) was added to the lysates. The mobility of XIAP was examined by immunoblotting.

(B) Other IAPs undergo a mobility shift on NuPAGE in the presence of copper. The indicated IAPs were transiently expressed in HEK 293 cells, copper sulfate (50 μM) was added to the media, and cell lysates were subsequently examined by immunoblotting using the relevant antibodies.

including those lacking a GST tag, confirming a strong and specific affinity of XIAP for copper. The recovered material migrated in the shifted position (Figure 4B, top), as seen also with the beads in which copper had been directly chelated (Figure 4A). A similar experiment performed with whole-cell lysates demonstrated that only copper-loaded GSH beads and not native GSH beads were capable of specifically precipitating XIAP, and the recovered protein migrated in the shifted position (Figure 4C). Taken together, these results indicate that XIAP directly binds to copper and undergoes a conformational change manifested by an alteration in its electrophoretic mobility.

The studies described above and in Figure 4 indicate a direct interaction between XIAP and copper. Because numerous previous reports have described critical roles for cysteine and histidine residues in copper binding (Adman, 1991), we tested the possibility that these residues may also be involved in the copper-XIAP interaction. Iodoacetamide (IAM) is an alkylating agent that avidly binds cysteine thiols and, thus, can neutralize the ability of cysteine residues to bind copper. We therefore compared the ability of XIAP to undergo a copper-induced mobility shift in whole-cell lysates, in the presence and absence of IAM. Significantly, IAM was sufficient to prevent the copper-mediated shift of XIAP (Figure 4D, top). Conversely, the addition of diethyl pyrocarbonate (DEPC), a histidine selective reagent, did not ablate the shift (Figure 4D, bottom). These results indicate that copper binds to cysteine, but not histidine residues within XIAP.

The altered mobility shift of XIAP observed after copper treatment, its reversibility by copper chelation, and the ability of XIAP to bind directly to copper are all suggestive of a conformational change induced by copper binding. To explore in more detail the possibility that XIAP undergoes a change in its conformation after binding to copper, we performed limited proteolytic digestion analysis of purified, recombinant XIAP in its free or copper-shifted form by using trypsin (Figure 4E, left) and proteinase K (Figure 4E, right). As shown in Figure 4E, the copper bound form of XIAP exhibits very different patterns of digestion to native XIAP, with both proteolytic enzymes over a 10 min period at 37ºC, strongly indicating that XIAP adopts a distinct conformation when bound to copper. The resistance of copper bound XIAP to proteases seen here reflects a conformational change in the protein and does not necessarily signify an altered susceptibility to degradation in vivo. The digestion patterns obtained with an unrelated control protein, bovine serum albumin, were identical in the presence and absence of copper with both proteinase K and trypsin (data not shown), indicating that their proteolytic activity was unaffected by the supplemental copper.

Copper Binding Is Mediated by Multiple Regions in XIAP

The iodoacetamide experiment shown in Figure 4D indicated that cysteine residues are required for XIAP to bind copper, prompting us to examine the domains within XIAP that might mediate copper binding. XIAP contains three BIR domains that are known to coordinate zinc, consistent with their similarities to zinc fingers (Hinds et al., 1999; Sun et al., 1999). These BIR domains are cysteine rich, and similarly, the carboxy-terminal RING finger domain present in XIAP is also rich in cysteine residues (Yang et al., 2000) and known to coordinate zinc. Therefore, the potential involvement of various domains of XIAP in copper binding was evaluated by testing the ability of truncated versions of the protein to undergo the mobility shift after addition of copper sulfate to the lysate. As shown in Figure 5A, the amino-terminal portion of XIAP containing the three BIR domains and lacking the RING finger domain was capable of undergoing a mobility shift as were the BIR1-2 and BIR2-3 constructs. In addition, a truncation mutant lacking all BIR domains and containing the RING finger domain

was also capable of undergoing the mobility shift. These results indicate that the BIR and RING domains of XIAP are all likely involved in copper binding, and these results are consistent with both the stepwise nature of the mobility shift observed in vitro (Figure 3B) and the known requirement of cysteine residues for copper binding to XIAP.

Copper Can Induce Mobility Shift of Other IAPs

Given the structural and functional similarities between various members of the IAP family, we investigated whether the electrophoretic mobility shift observed with XIAP could also be induced with other IAPs. To this end, HEK 293 cells were transfected with expression vectors for the IAPs indicated in Figure 5B, and the cells were then cultured in media supplemented with copper sulfate. Interestingly, this resulted in a mobility shift for the prototype baculoviral Op-IAP, suggesting that the copper binding properties of IAPs might be evolutionarily conserved. Although several other members of the IAP family did not appear to shift, treatment of cIAP-2-expressing cells with copper resulted in a redistribution of the doublet typically observed after overexpression of this gene into predominantly the faster-migrating species. These findings suggest that the ability of XIAP to bind copper is likely to be shared with several other IAP family members.

Copper Bound XIAP Exhibits Impaired Caspase-3 Inhibitory Activity and Renders Cells More Susceptible to Apoptotic Stimuli

Protection from apoptosis by XIAP relies primarily on its ability to inhibit caspases (Deveraux and Reed, 1999). Therefore, the ability of untreated and copper bound XIAP to inhibit caspase-3 was compared. Preliminary experiments revealed that even trace amounts of free copper abrogate caspase-3 activity (A.R.M. and C.S.D., unpublished data). We therefore devised a strategy to test the caspase inhibitory properties of copper bound XIAP in the absence of free copper. Recombinant GST or GST-XIAP were first adsorbed onto native or copper bound GSH Sepharose beads, which were subsequently washed to remove free copper. This allowed us to induce the copper bound form of XIAP but remove excess free copper from the system. In control samples, copper immobilized onto the GSH beads did not substantially affect the assay when compared to other negative controls such as native GSH beads either alone or bound to GST.

The enzymatic activity of recombinant caspase-3 was determined by its ability to cleave the fluorogenic substrate DEVD-AFC in the presence of increasing amounts of recombinant native or copper bound GST-XIAP. The caspase-3 activity in the presence of GST-XIAP was compared to that seen in the presence of equal amounts of GST to derive a percentage activity (Figure 6A). As expected, increasing amounts of GST-XIAP bound to native GSH Sepharose beads resulted in progressive inhibition of caspase-3 activity. However, GST-XIAP immobilized onto copper bound GSH beads no longer inhibited caspase-3. These results indicated that binding of copper by XIAP induces a loss of caspase inhibition, most likely due to the resulting conformational changes.

The effect of copper binding on the ability of XIAP to bind to caspase-3 was then investigated. Again,

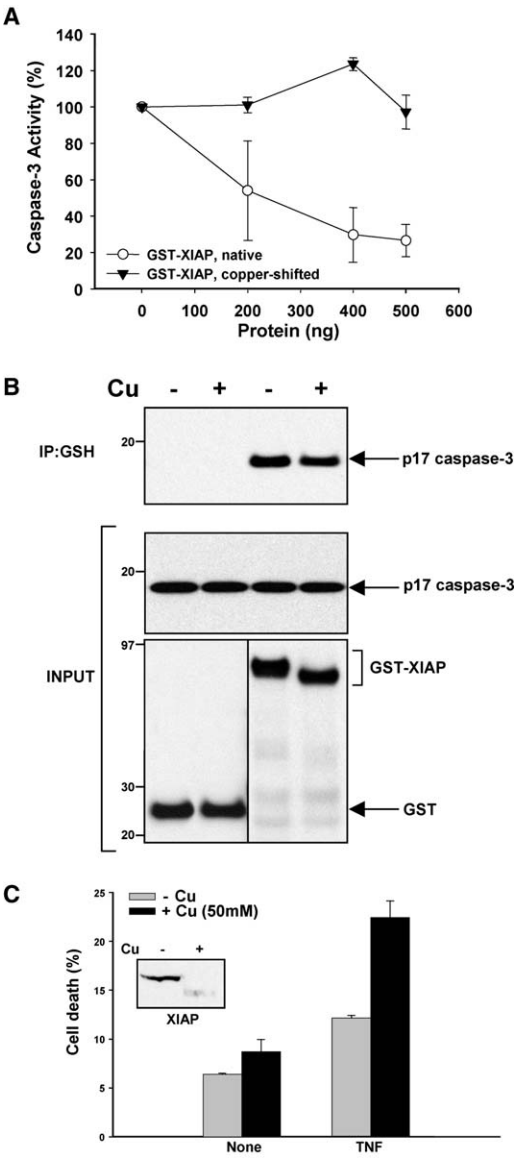

Figure 6. Copper Bound XIAP Does Not Inhibit Caspase 3 and Decreases the Threshold for Apoptosis

(A) Effects of the copper-induced mobility shift on the caspase-3 inhibitory activity of XIAP. Caspase-3 activity in the presence of copper-shifted GST-XIAP is compared to the native GST-XIAP control. Recombinant GST and GST-XIAP were mixed with glutathione beads, either untreated or after copper immobilization, the latter resulting in a copper-induced mobility shift. Caspase-3 was then added and its enzymatic activity determined by the cleavage of the fluorogenic substrate DEVD-AFC, and the activity in the presence of GST-XIAP was compared to the corresponding GST control to derive a percentage activity. The mean percentage activity and standard deviation of three samples per group are presented.

(B) The ability of native and copper bound GST-XIAP to bind caspase-3 was determined by coprecipitation and immunoblotting as indicated.

(C) Cells expressing the copper bound form of XIAP are more susceptible to apoptosis. HEK 293 cells were grown in the presence of additional copper sulfate (50 μM), and a combination of TNF (500 U) and CHX (60 μg/ml) was used to induce cell death. PI staining was used to identify dead cells by flow cytometry. The mean and standard deviation of three samples per group are shown.

recombinant GST or GST-XIAP was first bound to GSH Sepharose beads (either untreated or copper bound) and mixed with recombinant caspase-3. After precipitation and washing of the beads, the presence of caspase-3 was determined by immunoblotting (Figure 6B). Interestingly, the copper bound form of XIAP was still capable of binding caspase-3, despite its inability to inhibit caspase-3 enzymatic activity.

Based on the finding that copper bound XIAP is a poor inhibitor of caspase-3, we next investigated whether cells expressing the mobility-shifted form of XIAP were more susceptible to apoptotic stimuli. Cells were cultured in media supplemented with copper to induce the shifted form of XIAP (Figure 6C, inset) and then challenged with tumor necrosis factor (TNF) as a death stimulus. Although at this time-point, the dose of TNF used (500 U) resulted in minimal cell death in control cultures, cells expressing the mobility shifted form of XIAP were greatly sensitized to death (Figure 6C), and this occurred under conditions in which copper did not induce ROS formation (Figure 2C). Although the possibility cannot formally be excluded that copper can sensitize these cells to apoptosis through XIAP-independent pathways, these data suggest that at least one way to achieve this sensitization can be through the inactivation of XIAP.

Discussion

XIAP was originally identified as a mammalian homolog of the antiapoptotic protein Op-IAP and has since been found to bind and directly inhibit caspase-3, caspase-7, and caspase-9 (Chai et al., 2001; Deveraux and Reed, 1999; Riedl et al., 2001; Shiozaki et al., 2003). In addition to its role in regulating apoptosis, XIAP can also regulate intracellular copper levels by functioning as an E3 ubiquitin ligase for COMMD1, a factor involved in copper homeostasis. Consistent with this, tissues from *Xiap*-deficient mice contain elevated levels of COMMD1, as well as reduced levels of copper (Burstein et al., 2004). In light of this role for XIAP in copper homeostasis, we investigated the potential effects of copper on XIAP.

In this study, we demonstrate that in the presence of elevated copper, XIAP levels are markedly reduced both in inherited and acquired copper toxicosis disorders and that XIAP adopts an alternative conformation that has enhanced electrophoretic mobility in polyacrylamide gels, even under reducing, denaturing conditions. This conformational change is specifically induced by copper and occurs as a result of direct binding of the metal to multiple cysteine residues within XIAP. This finding is consistent with previous studies that have shown that other copper binding proteins such as ATP7B utilize cysteine residues to complex copper (Ralle et al., 2004). The BIR domains and the RING finger, which are all rich in cysteines, appear to be capable of binding copper, and the deletion studies performed here confirmed that multiple regions of XIAP can bind to copper. Additionally, other IAPs such as Op-IAP and cIAP-2 (Figure 5B) are also affected by intracellular copper accumulation, raising the possibility that the functions of IAPs in general might be affected under conditions of copper excess. Thus, copper overload may have a more profound effect on the apoptotic threshold beyond XIAP inactivation alone.

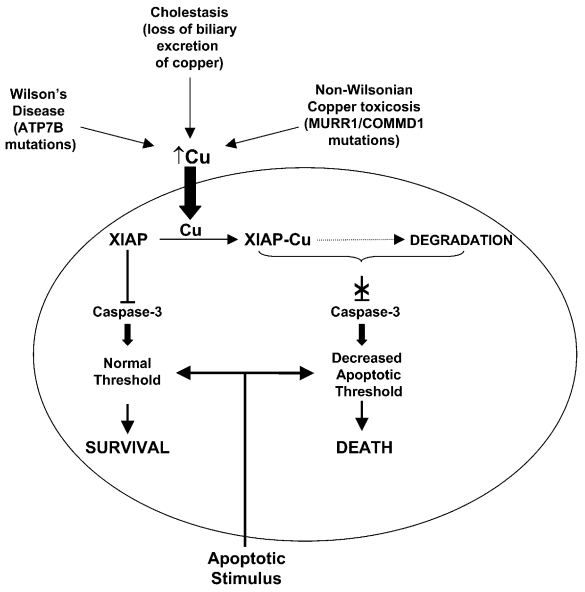

Figure 7. Overview of the Relationship between Copper, XIAP, and the Apoptotic Threshold

Intracellular copper accumulation results in a copper-induced conformational change of XIAP, thereby increasing its intracellular degradation and decreasing its ability to inhibit caspase-3. These changes result in a lowering of the apoptotic threshold and increased cell death in response to apoptotic stimuli.

In its copper bound state, XIAP is more susceptible to degradation than in its native form and is greatly impaired in its ability to inhibit caspase-3 despite the fact that there is no observable difference in its ability to bind the active p-17 caspase-3 fragment. Structural studies indicate that the interaction between XIAP and caspase-3 results in steric interference of the enzymatic site of caspase-3 by a domain in XIAP located just upstream of BIR2 (Riedl et al., 2001). The fact that the copper bound form of XIAP still binds caspase-3 but does not inhibit its activity implies that the mechanism of binding does not involve the active site of the enzyme. This finding is not surprising in light of the conformational change that XIAP undergoes when bound to copper, as demonstrated by the different digestion patterns seen with native and copper bound XIAP with proteinase K and trypsin. Importantly, cells expressing the mobility-shifted form of XIAP are more sensitive to apoptotic stimuli, and this is probably due to a decrease in XIAP levels in conjunction with the inability of the copper bound form of the protein to inhibit caspase-3.

These findings provide a provocative and unexpected link between cellular copper homeostasis and the control of apoptosis. Abnormal copper accumulation such as that resulting from Wilson's disease or chronic cholestasis is accompanied by cell death that has long been attributed to a direct toxic effect of copper. The data presented here suggest that in the setting of intracellular copper accumulation, XIAP undergoes a reversible conformational change that enhances its susceptibility to intracellular degradation and significantly decreases its ability to inhibit caspase-3. This results in a lowering of the apoptotic threshold of the cell and, in the presence of an apoptotic stimulus, leads to increased cell

death (Figure 7). Future studies will determine the extent to which this process contributes to the pathophysiology of copper toxicosis diseases.

This change in the biological properties of XIAP after copper binding is akin to that observed in other proteins that have a high affinity for copper. Amyloid-β-protein (Aβ) and prion protein (PrP^c) both avidly bind copper, and this interaction plays an important role in the eventual development of Alzheimer's disease (Bush et al., 2003) and transmissible spongiform encephalopathies, respectively (Millhauser, 2004). In the same way, the lowering of the apoptotic threshold in copper overload disorders may play a pivotal role in hastening cell death, resulting in the accelerated development of a disease phenotype. This raises the intriguing possibility that copper chelator therapy in Wilson's disease may be effective not only because excess copper is removed from the cell but also because the apoptotic threshold is normalized. Conversely, harnessing the effects of copper on XIAP may have practical applications in tumors, because it would be predicted that increases in copper may actually function synergistically with small molecule XIAP antagonists to sensitize cells to apoptosis.

Experimental Procedures

Plasmids

The plasmids pEBG-BIR1, pEBG-BIR2, pEBG-BIR3, pEBG-BIR1-2, pEBG-BIR2-3, and pEBG-BIR1-2-3 were generated by PCR using pEBB-XIAP as a template (boundaries are indicated in Figure 5). The plasmids pEBB-FLAG-XIAP-HA and pMAL-c2x-XIAP were derived by incorporating the XIAP coding sequence into the vectors pEBB-FLAG-HA and pMAL-c2x, respectively. The plasmids pEBG-ΔBIR, pEBG-ΔLOOP, pEBG-ΔRING and pEBG-XIAP, pcDNA3-OpIAP-HA, pcDNA3-Myc_6-cIAP-2, pcDNA3-Myc_6-NAIP, and pEBB-cIAP-1 have been described previously (Duckett et al., 1998; Liston et al., 1996).

Cell Culture, Transfection, and Hepatocyte Isolation

Human embryonic kidney 293 cells were cultured in DMEM supplemented with 10% FBS and 2 mM L-glutamine. A standard calcium phosphate transfection protocol (Duckett et al., 1997) was used to transfect 293 cells in all cases. *Atp7b*$^{tx\text{-}J}$ toxic milk mice (Coronado et al., 2001) and littermate controls were obtained from The Jackson Laboratory, Bar Harbor, ME. Hepatocytes were isolated by a modified in situ collagenase perfusion technique (Wan et al., 1995).

In Vitro Induction of Copper-Mediated XIAP Mobility Shift

Recombinant XIAP and GST-XIAP were prepared as previously described (Lewis et al., 2004). MBP-XIAP fusion protein was produced by following the manufacturer's instructions (NEB). The indicated concentrations of copper sulfate were added to whole-cell lysates, recombinant XIAP, and GST-XIAP on ice. After mixing, the samples were immediately resolved on denaturing NuPAGE 4%–12% polyacrylamide gradient gels as described below. In the stated experiments, after the addition of copper to the lysates as described above, increasing concentrations (0.156 mM, 1.56 mM, and 7.8 mM) of two different copper chelators, BCS (Sigma) and TM (Sigma), were added to the lysates and incubated on ice for 2 hr.

Precipitations Using Metal-Chelated Beads

Metal-free beads or ones with copper, zinc, or calcium immobilized onto a pentadentate chelator coupled to a quartz base matrix (PDC-SLQ free, Cu-PDC-SLQ, Zn-PDC-SLQ, and Ca-PDC-SLQ) were obtained from Affiland (Liege, Belgium). In addition, copper was also immobilized onto GSH by rotating equal volumes of GSH Sepharose beads (GE Healthcare) with copper sulfate (50 mM) at 4ºC for 1 hr. The beads were then washed five times (twice the bead bed volume) with EDTA-free 1% Triton lysis buffer (25 mM HEPES, 100 mM NaCl, 10% glycerol, and 1% Triton X-100) to remove excess unbound copper. The above beads were then used to precipitate recombinant XIAP (untagged or tagged with GST or MBP) and protein from HEK 293 cell lysates as indicated. Thirty microliters of beads was added to either recombinant protein or whole-cell lysates and rotated at 4ºC for 2 hr. The beads were then washed four times with EDTA-free 1% Triton lysis buffer, pelleted, and the precipitate resuspended in LDS loading buffer for immunoblotting.

Antibodies, Immunoblotting, and Immunoprecipitation

All tissue samples were lysed in Laemmli buffer (0.0625 mM Tris-HCl, 2% SDS, 10% glycerol, and 5% β-mercaptoethanol). Lysates from cultured cells were prepared with a Triton X-100 lysis buffer (25 mM HEPES, 100 mM NaCl, 10% glycerol, and 1% Triton X-100) supplemented with protease inhibitors. Protein samples were resolved by using 4%–12% gradient Novex Bis-Tris gels (Invitrogen), transferred to nitrocellulose membranes (Invitrogen), and blocked with 5% milk solution in TBS containing 0.05%–0.2% Tween-20. The membranes were incubated with the relevant primary antibodies followed by incubation with HRP-conjugated secondary antibodies (GE Healthcare). Antibody detection was performed by the Enhanced Chemiluminescence (ECL) Western blot analysis system (GE Healthcare). Antibodies against XIAP (Transduction Labs), GST (Santa Cruz), FLAG (Sigma), HA (Sigma), β-actin (Sigma), and COMMD1 (Burstein et al., 2005) were used.

Cell Viability Studies

Copper (50 μM) was added to HEK 293 cells as described above. After 48 hr, a combination of TNF (500 U; Roche) and CHX (60 μg/ml; Sigma) was used as the apoptotic stimulus. Alternatively, etoposide (30 μg/ml) alone was added in the absence of copper. After incubation for 16 hr, the cells were collected in 5 ml of PBS and washed once with 3 ml PBS. The samples were centrifuged at 200 × g for 5 min, the PBS was aspirated, and the cells were washed once more with 1 ml PBS. After further centrifugation at 200 × g for 5 min, the pelleted cells were resuspended in 0.5 ml PBS containing 2 μg/ml propidium iodide (PI) and incubated on ice for 10 min. PI-positive dead cells were then detected by flow cytometry.

Detection of Reactive Oxygen Species

The fluoroprobe 5-(and 6-)chloromethyl-2′,7′-dichlorodihydrofluorescein diacetate, acetyl ester (CM-H_2DCFDA, Invitrogen) was used to detect ROS production. Either copper (50 μM) or etoposide (30 μg/ml) was added to HEK 293 cells for 48 and 16 hr, respectively. Subsequently, CM-H_2DCFDA was added to the cells to a final concentration of 1 μM for 30 min, and the cells were then detached by using trypsin after being washed with 1 ml PBS. The samples were centrifuged at 200 × g for 5 min, the PBS was aspirated, and the cells were washed once more with 2 ml PBS. After further centrifugation at 200 × g for 5 min, the pelleted cells were resuspended in 0.5 ml PBS and ROS-positive cells were detected by flow cytometry.

Degradation Studies

HEK 293 culture media was supplemented with copper sulfate (50 μM) to induce the mobility shift of XIAP. After 48 hr, CHX (30 μg/ml) was added to the growth media to inhibit de novo protein synthesis, and the cells were then lysed at different time points as indicated. The samples were then prepared for immunoblot analysis, and XIAP and β-actin were identified by immunoblotting.

Protease Digestion

The copper bound form of the protein was generated by adding copper sulfate (1.56 mM) directly to recombinant MBP-XIAP. and binding of copper to the protein was confirmed by the presence of the mobility shift on the Coomassie blots. The proteolytic sensitivity of both native and copper bound MBP-XIAP was determined by carrying out timed digests with trypsin and proteinase K (Jakob et al., 2000). The samples were separated by SDS-PAGE and the protein bands visualized by colloidal Coomassie staining (Invitrogen).

Supplemental Data

Supplemental Data include one figure and can be found with this article online at http://www.molecule.org/cgi/content/full/21/6/775/DC1/.

Acknowledgments

We thank Drs. Cisca Wijmenga, Leo Klomp, and Casey Wright for their insightful suggestions, Dr. Hellan Kang for helping with hepatocyte isolation from toxic milk mice, Amanda Wilkinson for technical assistance, and Drs. P. Liston and R. Korneluk for the pcDNA3-Myc_6-cIAP-2 and NAIP plasmids. This work was supported in part by the University of Michigan Biological Scholars Program, Department of Defense IDEA Award PC040215, and National Institutes of Health Grant GM067827 to C.S.D.; by an American Gastroenterological Association Research Scholar Award, a Merit Review Entry Program Award, and a Veterans Education and Research Association of Michigan Award to E.B.; by a Department of Defense Prostate Cancer Research Program Postdoctoral Training Award PC040393 to J.C.W; by US Food and Drug Administration grants FD-R-002153 and FD-R-002132 and a General Clinical Research Center grant M01-RR00042 to G.J.B.; and by an American Cancer Society grant RSG-05-029-01-CCG to S.B.B.

Received: April 19, 2005
Revised: November 18, 2005
Accepted: January 30, 2006
Published: March 16, 2006

References

Adman, E.T. (1991). Copper protein structures. Adv. Protein Chem. *42*, 145–197.

Brewer, G.J. (2000). Recognition, diagnosis, and management of Wilson's disease. Proc. Soc. Exp. Biol. Med. *223*, 39–46.

Buiakova, O.I., Xu, J., Lutsenko, S., Zeitlin, S., Das, K., Das, S., Ross, B.M., Mekios, C., Scheinberg, I.H., and Gilliam, T.C. (1999). Null mutation of the murine ATP7B (Wilson disease) gene results in intracellular copper accumulation and late-onset hepatic nodular transformation. Hum. Mol. Genet. *8*, 1665–1671.

Burstein, E., Ganesh, L., Dick, R.D., van De Sluis, B., Wilkinson, J.C., Lewis, J., Klomp, L.W.J., Wijmenga, C., Brewer, G.J., Nabel, G.J., and Duckett, C.S. (2004). A novel role for XIAP in copper homeostasis through regulation of MURR1. EMBO J. *23*, 244–254.

Burstein, E., Hoberg, J.E., Wilkinson, A.S., Rumble, J.M., Csomos, R.A., Komarck, C.M., Maine, G.N., Wilkinson, J.C., Mayo, M.W., and Duckett, C.S. (2005). COMMD proteins: A novel family of structural and functional homologs of MURR1. J. Biol. Chem. *280*, 22222–22232.

Bush, A.I., Masters, C.L., and Tanzi, R.E. (2003). Copper, beta-amyloid, and Alzheimer's disease: tapping a sensitive connection. Proc. Natl. Acad. Sci. USA *100*, 11193–11194.

Chai, J., Shiozaki, E., Srinivasula, S.M., Wu, Q., Dataa, P., Alnemri, E.S., and Shi, Y. (2001). Structural basis of caspase-7 inhibition by XIAP. Cell *104*, 769–780.

Clem, R.J., Sheu, T.-T., Richter, B.W.M., He, W.-W., Thornberry, N.A., Duckett, C.S., and Hardwick, J.M. (2001). c-IAP1 is cleaved by caspases to produce a pro-apoptotic C-terminal fragment. J. Biol. Chem. *276*, 7602–7608.

Coronado, V., Nanji, M., and Cox, D.W. (2001). The Jackson toxic milk mouse as a model for copper loading. Mamm. Genome *12*, 793–795.

Deveraux, Q.L., and Reed, J.C. (1999). IAP family proteins-suppressors of apoptosis. Genes Dev. *13*, 239–252.

Duckett, C.S., Nava, V.E., Gedrich, R.W., Clem, R.J., Van Dongen, J.L., Gilfillan, M.C., Shiels, H., Hardwick, J.M., and Thompson, C.B. (1996). A conserved family of cellular genes related to the baculovirus *iap* gene and encoding apoptosis inhibitors. EMBO J. *15*, 2685–2694.

Duckett, C.S., Gedrich, R.W., Gilfillan, M.C., and Thompson, C.B. (1997). Induction of nuclear factor κB by the CD30 receptor is mediated by TRAF1 and TRAF2. Mol. Cell. Biol. *17*, 1535–1542.

Duckett, C.S., Li, F., Wang, Y., Tomaselli, K.J., Thompson, C.B., and Armstrong, R.C. (1998). Human IAP-like protein regulates programmed cell death downstream of Bcl-x_L and cytochrome c. Mol. Cell. Biol. *18*, 608–615.

Fuentealba, I.C., and Aburto, E.M. (2003). Animal models of copper-associated liver disease. Comp. Hepatol. *2*, 5.

Gitlin, J.D. (2003). Wilson disease. Gastroenterology *125*, 1868–1877.

Hamza, I., and Gitlin, J.D. (2002). Copper chaperones for cytochrome c oxidase and human disease. J. Bioenerg. Biomembr. *34*, 381–388.

Hinds, M.G., Norton, R.S., Vaux, D.L., and Day, C.L. (1999). Solution structure of a baculoviral inhibitor of apoptosis (IAP) repeat. Nat. Struct. Biol. *6*, 648–651.

Jakob, U., Eser, M., and Bardwell, J.C. (2000). Redox switch of hsp33 has a novel zinc-binding motif. J. Biol. Chem. *275*, 38302–38310.

Klomp, A.E.M., van de Sluis, B., Klomp, L.W.J., and Wijmenga, C. (2003). The ubiquitously expressed MURR1 protein is absent in canine copper toxicosis. J. Hepatol. *39*, 703–709.

Lewis, J., Burstein, E., Birkey Reffey, S., Bratton, S.B., Roberts, A.B., and Duckett, C.S. (2004). Uncoupling of the signaling and caspase-inhibitory properties of XIAP. J. Biol. Chem. *279*, 9023–9029.

Liston, P., Roy, N., Tamai, K., Lefebvre, C., Baird, S., Cherton-Horvat, G., Farahani, R., McLean, M., Ikeda, J.-E., MacKenzie, A., and Korneluk, R.G. (1996). Suppression of apoptosis in mammalian cells by NAIP and a related family of IAP genes. Nature *379*, 349–353.

Llanos, R.M., and Mercer, J.F. (2002). The molecular basis of copper homeostasis copper-related disorders. DNA Cell Biol. *21*, 259–270.

Mercer, J.F. (2001). The molecular basis of copper-transport diseases. Trends Mol. Med. *7*, 64–69.

Miller, L.K. (1999). An exegesis of IAPs: salvation and surprises from BIR motifs. Trends Cell Biol. *9*, 323–328.

Millhauser, G.L. (2004). Copper binding in the prion protein. Acc. Chem. Res. *37*, 79–85.

Rae, T.D., Schmidt, P.J., Pufahl, R.A., Culotta, V.C., and O'Halloran, T.V. (1999). Undetectable intracellular free copper: the requirement of a copper chaperone for superoxide dismutase. Science *284*, 805–808.

Ralle, M., Lutsenko, S., and Blackburn, N.J. (2004). Copper transfer to the N-terminal domain of the Wilson disease protein (ATP7B): X-ray absorption spectroscopy of reconstituted and chaperone-loaded metal binding domains and their interaction with exogenous ligands. J. Inorg. Biochem. *98*, 765–774.

Riedl, S.J., and Shi, Y. (2004). Molecular mechanisms of caspase regulation during apoptosis. Nat. Rev. Mol. Cell Biol. *5*, 897–907.

Riedl, S.J., Renatus, M., Schwarzenbacher, R., Zhou, Q., Sun, C., Fesik, S.W., Liddington, R.C., and Salvesen, G.S. (2001). Structural basis for the inhibition of caspase-3 by XIAP. Cell *104*, 791–800.

Shiozaki, E.N., Chai, J., Rigotti, D.J., Riedl, S.J., Li, P., Srinivasula, S.M., Alnemri, E.S., Fairman, R., and Shi, Y. (2003). Mechanism of XIAP-mediated inhibition of caspase-9. Mol. Cell *11*, 519–527.

Sun, C., Cai, M., Gunasekera, A.H., Meadows, R.P., Wang, H., Chen, J., Zhang, H., Wu, W., Xu, N., Ng, S.C., and Fesik, S.W. (1999). NMR structure and mutagenesis of the inhibitor-of-apoptosis protein XIAP. Nature *401*, 818–822.

Tao, T.Y., Liu, F., Klomp, L., Wijmenga, C., and Gitlin, J.D. (2003). The copper toxicosis gene product murr1 directly interacts with the Wilson disease protein. J. Biol. Chem. *278*, 41593–41596.

Torres, A.S., Petri, V., Rae, T.D., and O'Halloran, T.V. (2001). Copper stabilizes a heterodimer of the yCCS metallochaperone and its target superoxide dismutase. J. Biol. Chem. *276*, 38410–38416.

Uren, A., Pakusch, M., Hawkins, C., Puls, K.L., and Vaux, D.L. (1996). Cloning and expression of apoptosis inhibitory proteins homologs that function to inhibit apoptosis and/or bind tumor necrosis factor receptor-associated factors. Proc. Natl. Acad. Sci. USA *93*, 4974–4978.

van De Sluis, B., Rothuizen, J., Pearson, P.L., van Oost, B.A., and Wijmenga, C. (2002). Identification of a new copper metabolism gene by positional cloning in a purebred dog population. Hum. Mol. Genet. *11*, 165–173.

Vaux, D.L., and Silke, J. (2005). IAPs, RINGs and ubiquitylation. Nat. Rev. Mol. Cell Biol. *6*, 287–297.

Wan, Y., Freeswick, P.D., Khemlani, L.S., Kispert, P.H., Wang, S.C., Su, G.L., and Billiar, T.R. (1995). Role of lipopolysaccharide (LPS), interleukin-1, interleukin-6, tumor necrosis factor, and dexamethasone in regulation of LPS-binding protein expression in normal hepatocytes and hepatocytes from LPS-treated rats. Infect. Immun. *63*, 2435–2442.

Yang, Y., Fang, S., Jensen, J.P., Weissman, A.M., and Ashwell, J.D. (2000). Ubiquitin protein ligase activity of IAPs and their degradation in proteasomes in response to apoptotic stimuli. Science *288*, 874–877.

Molecular and Cellular Biochemistry **286:** 67–76, 2006.
DOI: 10.1007/s11010-005-9094-2

Xaf1 can cooperate with TNFα in the induction of apoptosis, independently of interaction with XIAP

Yan Xia,[1] Rachel Novak,[1] Jennifer Lewis,[2] Colin S. Duckett[2] and Andrew C. Phillips[1]

[1]*Medical College of Georgia, Institute of Molecular Medicine and Genetics, CB2803, 1120 15th Street, Augusta, GA 30912, USA;* [2]*University of Michigan, Departments of Pathology and Internal Medicine, University of Michigan Medical School, Room 5315, 1301 Catherine, Ann Arbor, MI 48109-0602, USA*

Received 14 October 2005; accepted 28 November 2005

Abstract

XIAP-associated factor 1 (Xaf1) binds XIAP and re-localizes it to the nucleus, thus inhibiting XIAP activity and enhancing apoptosis [1]. Xaf1 expression is reduced or absent in tumor samples and cell lines suggesting it may function as a tumor suppressor [2–5]. To further study Xaf1 function we generated Xaf1 inducible cells in the osteosarcoma cell line Saos-2. Despite Xaf1 inducing apoptosis that is dramatically enhanced by TNFα we find no evidence for an interaction between Xaf1 and XIAP. Furthermore, Xaf1 expression sensitized XIAP$^{-/-}$ fibroblasts to TNFα, demonstrating the existence of a novel mechanism of Xaf1 induced apoptosis distinct from antagonizing XIAP. Xaf1 expression promotes cytochrome c release that cannot be blocked by inhibition of caspase activity. This implicates a role for the mitochondrial apoptotic pathway, consistent with the ability of Bcl2 to block Xaf1 induced apoptosis. The data indicate that in Saos2 cells Xaf1 activates the mitochondrial apoptotic pathway to facilitate cytochrome c release, thus amplifying apoptotic signals from death receptors. (Mol Cell Biochem **286:** 67–76, 2006)

Key words: Xaf1, XIAP, TNFα, cytochrome c, caspase, Bcl2, tumor suppressor

Introduction

Apoptosis is an evolutionarily conserved form of cell death, which plays critical roles during development, differentiation and tissue homeostasis of multi-cellular organisms. Defects in apoptosis play an important role in the pathogenesis of a number of diseases including cancer, neurodegenerative and auto-immune diseases [6]. Central mediators of the apoptotic process are the caspases. These proteases are synthesized as zymogens that are activated by either an increase in local concentration or by cleavage by other caspases (or in some cases non-caspase proteases) [7]. This can lead to a cascade of caspase activation, eventually mediating the orderly destruction of the cell [7, 8].

Two major pathways of apoptosis are described as the death receptor (or extrinsic) and the mitochondrial (or intrinsic). In both pathways apical initiator caspases are activated which in turn activate other caspases. The extrinsic pathway is activated by ligation of death receptors such as Fas and Tumor Necrosis Factor Receptor (TNFR) with their appropriate ligand. This results in the formation of a signaling complex activating caspase 8 [9]. The intrinsic or mitochondrial pathway is regulated by members of the Bcl2 family, which either promote or inhibit apoptosis [10, 11]. This pathway

Address for offprints: Andrew C. Phillips, Medical College of Georgia, Institute of Molecular Medicine and Genetics,CB2803, 1120 15th Street, Augusta, GA 30912, USA (E-mail: anphillips@mcg.edu)

can be activated by a variety of stresses including radiation and chemotherapeutic agents resulting in the release of cytochrome c and other pro-apoptotic molecules from the mitochondria into the cytosol. Cytochrome c binds to Apaf1 forming a macromolecular structure termed the apoptosome that recruits and activates caspase 9 [12].

Apoptosis is regulated post activation of caspases, by the inhibitor of apoptosis proteins (IAPs), that bind and inhibit the activity of caspases [13]. In many experimental systems, the X-linked inhibitor of apoptosis (XIAP) is the most potent of the IAPs, binding and inhibiting the activity of several caspases, notably caspases 3, 7 and 9 [14, 15]. In addition to the activation of caspases, efficient induction of apoptosis requires relief of IAP-mediated caspase inhibition. A number of proteins that bind and antagonize IAP function have been identified including the mitochondrial sequestered SMAC/Diablo and HtrA2/Omi [16, 17]. These proteins are released from the mitochondria in response to apoptotic signals and inhibit IAP function.

In addition to these mitochondrial sequestered proteins, other proteins have been identified that can modulate XIAP activity, including Xaf1. Xaf1 was isolated as an XIAP interacting protein in a yeast 2-hybrid screen and antagonizes XIAP caspase inhibition by direct interaction and relocalization of XIAP from cytosol to the nucleus [1, 18]. Xaf1 expression has been found to be reduced or absent in multiple tumor cell lines, in comparison to normal cells [4]. In addition, expression is lost in a subset of gastric, melanoma and colon cancer samples, suggesting that Xaf1 may function as a tumor suppressor [2, 3, 5].

To further investigate Xaf1 function we generated Xaf1 inducible Saos-2 cell lines. Doxycycline treatment results in accumulation of Xaf1 in the nucleus and apoptosis that is enhanced by treatment with other inducers of apoptosis, most dramatically TNFα. Despite Xaf1 promoting apoptosis in this cell line, XIAP remains in the cytosol, and we see no evidence of an interaction between these proteins. In addition, expression of Xaf1 in XIAP null fibroblasts renders these cells sensitive to TNFα treatment, demonstrating a XIAP-independent function of Xaf1. Furthermore we demonstrate that Xaf1 can induce apoptosis by activation of the mitochondrial pathway, promoting cytochrome c release that cannot be inhibited by the caspase inhibitor z-VAD. Our data reveal the existence of a previously unidentified function of Xaf1 in facilitating cytochrome c release to enhance apoptosis by other signals.

Materials and methods

Transfection and cell culture

Saos-2 cells and mouse fibroblasts were maintained in Dulbecco's modified Eagle's medium supplemented with 10% fetal bovine serum, 2 mM L-glutamine (Cellgro), 100 U/ml penicillin and streptomycin (Cellgro). For transfections, 5×10^5 cells were transfected with 10 μg of expression plasmid and 2 μg of pCMV CD20 expression plasmid by calcium phosphate precipitation. Xaf1 inducibles were generated using methods previously described [19, 20]. Parallel transfections allowed isolation of Xaf1 inducibles and cells containing only the empty vector as controls. The cells were maintained in Dulbecco's Modified Eagle's Medium supplemented with 10% fetal bovine serum (Tet System Approved FBS, BD Biosciences), 2 mM L-glutamine (Cellgro), 100 U/ml penicillin and streptomycin (Cellgro).

Immunoprecipitations and immunoblotting

Cells were harvested in Cell Lysis Buffer (20 mM Tris pH 7.4, 150 mM NaCl, 1 mM EDTA, 1 mM EGTA, 1% Triton X100 and complete proteinase inhibitors). Cellular debris was removed by centrifugation at 13000 g at 4°C for 10 minutes. For immunoprecipitations, the cell lysates were pre-cleared with 20 μl of protein A-sepharose beads in Cell Lysis Buffer (Pierce, 20398), and then incubated with appropriate antibodies at 4°C for 2 hours, followed by addition of 20 μl protein A-Sepharose beads and incubation at 4°C for 30 minutes. Immunoprecipitates were washed 4 times with Cell Lysis Buffer and once with PBS. Bound proteins were eluted and resolved by SDS-PAGE, and transferred to PVDF membranes (Hybond-P, Amersham). Membranes were blocked in TBST containing 5% skimmed milk, and then incubated for 2 hours with specific antibodies (anti-Flag M2 (Sigma, F3165), anti-GFP JL-8 (Clontech, 8371-2), anti-HA F-7 (Santa Cruz, E289), anti-actin (Sigma, A2066), anti-Xaf1 (IMGENEX, IMG-379), and anti-XIAP (Stressgen, AAM-50). The membranes were then washed, and incubated for 1 hour with horseradish peroxidase (HRP)-conjugated anti-mouse or anti-rabbit antibodies (Amersham Biosciences, NA931V/NA934V). Visualization of protein bands was accomplished using enhanced chemiluminescence (Amersham Biosciences) according to the manufacturer's instructions.

Immunofluorescence microscopy

Cells grown on cover slips were fixed in 4% paraformaldehyde for 10 minutes at room temperature, rinsed three times in PBS, permeabilized with cold 0.2% TritonX-100/PBS for 5 minutes, and then blocked for 2 hours (3% BSA and 10% FBS in PBS) at room temperature. Cells were incubated with various antibodies (anti-HA F-7 Santa Cruz E289, anti-HILP/XIAP BD Transduction Laboratories 610763, at 1:200 dilution) for 2 hours at room temperature, rinsed three times in PBS, and then incubated with anti-mouse Alexa 488 or

anti-rat Alexa 594 (Molecular Probes, A11008/A11007) 1:200 for 1 hour at room temperature. Cells were then washed, and stained with DAPI (30 nM) for 10 min at room temperature prior to mounting on glass slides using anti-fade (Molecular Probes).

DNA content analysis

Saos-Xaf1 inducible cells (3×10^5) were treated as indicated with doxycycline (Fisher, 2 μg/ml), TNFα (Endogen, 2 ng/ml), CHX (Fisher, cycloheximide, 4 μg/ml) Apo2L/Trail (Cellsciences, 4 μg/ml), Z-VAD-fmk (CalBiochem, 50 μM) and Adriamycin (Sigma, 2 μg/ml). Floating and attached cells were collected, pooled washed in PBS and fixed with methanol for 2 hours at 4°C. The cells were washed in PBS and re-suspended in PBS supplemented with propidium iodide (Fisher, 50 μg/ml) and RNAse A (Sigma, 50 μg/ml). DNA content was assessed by flow cytometry as previously described [20], and cells with less than 2N DNA content are scored as apoptotic. Apoptosis in transfected cells is measured in the same manner, with identification of transfected cell by co-transfection of a CD20 expression plasmid and staining as previously described [20].

Cell fractionation

Cells (1×10^6) were isolated by trypsinization. The cell pellets were washed in ice cold PBS and re-suspended in 200 μl buffer A (10 mM Hepes (pH 7.9), 10 mM KCl, 0.1 mM EDTA, 0.1 mM EGTA, 1 mM DTT, 0.5 mM PMSF and complete proteinase inhibitor (Calbiochem), and incubated on ice for 15 minutes. After addition of 12.5 μl 10% NP-40, the pellets were vortexed for 15 seconds and spun at 13000 rpm 1 minute at 4°C in a microfuge. Supernatants containing cytoplasmic protein were collected. The pellets were washed 3 times with buffer A, vortexed for 15 min after addition of 30 μl buffer C (20 mM Hepes (pH 7.9), 420 mM NaCl, 1 mM EDTA, 1 mM EGTA, 1 mM DTT, 1mM PMSF and proteinase inhibitors) centrifuged 13000 rpm for 5 min at 4°C. The supernatant containing nuclear proteins was collected [21]. The nuclear and cytoplasmic fractions were resolved by SDS PAGE and analyzed by western blot.

Cytochrome c flow cytometery assay

Cells (2×10^5) were collected by trypsinization, rinsed in PBS, and incubated in 200 μl digitonin solution (digitonin 50 μg/ml (Calbiochem), 100 mM KCl in PBS) on ice for 5 min. Cells were fixed using 500 μl of 4% paraformadehyde at room temperature for 20 minutes. Cells were washed three times in PBS, blocked for 1 hour in 500 μl blocking buffer (3% BSA, 0.05% Saponin (Sigma) in PBS), followed by incubation with anti-cytochrome c antibody 1:200 (Pharmingen, 6H2.B4) overnight at 4°C. Cells were washed three times with PBS and incubated for 1 hour in 50 μl of anti-Ig-FITC (DAKO, F0479) diluted 1:10 in PBS. The cells were rinsed in PBS, and re-suspended in 400 μl of PBS containing RNAse A (50 μg/ml) and propidium iodine (50 μg/ml) and incubated at room temperature for 1 hour. Measurement of DNA content was assessed in FL2 and cytochrome c fluorescence was measured in FL1 using a Becton Dickenson FACScalibur.

Results

Xaf1 induces apoptosis in Saos-2 cells

We established HA-Xaf1 inducible cell lines in the human osteosarcoma tumor cell line Saos-2. Five clones that were capable of significant induction of Xaf1 in response to doxycycline treatment were analyzed in initial experiments, and compared to clones containing only empty vector. Treatment of empty vector controls demonstrated no effect of doxycycline on the growth or apoptosis of Saos2 cells (data not shown). All Xaf1 clones behaved in a similar fashion, and the results from a typical clone are presented. Treatment of doxycycline results in accumulation of detectable levels of Xaf1 by 8 hours and as previously reported (Fig. 1A),Xaf1 is located throughout the nucleus [1], however, we also see predominant staining in sub-nuclear spots that have the appearance of nucleoli (Fig. 1B).

To determine if Xaf1 expression modulates cell cycle distribution and/or induces apoptosis in Saos2 cells, Xaf1 was induced and DNA content was measured by propidium iodide staining and flow cytometry (Fig. 1C and D). Apoptotic cells (those with less than 2N DNA content) begin accumulating at 12 hours after doxycycline treatment and increase to around 20–25% at 24 hours. In contrast, no significant effect on the cell cycle distribution is seen, with the small changes in proportion of cells in G1, S, and G2/M most likely an indirect consequence of the loss of cells by apoptosis.

Xaf1 cooperates with TNFα in the induction of apoptosis

XIAP is a broad specificity inhibitor of apoptosis, blocking cell death induced by both the death receptor and mitochondrial apoptotic pathways by direct interaction with caspases [13]. Relief of XIAP inhibition of caspase activity by Xaf1 expression would be predicted to cooperate with multiple inducers of apoptosis. This is supported by work from other investigators, indicating that Xaf1 enhances apoptosis induced by a variety of agents [1, 18].

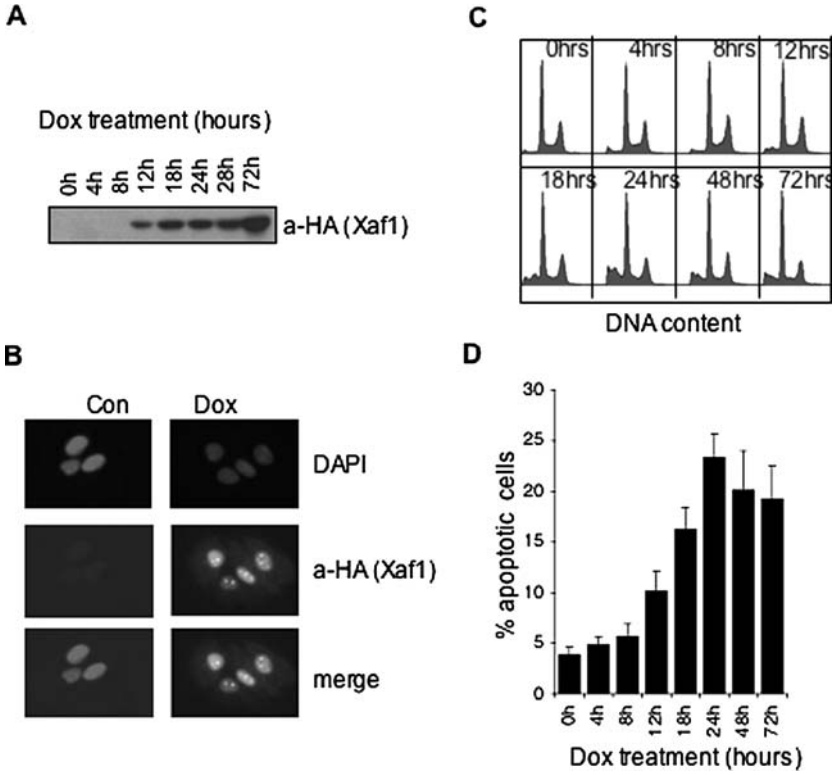

Fig. 1. Xaf1 induces apoptosis. Xaf1 tetracycline inducible cell lines were generated in Saos-2 cells. (A) Western blot showing accumulation of Xaf1 after addition of doxycycline for the times indicated. (B) Immunofluorescence of cells treated (where indicated) with doxycycline for 18 hours. Cells are stained with anti-HA (Xaf1 Green) and DAPI (Blue). (C) Flow cytometric profiles showing DNA content (x-axis) against cell number (y-axis) for Xaf1 inducible cells treated with doxycycline for the times indicated in the figure. (D) Average percentage of apoptotic cells (cells with less than 2N DNA content scored as apoptotic) after doxycycline treatment for the times indicated in the figure.

We tested if Xaf1 expression cooperated with the death receptor ligands TNFα and Apo2L/TRAIL in the induction of apoptosis in Saos-2 cells. Low levels of TNFα do not induce apoptosis in Saos-2 cells (2 ng/ml) [22], however, in combination with the inhibition of protein synthesis, these cells undergo dramatic apoptosis indicating the presence of functional receptors (Fig. 2A and 2B).In the Xaf1 inducible cell lines, treatment with TNFα induces around 10% apoptosis in the absence of doxycycline treatment (level in parental Saos2 and control lines is 2–3%) and this is increased to 50% after induction of Xaf1 for 24 hours. This rate of apoptosis is sufficient to eliminate almost all of the cells in culture. The observation that Xaf1 clones have increased sensitivity to apoptosis compared to the empty vector controls in the absence of doxycycline is presumably a consequence of some 'leakiness' in the system, suggesting that low levels of Xaf1 undetectable by western blot inhibit cell survival. In contrast to TNFα, this level of Apo2L/TRAIL does not significantly cooperate with Xaf1 in the induction of apoptosis, even though inhibition of protein synthesis was capable of rendering these cells extremely sensitive to this ligand (Fig. 2A and 2B). Increasing levels of Apo2L leads to an induction of apoptosis that was enhanced by Xaf1 expression, although the cooperation was not as dramatic as with TNFα (data not shown).

Xaf1 expression rendered Saos2 cells sensitive to UV induced apoptosis. In contrast, Adriamycin was unable to cooperate with Xaf1 in the induction of apoptosis. Despite Adriamycin inducing significant apoptosis alone, expression of Xaf1 did not increase the level of apoptosis (Fig. 2A and 2B).

XIAP independent function of Xaf1

To determine if the synergy between Xaf1 and TNFα was a consequence of an inhibition of XIAP function we first determined if these proteins were co-localized in the cell. Xaf1 is a nuclear protein and can re-localize XIAP from the cytosol to the nucleus [1]. In absence of doxycycline treatment, the sub-cellular localization of XIAP was determined to be in the cytosol, with staining typical for that seen in other cell types for this IAP. Induction of Xaf1 expression did not change the localization or staining pattern of XIAP (Fig. 3A).To confirm these results and obtain a more quantitative measure of the

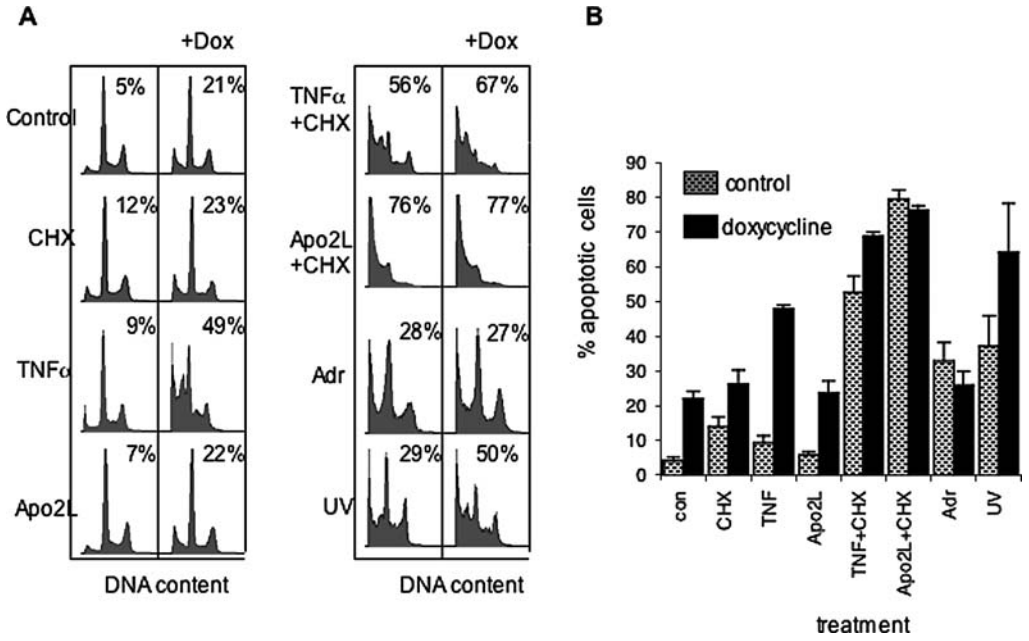

Fig. 2. Xaf1 cooperates with TNFα in the induction of apoptosis. (A) Flow cytometric profiles showing DNA content (x-axis) against cell number (y-axis) for Xaf1 inducible cells treated with doxycycline (DOX), cycloheximide (CHX), TNFα, Apo2L, Adriamycin and UV as indicated as indicated in the figure. The number in each box indicates percentage of apoptotic cells. (B) Average levels of apoptosis for Xaf1 inducible cells treated with the agents indicated in the Fig., with (solid bar) and without (hatched) doxycycline treatment.

location of Xaf1 and XIAP we treated the Xaf1 inducible cells with doxycycline, TNFα and doxycycline and TNFα together and fractionated the cells. Total cell extract indicates that the levels of XIAP are unchanged by either Xaf1 expression or Xaf1 and TNFα treatment in combination (Fig. 3B). Comparison of the nuclear and cytoplasmic fractions indicated that almost all detectable XIAP is in the cytosol and all almost all Xaf1 is in the nucleus (Fig. 3C). Even under conditions where Xaf1 is dramatically enhancing TNFα induced apoptosis, Xaf1 and XIAP are not co-localized.

One concern may be that in the generation of the lines, there may have been selection against cells in which Xaf1 and XIAP co-localized, since Xaf1 reduced colony formation relative to empty vector control plasmid. To test this, we transiently expressed HA-Xaf1 and Flag-XIAP in the parental Saos-2 cells, and performed immuno-precipitation to determine if there was any detectable interaction in this cell type. No interaction could be detected, nor can any co-localization be seen (Fig. 3D and data not shown).

These experiments provide strong evidence that Xaf1 is inducing apoptosis independently of XIAP. However, it is possible that a small fraction of total Xaf1 is sufficient to inhibit XIAP function in the cytosol. To eliminate this possibility we utilized fibroblasts derived from XIAP deficient mice [23]. These cells were transfected with Xaf1 and control vector expression constructs and treated with TNFα for 24 hours. Transfected cells were identified by staining positive for the transfection marker CD20, and apoptosis was assessed by measuring DNA content. Xaf1 expression increased the sensitivity of these fibroblasts to TNFα (Fig. 3E), clearly demonstrating a XIAP independent function of Xaf1.

Xaf1 and Xaf1+TNFα induced apoptosis require activation of the mitochondrial pathway

Although for convenience the death receptor and mitochondrial pathways are described separately, many cells require amplification of the apoptotic signal generated by death receptors through activation of the intrinsic pathway [24]. In some cell types this linking of the pathways is provided by the caspase 8 mediated cleavage of the BH3-only protein BID, this cleaved form translocates to the mitochondria triggering mitochondrial outer membrane permeabilization (MOMP) and release of cytochrome c [25, 26]. To determine if there is a requirement for activation of the mitochondrial apoptotic pathway for Xaf1 or Xaf1 and TNFα in combination to induce apoptosis, we transiently transfected the Xaf1 inducibles with Bcl2 expression constructs. The cells were treated with doxycycline, TNFα or both as indicated (Fig. 4),and apoptosis was assessed in the transfected population. Baculovirus p35 was utilized as a positive control, functioning as a broad specificity caspase inhibitor [27], and inhibited apoptosis induced by both Xaf1 expression and Xaf1 and TNFα in combination. Expression of Bcl2

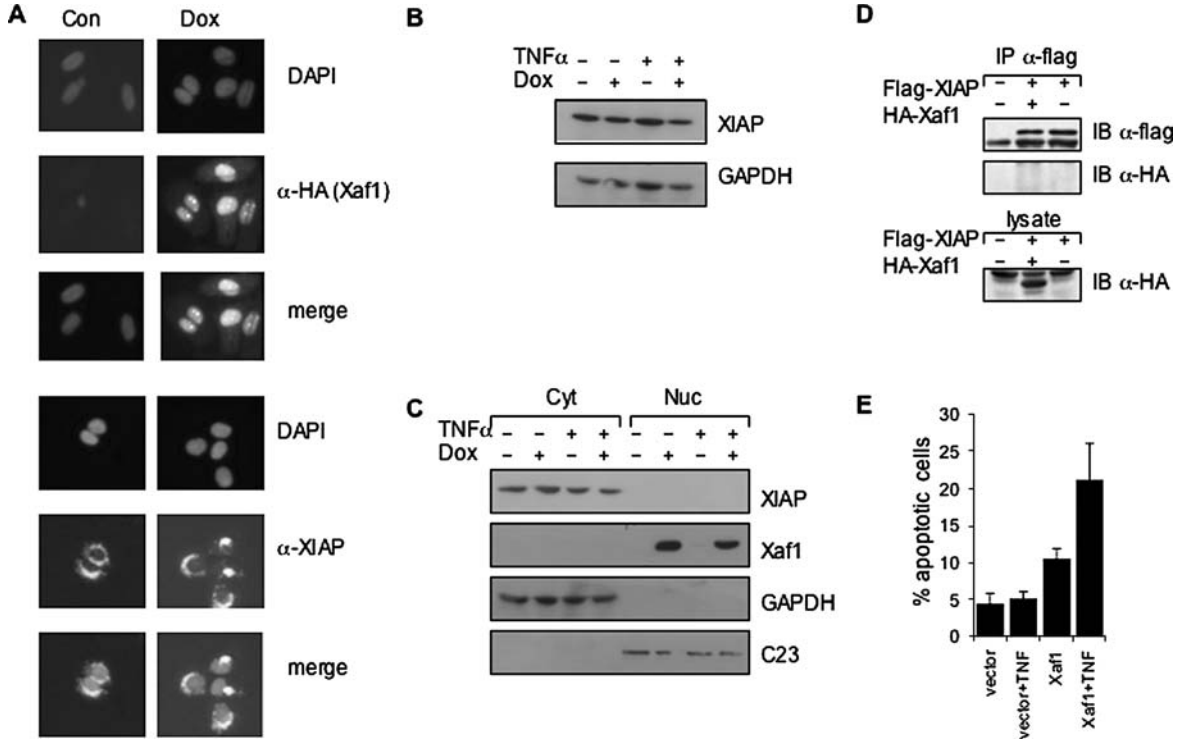

Fig. 3. XIAP independent function of Xaf1 (A) Immunofluorescence of cells treated (as indicated) with doxycycline for 18 hours. In the top three panels, cells are stained with anti-HA (Xaf1 Green) or anti-XIAP and DAPI (Blue). In the lower three panels cells are stained with anti-XIAP (Green) or anti-XIAP and DAPI (Blue). (B) Western blot showing XIAP levels after treatment with doxycycline, TNFα, doxycycline and TNFα for 24 hours. (C) Xaf1 inducible cells were treated with doxycycline, TNFα, doxycycline and TNFα for 24 hours as indicated in the figure. Western blot showing the levels of Xaf1 and XIAP in the nuclear and cytoplasmic fractions. Successful separation of nuclear and cytoplasmic fractions is verified by blotting for GAPDH (cytoplasmic) and C23 (nuclear). (D) Extracts of Saos2 cells transfected with plasmids encoding Flag-XIAP and HA-Xaf1 as indicated were immuno-precipitated with α-Flag and immuno-blotted with α-HA and α-Flag as indicated. Lower panel is a western blot using extract corresponding to 10% of protein used in the immuno-precipitation. (E) XIAP$^{-/-}$ mouse fibroblasts were transiently transfected with plasmids driving expression of Xaf1 or control empty vector and pCMV-CD20. The cells were treated with TNFα(20 ng/ml) for 24 hours, and apoptosis was measured by flow cytometry (those cells with less than 2N DNA content are scored as apoptotic). The graph expresses the average apoptotic rate for cells expressing CD20.

also inhibited all apoptosis triggered by Xaf1, and Xaf1 and TNFα in combination demonstrating that the apoptosis induced by Xaf1 requires engagement of the mitochondrial apoptotic pathway (Fig. 4).

Xaf1 triggers cytochrome c release

Bcl2 inhibition of Xaf1 induced apoptosis indicates a requirement for activation of the mitochondrial pathway. Although activation of the mitochondrial pathway by death receptors is caspase dependent, activation of this pathway can occur in a caspase independent manner. For example p53 induces expression of the BH3 only proteins PUMA and Noxa that antagonize Bcl2 function, promoting cytochrome c release [28, 29]. If Xaf1 is functioning only to relieve IAP mediated repression of caspase activity, then we would predict that caspase activity would be necessary for the Xaf1 mediated engagement of the mitochondrial pathway, leading to the release of cytochrome c and other pro-apoptotic molecules. By use of the pan-caspase inhibitor z-VAD, we can determine if caspase activity is necessary for the release of cytochrome c from the mitochondria.

As a quantitative measure of cytochrome c release we utilized flow cytometry. Digitonin permeabilization of the cell membrane allows cytochrome c that is not retained in the mitochondria to be leached out of the cell [30]. By minor modification of this protocol, we could measure DNA content and cytochrome c fluorescence on the same cells, allowing us to demonstrate the effectiveness of z-VAD caspase inhibition. Since DNA fragmentation is dependent on caspase activity, z-VAD blocks DNA fragmentation even if cytochrome c has been released from the mitochondria. We treated the cells with doxycycline for 18 hours and measured cytochrome c release and DNA content. As a control we treated cells with cycloheximide (CHX) and TNFα, as this results in a caspase dependent release of cytochrome c. Xaf1 expression triggered cytochrome c release, as more dramatically

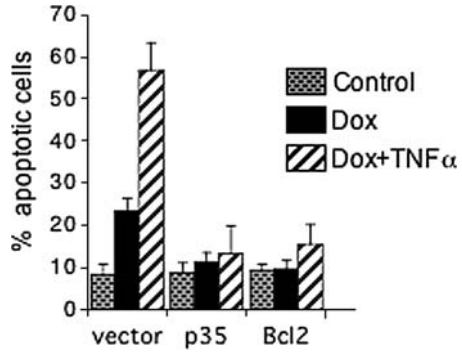

Fig. 4. Bcl2 inhibits Xaf1 induced apoptosis. The Xaf1 inducible cells were transiently transfected with p35, Bcl2 or control empty vector expression plasmids and pCMV-CD20. The cells were treated with doxycycline (2 μg/ml), TNFα(2 ng/ml), or TNFα and doxycycline 24 hours and apoptosis was measured by flow cytometry. The graph expresses the average apoptotic rate for cells expressing CD20.

did Xaf1+TNFα and CHX+TNFα treatment (Fig. 5A and B).Addition of z-VAD efficiently blocked cytochrome c release of the CHX+TNFα treated cells, in contrast the Xaf1 mediated release of cytochrome c was unaffected by z-VAD treatment (Fig. 5A and B). However, z-VAD treatment resulted in complete inhibition of Xaf1 mediated DNA fragmentation, indicating successful inhibition of caspase activity by z-VAD (Fig. 5B). Although TNFα and CHX induced dramatic release of cytochrome c, this was fully inhibited by z-VAD (Fig. 5C shows the results normalized, indicating almost 100% inhibition of cytochrome c release for TNFα and CHX treatment).

Treatment of cells with doxycycline and TNFα generates a similar level of DNA fragmentation and cytochrome c release as TNFα+CHX. In contrast although z-VAD treatment blocked DNA fragmentation efficiently, cytochrome c release was only partially blocked. This result is what we would predict as although TNFα promotes cytochrome c release by a caspase dependent mechanism, Xaf1 mediated cytochrome c release was not blocked by z-VAD. This data suggests that Xaf1 facilitates cytochrome c release independently of caspase activation, indicating that Xaf1 has apoptotic properties in addition to the relief of XIAP-mediated (or other IAP) caspase inhibition.

Discussion

We extended previous findings indicating that Xaf1 can cooperate with a number of agents in the induction of apoptosis to Saos2 cells. Xaf1 cooperated with both TNFα and Apo2L/TRAIL, although more dramatically with TNFα

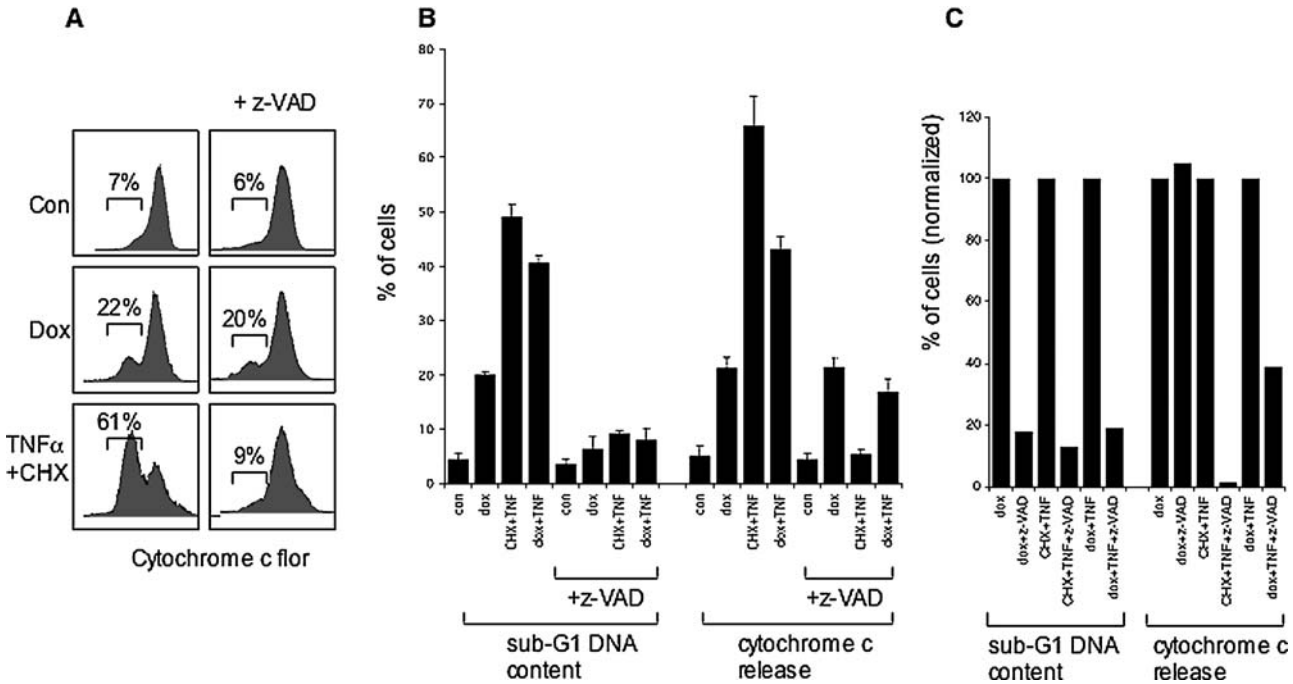

Fig. 5. Xaf1 triggers cytochrome c release by a caspase independent mechanism. The effect of z-VAD on Xaf1 induced apoptosis and cytochrome c release was measured by flow cytometry. Xaf1 inducible cells were treated as indicated with doxycycline, TNFα, CHX, and z-VAD for 24 hours. (A) Flow cytometric profiles showing log cytochrome c fluorescence (x-axis) and cell number (y-axis). (B) Average percentage of cells with less than 2N DNA content (apoptotic), and percentage of cells with released cytochrome c. (C) The results after normalization, showing relative inhibition of DNA fragmentation and cytochrome c release in the presence of z-VAD.

(Fig. 2 and data not shown). UV irradiation induced apoptosis was also enhanced by Xaf1 expression, however the chemotherapeutic drug Adriamycin was unable to cooperate with Xaf1, despite being capable of inducing apoptosis alone. The reason for the differences is unclear but may be related to the apoptotic pathways these agents stimulate, with Xaf1 perhaps cooperating more efficiently with death receptor signaling. Although UV can activate the mitochondrial apoptotic pathway [31–33], in some cell types UV can cross link the Fas receptor and TNFR1, independently of their ligands [34, 35]. However, further work is required to determine if Xaf1 cooperation is limited to agents activating death receptor signaling, and why Xaf1 cooperates more efficiently with TNFα than Apo2L/TRAIL.

Cooperation between Xaf1 and death receptors such as TNFR could occur at a number of levels. XIAP can inhibit apoptosis upstream of MOMP in response to death receptor signaling, by preventing full processing of caspase 3 [36]. Expression of Xaf1 would be predicted to neutralize XIAP repression of caspases thus enhancing death receptor induced apoptosis. Although work from other investigators indicates that that Xaf1 can function in this manner in some cell types [1, 18], the data here show no evidence for a Xaf1-XIAP interaction in Saos2 cells. Furthermore Xaf1 was able to sensitize XIAP$^{-/-}$ fibroblasts to TNFα, indicating that Xaf1 can promote apoptosis independently of XIAP (Fig. 6).

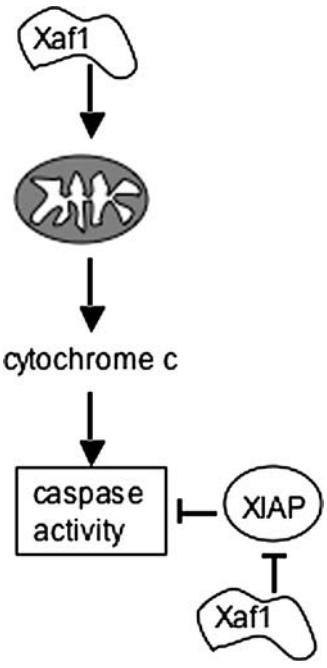

Fig. 6. Xaf1 can regulate apoptosis upstream and downstream of caspase activation. The model illustrates the points in the apoptotic cascade that Xaf1 can function. In addition to binding to XIAP reported by other investigators [1], our data demonstrate that Xaf1 can stimulate apoptosis by promoting the release of cytochrome c in a caspase independent manner.

Further studies are required to determine what signals control the interaction of Xaf1 and XIAP and the sub-cellular localization of these proteins, as well as the functional consequences. In addition to our data showing no co-localization, Leaman *et al*. have shown that interferon induced induction of Xaf1 results in Xaf1 accumulation in both nucleus and cytoplasm, however XIAP remains cytoplasmic [18]. XIAP has been reported in the nucleus in a number of papers, and interestingly can relocate from the cytosol to the nucleus in response to a number of stress signals [37–40]. Clearly in different cell types and/or under different conditions these proteins can locate to different sub-cellular compartments. An interesting possibility is that in response to certain stress conditions XIAP relocates to the nucleus to antagonize Xaf1 function, rather that Xaf1 antagonizing XIAP.

An obligatory role for the mitochondrial pathway in Xaf1 induced apoptosis is supported by the ability of Xaf1 alone to promote cytochrome c release, which cannot be inhibited by z-VAD. This data suggests that in Saos2 cells Xaf1 does not induce apoptosis by relief of IAP-mediated caspase inhibition. Further support for a role for the mitochondrial pathway in Xaf1 induced apoptosis is provided by our data demonstrating that Bcl2 can block Xaf1 induced apoptosis. Our data implicate Xaf1 as functioning upstream of the mitochondria in a caspase independent manner. All of the data are consistent with a role in facilitating cytochrome c release from mitochondria to amplify apoptotic signals. This may explain, at least in part, why Xaf1 cooperates with death receptor ligands such as TNFα, but not Adriamycin which itself can activate the mitochondrial apoptotic pathway.

How Xaf1 promotes cytochrome c release independently of caspase activation is unclear. A direct role at the mitochondria seems unlikely since almost all detectable Xaf1 is in the nucleus. However, since Bcl2 can inhibit Xaf1 induced apoptosis it is possible that the mechanism could involve the modulation of the level, activity, or location of BH family protein(s). A large family of Bcl2 related proteins exist including proteins that inhibit or induce apoptosis including certain BH3 only proteins that play key roles in activating this apoptotic pathway by antagonizing Bcl2-like proteins [28, 29, 41, 42]. Since Xaf1 expression is lost in a variety of tumor types and may function as a tumor suppressor further experiments to determine how Xaf1 induces apoptosis are warranted [2, 3, 5].

Acknowledgements

We would like to thank Krutika Haridas for technical assistance, Bob Korneluk and Peter Liston for providing the HA-Xaf1 construct and Colin Duckett, Gabriel Nunez, Alain Israel, Ed Harlow and Nancy Rice for the Flag-XIAP, p35, I-kB, CD20, and NF-kB expression constructs. The work

was supported in part by Georgia Cancer Coalition Distinguished Scholar Award GCC00032 to A.C.P, and a University of Michigan Biological Scholars Program, Department of Defense IDEA Award PC040215 and National Institutes of Health Grant GM067827 to C.S.D.

References

1. Liston P, Fong WG, Kelly NL, Toji S, Miyazaki T, Conte D, Tamai K, Craig CG, McBurney MW, Korneluk RG: Identification of XAF1 as an antagonist of XIAP anti-caspase activity. Nature Cell Biology 3: 128–133, 2001
2. Ng KC, Campos EI, Martinka M, Li G: XAF1 expression is significantly reduced in human melanoma. J Invest Dermatol 123: 1127–1134, 2004
3. Ma TL, Ni PH, Zhong J, Tan JH, Qiao MM, Jiang SH: Low expression of XIAP-associated factor 1 in human colorectal cancers. Chin J Dig Dis 6: 10–14, 2005
4. Fong WG, Liston P, Rajcan-Separovic E, St Jean M, Craig C, Korneluk RG: Expression and genetic analysis of XIAP-associated factor 1 (XAF1) in cancer cell lines. Genomics 70: 113–122, 2000
5. Byun DS, Cho K, Ryu BK, Lee MG, Kang MJ, Kim HR, Chi SG: Hypermethylation of XIAP-associated factor 1, a putative tumor suppressor gene from the 17p13.2 locus, in human gastric adenocarcinomas. Cancer Res 63: 7068–7075, 2003
6. Brunner T, Mueller C. Apoptosis in disease: about shortage and excess. Essays Biochem 39: 119–130, 2003
7. Thornberry NA, Lazebnik Y: Caspases: enemies within. Science 281: 1312–1316, 1998
8. Slee EA, Harte MT, Kluck RM, Wolf BB, Casiano CA, Newmeyer DD, Wang HG, Reed JC, Nicholson DW, Alnemri ES, Green DR, Martin SJ: Ordering the cytochrome c-initiated caspase cascade: hierarchical activation of caspases-2, -3, -6, -7, -8, and -10 in a caspase-9-dependent manner. J Cell Biol 144: 281–292, 1999
9. Ashkenazi A, Dixit VM: Apoptosis control by death and decoy receptors. Curr Opin Cell Biol 11: 255–260, 1999
10. Brenner C, Kroemer G: Apoptosis. Mitochondria–the death signal integrators. Science 289: 1150–1151, 2000
11. Sharpe JC, Arnoult D, Youle RJ: Control of mitochondrial permeability by Bcl-2 family members. Biochim Biophys Acta 1644: 107–113, 2004
12. Green DR, Reed JC: Mitochondria and apoptosis. Science 281: 1309–1312, 1998
13. Salvesen GS, Duckett CS: IAP proteins: Blocking the road to death's door. Nature Reviews Molecular Cell Biology 3: 401–410, 2002
14. Deveraux QL, Takahashi R, Salvesen GS, Reed JC: X-linked IAP is a direct inhibitor of cell-death proteases. Nature 388: 300–304, 1997
15. Suzuki Y, Nakabayashi Y, Nakata K, Reed JC, Takahashi R: X-linked inhibitor of apoptosis protein (XIAP) inhibits caspase-3 and-7 in distinct modes. Journal of Biological Chemistry 276: 27058–27063, 2001
16. Du CY, Fang M, Li YC, Li L, Wang XD: Smac, a mitochondrial protein that promotes cytochrome c- dependent caspase activation by eliminating IAP inhibition. Cell 102: 33–42, 2000
17. Suzuki Y, Imai Y, Nakayama H, Takahashi K, Takio K, Takahashi R: A serine protease, HtrA2, is released from the mitochondria and interacts with XIAP, inducing cell death. Molecular Cell 8: 613–621, 2001
18. Leaman DW, Chawla-Sarkar M., Vyas K, Reheman M, Tamai K, Toji S, Borden EC: Identification of X-linked inhibitor of apoptosis-associated factor-1 as an interferon-stimulated gene that augments TRAIL Apo2L-induced apoptosis. J Biol Chem 277: 28504–28511, 2002
19. Bates S, Ryan KM, Phillips AC, Vousden KH: Cell cycle arrest and DNA endoreduplication following p21(Waf1/Cip1) expression. Oncogene 17: 1691–1703, 1998.
20. Phillips AC, Bates S, Ryan KM, Helin K, Vousden KH: Induction of DNA synthesis and apoptosis are separable functions of E2F-1. Genes & Development 11: 1853–1863, 1997
21. Wadman IA, Osada H, Grutz GG, Agulnick AD, Westphal H, Forster A, Rabbitts TH: The LIM-only protein Lmo2 is a bridging molecule assembling an erythroid, DNA-binding complex which includes the TAL1, E47, GATA-1 and Ldb1/NLI proteins. Embo J 16: 3145–3157, 1997
22. Phillips AC, Ernst MK, Bates S, Rice NR, Vousden KH: E2F-1 potentiates cell death by blocking antiapoptotic signaling pathways. Molecular Cell 4: 771–781, 1999
23. Harlin H, Reffey SB, Duckett CS, Lindsten T, Thompson, CB: Characterization of XIAP-deficient mice. Molecular and Cellular Biology 21: 3604–3608, 2001
24. Green DR: Apoptotic pathways: the roads to ruin. Cell 94: 695–698, 1998
25. Luo X, Budihardjo I, Zou H, Slaughter C, Wang X: Bid, a Bcl2 interacting protein, mediates cytochrome c release from mitochondria in response to activation of cell surface death receptors. Cell 94: 481–490, 1998
26. Li H, Zhu H, Xu CJ, Yuan J: Cleavage of BID by caspase 8 mediates the mitochondrial damage in the Fas pathway of apoptosis. Cell 94: 491–501, 1998
27. Manji GA, Hozak RR, LaCount DJ, Friesen PD: Baculovirus inhibitor of apoptosis functions at or upstream of the apoptotic suppressor P35 to prevent programmed cell death. Journal of Virology 71: 4509–4516, 1997
28. Nakano K, Vousden KH: PUMA, a novel proapoptotic gene, is induced by p53. Molecular Cell 7: 683–694, 2001
29. Yu J, Zhang L, Hwang PM, Kinzler KW, Vogelstein B: PUMA induces the rapid apoptosis of colorectal cancer cells. Mol Cell 7: 673–682, 2001
30. Waterhouse NJ, Trapani J: A. A new quantitative assay for cytochrome c release in apoptotic cells. Cell Death Differ 10: 853–855, 2003
31. Scoltock AB, Cidlowski JA: Activation of intrinsic and extrinsic pathways in apoptotic signaling during UV-C-induced death of Jurkat cells: the role of caspase inhibition. Exp Cell Res 297: 212–223, 2004
32. Guzman E, Langowski JL, Owen-Schaub L: Mad dogs, Englishmen and apoptosis: the role of cell death in UV-induced skin cancer. Apoptosis 8: 315–325, 2003
33. Hakem R, Hakem A, Duncan GS, Henderson JT, Woo M, Soengas MS, Elia A, de la Pompa JL, Kagi D, Khoo W, Potter J, Yoshida R, Kaufman SA, Lowe SW, Penninger JM, Mak TW: Differential requirement for caspase 9 in apoptotic pathways in vivo. Cell 94: 339–352, 1998
34. Aragane Y, Kulms D, Metze D, Wilkes G, Poppelmann B, Luger TA, Schwarz T: Ultraviolet light induces apoptosis via direct activation of CD95 (Fas/APO-1) independently of its ligand CD95L. J Cell Biol 140: 171–182, 1998
35. Sheikh MS, Antinore MJ, Huang Y, Fornace AJ, Jr: Ultraviolet-irradiation-induced apoptosis is mediated via ligand independent activation of tumor necrosis factor receptor 1. Oncogene 17: 2555–2563, 1998
36. Wilkinson JC, Cepero E, Boise LH, Duckett CS: Upstream regulatory role for XIAP in receptor-mediated apoptosis. Mol Cell Biol 24: 7003–7014, 2004
37. Sauerwald TM, Betenbaugh MJ, Oyler GA: Inhibiting apoptosis in mammalian cell culture using the caspase inhibitor XIAP and deletion mutants. Biotechnol Bioeng 77: 704–716, 2002
38. Galvan V, Kurakin AV, Bredesen DE. Interaction of checkpoint kinase 1 and the X-linked inhibitor of apoptosis during mitosis. FEBS Lett 558: 57–62, 2004
39. Nowak D, Boehrer S, Brieger A, Kim SZ, Schaaf S, Hoelzer D, Mitrou PS, Weidmann E, Chow KU: Upon drug-induced apoptosis in

lymphoma cells X-linked inhibitor of apoptosis (XIAP) translocates from the cytosol to the nucleus. Leuk Lymphoma 45: 1429–1436, 2004
40. Siegelin M, Touzani O, Toutain J, Liston P, Rami A: Induction and redistribution of XAF1, a new antagonist of XIAP in the rat brain after transient focal ischemia. Neurobiol Dis, 2005
41. Oda E, Ohki R, Murasawa H, Nemoto J, Shibue T, Yamashita T, Tokino T, Taniguchi T, Tanaka N: Noxa, a BH3-only member of the Bcl-2 family and candidate mediator of p53-induced apoptosis. Science 288: 1053–1058, 2000
42. Jeffers JR, Parganas E, Lee Y, Yang C, Wang J, Brennan J, MacLean KH, Han J, Chittenden T, Ihle JN, McKinnon PJ, Cleveland JL, Zambetti GP: Puma is an essential mediator of p53-dependent and -independent apoptotic pathways. Cancer Cell 4: 321–328, 2003

Breast Cancer Res Treat (2008) 107:235–242
DOI 10.1007/s10549-007-9542-7

PRECLINICAL STUDY

EZH2 regulates the transcription of estrogen-responsive genes through association with REA, an estrogen receptor corepressor

Clara Hwang · Veda N. Giri · John C. Wilkinson · Casey W. Wright · Amanda S. Wilkinson · Kathleen A. Cooney · Colin S. Duckett

Received: 1 February 2007 / Accepted: 12 February 2007 / Published online: 24 April 2007

Abstract Enhancer of zeste homolog 2 (EZH2) is a histone methyltransferase polycomb group (PcG) protein, which has been implicated in the process of cellular differentiation and cancer progression for both breast and prostate cancer. Although transcriptional repression by histone modification appears to contribute to the process of cellular differentiation, it is unclear what mediates the specificity of PcG proteins. Since EZH2 requires a binding partner for its histone methyltransferase activity, we surmised that evaluating interacting proteins might shed light on how the activity of EZH2 is regulated. Here we describe the identification of a novel binding partner of EZH2, the repressor of estrogen receptor activity (REA). REA functions as a transcriptional corepressor of the estrogen receptor and can potentiate the effect of anti-estrogens. REA expression levels have also previously been associated with the degree of differentiation of human breast cancers. We show here that EZH2 can also mediate the repression of estrogen-dependent transcription, and that moreover, the ability of both REA and EZH2 to repress estrogen-dependent transcription are mutually dependent. These data suggest that EZH2 may be recruited to specific target genes by its interaction with the estrogen receptor corepressor REA. The identification of a novel interaction between EZH2 and REA, two transcription factors that have been linked to breast cancer carcinogenesis, may lead to further insights into the process of deregulated gene expression in breast cancer.

Keywords Cancer · Estradiol · Estrogen-dependent transcription · Estrogen receptor · EZH2 · REA

Clara Hwang and Veda N. Giri contributed equally to this work.

C. Hwang · K. A. Cooney · C. S. Duckett
Department of Internal Medicine, University of Michigan Medical School, Ann Arbor, MI 48109-0602, USA

V. N. Giri
Population Sciences and Medical Oncology, Fox Chase Cancer Center, Cheltenham, PA 19012, USA

J. C. Wilkinson · C. W. Wright · A. S. Wilkinson · C. S. Duckett (✉)
Department of Pathology, University of Michigan Medical School, Room 2000, 109 Zina Pitcher Pl, Ann Arbor, MI 48109, USA
e-mail: colind@umich.edu

K. A. Cooney
Department of Urology, University of Michigan Medical School, Ann Arbor, MI 48109, USA

Introduction

A growing body of evidence is accumulating to suggest a relationship between the fields of cancer biology and epigenetics, the study of heritable changes in gene function that occur without a change in DNA sequence [1]. These heritable changes, which are independent of DNA sequence, thus establish cellular identity within a multicellular organism. A major determinant of these heritable changes is modification of chromatin, the term for the structures formed by histone proteins and chromosomal DNA. Transcriptional regulation has been shown to depend in part on the dynamic change between open and compacted chromatin structure. Significantly, a growing number of genes involved in chromatin regulation have been implicated in cancer, including *BRCA1*, histone deacetylases (HDAC), and members of the polycomb group (PcG) of proteins.

Much recent interest has focused on EZH2, a PcG protein. EZH2 is a homolog of the *Drosophila* protein Enhancer of zeste, critical to development and cell differentiation [2–5]. The catalytic activity of EZH2 is contained in its SET domain, which methylates histone lysine residues, affecting chromatin structure and gene transcription. The catalytic activity of EZH2 appears to be regulated by its binding partners, since the multimeric complexes containing EZH2 change during differentiation, along with their substrate specificity [6]. EZH2 is critical for embryonic development, as demonstrated by the phenotype of EZH2-null mice, which is embryonic lethal [6]. Furthermore, EZH2 is preferentially expressed in embryonic tissues and is normally not expressed in terminally differentiated adult tissues. In contrast, EZH2 appears to be overexpressed in various malignancies, including steroid-dependent malignancies such as breast cancer, prostate cancer, multiple myeloma and lymphoma [7–18]. EZH2 overexpression also correlates strongly with tumor differentiation and pathologic grade for both breast and prostate cancer [7–9]. This observation may follow from the preferential expression of EZH2 in embryonic over terminally differentiated tissues. In addition to the finding of EZH2 overexpression in neoplastic cells, EZH2 overexpression is a powerful independent prognostic factor, correlating with metastatic disease and survival for both prostate and breast cancer [7, 8]. EZH2 also appears to be important in conferring a malignant phenotype to cells, and may be a *bona fide* oncogene. Knockdown of EZH2 dramatically reduces proliferation and induces growth arrest in prostate cancer and multiple myeloma cell lines [7, 10, 17]. Conversely, overexpression of EZH2 contributes to anchorage-independent growth, an invasive phenotype, and growth-factor independence [7, 10]. Finally, the overexpression of EZH2 is sufficient to induce oncogenic potential in a xenograft model [10].

Although EZH2 appears to play a role in neoplastic transformation, it remains unclear how EZH2 may contribute to the regulation of various developmental programs and their deregulation in cancer. Furthermore, although it has been shown that EZH2 expression correlates with differentiation of hormone-sensitive epithelial tissues such as breast and prostate, the mechanism underlying this correlation has not yet been determined. Since EZH2 requires a binding partner for its histone methyltransferase activity, we postulated that evaluating interacting proteins might shed light on how the activity of EZH2 is regulated. Using a biochemical screen to identify EZH2-interacting proteins, we have identified Repressor of Estrogen receptor Activity (REA) as a novel binding partner of EZH2 and confirmed this interaction in human cells. EZH2 was also found to repress estrogen-dependent signaling in a manner dependent on the presence of REA. Together, these data suggest that EZH2 and REA cooperate to regulate transcription of estrogen-dependent genes and may further our understanding of aberrant transcriptional regulation in hormonally regulated tumors such as breast and prostate cancer.

Materials and methods

Plasmids and RNA interference

The plasmids pEBB, pEBG, pEBB-FLAG, pEBB-HA, pEBB-CTAP, and pFG12 have been described previously [19–22]. EZH2 coding sequence was PCR amplified from an IMAGE EST clone 4521628 and subcloned into pEBB-CTAP, pEBB-FLAG and pEBG to construct pEBB-EZH2-TAP, pEBB-EZH2-FLAG, and pEBG-EZH2, respectively. The REA coding sequence was cloned from IMAGE EST clone 5728265 using PCR amplification and subcloned into pEBB-HA to generate pEBB-REA-HA. Sequences encoding a short-hairpin RNA targeting EZH2 or REA were subcloned into pFG12 for RNA-interference experiments using a lentiviral delivery system. All plasmids were sequenced to confirm correspondence with published data. Small interfering RNA oligonucleotides sequences were submitted to Qiagen for oligonucleotide synthesis. Sequences used for RNA interference are available upon request. pGL3-ERE2bf-TATA-luc and pSG5-ER were kindly provided by R. Koenig.

Cell culture, transfection, and co-precipitation

HEK293 and 293T cells were grown in Dulbecco's Modified Eagle's Medium (Cellgro, Herndon, VA, USA) and supplemented with 2 mM L-glutamine and 10% fetal bovine serum. MDA-MB-231 cells were grown in RPMI 1640 supplemented with 1% glutamax and 10% fetal bovine serum. When indicated, phenol-red free media and charcoal-stripped fetal bovine serum (Hyclone, Logan, UT, USA) were used to eliminate background estrogen signaling. A standard calcium phosphate method [23] was used to transfect both plasmid and siRNA into HEK293 cells and 293T cells. For transfection of siRNA, MDA-MB-231 cells were transfected with lipofectamine (Invitrogen, Carlsbad, CA, USA) using a protocol provided by the supplier. Alternatively, the Amaxa nucleofection system was employed, using program A-23 and nucleofector solution T, according to the recommendations of the manufacturer. Lentiviral production using 293T-cells was performed as previously described [22].

For co-precipitation experiments, HEK293 cells were transfected with pEBG-EZH2, pEBB-REA-HA or appropriate control plasmids. Cell lysates were prepared with Triton-X 100 lysis buffer. Glutathione sepharose beads (Amersham, Piscataway, NJ, USA) were added and the

samples were incubated at 4°C for 3-6 h. After washing beads four times with lysis buffer, pelleted material was resuspended in LDS loading buffer (Invitrogen) and used for immunoblotting as described below.

Tandem affinity purification

HEK293 cells were transfected with 12 μg of pEBB-EZH2-TAP plasmid per 15-cm plate. After 2 days, cells were harvested and lysed in Triton lysis buffer (25 mM HEPES, 100 mM NaCl, 1 mM EDTA, 10% glycerol, 1% Triton X-100, protease inhibitors); cell lysate was supplemented with NaCl and Nonidet P-40. Lysate was applied to a chromatography column containing IgG-Sepharose beads (Amersham) and incubated for 2 h at 4°C. The column was drained and washed with IPP150 buffer (10 mM Tris–HCl, pH+ 8.0, 150 mM NaCl, 0.1% Nonidet P-40, protease inhibitors) and TEV cleavage buffer (10 mM Tris–HCl, pH+ 8.0, 150 mM NaCl, 0.1% Nonidet P-40, 0.5 mM EDTA, 1 mM dithiothreitol, protease inhibitors). After incubation for 2 h at 16°C in TEV cleavage buffer supplemented with TEV enzyme (Invitrogen), the eluate was collected and supplemented with $CaCl_2$ and IPP150 calmodulin binding buffer (10 mM Tris–HCl, pH+ 8.0, 150 mM NaCl, 0.1% Nonidet P-40, 1 mM magnesium acetate, 1 mM imidazole, 2 mM CaCl2, 10 mM β-mercaptoethanol). The supplemented eluate was applied to a chromatography column containing calmodulin 4B beads (Amersham) and incubated at 4°C for 1 h. After this incubation, the column was drained and washed with IPP150 calmodulin binding buffer. A final eluate was collected after incubation at 4°C with IPP150 calmodulin elution buffer (10 mM Tris–HCl, pH+ 8.0, 150 mM NaCl, 0.1% Nonidet P-40, 1 mM magnesium acetate, 1 mM imidazole, 2 mM EGTA, 10 mM β-mercaptoethanol). Proteins were precipitated by adding cold 10% trichloroacetic acid in acetone and incubation overnight at –20°C. The samples were centrifuged at 4°C (10,000×g for 30 min) and precipitate was then rinsed in 100% acetone and allowed to air dry. These protein precipitates were submitted to the Proteomics Centre (http://www.protein-centre.com) at the University of Victoria for tryptic digestion, high-performance liquid chromatography separation, and tandem mass spectrometry (MS/MS) to determine peptide sequences. REA was identified as a putative EZH2-interacting protein based upon the peptide sequence QVAQQEAQR.

Western blot analyses

Whole cell extracts were prepared with Triton lysis buffer or RIPA lysis buffer (PBS, 1% NP-40, 0.5% sodium deoxycholate, 0.1% SDS) supplemented with 1 mM PMSF, one protease inhibitor tablet (Roche, Penzberg, Germany) per 10 ml of buffer, and 10 mM DTT. Proteins were separated by electrophoresis on 4–12% gradient Novex Bis–Tris gels (Invitrogen), transferred to nitrocellulose membranes (Invitrogen) and blocked with 5% milk solution in TBS containing between 0.05 and 0.1% Tween-20, dependent on the antibody. The membranes were incubated with the relevant primary and secondary antibodies followed by antibody detection. Antibody detection was performed with an enhanced chemiluminescence system according to the manufacturer's directions (Amersham). Primary HRP-conjugated antibodies against FLAG and HA were obtained from Sigma, St.Louis, MO, USA. Other primary antibodies used included rabbit polyclonal antibodies against GST (Santa Cruz, CA, USA), REA and EZH2 (Upstate, NJ, USA), and a mouse monoclonal antibody against β-actin (Sigma). Secondary antibodies used were HRP-conjugated donkey anti-rabbit and HRP-conjugated sheep anti-mouse (Amersham).

Confocal and fluorescence microscopy

HEK293 cells (5×10^4 per well) were plated on poly lysine coated chambered coverglass slides. Cells were transfected by calcium phosphate precipitation with pEBB-EZH2-FLAG, pEBB-REA-HA or both. Twenty-four hours after transfection cells were washed with D-PBS (Dulbecco's phosphate-buffered saline), fixed in 4% paraformaldehyde, and then permeablized in a solution of 0.1% Triton X-100/1% goat serum in D-PBS. Antibody staining was completed as follows: cells were blocked with 20% goat serum in D-PBS for 1 h at room temperature and then incubated with primary antibodies (anti-FLAG-FITC, anti-HA-Alexa594) for 1 h at room temperature in the dark. Following three washes with D-PBS, cells were stained with Hoechst 33342, chamber slides were allowed to air dry, and mounted with Pro-long Gold (Molecular probes, Eugene, OR, USA/Invitrogen) according to manufacturer's instructions. Samples were then examined using a Zeiss Axiovert 100 M Confocal microscope equipped with a Zeiss LSM 510 spectrometer.

Luciferase assay

For luciferase reporter experiments, cells were seeded in 6-well plates and transfected with the relevant plasmids and siRNA, in addition to an estrogen receptor-expressing plasmid (pSG5-ER) and the reporter plasmid pGL3-ERE2bf-TATA-luc. The following day, cells were exposed to β-estradiol (Sigma) at a final concentration of 10^{-8} M, or an equivalent volume of ethanol, the vehicle used to solubilize β-estradiol. The Promega reporter lysis buffer and luciferase assay kit were used, with assays performed

according to the manufacturer's protocol. Cells were assayed for luciferase reporter activity 1 day after estrogen treatment.

Results

Although EZH2 contains the enzymatic domain responsible for histone methylation, its target specificity appears to be driven by its binding partners [6]. For this reason, and due to the apparent role of EZH2 in cell-identity and cancer progression, we were interested in identifying novel EZH2-binding partners. Using the tandem affinity purification (TAP) system [24], a variety of peptides were isolated and sequenced to identify candidate binding partners of EZH2. This screen suggested an interaction between EZH2 and the Repressor of Estrogen Activity (REA) protein. REA has been reported to act as a corepressor in estrogen-dependent transcription by binding to the estrogen receptor [25]. In addition, a decreased level of REA expression has been correlated with high-grade, poorly differentiated breast cancer [26]. Based on the novel nature of the interaction between EZH2 and REA and the potential role of REA in neoplasia, we chose to further investigate this interaction.

The interaction between REA and EZH2 was confirmed through a GST-fusion protein pull-down experiment. GST was fused to the EZH2 protein and co-transfected into cells with plasmid expressing REA fused to an HA tag. REA-HA was found to co-precipitate with EZH2-GST in extracts from cells transfected with both plasmids (Fig. 1a). REA-HA did not co-precipitate with GST alone, indicating the specific nature of this interaction. The interaction between EZH2 and REA was further analyzed in co-localization experiments. The subcellular localization patterns of both EZH2 and REA were examined using an immunofluorescence approach. HEK293 cells were transfected with plasmids encoding both EZH2-FLAG and REA-HA and stained with FITC-conjugated anti-FLAG and Alexa-594 conjugated anti-HA prior to analysis by confocal microscopy. As shown in Fig. 1b, REA displayed a predominantly cytoplasmic localization, with a small portion of the protein detected in the nucleus. In contrast, EZH2 was completely nuclear, with no detectable fluorescence in the cytoplasm. Interestingly, EZH2 localization within the nucleus was in the form of discrete foci, rather than diffuse within each nucleus.

Since REA has previously been shown to bind the estrogen receptor and repress transcription [25, 27], we asked whether EZH2 might also play a role in estrogen-dependent transcription. RNA interference was used to reduce levels of EZH2 and examine the role of EZH2 in this system. HEK293 cells were transfected with a siRNA oligonucleotide specific for the EZH2 transcript (siEZH2). The protein levels of endogenous EZH2 were specifically and effectively reduced with siEZH2, as shown in Fig. 2a. This siRNA was used to evaluate the effect of EZH2 depletion on the expression of a luciferase reporter construct whose promoter contained canonical estrogen-response elements. As expected, when transfected into both HEK293 cells and MDAMB231 cells, transcription was robustly activated by the addition of estradiol (E2) to the cell media (Fig. 2b, c, first three bars). In both of these systems, there was little basal activity in the absence of estradiol. When EZH2 levels were reduced in HEK293 cells, estrogen-dependent transcription was increased

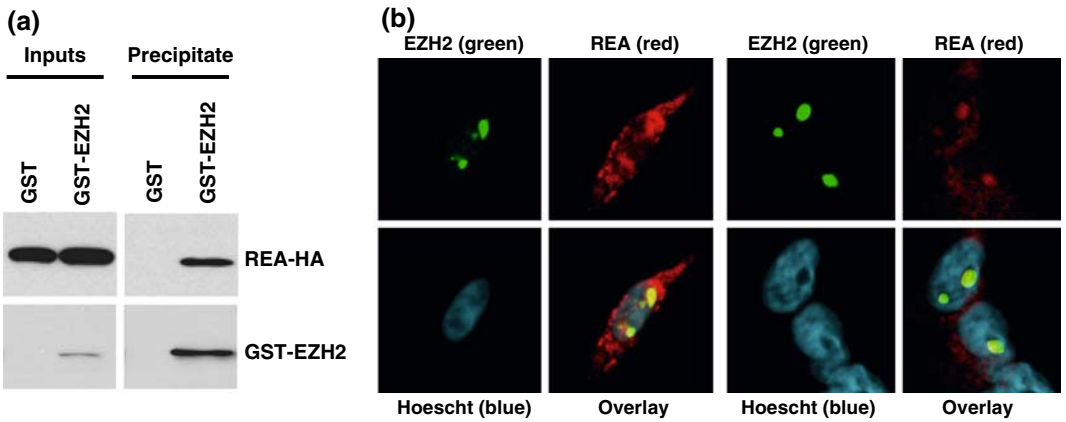

Fig. 1 Interaction between EZH2 and REA. (**a**) GST-pulldown assay using EZH2-GST. HEK293 cells were co-transfected with REA-HA and either EZH2-GST or GST. Cell lysates were prepared and purified using the affinity of GST for glutathione. Input lysates and pulldowns were immunoblotted and probed for either HA (*top panels*) or GST (*bottom panels*). (**b**) Co-localization of EZH2 and REA. HEK293 cells were co-transfected with separate plasmids constructed to express EZH2-FLAG and REA-HA fusion proteins. Immunofluorescence staining was performed using anti-FLAG (*green, left upper panel*) and anti-HA antibodies (*red, right upper panel*). Nuclei were stained with Hoescht (*blue, left lower panel*). The overlay image is shown in the right lower panel.

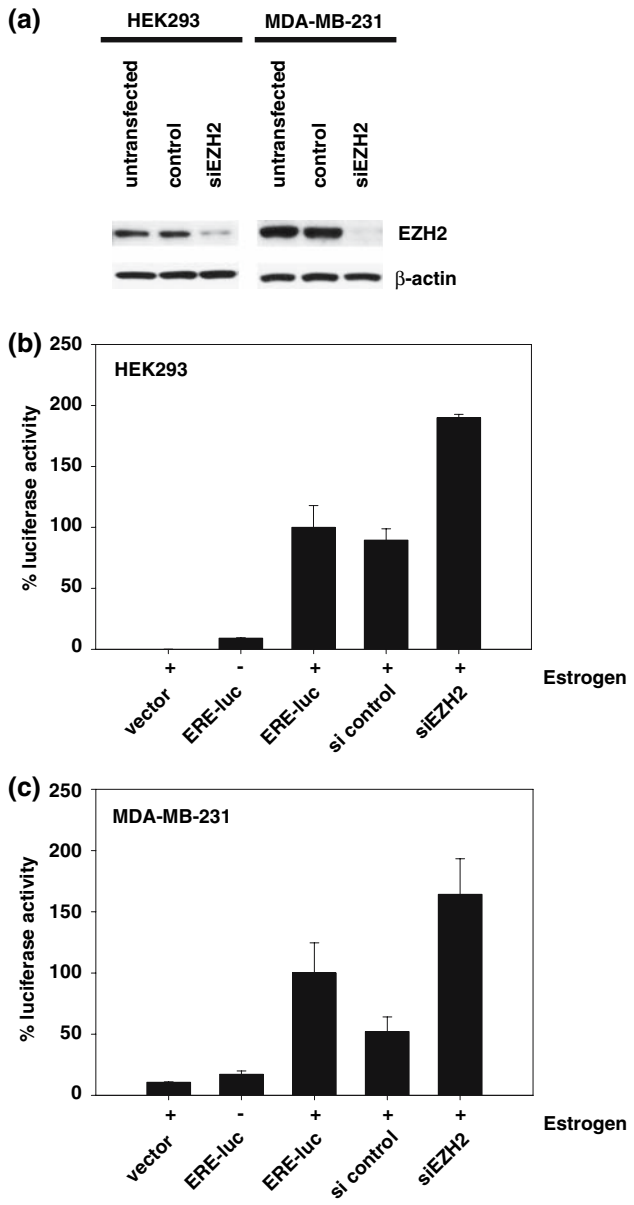

◄ **Fig. 2** siRNA-mediated reduction in EZH2 expression increases ERE-dependent transcription. (**a**) HEK293 cells were transfected with either siEZH2 or siGFP using a calcium phosphate method. Lysates were prepared for Western blot analysis and probed using an antibody that recognized endogenous EZH2. Transfection of siEZH2 was able to efficiently decrease EZH2 expression in HEK293 cells. Similar results were achieved using siEZH2 to reduce the expression of EZH2 in MDA-MB-231 breast cancer cells. (**b**) Estrogen-dependent transcription was evaluated using a luciferase reporter system. Transcription of the luciferase gene from the plasmid pGL3-ERE2bf-TATA-luc is estrogen-dependent due to the two estrogen-response elements (*ERE*) in its promoter. pSG5-ER, which expresses the estrogen receptor (*ER*), was co-transfected with pGL3-ERE2bf-TATA-luc to enable estrogen-mediated transcription. Cells were cultured in phenol red-free media supplemented with charcoal-stripped serum to eliminate substances that would cross-react with the estrogen receptor. Luciferase transcription was confirmed to be estrogen dependent (+E2). Transcription increased with transfection of siEZH2 compared to siGFP control. (**c**) Estrogen-dependent transcription was also evaluated in MDA-MB-231 cells in a similar fashion. EZH2 levels were reduced with the introduction of a small interfering RNA oligonucleotide and the effect on transcription of pGL2-ERE2bf-TAT-luc was examined.

(Fig. 2b). This increase in estrogen-dependent transcription did not occur with a control siRNA oligonucleotide, indicating the specific nature of this result. Similar results were obtained from a parallel analysis in MDA-MB-231 cells, a breast cancer cell line. Estrogen-dependent transcription was increased when EZH2 levels were reduced using siEZH2 (Fig. 2c).

Since decreasing the expression of EZH2 increased ERE-dependent transcription, we also asked if the converse was also true; that is, if overexpression of EZH2 would repress transcription in this system. EZH2- and REA-expressing plasmids were transfected into an MDA-MB-231 cell line. Consistent with previous reports, REA repressed transcription from the ERE-luciferase reporter plasmid. Moreover, overexpression of EZH2 was also shown to repress transcription from an estrogen-dependent promoter, a novel observation. The effects of REA and EZH2 on estrogen-dependent transcription were further examined to determine if their effects were additive. When REA and EZH2 were co-transfected, transcriptional levels were repressed, but only to the same level as with REA or EZH2 alone, indicating that the transcriptional effects of REA and EZH2 in this system were not additive (Fig. 3b).

Finally, the repression of estrogen-dependent transcription by REA and EZH2 was investigated to assess whether REA and EZH2 acted independently or were mutually dependent. To answer this question, cell lines in which EZH2 or REA expression was stably reduced were established. A decrease in REA and EZH2 expression is demonstrated by Western blot of lysates from these cells (Fig. 3a). ERE-dependent transcription in these cell lines was examined. In a manner similar to our results with transient reduction of EZH2, transcription from the ERE-luciferase reporter construct increased when either REA or EZH2 levels were reduced in a stable fashion (Fig. 3b). The effect of EZH2 or REA overexpression was then evaluated in the absence of the other protein. Significantly, EZH2-mediated repression was abrogated in cell lines expressing the shREA knockdown construct (Fig. 3c). In addition, reducing the expression of EZH2 resulted in attenuation of REA-mediated repression. These results indicate that the repression of estrogen-dependent transcription by EZH2 is dependent on the presence of REA and that the transcriptional repression of REA also depends in part upon EZH2. Together, these data suggest a model in which EZH2 and REA are recruited together to promoters containing estrogen-response elements to modulate ER-dependent transcription.

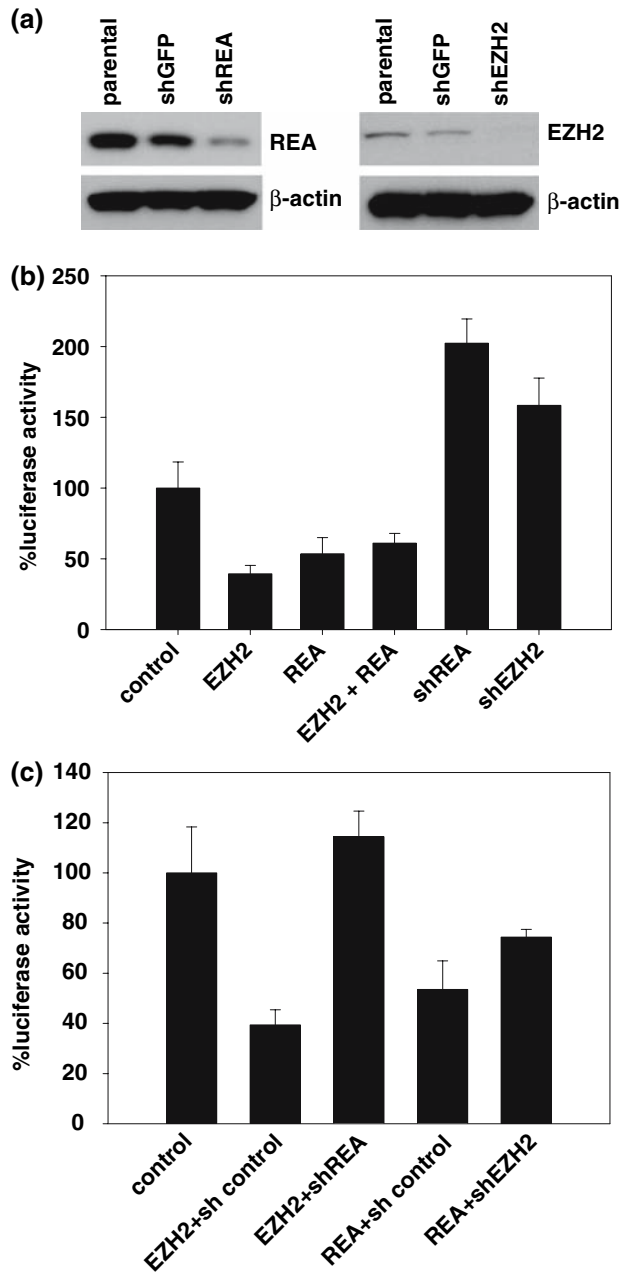

Fig. 3 Effects of EZH2 and REA expression on ERE-transcription in a lentiviral system. (**a**) MDA-MB-231 cells were infected with lentivirus constructs designed to express short hairpin RNA that interfere with either REA, EZH2 or GFP expression. Immunoblotting with anti-REA (*left panel*) or anti-EZH2 (*right panel*) demonstrates reduced expression of target proteins. (**b**) Cell lines were transfected and luciferase activity was determined under various conditions: control (shGFP and pEBB); EZH2 (shGFP and pEBB-EZH2-Flag); REA (shGFP and pEBB-REA-HA); EZH2 + REA (shGFP, pEBB-EZH2-Flag, and pEBB-REA-HA); shREA (shREA and pEBB); shEZH2 (shEZH2 and pEBB). (**c**) Cell lines were transfected as follows and luciferase activity was determined: control (shGFP and pEBB); EZH2 and sh control (shGFP and pEBB-EZH2-Flag); EZH2 and shREA (shREA and pEBB-EZH2-Flag); REA and sh control (shGFP and pEBB-REA-HA); REA and shEZH2 (shFZH2 and pEBB-REA-HA)

Discussion

In this study, we report a novel interaction between the transcription factors EZH2 and REA. The protein REA was identified based on a peptide sequence obtained from a biochemical screen searching for EZH2-binding partners. This interaction was confirmed using full-length protein and a GST-pulldown technique (Fig. 1a). Examination of EZH2 and REA localization patterns also displayed significant overlap between their subcellular localization (Fig. 1b). EZH2 and REA were observed to co-localize within discrete nuclear foci. Interestingly, only a subset of REA was found to localize in these nuclear foci while the remainder was seen within the cytoplasm. On the other hand, EZH2 was only visualized within these discrete nuclear foci.

EZH2 was also shown to modulate the transcriptional activity of the estrogen receptor (Figs. 2, 3). The ability of EZH2 to methylate specific histone lysine residues has been associated with a compacted chromatin structure and transcriptional repression. It is possible that the transcriptional repression seen in response to overexpression of EZH2 may be a nonspecific effect. However, the repression of EZH2 of estrogen-repressor mediated transcription appears to be dependent on REA. When the expression of REA was silenced by an RNA interference approach, there was no repression of estrogen receptor transcription seen with EZH2 overexpression. In addition, silencing EZH2 repression partially reverses the transcriptional repression seen with REA. These data suggest that the interaction of REA and EZH2 is responsible for the recruitment of EZH2 to ERE-containing promoters and the dampening of ER transcription.

Kurtev et al. have previously shown that REA interacts with both classes I and II HDAC [28]. HDAC are also chromatin-modifying enzymes that have been implicated in development and carcinogenesis. Based on their observations, Kurtev et al. proposed that REA acts as a corepressor by recruiting HDAC to nuclear receptor target genes. They demonstrated that REA-mediated transcriptional repression of estrogen receptor activity is partially reversed by a specific histone deacetylase inhibitor, trichostatin A. Because this reversal was only partial, they suggested that the transcriptional effects of REA may be mediated in part by a HDAC-independent mechanism. This conjecture is further supported by their demonstration that REA contains a domain able to repress ER transcription but does not bind to HDAC. The interaction of REA with EZH2, a histone lysine methyltransferase, may, at least in part, explain the HDAC-independent repressive properties of REA.

Although EZH2 has been associated with embryonic development and the determination of cellular identity, it

is unclear how EZH2-mediated repression coordinates the transcription of a specific set of genes involved in differentiation. REA also appears to play a critical role in embryonal development, as REA-deficiency in the mouse is embryonic lethal at embryonic day 9 [29]. REA acts a corepressor in estrogen-dependent transcription by binding to the estrogen receptor [25, 27]. Significantly, a decreased level of REA expression is correlated with high-grade, poorly differentiated breast cancer [26, 30]. This may be due to the repression of genes that are normally induced by estrogen and the estrogen receptor. The interaction of EZH2 and REA may, in a similar fashion, shed light on the association seen between EZH2 overexpression and the degree of differentiation seen in human breast cancer cases.

The association of nuclear receptors and chromatin remodeling proteins in cancer echoes findings of other model systems. For example, the remarkable clinical success of differentiation therapy in acute promyelocytic leukemia was dependent on the ability of retinoic acid to reverse the differentiation block induced by aberrant recruitment of HDAC to retinoic acid target genes [31]. This HDAC recruitment is mediated by N-Cor and SMRT, corepressors of the retinoic acid receptor. In a similar fashion, mounting evidence also points to the importance of histone-modifying enzymes in breast and prostate cancer, solid tumors, which are steroid hormone-dependent. The data presented here contribute to our understanding of the relationship between chromatin-modifying enzymes such as EZH2 in the differentiation of hormonally regulated tissues. Unraveling the key determinants of differentiation in these cell types and neoplasms may yield to the identification of potential targets for differentiation therapy in solid tumors.

Acknowledgments We thank Dr. Ron Koenig of the University of Michigan for his kind gift of the ER-expressing and ERE-luciferase reporter plasmids. We also acknowledge members of the Duckett lab for helpful discussions and critical reading of this manuscript. In addition, we specifically thank Karolyn Oetjen and David Kosoff for their contributions to this work. This work was supported by a grant from the Department of Defense (W81XWH-04-1-0314).

References

1. Ting AH, McGarvey KM, Baylin SB (2006) The cancer epigenome—components and functional correlates. Genes Dev 20:3215–3231
2. Cao R, Wang L, Wang H, Xia L, Erdjument-Bromage H, Tempst P, Jones RS, Zhang Y (2002) Role of histone H3 lysine 27 methylation in polycomb-group silencing. Science 298:1039–1043
3. Czermin B, Melfi R, McCabe D, Seitz V, Imhof A, Pirrotta V (2002) Drosophila enhancer of zeste/ESC complexes have a histone H3 methyltransferase activity that marks chromosomal polycomb sites. Cell 111:185–196
4. Kuzmichev A, Nishioka K, Erdjument-Bromage H, Tempst P, Reinberg D (2002) Histone methyltransferase activity associated with a human multiprotein complex containing the enhancer of zeste protein. Genes Dev 16:2893–2905
5. Muller J, Hart CM, Francis NJ, Vargas ML, Sengupta A, Wild B, Miller EL, O'Connor MB, Kingston RE, Simon JA (2002) Histone methyltransferase activity of a *Drosophila* polycomb group repressor complex. Cell 111:197–208
6. Kuzmichev A, Margueron R, Vaquero A, Preissner TS, Scher M, Kirmizis A, Ouyang X, Brockdorff N, Abate-Shen C, Farnham P, Reinberg D (2005) Composition and histone substrates of polycomb repressive group complexes change during cellular differentiation. Proc Natl Acad Sci USA 102:1859–1864
7. Varambally S, Dhanasekaran SM, Zhou M, Barrette TR, Kumar-Sinha C, Sanda MG, Ghosh D, Pienta KJ, Sewalt RG, Otte AP, Rubin MA, Chinnaiyan AM (2002) The polycomb group protein EZH2 is involved in progression of prostate cancer. Nature 419:624–629
8. Kleer CG, Cao Q, Varambally S, Shen R, Ota I, Tomlins SA, Ghosh D, Sewalt RG, Otte AP, Hayes DF, Sabel MS, Livant D, Weiss SJ, Rubin MA, Chinnaiyan AM (2003) EZH2 is a marker of aggressive breast cancer and promotes neoplastic transformation of breast epithelial cells. Proc Natl Acad Sci USA 100:11606–11611
9. Raaphorst FM, Meijer CJ, Fieret E, Blokzijl T, Mommers E, Buerger H, Packeisen J, Sewalt RA, Otte AP, van Diest PJ (2003) Poorly differentiated breast carcinoma is associated with increased expression of the human polycomb group EZH2 gene. Neoplasia 5:481–488
10. Croonquist PA, Van Ness B (2005) The polycomb group protein enhancer of zeste homolog 2 (EZH2) is an oncogene that influences myeloma cell growth and the mutant ras phenotype. Oncogene 24:6269–6280
11. Weikert S, Christoph F, Kollermann J, Muller M, Schrader M, Miller K, Krause H (2005) Expression levels of the EZH2 polycomb transcriptional repressor correlate with aggressiveness and invasive potential of bladder carcinomas. Int J Mol Med 16:349–353
12. Visser HP, Gunster MJ, Kluin-Nelemans HC, Manders EM, Raaphorst FM, Meijer CJ, Willemze R, Otte AP (2001) The polycomb group protein EZH2 is upregulated in proliferating, cultured human mantle cell lymphoma. Br J Haematol 112:950–958
13. van Kemenade FJ, Raaphorst FM, Blokzijl T, Fieret E, Hamer KM, Satijn DP, Otte AP, Meijer CJ (2001) Coexpression of BMI-1 and EZH2 polycomb-group proteins is associated with cycling cells and degree of malignancy in B-cell non-Hodgkin lymphoma. Blood 97:3896–3901
14. Sudo T, Utsunomiya T, Mimori K, Nagahara H, Ogawa K, Inoue H, Wakiyama S, Fujita H, Shirouzu K, Mori M (2005) Clinicopathological significance of EZH2 mRNA expression in patients with hepatocellular carcinoma. Br J Cancer 92:1754–1758
15. Raaphorst FM, van Kemenade FJ, Blokzijl T, Fieret E, Hamer KM, Satijn DP, Otte AP, Meijer CJ (2000) Coexpression of BMI-1 and EZH2 polycomb group genes in Reed–Sternberg cells of Hodgkin's disease. Am J Pathol 157:709–715
16. Dukers DF, van Galen JC, Giroth C, Jansen P, Sewalt RG, Otte AP, Kluin-Nelemans HC, Meijer CJ, Raaphorst FM (2004) Unique polycomb gene expression pattern in Hodgkin's lymphoma and Hodgkin's lymphoma-derived cell lines. Am J Pathol 164:873–881
17. Bracken AP, Pasini D, Capra M, Prosperini E, Colli E, Helin K (2003) EZH2 is downstream of the pRB-E2F pathway, essential for proliferation and amplified in cancer. EMBO J 22:5323–5335
18. Breuer RH, Snijders PJ, Smit EF, Sutedja TG, Sewalt RG, Otte AP, van Kemenade FJ, Postmus PE, Meijer CJ, Raaphorst FM

(2004) Increased expression of the EZH2 polycomb group gene in BMI-1-positive neoplastic cells during bronchial carcinogenesis. Neoplasia 6:736–743
19. Duckett CS, Li F, Wang Y, Tomaselli KJ, Thompson CB, Armstrong RC (1998) Human IAP-like protein regulates programmed cell death downstream of Bcl-x_L and cytochrome c. Mol Cell Biol 18:608–615
20. Lewis J, Burstein E, Birkey Reffey S, Bratton SB, Roberts AB, Duckett CS (2004) Uncoupling of the signaling and caspase-inhibitory properties of XIAP. J Biol Chem 279:9023–9029
21. Burstein E, Hoberg JE, Wilkinson AS, Rumble JM, Csomos RA, Komarck CM, Maine GN, Wilkinson JC, Mayo MW, Duckett CS (2005) COMMD proteins: a novel family of structural and functional homologs of MURR1. J Biol Chem 280:22222–22232
22. Maine GN, Mao X, Komarck CM, Burstein E (2007) COMMD1 promotes the ubiquitination of NF-kappaB subunits through a cullin-containing ubiquitin ligase. EMBO J 26:436–447
23. Duckett CS, Nava VE, Gedrich RW, Clem RJ, Van Dongen JL, Gilfillan MC, Shiels H, Hardwick JM, Thompson CB (1996) A conserved family of cellular genes related to the baculovirus *iap* gene and encoding apoptosis inhibitors. EMBO J 15:2685–2694
24. Puig O, Caspary F, Rigaut G, Rutz B, Bouveret E, Bragado-Nilsson E, Wilm M, Seraphin B (2001) The tandem affinity purification (TAP) method: a general procedure of protein complex purification. Methods 24:218–229
25. Delage-Mourroux R, Martini PG, Choi I, Kraichely DM, Hoeksema J, Katzenellenbogen BS (2000) Analysis of estrogen receptor interaction with a repressor of estrogen receptor activity (REA) and the regulation of estrogen receptor transcriptional activity by REA. J Biol Chem 275:35848–35856
26. Simon SL, Parkes A, Leygue E, Dotzlaw H, Snell L, Troup S, Adeyinka A, Watson PH, Murphy LC (2000) Expression of a repressor of estrogen receptor activity in human breast tumors: relationship to some known prognostic markers. Cancer Res 60:2796–2799
27. Montano MM, Ekena K, Delage-Mourroux R, Chang W, Martini P, Katzenellenbogen BS (1999) An estrogen receptor-selective coregulator that potentiates the effectiveness of antiestrogens and represses the activity of estrogens. Proc Natl Acad Sci USA 96:6947–6952
28. Kurtev V, Margueron R, Kroboth K, Ogris E, Cavailles V, Seiser C (2004) Transcriptional regulation by the repressor of estrogen receptor activity via recruitment of histone deacetylases. J Biol Chem 279:24834–24843
29. Park SE, Xu J, Frolova A, Liao L, O'Malley BW, Katzenellenbogen BS (2005) Genetic deletion of the repressor of estrogen receptor activity (REA) enhances the response to estrogen in target tissues in vivo. Mol Cell Biol 25:1989–1999
30. Murphy LC, Simon SL, Parkes A, Leygue E, Dotzlaw H, Snell L, Troup S, Adeyinka A, Watson PH (2000) Altered expression of estrogen receptor coregulators during human breast tumorigenesis. Cancer Res 60:6266–6271
31. Claus R, Lubbert M (2003) Epigenetic targets in hematopoietic malignancies. Oncogene 22:6489–6496

MOLECULAR AND CELLULAR BIOLOGY, Jan. 2008, p. 237–247 Vol. 28, No. 1
0270-7306/08/$08.00+0 doi:10.1128/MCB.01065-07

Apoptosis-Inducing Factor Is a Target for Ubiquitination through Interaction with XIAP▽†

John C. Wilkinson,[1]‡ Amanda S. Wilkinson,[1]‡ Stefanie Galbán,[1] Rebecca A. Csomos,[1] and Colin S. Duckett[1,2]*

Departments of Pathology[1] and Internal Medicine,[2] University of Michigan, Ann Arbor, Michigan 48109

Received 15 June 2007/Returned for modification 19 July 2007/Accepted 8 October 2007

X-linked inhibitor of apoptosis (XIAP) is an inhibitor of apoptotic cell death that protects cells by caspase-dependent and independent mechanisms. In a screen for molecules that participate with XIAP in regulating cellular activities, we identified apoptosis-inducing factor (AIF) as an XIAP binding protein. Baculoviral IAP repeat 2 of XIAP is sufficient for the XIAP/AIF interaction, which is disrupted by Smac/DIABLO. In healthy cells, mature human AIF lacks only the first 54 amino acids, differing significantly from the apoptotic form, which lacks the first 102 amino-terminal residues. Fluorescence complementation and immunoprecipitation experiments revealed that XIAP interacts with both AIF forms. AIF was found to be a target of XIAP-mediated ubiquitination under both normal and apoptotic conditions, and an E3 ubiquitin ligase-deficient XIAP variant displayed a more robust interaction with AIF. Expression of either XIAP or AIF attenuated both basal and antimycin A-stimulated levels of reactive oxygen species (ROS), and when XIAP and AIF were expressed in combination, a cumulative decrease in ROS was observed. These results identify AIF as a new XIAP binding partner and indicate a role for XIAP in regulating cellular ROS.

Apoptosis is a cellular death program critical to the development and homeostatic maintenance of all multicellular organisms (27, 39), and deregulated apoptosis has been implicated in many disease states (52). The principal biochemical mediators of apoptosis are caspases, cysteinyl proteases that are activated in a precisely orchestrated manner following various death triggers (12, 53). Apoptotic caspases are divided into two groups: initiator caspases, which respond to and are directly activated by apoptotic stimuli, and effector caspases, which carry out completion of the apoptotic program (3, 40).

Predominant among the molecules that play a role in controlling caspase activity are members of the inhibitor of apoptosis (IAP) family (13, 21). Among the eight mammalian IAP homologues that have been described, X-linked inhibitor of apoptosis (XIAP) (15, 32, 54) has emerged as the most potent suppressor of apoptosis. XIAP binds and inhibits the initiator caspase 9 (47, 50) and the effector caspases 3 (23, 44) and 7 (8) and can thus regulate multiple steps within the caspase cascade. While many IAP proteins can attenuate cell death, XIAP appears to be the only IAP homologue to directly inhibit caspases with high affinity (16).

Distinct patterns of caspase activation exist, and so far two major apoptotic pathways have been described. Ligation of members of the tumor necrosis factor receptor family activates an extrinsic death program by forming an intracellular death-inducing signaling complex (DISC) (35). The DISC recruits and activates initiator caspases, such as caspases 8 and 10, which in turn engage downstream effector caspases. In contrast, death signals such as cellular stress induce an intrinsic apoptotic program regulated predominantly by the mitochondria. These stimuli induce mitochondrial outer membrane permeabilization, thus allowing the cytoplasmic release of pro-apoptotic molecules sequestered within the mitochondria. Notable among these sequestered factors are cytochrome *c*, which along with the adaptor molecule Apaf-1 (31) forms an oligomeric complex known as the apoptosome (6) leading to caspase 9 activation. Additional factors include Smac/DIABLO (14, 58) and Omi/HtrA2 (19, 34, 59), which promote apoptosis in part by neutralizing XIAP-mediated caspase inhibition (7, 33, 48), and the flavoprotein apoptosis-inducing factor (AIF).

While cytochrome *c*, Smac/DIABLO, and Omi/HtrA2 promote cell death predominantly by caspase-dependent mechanisms, AIF was originally described as a caspase-independent mediator of cell death (51). Mitochondrial release of AIF ultimately results in AIF nuclear translocation and DNA binding (63) and is associated with chromatin condensation and internucleosomal DNA cleavage. Interestingly, AIF possesses NADH oxidase activity in vitro (36), and recent studies have described a protective role for AIF, in part through maintaining the expression and activity of complex I of the electron transport chain (55). Further studies in vivo have suggested a protective role for AIF against certain forms of oxidative stress (28), and loss of AIF in heart and brain results in severe defects, most likely caused by loss of mitochondrial integrity (9, 26).

Like AIF, XIAP is involved in several pathways both related to and distinct from apoptosis. Through interactions with members of the transforming growth factor β receptor family, XIAP regulates Smad-dependent transcriptional activation (2, 25, 61). Ectopic XIAP expression regulates stress-responsive

* Corresponding author. Mailing address: BSRB, Room 2057, 109 Zina Pitcher Place, Ann Arbor, MI 48109-2200. Phone: (734) 615-6414. Fax: (734) 763-2162. E-mail: colind@umich.edu.

† Supplemental material for this article may be found at http://mcb.asm.org/.

‡ Present address: Department of Biochemistry, Wake Forest University School of Medicine, Medical Center Boulevard, Winston-Salem, NC 27157.

▽ Published ahead of print on 29 October 2007.

pathways, including those involving N-terminal c-Jun kinase (JNK) (45, 46) and the transcription factor NF-κB (20, 29). Interestingly, the ability of XIAP to regulate these pathways can be uncoupled from its caspase-inhibitory activities (30), suggesting that these are distinct properties of the protein. XIAP also controls intracellular copper levels, both through ubiquitin ligase-dependent regulation of the copper binding protein COMMD1 (4) and by binding copper directly (37). In light of the fact that XIAP-deficient mice display no overt apoptotic phenotype (18), these findings suggest that in most normal tissues the primary function(s) of XIAP may be to regulate pathways distinct from those involving apoptotic caspase cascades. This is similar to many apoptotic regulators, such as cytochrome *c* and Bad, which under normal conditions participate in processes other than cell death regulation (17, 43).

To explore the possibility that XIAP regulates biological processes beyond those described above, we conducted a biochemical screen for XIAP-associated proteins and identified AIF as an XIAP binding protein. XIAP binds both the mature form of AIF present in healthy cells and the processed form of AIF released from mitochondria during apoptosis (41). The XIAP/AIF interaction depends on the presence of the second baculoviral IAP repeat (BIR) domain of XIAP and can be specifically displaced by Smac/DIABLO. Unlike that of XIAP antagonists, AIF overexpression fails to prevent XIAP-mediated caspase activation. Under both normal and apoptotic conditions XIAP induces AIF ubiquitination in a manner that does not result in degradation but instead appears to affect the stability of the XIAP/AIF interaction. Finally, XIAP and AIF combine to attenuate levels of both basal and antimycin A-stimulated reactive oxygen species (ROS). Taken together, these data define a novel interaction between two well-known regulators of the cell death pathway and provide the foundation for uncovering new mechanisms by which XIAP and AIF regulate both apoptotic and nonapoptotic cellular processes.

MATERIALS AND METHODS

Materials. Reagents were obtained as follows: protein G-coupled agarose, Ni-nitrilotriacetic acid (NTA) agarose, Glutamax, tobacco etch virus protease, Mitotracker Red, and phosphate-buffered saline from Invitrogen; glutathione-Sepharose 4B, calmodulin-Sepharose 4B, and immunoglobulin G (IgG)-Sepharose from Amersham; fetal bovine serum from HyClone; Dulbecco modified Eagle medium (DMEM) from Mediatech; ApoTarget protease assay kit from Biosource; DEVD–7-amino-4-trifluoromethyl coumarin from BioMol; site-directed mutagenesis kit from Stratagene; and protease inhibitor tablets from Roche. All other chemicals were from Sigma. Antibodies were obtained as follows: anti-XIAP and anti-AIF from BD-Pharmingen; anti-AIF from Santa Cruz Biotechnology; cleaved caspase 3 from Cell Signaling; anti-Smac/DIABLO from Calbiochem; anti-glutathione *S*-transferase (anti-GST) from Santa Cruz Biotechnology; anti-β-actin, horseradish peroxidase (HRP)-conjugated anti-FLAG, and HRP-conjugated antihemagglutinin (anti-HA) from Sigma; and HRP-conjugated anti-mouse and anti-rabbit antibodies from Amersham.

Cell culture, transfections, and plasmids. HEK 293 cells were grown in DMEM containing 10% fetal bovine serum supplemented with 2 mM Glutamax at 37°C in an atmosphere of 95% air and 5% CO_2. Transfections were performed by the method of calcium phosphate precipitation as described previously (15). pEBB XIAP-TAP and pEBB D148A/W310A XIAP-TAP were generated by subcloning wild-type (WT) and D148A/W310A XIAP into the pEBB tandem affinity purification (TAP) plasmid. The bimolecular fluorescence complementation (BiFC) plasmids pEBB YN and pEBB YC were generated by PCR using pBIFC-YN155 and pBIFC-YC155 (gifts of T. Kerppola, University of Michigan) as templates, respectively. pEBB YN-XIAP was generated by subcloning WT XIAP into pEBB-YN. pEBB AIF was generated by PCR using an expressed sequence tag clone containing full-length human AIF (Image clone 5740894) and was used to further subclone pEBB AIF-TAP, pEBB AIF-YFP, pEBB AIF-FLAG, and pEBB AIF-YC. pEBB Ub-Smac/DIABLO A1G and pEBB Ub-Smac/DIABLO ΔA1 were generated by site-directed mutagenesis (Stratagene) using pEBB Ub-Smac/DIABLO as template. pEBB Ub-Δ54AIF-FLAG and pEBB Ub-Δ102AIF-FLAG were generated by PCR using pEBB-AIF-FLAG as template followed by replacement of the Smac/DIABLO sequence within the pEBB Ub-Smac/DIABLO-FLAG construct. These plasmids were then used as templates for PCR amplification in the subcloning of pEBB Ub-Δ54AIF, pEBB Ub-Δ102AIF, pEBB Ub-Δ102AIF-YFP, and pEBB Ub-Δ102AIF-YC. All remaining plasmids used in this study have been reported previously (4, 5, 60).

TAP. Cells were seeded into a total of 10 15-cm plates and then transfected with 12 μg of pEBB XIAP-TAP or pEBB D148A/W310A XIAP-TAP per plate. Two days after transfection, the cells were harvested, lysed, and subjected to TAP as described previously (5). Final purified samples were submitted to the Proteomics Centre at the University of Victoria for further processing including trypsin digestion, high-pressure liquid chromatography separation, and tandem mass spectrometry to determine peptide sequences.

Cell lysis, Coomassie blue staining, immunoblot analysis, and immunoprecipitation. Cell lysates were prepared in either RIPA buffer (phosphate-buffered saline containing 1% NP-40, 0.5% sodium deoxycholate, 0.1% sodium dodecyl sulfate [SDS]) or Triton lysis buffer (25 mM HEPES, pH 7.9, 100 mM NaCl, 1% Triton X-100, 1 mM EDTA, 10% glycerol, 1 mM NaF, 1 mM $NaVO_4$) (both lysis buffers were supplemented with 1 mM dithiothreitol, 1 mM phenylmethylsulfonyl fluoride, and 1 protease inhibitor cocktail tablet per 10 ml prior to use), normalized for protein content, and then separated by SDS-polyacrylamide gel electrophoresis (PAGE) using 4 to 12% gradient SDS-polyacrylamide gels (Invitrogen). Coomassie blue staining was performed using the Colloidal Blue staining kit (Invitrogen) according to the manufacturer's instructions. For immunoblot analysis, SDS-PAGE was followed by transfer to nitrocellulose membranes (Invitrogen), which were then blocked with 5% milk in Tris-buffered saline containing 0.02 to 0.2% Tween, followed by incubation with the indicated antibodies for 1 h at room temperature. Following washing, membranes were incubated with HRP-conjugated anti-mouse IgG or anti-rabbit IgG secondary antibodies for 45 min at room temperature and visualized by enhanced chemiluminescence. For immunoprecipitation experiments, cell lysates (Triton lysis buffer) were normalized for protein content and incubated with indicated antibodies for 2 h at 4°C. Protein G-coupled agarose beads were then added and incubated for 1 h. For precipitation of GST-tagged proteins or His_6-ubiquitin-conjugated proteins, glutathione-Sepharose beads or nickel agarose beads were added and the samples were incubated at 4°C for 2 h. Agarose beads were recovered by centrifugation and washed in Triton buffer, and precipitated proteins were eluted by adding lithium dodecyl sulfate sample buffer and heating the mixture to 95°C for 5 min. Recovered proteins were then separated by electrophoresis, and immunoblot analysis was carried out as described above.

Amino-terminal protein sequencing. Cells were seeded in five 15-cm plates and transfected with 12 μg each of pEBB AIF-TAP. After 2 days, cell lysates were subjected to TAP as described above, except that the final eluate was collected as a single fraction and was not precipitated with trichloroacetic acid. A portion of the eluate was analyzed by colloidal Coomassie blue staining as described above. The remaining sample was then submitted to the Proteomics Centre at the University of Victoria for further processing, including separation by SDS-PAGE, transfer to polyvinylidene difluoride (PVDF), and amino-terminal protein sequencing by Edman degradation.

Fluorescence microscopy/BiFC. Cells were seeded on polylysine-coated chambered coverglass slides and then transfected as follows: for plasmids encoding yellow fluorescent protein (YFP) fusion proteins, a total of 2 μg of each plasmid was used per well; for BiFC plasmids, 1 μg of each plasmid encoding a BiFC fusion protein (YN or YC, 2 μg total DNA) was used per well. Twenty-four hours after transfection, medium was replaced with phenol red-free DMEM and cells were incubated for an additional 24 h. Cells were then stained with Hoechst 33342 and Mitotracker Red (Molecular Probes/Invitrogen) and examined using a Zeiss Axiovert 100 M confocal microscope equipped with a Zeiss LSM 510 spectrometer.

Caspase activity assay. Cells were seeded in six-well plates; transfected 24 h later with pEBB-GFP, pCDNA3-Bax, and other plasmids; and then incubated at 37°C for 16 h. Floating and attached cells were harvested, and caspase 3 assays were performed as described previously (60).

Measurement of intracellular ROS levels. Cells were seeded in six-well plates and transfected by calcium phosphate. After 48 h cells were left untreated or treated with 10 μg/ml antimycin A for 1 hour at 37°C. Following treatment cells were incubated with the ROS indicator dye CM-H_2DCF-DA (Molecular Probes/Invitrogen) for an additional 30 min at 37°C. Cells were then harvested by

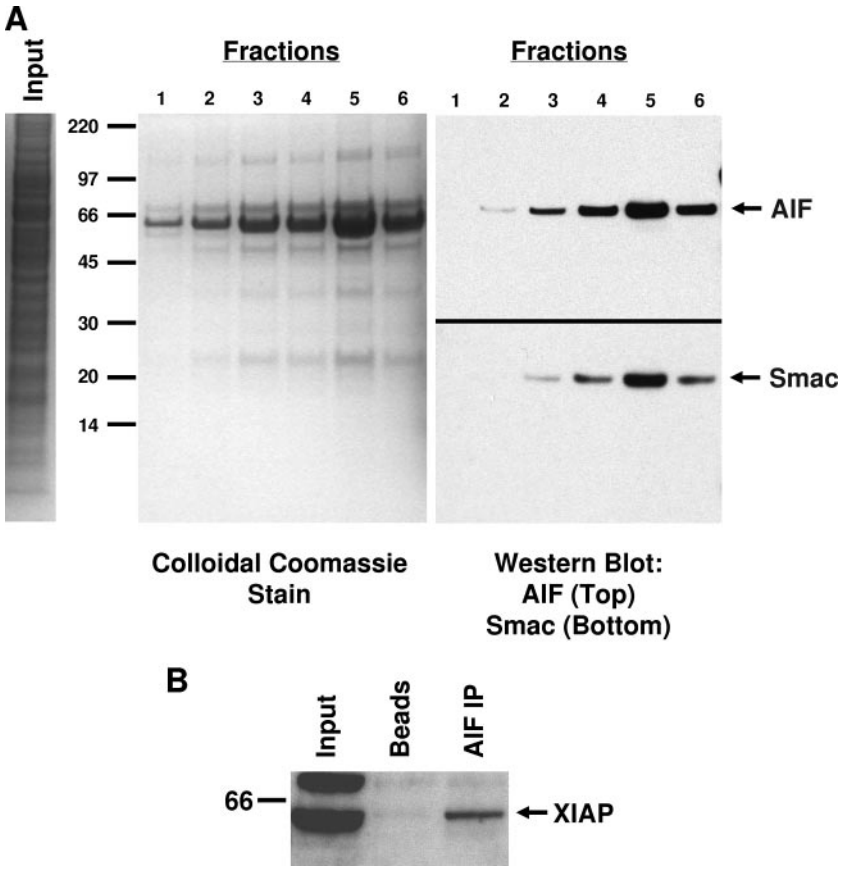

FIG. 1. AIF is an XIAP-associated factor. (A) D148A/W310A XIAP-TAP was expressed in HEK 293 cells. A cell lysate was prepared and subjected to TAP. Total protein in input and final eluted fractions was visualized by SDS-PAGE and Coomassie blue staining (left and middle panels), showing XIAP bait protein and associated factors. Eluted fractions were pooled, precipitated with trichloroacetic acid, and digested with trypsin, and peptides were identified by mass spectrometry. Eluted fractions were also immunoblotted for the presence of AIF and Smac (right panel). (B) Untransfected HEK 293 cell lysate was precipitated with either beads alone or beads bound to an AIF-specific antibody, and the presence of XIAP in precipitated complexes was assessed by immunoblot analysis. Numbers at left of the panels are molecular masses in kilodaltons.

trypsinization and analyzed using either a Beckman-Coulter Cytomics FC 500 or a Becton Dickinson FACSCalibur flow cytometer.

RESULTS

To identify factors that participate with XIAP in regulating caspase-independent processes, a biochemical screen for XIAP-associated proteins was performed using the TAP method (42). This screen employed as bait the XIAP variant D148A/W310A, which fails to inhibit caspases 3, 7, and 9 (30), in fusion with a carboxy-terminal TAP tag, which was chosen in order to avoid masking potential interaction partners due to XIAP/caspase interactions. Coomassie blue staining of purification eluates showed a significant amount of bait material, as well as a number of additional bands of both higher and lower molecular weights (Fig. 1A, left panel). Purified material was precipitated by trichloroacetic acid and digested with trypsin, and potential XIAP-interacting proteins were identified by liquid chromatography-tandem mass spectrometry analysis of generated peptides. This approach identified a number of novel XIAP-associated proteins (see Table S1 in the supplemental material), including the mitochondrial flavoprotein AIF. The presence of AIF in eluted fractions was confirmed by immunoblot analysis, using Smac/DIABLO as a control (Fig. 1A, right panel). Given the roles that both XIAP and AIF play in regulating apoptotic and nonapoptotic processes, this interaction represents a potentially novel finding for cellular regulation and became the focus for further characterization. The ability of XIAP and AIF to coassociate was confirmed with endogenous proteins by immunoprecipitation analysis. AIF was precipitated from HEK 293 cells, and the presence of XIAP was assessed by immunoblot analysis. As shown in Fig. 1B, XIAP was readily detected in AIF immune complexes, confirming the association between endogenous XIAP and AIF.

The structural determinants within XIAP that are required for binding to AIF were next assessed. XIAP contains three amino-terminal BIR domains followed by a RING domain at the carboxy terminus. Plasmids encoding XIAP domains in fusion with GST were transfected into HEK 293 cells along with a plasmid encoding full-length human AIF with a FLAG tag at the carboxy terminus. Cellular lysates were then precipitated with glutathione beads, and the presence of AIF in

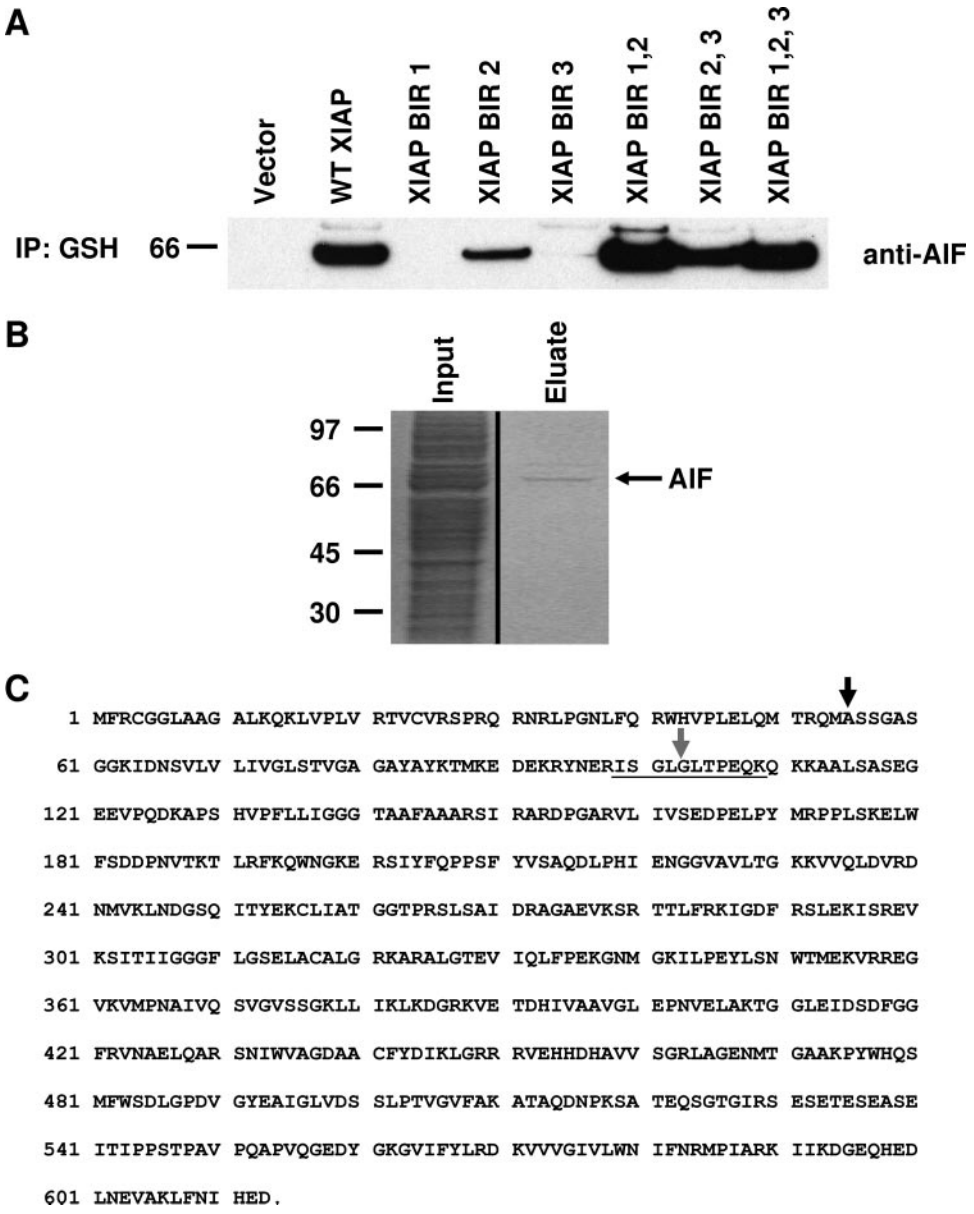

FIG. 2. BIR2 of XIAP binds AIF; mature AIF begins at residue 55. (A) HEK 293 cells were transfected with plasmids encoding various XIAP domain truncations in fusion with GST along with a plasmid encoding full-length human AIF. Cell lysates were prepared, and XIAP was precipitated with glutathione (GSH) beads. The presence of AIF in precipitated complexes was determined by immunoblotting. (B) Full-length human AIF-TAP was expressed in HEK 293 cells. AIF was precipitated from cell lysates using IgG-Sepharose beads; eluted proteins were then separated by SDS-PAGE and transferred to PVDF membranes. Following Coomassie blue staining, the AIF band was excised and subjected to Edman degradation in order to determine the mature amino terminus. Numbers at left of panels A and B are molecular masses in kilodaltons. (C) Primary sequence of full-length human AIF. The underlined sequence is one of four AIF peptides recovered from analysis of XIAP-TAP. The gray arrow is the first residue of mature AIF as reported by reference 51; the black arrow is the first residue of mature human AIF as determined by this study.

precipitated complexes was assessed by immunoblot analysis. As shown in Fig. 2A, XIAP BIR2 was found to be sufficient to precipitate AIF, indicating that this region is critical for AIF association.

AIF undergoes amino-terminal processing to generate the mature form, originally reported to begin at residue 102 in the mouse protein (residue 103 in human) (51). When examining the peptides recovered from the XIAP-TAP screen, we observed that one AIF-specific peptide spanned the region surrounding residue 103 (Fig. 2C), raising the possibility that mature AIF begins at a position farther upstream than originally reported. To test this possibility, full-length human AIF in fusion with a carboxy-terminal TAP tag was expressed in HEK 293 cells. TAP-tagged AIF then was recovered from cell lysates by TAP, subjected to SDS-PAGE, transferred to a PVDF membrane, and visualized by Coomassie blue staining (Fig. 2B). The band corresponding to AIF was excised, and Edman degradation was performed to determine the mature

amino terminus. These results indicated that the mature terminus of human AIF begins at residue 55, rather than the residue originally reported (Fig. 2C). This observation is in agreement with a recent study characterizing the processing of rat AIF expressed in HeLa cells (41), which indicated that AIF exists in two forms within cells: a mature, nonapoptotic form truncated to position 54 (residue 55 in the human protein) and an apoptotic form truncated to position 102 (residue 103 in the human protein).

Like AIF, the XIAP antagonist Smac/DIABLO undergoes proteolytic processing to generate a mature amino terminus, which contains a canonical IAP binding motif (IBM). IBMs have a strong preference for an alanine residue in the first position, and alteration of this alanine is often sufficient to prevent IAP binding (57). Neither the healthy nor the apoptotic forms of AIF appear to contain a consensus IBM sequence, though this possibility could not be ruled out. Thus, to compare the abilities of both the healthy and mature forms of AIF to interact with XIAP, two different AIF encoding strategies were used. In the first approach, cDNAs encoding either the Δ54 or the Δ102 form of AIF were expressed following a single start codon (met-Δ54AIF and met-Δ102AIF, respectively [Fig. 3A]). However, this approach results in the incorporation of a methionine residue at the amino terminus of each protein that could potentially interfere with binding to XIAP. We therefore chose an alternative strategy in which each AIF variant was expressed in fusion with a ubiquitin polypeptide at the amino terminus (24). Ubiquitin undergoes cotranslational processing, resulting in a proteolytic event at the extreme carboxy-terminal diglycine of ubiquitin. This event releases ubiquitin and leaves the amino terminus of AIF free of any additional residues. Therefore, we generated Ub-Δ54AIF and Ub-Δ102AIF fusion polypeptides, which undergo processing into the healthy and apoptotic AIF forms, respectively (Fig. 3A).

The panel of AIF variants was then tested for interaction with XIAP. As shown in Fig. 3A, XIAP efficiently precipitated all forms of AIF except Ub-Δ102AIF. The ability of XIAP to bind both met-Δ54AIF and met-Δ102AIF confirms the lack of an IBM at the amino terminus of AIF and suggests that AIF binds XIAP through a non-IBM motif. When input material was immunoblotted for AIF, a pattern of laddering consistent with ubiquitination was observed for the full-length, Ub-Δ54AIF, and Ub-Δ102AIF variants and was noticeably absent for both the met-Δ54 and met-Δ102 forms. Since met-Δ102AIF protein bound XIAP efficiently, in contrast to the Ub-Δ102AIF form, which failed to bind but displayed the greatest extent of laddering, these data raised the possibility that AIF may be a target for ubiquitination, which may in turn regulate stability of the XIAP/AIF complex.

XIAP possesses E3 ubiquitin ligase activity, a property that is conferred by the RING domain at the carboxy terminus (62). The data presented above suggested that AIF is ubiquitinated and may thus be a substrate for the E3 ligase activity of XIAP. To test this possibility, cells were transfected with plasmids encoding His-tagged ubiquitin and either full-length AIF, Ub-Δ54AIF, or Ub-Δ102AIF in the absence and presence of XIAP. Ni-NTA beads were then used to precipitate ubiquitinated proteins from cell lysates, and the presence of AIF in these complexes was determined by immunoblotting (Fig. 3B).

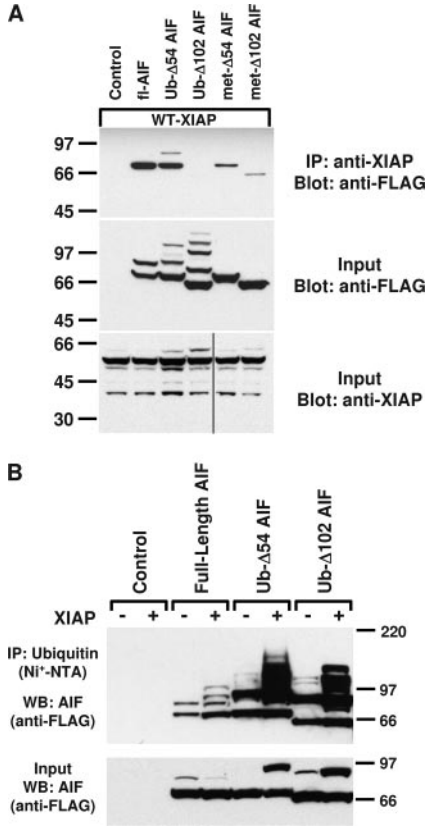

FIG. 3. XIAP binds AIF variants and mediates AIF ubiquitination. (A) HEK 293 cells were transfected with a plasmid encoding WT-XIAP along with control, full-length AIF, Ub-Δ54AIF, Ub-Δ102AIF, met-Δ54AIF, or met-Δ102AIF expression plasmids. Cell lysates were then prepared and precipitated with anti-XIAP. The presence of AIF in precipitated complexes was determined by immunoblot analysis for the FLAG tag present at the carboxy terminus of each AIF protein (top panel). Equivalent expression of XIAP and AIF variants was confirmed by immunoblotting input lysates with anti-FLAG (middle panel) or anti-XIAP (bottom panel). The black line present in the bottom panel indicates removal of a single empty lane solely for the purpose of clarity. (B) HEK 293 cells were transiently transfected with His-tagged ubiquitin and plasmids expressing full-length AIF-FLAG, Ub-Δ54AIF-FLAG, and Ub-Δ102AIF-FLAG in the absence and presence of an XIAP expression plasmid. Ubiquitinated material was then precipitated using Ni-NTA beads, and the presence of FLAG-tagged proteins (AIF) in precipitated complexes was detected by immunoblot analysis. Numbers at left of panel A and at right of panel B are molecular masses in kilodaltons.

All three AIF variants displayed significant basal ubiquitination in the absence of overexpressed XIAP, possibly due to either endogenous XIAP or alternative E3 ligases. Upon XIAP overexpression the amount of ubiquitinated material recovered for all three forms of AIF, including Ub-Δ102AIF, increased substantially above basal levels. These data suggest that both the healthy and apoptotic forms of AIF are targets for XIAP-mediated ubiquitination. Interestingly, AIF ubiquitination by XIAP did not result in degradation (as shown by AIF input levels), suggesting that this process does not target AIF to the proteasome and raising the possibility that ubiquitination of AIF by XIAP may instead alter the enzymatic or death-inducing properties of the molecule.

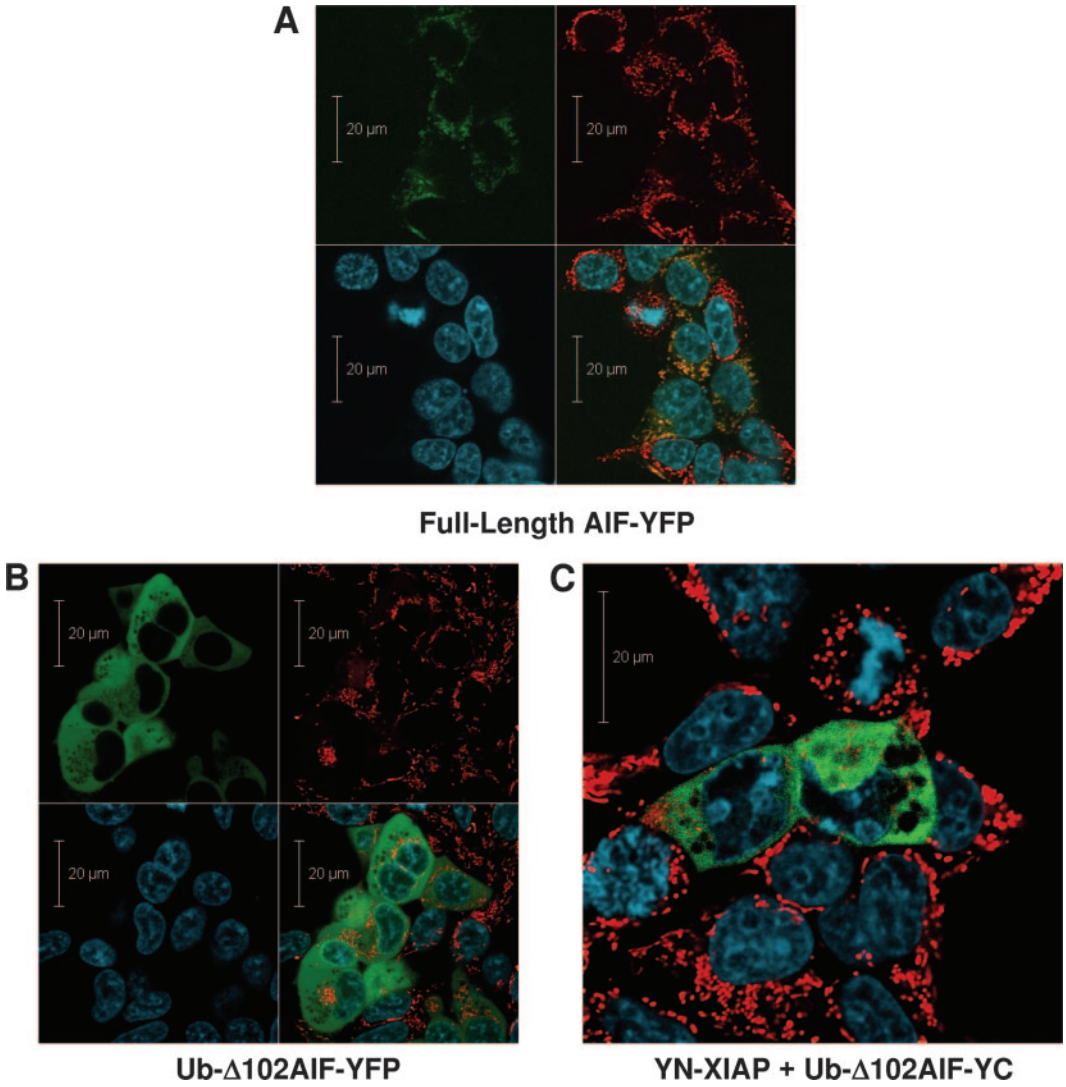

FIG. 4. Fluorescence complementation analysis of the XIAP/AIF interaction. (A and B) Full-length AIF (A) and Ub-Δ102AIF (B) in fusion with YFP at the carboxy terminus (here shown in green) were expressed in HEK 293 cells. Cells were stained with Mitotracker Red (red staining) and Hoechst stain (blue staining). The cellular localization of AIF proteins was then determined by confocal microscopy. (C) BiFC was used to examine the XIAP/AIF interaction. YN-XIAP was coexpressed with Ub-Δ102AIF-YC. The green fluorescence observed is indicative of a cytoplasmic interaction between XIAP and Δ102 AIF. Cells were additionally stained with both Mitotracker Red (red) and Hoechst stain (blue).

Since XIAP must bind a substrate in order to induce its ubiquitination, the data presented above suggest that XIAP and Ub-Δ102AIF interact within cells, despite our inability to coprecipitate these two molecules (Fig. 3A). To test this possibility, the BiFC approach (22) was used as an alternative means to investigate the interaction between XIAP and Ub-Δ102AIF. This method is based on the separation of YFP into amino (YN)- and carboxy (YC)-terminal domains, neither of which is fluorescent when the two are coexpressed in cells. When separately fused to two interacting molecules, these YFP domains may recombine, resulting in cellular fluorescence. Thus, this approach not only allows the detection of protein-protein interactions within a living cell but also identifies the subcellular compartment where the interaction occurs. Our laboratory and others have shown that XIAP resides predominantly in the cytoplasm (4). While native AIF in fusion with the complete YFP polypeptide displayed a clear, punctate, mitochondrial localization (Fig. 4A), Ub-Δ102AIF-YFP exhibited a diffuse, cytoplasmic localization pattern (Fig. 4B). When the BiFC combination of YN-XIAP and Ub-Δ102AIF-YC was examined by confocal microscopy, a strong fluorescent signal localized to the cytoplasm was observed (Fig. 4C). Thus, by using the BiFC approach, which is highly sensitive to lower-affinity protein-protein interactions, binding between XIAP and Ub-Δ102AIF was observed in living cells.

The data presented in Fig. 3 and 4 strongly suggest that XIAP binds and ubiquitinates both the healthy and apoptotic forms of AIF, though binding to the latter is transient, with complex stability decaying quickly as AIF becomes ubiquitinated. Thus, the XIAP variant H467A, which lacks E3 ubiquitin ligase activity, should be able to effectively precipitate

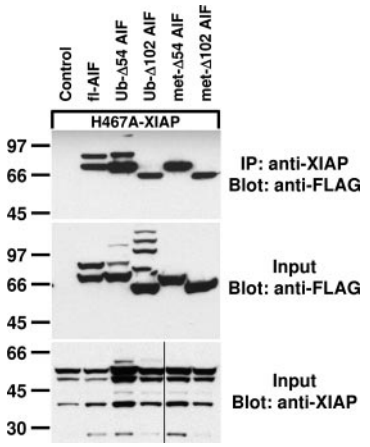

FIG. 5. H467A-XIAP immunoprecipitates all AIF variants. (A) HEK 293 cells were transfected with a plasmid encoding H467A-XIAP along with control, full-length AIF, Ub-Δ54AIF, Ub-Δ102AIF, met-Δ54AIF, or met-Δ102AIF expression plasmids. XIAP was then immunoprecipitated from cell lysates, and the presence of AIF was determined by immunoblot analysis using anti-FLAG (top panel). Equivalent expression of XIAP (bottom panel) and AIF variants (middle panel) was confirmed by immunoblotting input lysates. The black line present in the bottom panel indicates removal of a single empty lane solely for the purpose of clarity. Note that this experiment was carried out in parallel to that shown for WT-XIAP in Fig. 3A so that efficiency of AIF coprecipitation could be compared between the two XIAP variants. Numbers at left are molecular masses in kilodaltons.

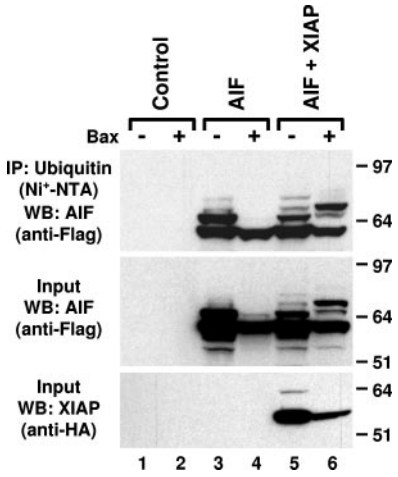

FIG. 6. XIAP ubiquitinates AIF following induction of apoptosis. HEK 293 cells were transfected with His-tagged ubiquitin and either control plasmids (lanes 1 and 2), full-length AIF-FLAG (lanes 3 and 4), or full-length AIF-FLAG and XIAP expression plasmids (lanes 5 and 6), in the absence (lanes 1, 3, and 5) and presence (lanes 2, 4, and 6) of a plasmid encoding Bax. Ubiquitinated material was then precipitated using Ni-NTA beads, and the presence of FLAG-tagged proteins (AIF) in precipitated complexes was detected by immunoblot analysis. Numbers at right are molecular masses in kilodaltons.

Ub-Δ102AIF. As shown in Fig. 5, Ub-Δ102AIF was readily detectable in H467A-XIAP immune complexes, confirming that the lack of detectable Ub-Δ102AIF in WT-XIAP immunoprecipitates is most likely due to XIAP-mediated ubiquitination of Ub-Δ102 AIF, resulting in destabilization of the complex. Furthermore, the remaining forms of AIF appear to precipitate more efficiently with H467A-XIAP than with the WT protein (compare Fig. 5 with Fig. 3A), suggesting that a lack of XIAP-mediated ubiquitination may stabilize these complexes as well.

While the data presented thus far demonstrate that XIAP binds to and ubiquitinates multiple forms of AIF, due to the fact that these data were obtained under postlysis conditions (solubilizing both XIAP and AIF) and/or employed AIF variants that were cytoplasmically localized, a question arises regarding the physiological conditions in which XIAP and AIF interact. This is because in healthy cells XIAP resides predominantly in the cytoplasm, whereas AIF is found in the intermembrane space of the mitochondria; thus, these molecules are normally sequestered in different cellular compartments. To explore this question, a functional approach was employed in which the ubiquitination status of AIF was examined during apoptosis, a condition in which release of AIF from the mitochondria should allow association with XIAP. Bax overexpression in HEK 293 cells induces caspase-dependent cell death and was used as a convenient method of apoptosis induction. Cells were transfected with a plasmid encoding His-tagged ubiquitin along with control, full-length AIF, or full-length AIF and XIAP expression plasmids, in the absence or presence of a plasmid encoding Bax. Ni-NTA beads were then used to precipitate ubiquitinated proteins from cell lysates, and the presence of AIF in precipitated complexes was determined by immunoblot analysis. As shown in Fig. 6, full-length AIF in healthy cells exhibited a moderate amount of ubiquitination in the absence of XIAP, and little to no change was observed following XIAP coexpression (compare lanes 3 and 5), consistent with the results in Fig. 3B. Importantly, the presence of XIAP induced a significantly greater amount of AIF ubiquitination under apoptotic conditions compared to cells lacking the XIAP plasmid (compare lanes 4 and 6), and the electrophoretic mobilities of the detected species were significantly different from the mobilities of those detected in the absence of Bax (compare lanes 5 and 6). These results demonstrate that under apoptotic conditions significant XIAP-mediated ubiquitination of AIF occurs and suggest that XIAP and AIF associate as the cell death cascade proceeds.

In light of the above observation, the effects of XIAP/AIF association on apoptosis were explored further. Our screen isolated AIF by using an XIAP variant incapable of inhibiting caspases, suggesting that the interface of XIAP to which AIF binds may differ from that employed by caspases. Since Smac/DIABLO binds to XIAP in a competitive manner with respect to caspases, this raised the question of whether Smac/DIABLO could also block the XIAP/AIF interaction. XIAP was expressed along with either WT Smac/DIABLO or the Smac/DIABLO mutant Δ1A or A1G, and the ability of Smac/DIABLO to prevent XIAP/AIF association was evaluated by coprecipitation. As shown in Fig. 7, the presence of WT Smac/DIABLO completely prevented the association between XIAP and AIF, whereas the IBM mutants, which fail to bind XIAP, also fail to prevent XIAP/AIF association. These data suggest that the XIAP associations with Smac/DIABLO and AIF are mutually exclusive.

XIAP is a well-characterized caspase inhibitor, a property that allows XIAP to protect cells from a variety of apoptotic stimuli (21). As described above for Fig. 6, in HEK 293 cells

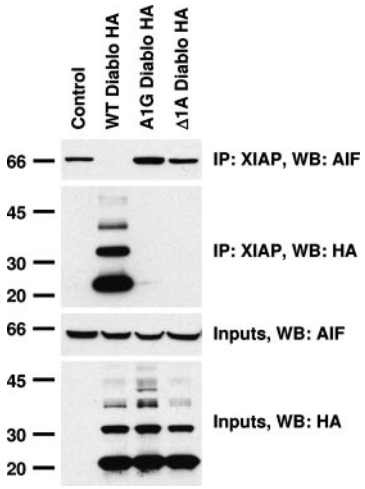

FIG. 7. Smac/DIABLO disrupts the XIAP/AIF interaction. HEK 293 cells were transfected with a plasmid encoding WT-XIAP along with either control, DIABLO-HA, Δ1A-DIABLO-HA, or A1G-DIABLO-HA expression plasmid. Cell lysates were then precipitated with anti-XIAP, and the presence of AIF (anti-AIF, top panel) or Smac/DIABLO (anti-HA, second panel from top) in immune complexes was determined by immunoblot analysis. Equivalent expression of AIF (third panel from top) and Smac/DIABLO (bottom panel) was assessed by immunoblot analysis of input lysates. Numbers at left are molecular masses in kilodaltons.

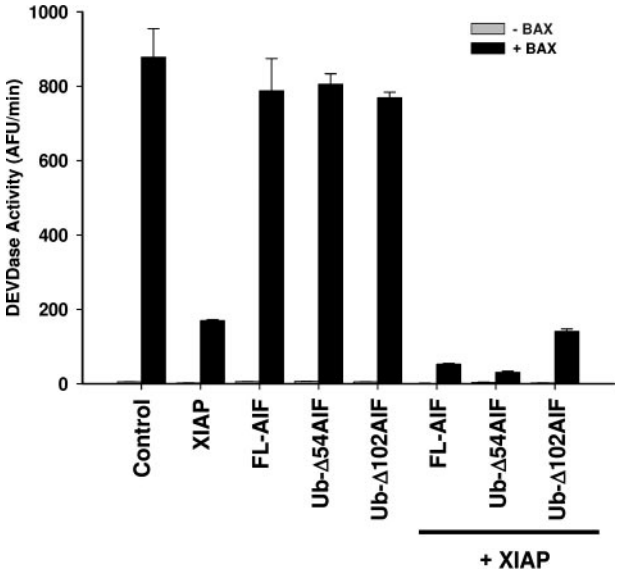

FIG. 8. AIF does not prevent XIAP-mediated caspase inhibition. HEK 293 cells were transfected with the indicated plasmids, cell lysates were prepared, and the activation of caspase 3 was determined by incubation with the fluorogenic caspase 3 substrate DEVD–7-amino-4-trifluoromethyl coumarin.

Bax overexpression effectively induces caspase-dependent death; in this setting XIAP overexpression effectively prevents apoptosis, and this protection can be reversed by coexpression of Smac/DIABLO (60). To determine if AIF, like other XIAP binding proteins, can neutralize XIAP-mediated caspase inhibition, we examined the effects of AIF expression in this model system. As shown in Fig. 8, Bax expression resulted in robust caspase activation, which was significantly reduced by expression of XIAP, as expected. When the three AIF variants (full length, Ub-Δ54, and Ub-Δ102) were expressed alone in the absence and presence of Bax, no noticeable differences were observed in the levels of caspase activity. Importantly, none of the AIF variants were capable of inducing caspase activation when expressed in the absence of cotransfected Bax, consistent with Fig. 4A and B, in which full-length AIF-YFP and Ub-Δ102AIF-YFP exhibited no toxicity. Finally, when coexpressed with XIAP none of the AIF variants were able to prevent XIAP-mediated caspase inhibition. Taken together, these data suggest that the interaction between XIAP and AIF does not alter the caspase-inhibitory properties of XIAP, indicating that AIF does not function as an IAP antagonist, and further raise the possibility that the interaction between XIAP and AIF serves to regulate caspase-independent functions of both proteins.

While the results of Fig. 6 confirm that an interaction occurs between XIAP and AIF following permeabilization of the outer mitochondrial membrane, they do not rule out the possibility that XIAP and AIF may coregulate within cells that are not undergoing apoptosis. The enzymatic and signal-transducing properties of AIF in healthy cells are presently ill defined, with the best-described property being in vitro NADH-oxidase activity (36). Since AIF can affect the oxidative state of cells through this enzymatic function, the ability of AIF to regulate intracellular ROS levels was tested in the absence and presence of XIAP, both under basal conditions and following treatment with the ROS-generating agent antimycin A. HEK 293 cells were transfected with AIF or XIAP expression plasmids either individually or in combination prior to treatment with antimycin A. Cells were then stained with the general-purpose ROS indicator dye CM-H_2DCF-DA, and cellular fluorescence was determined by flow cytometry (Fig. 9). Whereas expression of full-length AIF resulted in a slight increase in both basal and antimycin A-stimulated ROS levels, both AIF truncation variants significantly reduced both basal and stimulated levels of ROS. Interestingly, XIAP was also capable of decreasing ROS, to an extent that exceeded that of all three AIF variants. Importantly, the coexpression of XIAP with each of the AIF variants resulted in a progressive decrease in observed ROS levels (both basal and stimulated), such that the combination of XIAP and AIF reduced ROS levels following antimycin A treatment to those observed in untreated control cells, suggesting that the combined effects of XIAP and AIF on ROS are to reduce overall cellular oxidative stress. This last observation also confirms that XIAP-mediated ubiquitination of AIF does not result in proteasomal degradation, since such an effect would have been expected to reverse the AIF-mediated decrease in ROS following coexpression of XIAP with AIF.

DISCUSSION

XIAP is a multifunctional protein that can regulate numerous intracellular signaling cascades. In order to identify factors that participate with XIAP in regulating both caspase-dependent and -independent pathways, we conducted a biochemical screen and identified AIF as an XIAP-associated protein. The physical association between AIF and XIAP requires the second BIR domain of the XIAP protein, a similar determinant

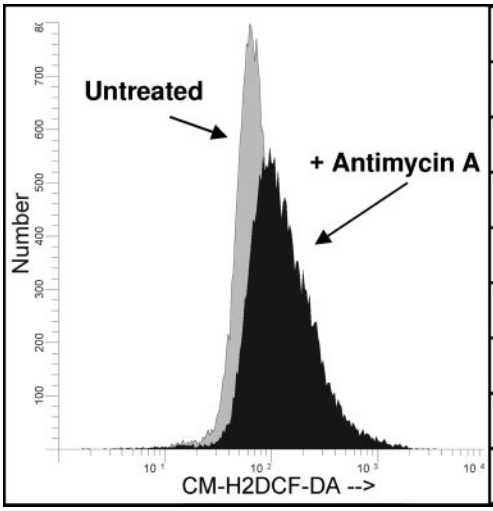

Sample	Untreated	+ Antimycin A
Control	83.37 ± 3.76	152.70 ± 14.0
FL-AIF	102.15 ± 3.04	171.55 ± 7.42
Ub-Δ54-AIF	65.75 ± 2.22	115.90 ± 14.1
Ub-Δ102-AIF	56.41 ± 3.20	100.90 ± 3.96
XIAP	44.72 ± 2.04	80.21 ± 2.84
FL-AIF + XIAP	62.30 ± 3.78	104.01 ± 15.7
Ub-Δ54-AIF + XIAP	37.89 ± 2.28	67.74 ± 3.40
Ub-Δ102-AIF + XIAP	35.62 ± 0.13	60.58 ± 4.74

FIG. 9. Effects of XIAP/AIF expression of ROS formation. HEK 293 cells were transfected with control or XIAP expression plasmids in the absence and presence of either full-length AIF, Ub-Δ54 AIF, or Ub-Δ102 AIF. Cells were then left untreated or treated with antimycin A and stained with the ROS-indicating dye CM-H_2-DCFDA, and cellular ROS levels were determined by flow cytometry. Representative histograms of untreated (gray) and antimycin A-treated (black) cells are shown, and values shown are the average ±1 standard deviation of three replicate measurements.

used by XIAP for interaction with caspases 3 and 7. However, AIF binds the XIAP variant D148A/W310A, a variant lacking caspase-inhibitory properties, suggesting that the nature of the interaction between XIAP and AIF is different from the nature of those between XIAP and the executioner caspases. Interestingly, Smac/DIABLO interferes with the binding of XIAP to AIF, suggesting that there is overlap in the binding epitopes within XIAP employed by these two mitochondrial proteins.

The XIAP/AIF interaction is complex due to the existence of two distinct forms of AIF, as well as to the differing extents of ubiquitination observed for these AIF variants. We show here that the mature form of human AIF in healthy cells lacks the first 54 amino-terminal residues, which is consistent with a previous report describing both healthy and apoptotic forms of rat AIF (41). XIAP binds both forms of AIF, and the extent of binding correlates with AIF ubiquitination status. Indeed, through the E3 ubiquitin ligase activity of its RING domain, XIAP induces the ubiquitination of AIF, and the Δ102 form appears to be a better substrate than the Δ54 form, explaining the failure of Δ102AIF to coprecipitate with WT XIAP. Importantly, the reduced ability of Δ102 to coprecipitate with XIAP is not a consequence of ubiquitination-induced AIF degradation, since AIF levels appear unaffected following ubiquitination by XIAP. Surprisingly, the XIAP variant H467A, which is devoid of E3 ubiquitin ligase activity, binds more robustly to all forms of AIF. We have previously reported that H467A XIAP is a dominant-negative protein with respect to E3 ligase activity (60); thus, the increased coprecipitation of AIF by H467A-XIAP may be due to a general reduction of AIF ubiquitination, resulting in increased affinity for XIAP.

Despite the ability of AIF to bind XIAP, this interaction does not result in an attenuation of the caspase-inhibitory properties of the XIAP protein. Indeed, not only does the coexpression of AIF fail to prevent XIAP from inhibiting Bax-mediated caspase activation and cell death, but a slight improvement to XIAP-mediated protection was observed when AIF was coexpressed. Interestingly, none of the forms of AIF studied, including the presumptively prodeath Δ102 form, were capable of inducing death when expressed alone. This observation is in contrast to previous reports describing the ability of AIF to kill cells with single-agent toxicity (51) and is consistent with more-recent studies suggesting that the death-promoting capacity of AIF is dependent upon prior caspase activation (1, 38).

While AIF was originally discovered as an agent involved in completing the apoptotic cascade (51), a unifying model describing the role of AIF in cell death remains elusive. Indeed, accumulating evidence suggests that the role of AIF in cell death varies tremendously in both a tissue-specific and a stimulus-dependent manner. For example, in neuronal cells AIF plays a key role in the completion of both caspase-dependent and -independent death pathways (10, 11), particularly following ischemia/reperfusion injury or glutamate excitotoxicity (10, 64). Conversely, not only does the loss of AIF in cardiomyocytes fail to prevent ischemia/reperfusion-induced death, but cells lacking AIF are more sensitive to this stimulus (56). In peripheral T cells, AIF is required for the successful completion of activation-induced cell death, but the absence of AIF has no effect on DNA damage-induced apoptosis (49). In light of these observations, our study defining the association between XIAP and AIF takes on new significance, as it suggests that these two molecules may coordinately regulate multiple forms of cell death in a tissue-specific manner.

Though in vitro studies have characterized the NADH-oxidase function of the protein, clear characterization of the enzymatic properties of AIF in a cellular context has not been reported. AIF loss-of-function studies, such as in mice with either natural reduction (28) or tissue-specific targeted deletion (9, 26) of AIF, suggest that AIF functions to preserve mitochondrial function. This may occur by AIF serving as a general-purpose antioxidant, through regulation of the activity and/or expression of complex I of the mitochondrial electron

transport chain or through maintenance of mitochondrial structure by as-yet-unknown mechanisms. We report here that the expression of either Δ54 or Δ102 AIF results in a decrease in the levels of ROS, consistent with a role for AIF as an antioxidant. Interestingly, expression of XIAP also appears to reduce cellular ROS levels, and the simultaneous expression of AIF and XIAP has an additive effect. Whether this is due to the XIAP/AIF interaction or is through the independent function of each protein is unclear. But to our knowledge this is the first report linking XIAP to the regulation of intracellular ROS, suggesting an additional mechanism by which XIAP controls cellular signal transduction.

Since the original description of XIAP as a high-affinity caspase inhibitor, a number of additional properties of XIAP have been described. Indeed, in light of the observation that mice lacking XIAP display no overt defects in apoptosis, it could be argued that the predominant in vivo function of XIAP is to participate in signal transduction cascades distinct from those involving caspases. Our observations here that XIAP is capable of interacting with AIF, that this interaction does not affect caspase inhibition by XIAP, and that both AIF and XIAP can additively reduce intracellular ROS levels support this point of view. As with XIAP, the apparent biological properties of AIF are complex. While originally described as a prodeath molecule capable of both caspase-dependent and -independent apoptotic functions, more-recent evidence points to a prosurvival activity for AIF, predominantly by preserving mitochondrial function and integrity. Experiments reported here show that enforced expression of AIF is not cytotoxic and may be protective since a general decrease in basal ROS levels was observed. The mechanism(s) by which AIF and XIAP regulate cellular oxidative stress, both separately and in combination, remains to be elucidated. However, a role for both proteins in this process highlights their multifaceted roles in controlling intracellular signaling.

We show that XIAP binds to and induces the ubiquitination of both the healthy and apoptotic forms of AIF. The possible consequences of this interaction require more complete definition, but since XIAP-mediated ubiquitination does not result in AIF degradation, they include alteration of AIF enzymatic activity, attenuation of the apoptotic effects of AIF, or alterations in as-yet-undefined properties of the AIF protein. Given the high level of attention cast towards regulators of the cell death cascade for the purposes of therapeutic intervention in human diseases, the data presented here raise the level of importance of understanding the total functions of both XIAP and AIF, as well as the significance of their interaction in vivo.

ACKNOWLEDGMENTS

We are grateful to T. Kerppola for providing BiFC plasmids and to L. Boise and E. Burstein for critical discussions.

This work was supported by the University of Michigan Biomedical Scholars Program (to C.S.D.), grants R01 GM067827 (to C.S.D.) and T32 CA09676 (to R.A.C.) from the National Institutes of Health, and grants W81XWH-04-1-0891 (to C.S.D.) and W81XWH-04-1-0854 (to J.C.W.) from the Department of Defense Prostate Cancer Research Program.

REFERENCES

1. **Arnoult, D., M. Karbowski, and R. J. Youle.** 2003. Caspase inhibition prevents the mitochondrial release of apoptosis-inducing factor. Cell Death Differ. **10:**845–849.
2. **Birkey Reffey, S., J. U. Wurthner, W. T. Parks, A. B. Roberts, and C. S. Duckett.** 2001. X-linked inhibitor of apoptosis protein functions as a cofactor in transforming growth factor-β signaling. J. Biol. Chem. **276:**26542–26549.
3. **Budihardjo, I., H. Oliver, M. Lutter, X. Luo, and X. Wang.** 1999. Biochemical pathways of caspase activation during apoptosis. Annu. Rev. Cell Dev. Biol. **15:**269–290.
4. **Burstein, E., L. Ganesh, R. D. Dick, B. van De Sluis, J. C. Wilkinson, J. Lewis, L. W. J. Klomp, C. Wijmenga, G. J. Brewer, G. J. Nabel, and C. S. Duckett.** 2004. A novel role for XIAP in copper homeostasis through regulation of MURR1. EMBO J. **23:**244–254.
5. **Burstein, E., J. E. Hoberg, A. S. Wilkinson, J. M. Rumble, R. A. Csomos, C. M. Komarck, G. N. Maine, J. C. Wilkinson, M. W. Mayo, and C. S. Duckett.** 2005. COMMD proteins: a novel family of structural and functional homologs of MURR1. J. Biol. Chem. **280:**22222–22232.
6. **Cain, K., D. G. Brown, C. Langlais, and G. M. Cohen.** 1999. Caspase activation involves the formation of the aposome, a large (approximately 700 kDa) caspase-activating complex. J. Biol. Chem. **274:**22686–22692.
7. **Chai, J., C. Du, J. W. Wu, S. Kyin, X. Wang, and Y. Shi.** 2000. Structural and biochemical basis of apoptotic activation by Smac/DIABLO. Nature **406:** 855–862.
8. **Chai, J., E. Shiozaki, S. M. Srinivasula, Q. Wu, P. Dataa, E. S. Alnemri, and Y. Shi.** 2001. Structural basis of caspase-7 inhibition by XIAP. Cell **104:**769–780.
9. **Cheung, E. C., N. Joza, N. A. Steenaart, K. A. McClellan, M. Neuspiel, S. McNamara, J. G. MacLaurin, P. Rippstein, D. S. Park, G. C. Shore, H. M. McBride, J. M. Penninger, and R. S. Slack.** 2006. Dissociating the dual roles of apoptosis-inducing factor in maintaining mitochondrial structure and apoptosis. EMBO J. **25:**4061–4073.
10. **Cheung, E. C., L. Melanson-Drapeau, S. P. Cregan, J. L. Vanderluit, K. L. Ferguson, W. C. McIntosh, D. S. Park, S. A. Bennett, and R. S. Slack.** 2005. Apoptosis-inducing factor is a key factor in neuronal cell death propagated by BAX-dependent and BAX-independent mechanisms. J. Neurosci. **25:** 1324–1334.
11. **Cregan, S. P., A. Fortin, J. G. MacLaurin, S. M. Callaghan, F. Cecconi, S. W. Yu, T. M. Dawson, V. L. Dawson, D. S. Park, G. Kroemer, and R. S. Slack.** 2002. Apoptosis-inducing factor is involved in the regulation of caspase-independent neuronal cell death. J. Cell Biol. **158:**507–517.
12. **Cryns, V., and J. Yuan.** 1998. Proteases to die for. Genes Dev. **12:**1551–1570.
13. **Deveraux, Q. L., and J. C. Reed.** 1999. IAP family proteins—suppressors of apoptosis. Genes Dev. **13:**239–252.
14. **Du, C., M. Fang, Y. Li, L. Li, and X. Wang.** 2000. Smac, a mitochondrial protein that promotes cytochrome *c*-dependent caspase activation by eliminating IAP inhibition. Cell **102:**33–42.
15. **Duckett, C. S., V. E. Nava, R. W. Gedrich, R. J. Clem, J. L. Van Dongen, M. C. Gilfillan, H. Shiels, J. M. Hardwick, and C. B. Thompson.** 1996. A conserved family of cellular genes related to the baculovirus *iap* gene and encoding apoptosis inhibitors. EMBO J. **15:**2685–2694.
16. **Eckelman, B. P., G. S. Salvesen, and F. L. Scott.** 2006. Human inhibitor of apoptosis proteins: why XIAP is the black sheep of the family. EMBO Rep. **7:**988–994.
17. **Hao, Z., G. S. Duncan, C. C. Chang, A. Elia, M. Fang, A. Wakeham, H. Okada, T. Calzascia, Y. Jang, A. You-Ten, W. C. Yeh, P. Ohashi, X. Wang, and T. W. Mak.** 2005. Specific ablation of the apoptotic functions of cytochrome C reveals a differential requirement for cytochrome C and Apaf-1 in apoptosis. Cell **121:**579–591.
18. **Harlin, H., S. B. Reffey, C. S. Duckett, T. Lindsten, and C. B. Thompson.** 2001. Characterization of XIAP-deficient mice. Mol. Cell. Biol. **21:**3604–3608.
19. **Hegde, R., S. M. Srinivasula, Z. Zhang, R. Wassell, R. Mukattash, L. Cilenti, G. DuBois, Y. Lazebnik, A. S. Zervos, T. Fernandes-Alnemri, and E. S. Alnemri.** 2002. Identification of Omi/HtrA2 as a mitochondrial apoptotic serine protease that disrupts IAP-caspase interaction. J. Biol. Chem. **277:** 432–438.
20. **Hofer-Warbinek, R., J. A. Schmid, C. Stehlik, B. R. Binder, J. Lipp, and R. de Martin.** 2000. Activation of NF-κB by XIAP, the X chromosome-linked inhibitor of apoptosis, in endothelial cells involves TAK1. J. Biol. Chem. **275:**22064–22068.
21. **Holcik, M., and R. G. Korneluk.** 2001. XIAP, the guardian angel. Nat. Rev. Mol. Cell Biol. **2:**550–556.
22. **Hu, C. D., Y. Chinenov, and T. K. Kerppola.** 2002. Visualization of interactions among bZIP and Rel family proteins in living cells using bimolecular fluorescence complementation. Mol. Cell **9:**789–798.
23. **Huang, Y., Y. C. Park, R. L. Rich, D. Segal, D. G. Myszka, and H. Wu.** 2001. Structural basis of caspase inhibition by XIAP. Differential roles of the linker versus the BIR domain. Cell **104:**781–790.
24. **Hunter, A. M., D. Kottachchi, J. Lewis, C. S. Duckett, R. G. Korneluk, and P. Liston.** 2003. A novel ubiquitin fusion system bypasses the mitochondria and generates biologically active Smac/DIABLO. J. Biol. Chem. **278:**7494–7499.
25. **Itoh, S., M. Thorikay, M. Kowanetz, A. Moustakas, F. Itoh, C. H. Heldin, and P. ten Dijke.** 2003. Elucidation of Smad requirement in transforming

growth factor-β type I receptor-induced responses. J. Biol. Chem. **278:**3751–3761.

26. **Joza, N., G. Y. Oudit, D. Brown, P. Benit, Z. Kassiri, N. Vahsen, L. Benoit, M. M. Patel, K. Nowikovsky, A. Vassault, P. H. Backx, T. Wada, G. Kroemer, P. Rustin, and J. M. Penninger.** 2005. Muscle-specific loss of apoptosis-inducing factor leads to mitochondrial dysfunction, skeletal muscle atrophy, and dilated cardiomyopathy. Mol. Cell. Biol. **25:**10261–10272.
27. **Kerr, J. F., A. H. Wyllie, and A. R. Currie.** 1972. Apoptosis: a basic biological phenomenon with wide-ranging implications in tissue kinetics. Br. J. Cancer **26:**239–257.
28. **Klein, J. A., C. M. Longo-Guess, M. P. Rossmann, K. L. Seburn, R. E. Hurd, W. N. Frankel, R. T. Bronson, and S. L. Ackerman.** 2002. The harlequin mouse mutation downregulates apoptosis-inducing factor. Nature **419:**367–374.
29. **Levkau, B., K. J. Garton, N. Ferri, K. Kloke, J. R. Nofer, H. A. Baba, E. W. Raines, and G. Breithardt.** 2001. XIAP induces cell-cycle arrest and activates nuclear factor-κB: new survival pathways disabled by caspase-mediated cleavage during apoptosis of human endothelial cells. Circ. Res. **88:**282–290.
30. **Lewis, J., E. Burstein, S. B. Reffey, S. B. Bratton, A. B. Roberts, and C. S. Duckett.** 2004. Uncoupling of the signaling and caspase-inhibitory properties of XIAP. J. Biol. Chem. **279:**9023–9029.
31. **Li, P., D. Nijhawan, I. Budihardjo, S. M. Srinivasula, M. Ahmad, E. S. Alnemri, and X. Wang.** 1997. Cytochrome *c* and dATP-dependent formation of Apaf-1/caspase-9 complex initiates an apoptotic protease cascade. Cell **91:**479–489.
32. **Liston, P., N. Roy, K. Tamai, C. Lefebvre, S. Baird, G. Cherton-Horvat, R. Farahani, M. McLean, J.-E. Ikeda, A. MacKenzie, and R. G. Korneluk.** 1996. Suppression of apoptosis in mammalian cells by NAIP and a related family of IAP genes. Nature **379:**349–353.
33. **Liu, Z., C. Sun, E. T. Olejniczak, R. P. Meadows, S. F. Betz, T. Oost, J. Herrmann, J. C. Wu, and S. W. Fesik.** 2000. Structural basis for binding of Smac/DIABLO to the XIAP BIR3 domain. Nature **408:**1004–1008.
34. **Martins, L. M., I. Iaccarino, T. Tenev, S. Gschmeissner, N. F. Totty, N. R. Lemoine, J. Savopoulos, C. W. Gray, C. L. Creasy, C. Dingwall, and J. Downward.** 2002. The serine protease Omi/HtrA2 regulates apoptosis by binding XIAP through a Reaper-like motif. J. Biol. Chem. **277:**439–444.
35. **Medema, J. P., C. Scaffidi, F. C. Kischkel, A. Shevchenko, M. Mann, P. H. Krammer, and M. E. Peter.** 1997. FLICE is activated by association with the CD95 death-inducing signaling complex (DISC). EMBO J. **16:**2794–2804.
36. **Miramar, M. D., P. Costantini, L. Ravagnan, L. M. Saraiva, D. Haouzi, G. Brothers, J. M. Penninger, M. L. Peleato, G. Kroemer, and S. A. Susin.** 2001. NADH oxidase activity of mitochondrial apoptosis-inducing factor. J. Biol. Chem. **276:**16391–16398.
37. **Mufti, A. R., E. Burstein, R. A. Csomos, P. C. Graf, J. C. Wilkinson, R. D. Dick, M. Challa, J. K. Son, S. B. Bratton, G. L. Su, G. J. Brewer, U. Jakob, and C. S. Duckett.** 2006. XIAP is a copper binding protein deregulated in Wilson's disease and other copper toxicosis disorders. Mol. Cell **21:**775–785.
38. **Munoz-Pinedo, C., A. Guio-Carrion, J. C. Goldstein, P. Fitzgerald, D. D. Newmeyer, and D. R. Green.** 2006. Different mitochondrial intermembrane space proteins are released during apoptosis in a manner that is coordinately initiated but can vary in duration. Proc. Natl. Acad. Sci. USA **103:**11573–11578.
39. **Nagata, S.** 1996. Apoptosis: telling cells their time is up. Curr. Biol. **6:**1241–1243.
40. **Nicholson, D. W.** 1999. Caspase structure, proteolytic substrates, and function during apoptotic cell death. Cell Death Differ. **6:**1028–1042.
41. **Otera, H., S. Ohsakaya, Z. Nagaura, N. Ishihara, and K. Mihara.** 2005. Export of mitochondrial AIF in response to proapoptotic stimuli depends on processing at the intermembrane space. EMBO J. **24:**1375–1386.
42. **Puig, O., F. Caspary, G. Rigaut, B. Rutz, E. Bouveret, E. Bragado-Nilsson, M. Wilm, and B. Seraphin.** 2001. The tandem affinity purification (TAP) method: a general procedure of protein complex purification. Methods **24:**218–229.
43. **Ranger, A. M., J. Zha, H. Harada, S. R. Datta, N. N. Danial, A. P. Gilmore, J. L. Kutok, M. M. Le Beau, M. E. Greenberg, and S. J. Korsmeyer.** 2003. Bad-deficient mice develop diffuse large B cell lymphoma. Proc. Natl. Acad. Sci. USA **100:**9324–9329.
44. **Riedl, S. J., M. Renatus, R. Schwarzenbacher, Q. Zhou, C. Sun, S. W. Fesik, R. C. Liddington, and G. S. Salvesen.** 2001. Structural basis for the inhibition of caspase-3 by XIAP. Cell **104:**791–800.
45. **Sanna, M. G., J. da Silva Correia, O. Ducrey, J. Lee, K. Nomoto, N. Schrantz, Q. L. Deveraux, and R. J. Ulevitch.** 2002. IAP suppression of apoptosis involves distinct mechanisms: the TAK1/JNK1 signaling cascade and caspase inhibition. Mol. Cell. Biol. **22:**1754–1766.
46. **Sanna, M. G., J. Da Silva Correia, Y. Luo, B. Chuang, L. M. Paulson, B. Nguyen, Q. L. Deveraux, and R. J. Ulevitch.** 2002. ILPIP, a novel anti-apoptotic protein that enhances XIAP-mediated activation of JNK1 and protection against apoptosis. J. Biol. Chem. **277:**30454–30462.
47. **Shiozaki, E. N., J. Chai, D. J. Rigotti, S. J. Riedl, P. Li, S. M. Srinivasula, E. S. Alnemri, R. Fairman, and Y. Shi.** 2003. Mechanism of XIAP-mediated inhibition of caspase-9. Mol. Cell **11:**519–527.
48. **Srinivasula, S. M., R. Hegde, A. Saleh, P. Datta, E. Shiozaki, J. Chai, R. A. Lee, P. D. Robbins, T. Fernandes-Alnemri, Y. Shi, and E. S. Alnemri.** 2001. A conserved XIAP-interaction motif in caspase-9 and Smac/DIABLO regulates caspase activity and apoptosis. Nature **410:**112–116.
49. **Srivastava, S., H. Banerjee, A. Chaudhry, A. Khare, A. Sarin, A. George, V. Bal, J. M. Durdik, and S. Rath.** 2007. Apoptosis-inducing factor regulates death in peripheral T cells. J. Immunol. **179:**797–803.
50. **Sun, C., M. Cai, R. P. Meadows, N. Xu, A. H. Gunasekera, J. Herrmann, J. C. Wu, and S. W. Fesik.** 2000. NMR structure and mutagenesis of the third Bir domain of the inhibitor of apoptosis protein XIAP. J. Biol. Chem. **275:**33777–33781.
51. **Susin, S. A., H. K. Lorenzo, N. Zamzami, I. Marzo, B. E. Snow, G. M. Brothers, J. Mangion, E. Jacotot, P. Costantini, M. Loeffler, N. Larochette, D. R. Goodlett, R. Aebersold, D. P. Siderovski, J. M. Penninger, and G. Kroemer.** 1999. Molecular characterization of mitochondrial apoptosis-inducing factor. Nature **397:**441–446.
52. **Thompson, C. B.** 1995. Apoptosis in the pathogenesis and treatment of disease. Science **267:**1456–1462.
53. **Thornberry, N. A., and Y. Lazebnik.** 1998. Caspases: enemies within. Science **281:**1312–1316.
54. **Uren, A., M. Pakusch, C. Hawkins, K. L. Puls, and D. L. Vaux.** 1996. Cloning and expression of apoptosis inhibitory protein homologs that function to inhibit apoptosis and/or bind tumor necrosis factor receptor-associated factors. Proc. Natl. Acad. Sci. USA **93:**4974–4978.
55. **Vahsen, N., C. Cande, J. J. Briere, P. Benit, N. Joza, N. Larochette, P. G. Mastroberardino, M. O. Pequignot, N. Casares, V. Lazar, O. Feraud, N. Debili, S. Wissing, S. Engelhardt, F. Madeo, M. Piacentini, J. M. Penninger, H. Schagger, P. Rustin, and G. Kroemer.** 2004. AIF deficiency compromises oxidative phosphorylation. EMBO J. **23:**4679–4689.
56. **van Empel, V. P., A. T. Bertrand, R. van der Nagel, S. Kostin, P. A. Doevendans, H. J. Crijns, E. de Wit, W. Sluiter, S. L. Ackerman, and L. J. De Windt.** 2005. Downregulation of apoptosis-inducing factor in harlequin mutant mice sensitizes the myocardium to oxidative stress-related cell death and pressure overload-induced decompensation. Circ. Res. **96:**e92–e101.
57. **Vaux, D. L., and J. Silke.** 2005. IAPs, RINGs and ubiquitylation. Nat. Rev. Mol. Cell Biol. **6:**287–297.
58. **Verhagen, A. M., P. G. Ekert, M. Pakusch, J. Silke, L. M. Connolly, G. E. Reid, R. L. Moritz, R. J. Simpson, and D. L. Vaux.** 2000. Identification of DIABLO, a mammalian protein that promotes apoptosis by binding to and antagonizing IAP proteins. Cell **102:**43–53.
59. **Verhagen, A. M., J. Silke, P. G. Ekert, M. Pakusch, H. Kaufmann, L. M. Connolly, C. L. Day, A. Tikoo, R. Burke, C. Wrobel, R. L. Moritz, R. J. Simpson, and D. L. Vaux.** 2002. HtrA2 promotes cell death through its serine protease activity and its ability to antagonise inhibitor of apoptosis proteins. J. Biol. Chem. **277:**445–454.
60. **Wilkinson, J. C., A. S. Wilkinson, F. L. Scott, R. A. Csomos, G. S. Salvesen, and C. S. Duckett.** 2004. Neutralization of Smac/Diablo by IAPs: a caspase-independent mechanism for apoptotic inhibition. J. Biol. Chem. **279:**51091–51099.
61. **Yamaguchi, K., S. Nagai, J. Ninomiya-Tsuji, M. Nishita, K. Tamai, K. Irie, N. Ueno, E. Nishida, H. Shibuya, and K. Matsumoto.** 1999. XIAP, a cellular member of the inhibitor of apoptosis protein family, links the receptors to TAB1-TAK1 in the BMP signaling pathway. EMBO J. **18:**179–187.
62. **Yang, Y., S. Fang, J. P. Jensen, A. M. Weissman, and J. D. Ashwell.** 2000. Ubiquitin protein ligase activity of IAPs and their degradation in proteasomes in response to apoptotic stimuli. Science **288:**874–877.
63. **Ye, H., C. Cande, N. C. Stephanou, S. Jiang, S. Gurbuxani, N. Larochette, E. Daugas, C. Garrido, G. Kroemer, and H. Wu.** 2002. DNA binding is required for the apoptogenic action of apoptosis inducing factor. Nat. Struct. Biol. **9:**680–684.
64. **Yu, S. W., H. Wang, M. F. Poitras, C. Coombs, W. J. Bowers, H. J. Federoff, G. G. Poirier, T. M. Dawson, and V. L. Dawson.** 2002. Mediation of poly-(ADP-ribose) polymerase-1-dependent cell death by apoptosis-inducing factor. Science **297:**259–263.

Cell Death and Differentiation (2008), 1–10

www.nature.com/cdd

X-linked inhibitor of apoptosis deficiency in the TRAMP mouse prostate cancer model

C Hwang[1,5], KA Oetjen[2,5], D Kosoff[2], KJ Wojno[3], MA Albertelli[4], RL Dunn[3], DM Robins[4], KA Cooney[1,3] and CS Duckett*[,1,2]

Deregulation of apoptotic pathways plays a central role in cancer pathogenesis. X-linked inhibitor of apoptosis protein (XIAP), is an antiapoptotic molecule, whose elevated expression has been observed in tumor specimens from patients with prostate carcinoma. Studies in human cancer cell culture models and xenograft tumor models have demonstrated that loss of XIAP sensitizes cancer cells to apoptotic stimuli and abrogates tumor growth. In view of these findings, XIAP represents an attractive antiapoptotic therapeutic target for prostate cancer. To examine the role of XIAP in an immunocompetent mouse cancer model, we have generated transgenic adenocarcinoma of the mouse prostate (TRAMP) mice that lack XIAP. We did not observe a protective effect of *Xiap* deficiency in TRAMP mice as measured by tumor onset and overall survival. In fact, there was an unexpected trend toward more aggressive disease in the *Xiap*-deficient mice. These findings suggest that alternative mechanisms of apoptosis resistance are playing a significant oncogenic role in the setting of *Xiap* deficiency. Our study has implications for XIAP-targeting therapies currently in development. Greater understanding of these mechanisms will aid in combating resistance to XIAP-targeting treatment, in addition to optimizing selection of patients who are most likely to respond to such treatment.
Cell Death and Differentiation advance online publication, 8 February 2008; doi:10.1038/cdd.2008.15

Apoptosis is a process of cell death that is tightly regulated by a cadre of both pro- and antiapoptotic proteins. In contrast to healthy cells, a hallmark of cancerous cells is the acquired capacity to evade this process of programmed cell death.[1,2] The acquisition of genetic lesions leading to oncogene activation normally triggers a program of apoptosis or senescence. Additionally, the tumor microenvironment often exposes malignant cells to apoptotic stimuli, such as hypoxia or activation of death receptors. Thus, suppression of the pathway leading to cell death has been suggested as a necessarily early event in the development of neoplasia.

Execution of the apoptotic cell death process is carried out by caspases, a family of cysteine aspartate proteases.[3,4] During apoptosis, loss of mitochondrial integrity or engagement of death receptors leads to the activation of initiator caspase-9 or -8, respectively. In either case, the initiator caspases cleave and activate effector caspases, including caspase-3 or -7. The cascade of caspase cleavage is regulated by X-linked inhibitor of apoptosis protein (XIAP). XIAP belongs to the IAP family, characterized by containing at least one zinc-binding baculovirus IAP repeat.[5] The only member of the IAP family that potently inhibits caspase activity, XIAP has been demonstrated to directly inhibit caspases-3, -7 and -9, blocking both intrinsic and extrinsic apoptotic signals.[6] Given its role in apoptosis, there has been much interest in understanding the role of XIAP in cancer and evaluating XIAP as a therapeutic target.[7–9]

XIAP overexpression has been reported in a variety of human cancers.[10–16] Increased XIAP levels have been linked to escaping anoikis and apoptosis induced by radiation, chemotherapy and death receptor ligands.[13,17–22] Furthermore, antagonism of XIAP has been reported to have antitumor activity in a number of models, including prostate cancer.[21,23–25] Consistent with an antiapoptotic role, high levels of XIAP have an adverse prognosis in certain cancers.[14,15] However, there was an unexpected favorable prognosis seen in prostate and non-small cell lung cancers with high levels of XIAP expression.[12,26]

We thus chose to further examine the role of XIAP in a tumor model that would resemble human cancer more closely than xenograft or *in vitro* studies. In this study, we describe an evaluation of prostate cancer development in the presence and absence of XIAP using the transgenic adenocarcinoma of the mouse prostate (TRAMP) model. Prostate-specific expression of SV40 T-antigen in TRAMP mice results in 100% penetrance of prostate tumors and a substantial proportion with metastatic disease.[27] XIAP expression is elevated in TRAMP tumors compared to normal prostate epithelium,[12] further justifying an evaluation of the effect of *Xiap* deficiency in this model.

[1]Department of Internal Medicine, University of Michigan Medical School, Ann Arbor, MI, USA; [2]Department of Pathology, University of Michigan Medical School, Ann Arbor, MI, USA; [3]Department of Urology, University of Michigan Medical School, Ann Arbor, MI, USA and [4]Department of Human Genetics, University of Michigan Medical School, Ann Arbor, MI, USA
*Corresponding author: CS Duckett, Department of Pathology and Internal Medicine, University of Michigan, BSRB, Room 2057, 109 Zina Pitcher Place, Ann Arbor, MI 48109-2200, USA. Tel.: +734 615 6414; Fax: +734 763 2162; E-mail: colind@umich.edu
[5]These authors contributed equally to this work.
Keywords: XIAP; BIRC4; prostate cancer
Abbreviations: c-IAP1, cellular inhibitor of apoptosis protein 1; c-IAP2, cellular inhibitor of apoptosis protein 2; IAP, inhibitor of apoptosis protein; MRI, magnetic resonance imaging; PIN, prostatic intraepithelial neoplasia; RIAP, rodent inhibitor of apoptosis protein; TRAMP, transgenic adenocarcinoma of mouse prostate; TUNEL, terminal dUTP nick end labeling; XIAP, X-linked inhibitor of apoptosis protein
Received 12.9.07; revised 20.12.07; accepted 07.1.08; Edited by A Villunger

Surprisingly, we found no evidence for a protective effect of *Xiap* deficiency in TRAMP mice. *Xiap*-deficient mice demonstrated no difference in tumor onset or overall survival compared to controls. Furthermore, tumor histology revealed similar patterns of differentiation and frequencies of apoptosis and proliferation in tumors from both groups. To our knowledge, these experiments represent the first examination of XIAP in an immunocompetent cancer model and differ markedly from previously published studies using xenografted cell lines. These results are relevant to the development of therapeutics, currently in clinical trials, that specifically antagonize XIAP.

Results

Loss of XIAP in TRAMP mice does not prevent tumor development or improve survival. *Xiap*-deficient TRAMP mice were generated with the hypothesis that mice deficient in XIAP may be protected from tumor formation compared to wild-type controls. Prostate size was monitored by magnetic resonance imaging (MRI). Representative MRI images from two littermate pairs of TRAMP mice are shown in Figure 1. In the first pair, tumor onset occurred sooner in the *Xiap*-deficient mouse compared to its wild-type littermate, but there was no appreciable difference in tumor onset or growth in the second littermate pair. Aggregate Kaplan–Meier analysis showed no difference between the two groups of mice (data not shown). The median age of tumor onset was 25.9 weeks for *Xiap*-deficient mice and 25.6 weeks for wild-type mice (*Xiap*-deficient mice $n=9$; wild-type mice $n=8$; $P=0.88$).

In addition to MRI, tumor onset was evaluated by abdominal palpation. The median age at the time of palpable tumor onset was 26.0 weeks in *Xiap*-deficient mice and 27.3 weeks in littermate controls (*Xiap*-deficient mice $n=13$; wild-type mice $n=11$). Kaplan–Meier analysis was used to compare the

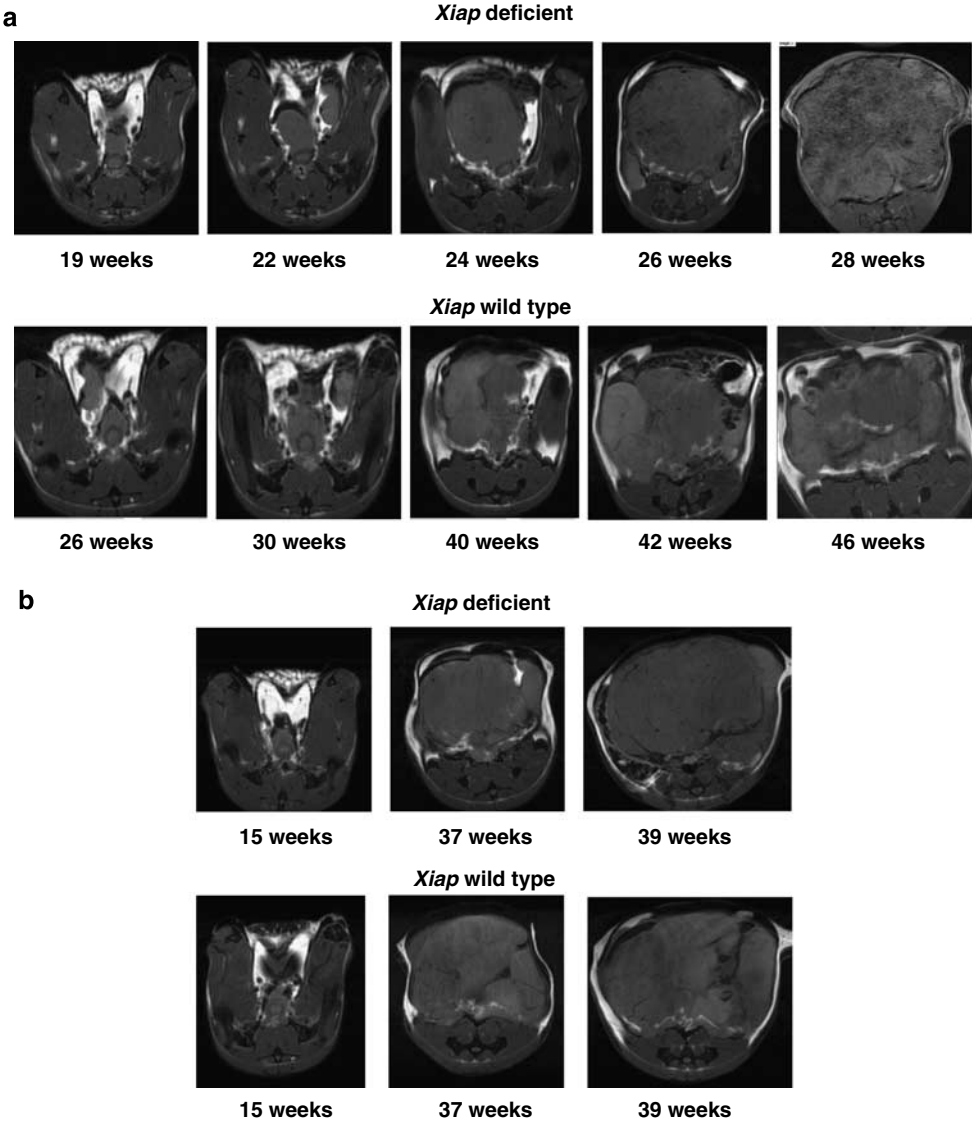

Figure 1 MRI images of prostate tumors in *Xiap*-deficient and wild-type TRAMP mice. MRI scans are shown for two representative pairs (**a**, **b**) of *Xiap*-deficient and wild-type TRAMP mice

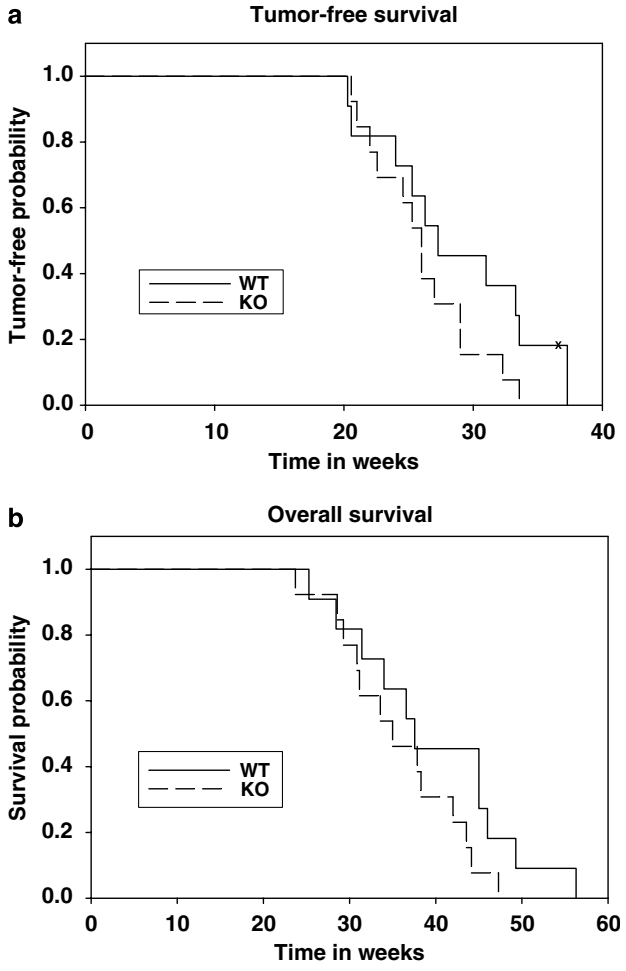

Figure 2 Kaplan–Meier analysis for tumor onset and overall survival. (**a**) Kaplan–Meier curves were plotted for *Xiap*-deficient (dotted line) and wild-type (solid line) TRAMP mice. The probability of remaining without tumor is plotted against age in weeks. One wild-type TRAMP mouse died from unknown causes at 36 weeks of age before evidence of tumor onset, and this mouse (x) was censored. A one-sided log-rank analysis yields a *P*-value of 0.924, indicating a 7.6% probability that *Xiap*-deficient mice would protect against tumor onset. (**b**) Kaplan–Meier curves were plotted for *Xiap*-deficient (dotted line) and wild-type (solid line) TRAMP mice. The probability of survival is plotted against age in weeks. A one-sided log rank analysis yields a *P*-value of 0.928, indicating a 7.2% probability that *Xiap* deficiency is protective for overall survival

probability of remaining without tumor between the two groups (Figure 2a). There was no evidence for a protective effect of *Xiap* deficiency in TRAMP mice. In fact, there was an unexpected trend for the *Xiap*-deficient mice to develop tumors earlier than wild-type controls, although the difference was not statistically significant (two-sided P-value $= 0.15$).

Although *Xiap* deficiency did not alter TRAMP tumor onset, inhibition of apoptosis by XIAP could contribute to a more lethal phenotype later in tumor progression. However, there was no evidence for a protective effect of *Xiap* deficiency in TRAMP mice on overall survival, and the trend for poorer outcome in the *Xiap*-deficient mice was again observed (Figure 2b). The median age at time of death was 35.0 weeks for *Xiap*-deficient TRAMP mice ($n = 13$), and the median age of control TRAMP mice at the time of death was 37.6 weeks ($n = 11$), but this difference was not statistically significant (two-sided P-value $= 0.15$).

***Xiap* deficiency does not retard growth of TRAMP tumors.** Since apoptosis may affect tumor growth without significantly impacting either tumor onset or overall survival, we hypothesized that a deficiency in XIAP may be expected to result in a decreased tumor burden. To assess tumor burden, the mass of the primary tumor at the time of necropsy was determined and tumor mass as a percentage of the mass of the mouse at necropsy was calculated. By both of these measures, *Xiap* deficiency did not result in a decrease in tumor burden as compared to wild-type controls (Figure 3a). Indeed, average tumor mass was somewhat greater in *Xiap*-deficient TRAMP mice (11.1 ± 5.06 g) than littermate controls (9.05 ± 4.78 g) despite the shortened survival observed above.

Although an effect on tumor burden at the time of death was not seen, tumor size may reflect the duration of growth as opposed to tumor growth rate. Thus, the time from palpable tumor to time of killing was measured. Generally, a prolonged duration between tumor onset and killing would indicate slower tumor growth. However, when *Xiap*-deficient TRAMP mice were compared to controls, there was no delay from the time of palpable tumor to time of killing (Figure 3b, last bars). As previously noted, the time to palpable tumor and time to death for *Xiap*-deficient TRAMP mice was shorter than controls.

Tumor growth was also assessed over time by clinical examination on a four-point scale. The time from palpable tumor to larger tumors was calculated and compared between *Xiap*-deficient TRAMP mice and controls. In agreement with our previous finding that *Xiap* deficiency does not delay time to killing or time from palpable tumor to killing, tumors in *Xiap*-deficient mice did not grow more slowly than tumors in controls (Figure 3c). To the contrary, the average time from palpable tumor to larger tumors (size 3 or 4) was seen to be shorter in *Xiap*-deficient mice.

***Xiap* deficiency does not result in less aggressive TRAMP tumors.** When tumor mass at autopsy was measured, it was observed that the mass of the primary tumor varied significantly, indicating that local growth did not always correspond to tumor lethality. Tumor aggressiveness also correlates with tumor grade and metastatic potential. Elevated expression of XIAP has been observed to correlate with higher tumor grades in renal cell carcinoma and breast cancer,[10,14] although this is not the case in other cancers.[26,28] To evaluate the effect of *Xiap* deficiency on tumor grade, tumor differentiation was assessed as another measure of tumor aggressiveness. Poorly and moderately differentiated carcinomas, as well as the more benign phylloides tumor, were observed in both *Xiap*-deficient and wild-type TRAMP mice. Examples of poorly differentiated and moderately differentiated primary tumors in both *Xiap*-deficient and wild-type mice are shown in Figure 4a. When tabulated, 67% (6/9) *Xiap*-deficient mice were noted to have carcinoma and the remainder (33%, 3/9) were phylloides. In comparison, 50% (4/8) of tumors from control mice were carcinoma and 50% (4/8) were phylloides. Among those

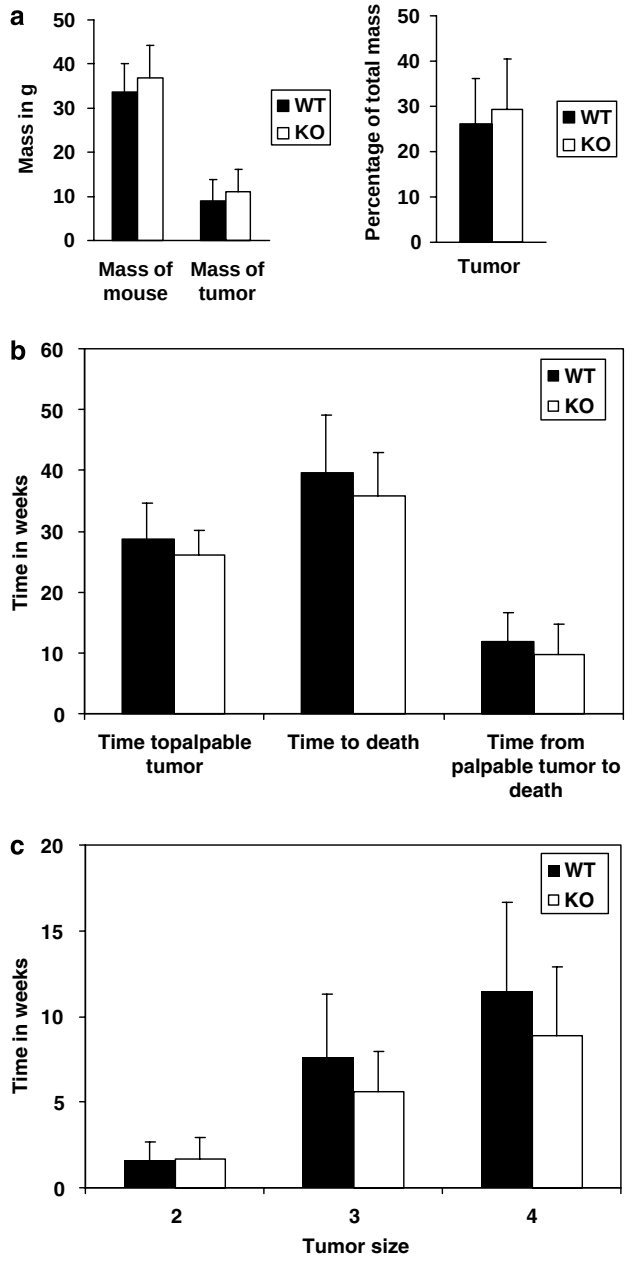

Figure 3 Comparison of tumor characteristics in *Xiap*-deficient and wild-type TRAMP mice. (**a**) Mass of animals and mass of tumors at necropsy were compared between the wild-type and *Xiap*-deficient mice. The tumor mass as a percentage of total mouse mass at the time of necropsy was also compared. Mean values are plotted with error bars representing one standard deviation. (**b**) Time to palpable tumor, time to death and time from palpable tumor to death were assessed for *Xiap*-deficient and wild-type mice. Mean values for each variable are plotted with error bars representing one standard deviation. (**c**) The time in weeks from tumor onset (size 1) to larger tumors (sizes 2–4) was calculated for each cohort of mice. Mean values for each variable are plotted with error bars representing one standard deviation

classified as carcinoma, tumors were poorly differentiated in 83% of *Xiap*-deficient mice (5/6 mice with carcinoma) and 50% of controls (2/4 mice with carcinoma). Overall, this equated to 56% of the entire cohort of *Xiap*-deficient mice with poorly differentiated carcinoma and 25% of the wild-type cohort (Figure 4b). Therefore, *Xiap*-deficient mice are not protected from more aggressive histologic subtypes of TRAMP tumors.

Xiap-deficient and control TRAMP mice were also evaluated for metastatic spread of tumor. An increase in XIAP has been implicated in resistance to anoikis and increased metastatic potential.[17,20] However, at necropsy, both *Xiap*-deficient and wild-type mice were observed to have pelvic nodal metastases and distant metastases. Metastatic deposits were confirmed histologically and representative images are presented in the right-hand panels of Figure 4a. When quantified, 56% (5/9) of *Xiap*-deficient TRAMP mice were noted to have metastases compared to 63% (5/8) of control TRAMP mice (Figure 4b). Evidence of distant metastases (liver and lung) was identified in three *Xiap*-deficient TRAMP mice (33%, 3/9 mice) compared to two control mice (25%, 2/8 mice). Thus, *Xiap*-deficient mice were not protected from metastatic spread. The majority of metastatic lesions in both *Xiap*-deficient and control TRAMP mice were poorly differentiated.

***Xiap* deficiency does not result in decreased incidence of pre-invasive lesions.** Elevation of XIAP expression has been observed in pre-invasive prostatic intraepithelial neoplasia (PIN) specimens from patients treated for prostate cancer as well as TRAMP mice.[12] To investigate the possibility that XIAP contributes to early tumor development, we studied the effect of loss of XIAP in a cohort of *Xiap*-deficient and control TRAMP mice who were followed until 25 weeks of age. Mice were assessed for prostate gland histology and micrometastatic disease (Table 1). None of the 25-week-old mice had evidence of micrometastases. There was no difference between *Xiap*-deficient and wild-type TRAMP mice in the incidence of PIN or microscopic carcinoma.

Loss of XIAP does not affect apoptosis or proliferation of tumor cells *in vivo*. Because of the accepted role of XIAP in cell death, we examined tumor specimens from *Xiap*-deficient mice by terminal dUTP nick end labeling (TUNEL) staining to assess the number of cells undergoing apoptosis (Figure 5a). There was no difference seen in TUNEL staining between the *Xiap*-deficient and wild-type tumors. Moreover, when quantitated, the apoptotic index was not increased in *Xiap*-deficient compared to wild-type TRAMP tumors (Figure 5b). In most tumors from both wild-type and *Xiap*-deficient TRAMP mice, the apoptotic index was on the order of 10 apoptotic cells per 1000, with only a few tumors exhibiting higher apoptotic indices. There did not seem to be a correlation between apoptotic index and histologic subtype. Of the three tumors with apoptotic indices greater than 15 cells per 1000, one was poorly differentiated, one was well differentiated and one was phylloides.

In view of previous work in resected lung cancer suggesting an increased proliferative and mitotic index in tumors with low XIAP expression,[26] we also performed an analysis of the proliferative rates present in these TRAMP tumors. Using both nuclear Ki-67 staining and mitotic figures as markers for proliferation, we did not observe any differences between the wild-type and *Xiap*-deficient TRAMP tumors (Figure 6).

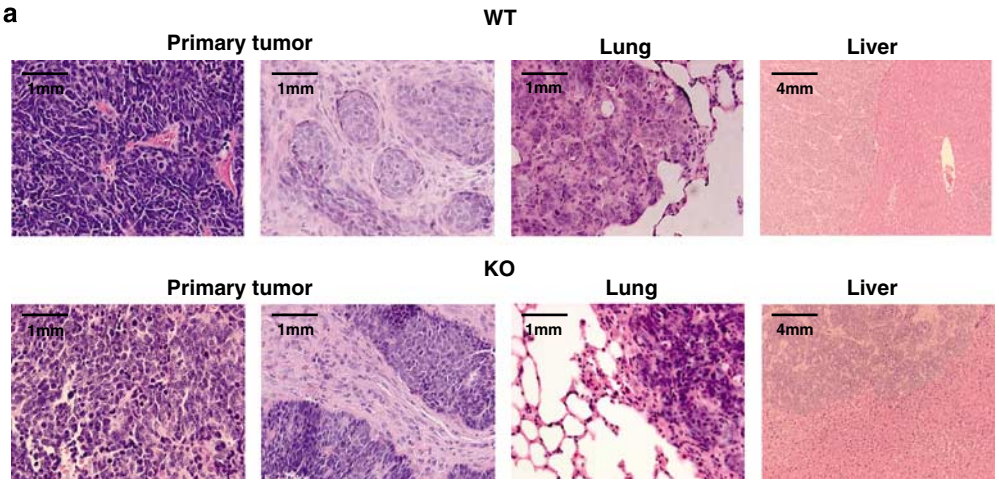

b

	Wild type	Knockout		*P*-value
Primary tumor				
Phylloides	4/8 50%	3/9 33%		0.49
Carcinoma	4/8 50%	6/9 67%		0.49
Poorly Differentiated	2/8 25%	5/9 56%		0.20
Moderately Differentiated	1/8 13%	1/9 11%		0.87
Well Differentiated	1/8 13%	0/9 0%		0.27
Metastases				
Mice with Metastases	5/8 63%	5/9 56%		0.77
Poorly Differentiated	4/8 50%	5/9 56%	*	0.82
Moderately Differentiated	1/8 13%	1/9 11%	*	0.93
Mice with distant metastases	2/8 25%	3/9 33%		0.71
Liver	1/8 13%	3/9 33%		0.31
Lung	2/8 25%	1/9 11%		0.45

*one mouse had separate metastases with poor and well-differentiated histology

Figure 4 Histology from primary and metastatic lesions of *Xiap*-deficient and wild-type TRAMP mice. (**a**) Examples of poorly differentiated tumors from wild-type and *Xiap*-deficient mice are shown in the left-most panels. Examples of moderately differentiated tumors are shown in the second set of panels. Metastases to liver and lung were also histologically confirmed and representative images are shown in the two right-most panels. (**b**) Results of histologic analysis for both primary and metastatic tumors were tabulated and compared between the wild-type and *Xiap*-deficient mice

Table 1 Histologic analysis of tumors from 25-week-old wild-type and *Xiap*-deficient TRAMP mice

	Wild type (%)	Knockout (%)	*P*-value
Primary tumor			
Phylloides	1/8 (13)	0/8 (0)	0.30
Carcinoma	2/8 (25)	2/8 (25)	1.00
Poorly differentiated	2/8 (25)	1/8 (13)	0.52
Well differentiated	0/8 (0)	1/8 (13)	0.30
PIN	5/8 (63)	6/8 (50)	0.59
Metastases			
Mice with metastases	0/8 (0)	0/8 (0)	1.00

Wild-type and *Xiap*-deficient mice were followed in cohorts of 10 mice until 25 weeks of age; eight of ten total mice were left in both groups at this time. Results from histologic analysis were tabulated and compared.

Finally, lysates from TRAMP tumors were assessed for expression of caspase-9 and the presence of active caspase-3 (Figure 7a). We did not detect any active caspase-3 in either wild-type or *Xiap*-deficient TRAMP tumors. This finding is consistent with our previous finding of generally low apoptotic rates in TRAMP prostate tumors.

***Xiap* deficiency does not increase c-IAP1 and c-IAP2 expression in TRAMP tumors.** Of the mammalian IAP family members, only cellular IAP1 (c-IAP1) and c-IAP2 are capable of binding caspases and might functionally compensate in the apoptotic pathway following loss of XIAP.[29] Furthermore, in the initial description of *Xiap*-deficient mice, it was found that c-IAP1 and c-IAP2 are overexpressed in *Xiap*-deficient mice.[30] For this reason, expression of c-IAP1 and c-IAP2 was examined in prostate tumor specimens from control and *Xiap*-deficient mice by immunoblot (Figure 7a). There was no obvious compensatory overexpression of c-IAP1 or c-IAP2 in the *Xiap*-deficient TRAMP tumors. Detection of c-IAP1 and c-IAP2 by immunoblot was quantified, and results are presented in Figure 7b. Not only was there no evidence of overexpression of c-IAP1 or c-IAP2, the mean level of c-IAP2 was actually decreased in the *Xiap*-deficient tumors compared to wild-type controls. Since levels of c-IAP1 and c-IAP2 are also subject to post-translational regulation,[31] expression of *c-iap1* and *c-iap2* transcripts was also examined by quantitative RT-PCR. Consistent with measurements of protein expression, expression of *c-iap1*

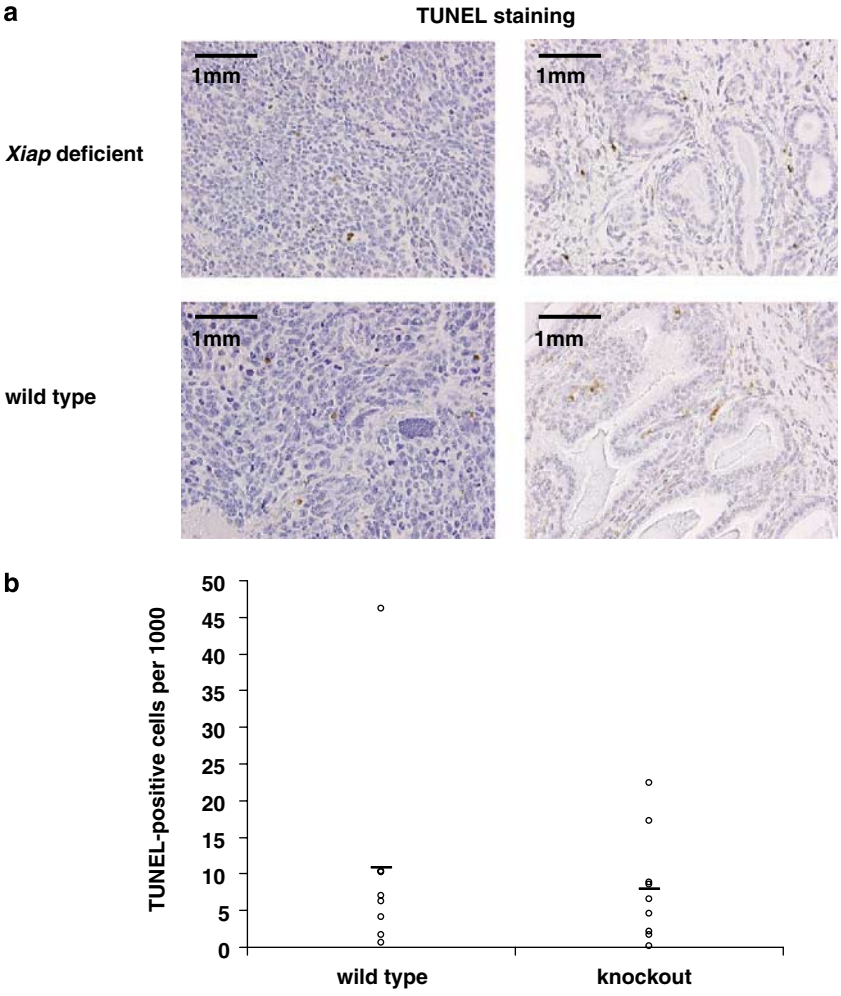

Figure 5 Frequency of apoptotic cells in *Xiap*-deficient tumors. (**a**) Primary prostate tumors were assessed for apoptotic cells using TUNEL staining. Representative images are shown from tumors with poorly differentiated carcinoma (left) and phylloides histology (right). (**b**) The number of TUNEL-positive cells per 1000 total cells was plotted for wild-type and *Xiap*-deficient mice. Mean values are represented by (—)

and *c-iap2* mRNA was not increased in *Xiap*-deficient tumors compared to controls (Figure 7c). Levels of *c-iap1* and *c-iap2* transcripts were actually somewhat less in the *Xiap*-deficient group, which was surprising but correlated with our observations of protein levels. In summary, compensation by c-IAP1 or c-IAP2 could not explain why *Xiap* deficiency did not protect TRAMP mice against tumor onset, growth or lethality.

Discussion

Malignant cells demonstrate a resistance to apoptosis, which allows these cells to survive in cellular environments that would typically induce cell death.[1] One proposed mechanism for the acquired capacity of cancer cells to evade apoptosis is antagonism of caspase activity through increased expression of XIAP. Elevated expression of XIAP has been demonstrated in cancers of various origins.[10–16] Not only is XIAP over-expressed in cancer, increased XIAP expression has been shown to contribute to apoptosis resistance and conversely, XIAP antagonism sensitizes cancer cells to multiple types of apoptotic stimuli *in vitro* and *in vivo*.[13,17–25,28,32–37] These apoptotic stimuli have included various chemotherapeutic agents, ionizing radiation, tumor necrosis factor-related apoptosis-inducing ligand, anoikis induction and immune clearance by cytotoxic lymphocytes. Despite these encouraging reports supporting a role for XIAP in the pathogenesis of cancer, there are data that are difficult to reconcile with the currently known functions of XIAP. Specifically, the paradoxical and dramatic favorable prognostic value of elevated XIAP levels observed in patients with resected prostate cancer does not correspond with the predicted increased resistance to apoptosis.[12] Interestingly, c-IAP1 and c-IAP2 expression correlated negatively with prognosis in this same group of patients.

We report here that *Xiap*-deficient TRAMP mice do not develop tumors later than wild-type TRAMP mice. Furthermore, *Xiap* deficiency does not lessen the lethality, metastatic potential, histologic grade or tumor growth of TRAMP tumors; in fact, the data suggested a trend of more aggressive behavior in *Xiap*-deficient TRAMP tumors. Thus, we conclude that although elevations of XIAP expression have been

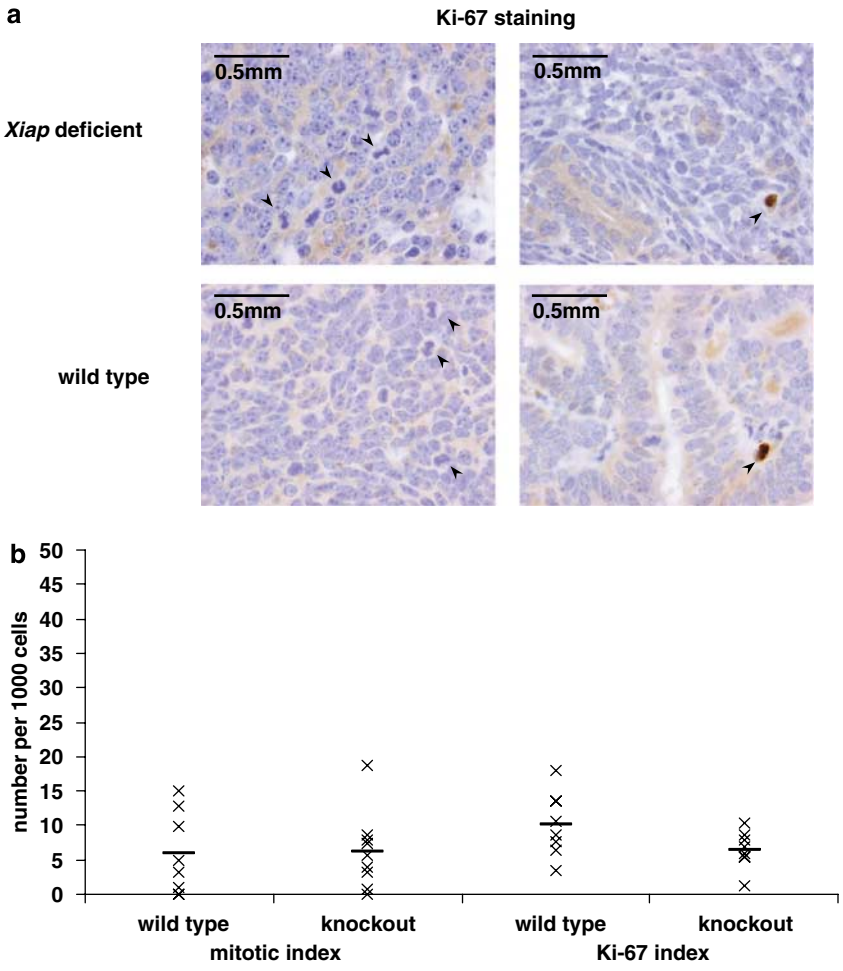

Figure 6 Proliferative indices in *Xiap*-deficient tumors. (**a**) Primary prostate tumors were stained immunohistochemically for Ki-67 (a proliferative marker). Ki-67 proliferative index and mitotic index were calculated. Representative images demonstrating both mitotic figures as well Ki-67-positive cells are shown in the left and right-hand panels, respectively. (**b**) The number of Ki-67-positive cells and the number of mitotic figures per 1000 total cells were plotted for wild-type and *Xiap*-deficient mice. Mean values are represented by (—)

observed in TRAMP tumors, upregulation of XIAP is not essential for transformation of prostate epithelium. It is possible that the aggressiveness of the TRAMP model, in which p53 and pRB are inhibited by the SV40 T-antigen, may have overwhelmed the ability to detect an effect of *Xiap* deficiency. In addition, the inhibition of p53 itself may be sufficient to inhibit apoptosis. However, the TRAMP model has been used to successfully establish a role for the antiapoptotic *Bcl-2* in tumorigenesis,[38] as well as to demonstrate that compounds such as green tea and celecoxib suppress tumorigenesis.[39,40]

These findings suggest that although XIAP is overexpressed in cancer it may not play a causal role in tumor pathogenesis. Conspicuously, evidence of *XIAP* mutations, translocations or amplifications, as is typically associated with classic oncogenes, has been absent in human cancers. Worth considering is the possibility that overexpression of XIAP may instead be a surrogate marker for other biologic behaviors. For example, XIAP is known to be upregulated by hypoxia[32] and thus may be overexpressed in tumors that are outgrowing a vascular supply.

Alternatively, XIAP may modulate apoptosis and tumor progression without being a classic oncogene. In this case, tumor formation in the absence of XIAP could occur if increased apoptosis was compensated by an increase in proliferation. In fact, although Ferreira *et al.*[26] did not observe a correlation between XIAP expression levels and apoptotic index in resected non-small cell lung cancer, they did note an increased proliferative and mitotic index in tumors with low XIAP expression. However, the surprising finding that *Xiap* deficiency did not result in an increase in the apoptotic index suggests that an increased proliferative index would not explain our findings. Indeed, when proliferative rate and mitotic index were assessed, there were no discernible differences between the wild-type and *Xiap*-deficient mice.

In addition, expression of the oncogenic SV40 T-antigen in the absence of XIAP may have selected for pathogenic mechanisms of apoptosis resistance that do not depend on XIAP. This selection pressure may be less acute in a clinical setting when XIAP antagonists are given after cancer has already developed. To explore the possibility of

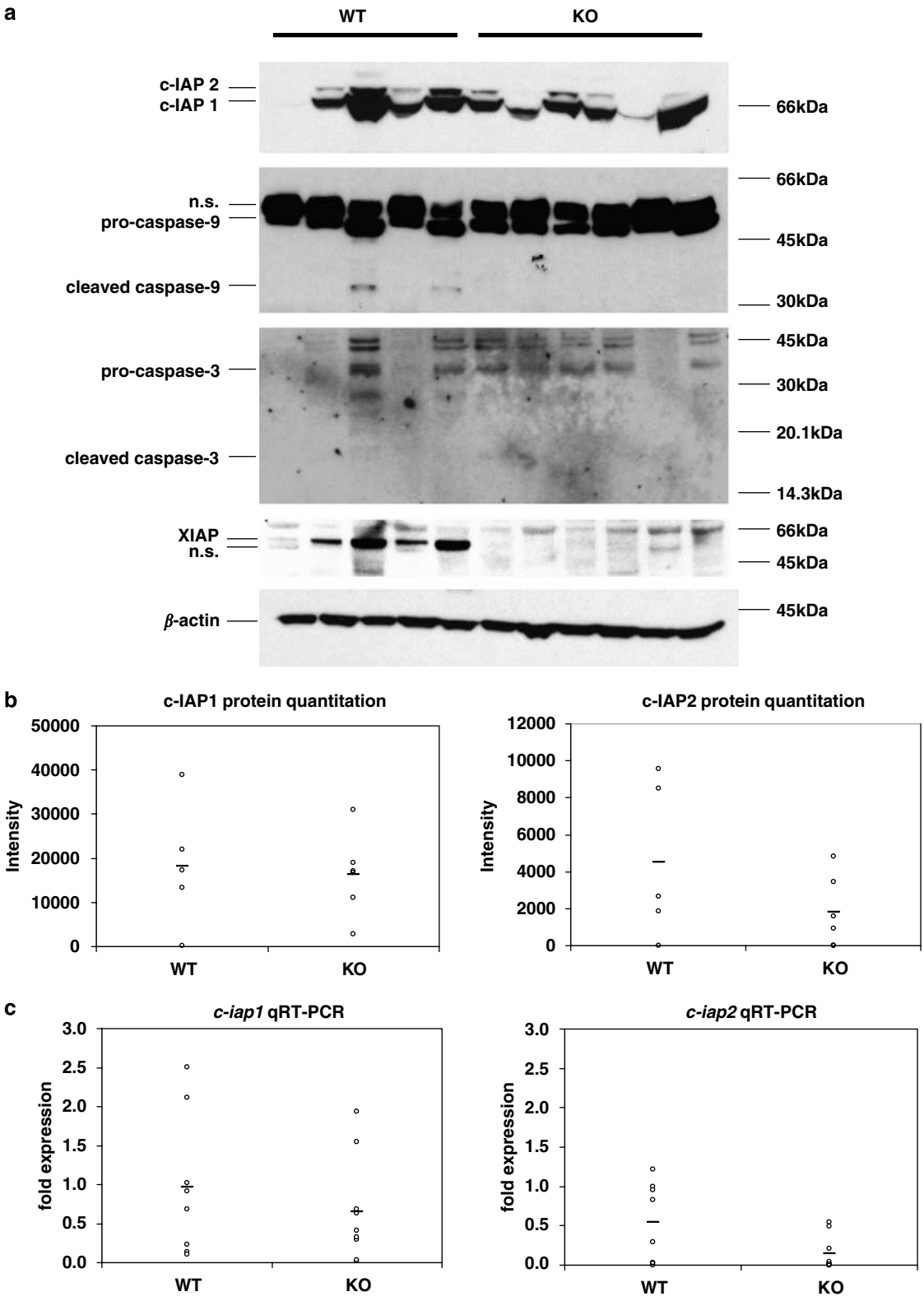

Figure 7 Expression of c-IAP1, c-IAP2 and other apoptotic proteins in Xiap-deficient TRAMP tumor specimens. (**a**) Immunoblot of c-IAP1 and c-IAP2 protein levels in primary tumor lysates. The same lysates were also probed for caspase-3 (full-length 32 kDa, cleaved form 19 or 17 kDa), caspase-9 (full-length 46 kDa, cleaved form 36 kDa) and XIAP (57 kDa). A β-actin immunoblot is shown to demonstrate equal total protein loading. (**b**) Expression levels of c-IAP1 and c-IAP2 protein based on immunoblotting were quantitated using ImageJ software. Relative intensity is plotted on the *y* axis. Mean values are represented by (—). (**c**) Expression of *c-iap1* and *c-iap2* mRNA in tumor specimens, as assessed by quantitative RT-PCR. Fold expression relative to normal prostate is plotted on the *y* axis for wild-type and *Xiap*-deficient cohorts. n.s. nonspecific

XIAP-independent mechanisms of apoptosis inhibition, c-IAP1 and c-IAP2 were evaluated as obvious candidates for a possible compensatory effect. No evidence for such a role was found based on levels of c-IAP1 and c-IAP2 overexpression. Moreover, although c-IAP1 and c-IAP2 are capable of binding caspases, the affinity of c-IAP1 or c-IAP2 for caspases is much lower than XIAP, and recent data suggest that both are incapable of inhibiting caspase activity.[29,41] If inhibition of caspases is relevant to the physiology of cancer cell biology and XIAP overexpression, it is unlikely that c-IAP1 or c-IAP2 can compensate for this activity.

Another possibility for our results is the absence of a significant apoptotic stimulus in our experiments. Although it has been reported that cancer cells can have high basal levels of apoptotic signaling molecules such as caspases-3 and -8,[42] we did not observe significant apoptotic activity in TRAMP tumors. It is interesting that the active 35-kDa form of caspase-9 was observed only in the wild-type mice. However, there did not appear to be a significant amount of active caspase-3 detected in either wild-type or *Xiap*-deficient mice. This finding correlates with the relatively low apoptotic indices in these tumors as assessed by TUNEL staining. The absence of an effective apoptotic stimulus may have negated any effect from *Xiap* deficiency. Synergy between XIAP antagonism has been seen when combined with an apoptosis-inducing stimulus, even if little effect is seen in the absence of such a stimulus. Future combinations of chemotherapy or radiation therapy with XIAP antagonism in this or other transgenic cancer models may help resolve this possibility. XIAP antagonists may also have more clinical efficacy if combined with traditional cytotoxic therapies.

Given the promising preclinical reports of XIAP-targeted therapy, it is not surprising that these agents are being developed for clinical use. XIAP is a particularly attractive therapeutic target, because the apparent health of *Xiap*-deficient mice suggests that the side effects of suppressing XIAP should be minimal. The present study is, to our knowledge, the first evaluation of the role of XIAP in an immunocompetent autochthonous tumor model. Contrary to the previously discussed preclinical reports, we did not observe a protective effect in *Xiap*-deficient mice. Moreover, the suggestion of an adverse impact of *Xiap* deficiency on tumor progression, in addition to previous accounts of an adverse prognosis associated with low XIAP levels in prostate and lung cancer, underscores the need for a better understanding of the physiologic function of XIAP. These findings have obvious implications for treatments targeting XIAP activity. Neoplastic cells likely develop antiapoptotic mechanisms that do not depend on XIAP overexpression, which may have greater importance in the setting of XIAP antagonism. Greater insight into these pathways will help in selection of patients who would benefit most from XIAP-targeted therapies, as well as in overcoming resistance to such therapies.

Materials and Methods

Animals. Generation and genotyping of TRAMP and *Xiap*-deficient mice have been previously described.[27,30] All mice were bred and maintained on a C57BL/6 background. TRAMP males were mated with $Xiap^{+/-}$ females to generate $Xiap^{-}$ TRAMP males, as well as $Xiap^{+}$ TRAMP males for controls. Research was conducted on a UCUCA-approved protocol in a manner consistent with the NIH Guidelines for the Care and Use of Laboratory Animals. Beginning at 12 weeks of age, weekly abdominal palpation by two independent observers was used to determine tumor onset. Mice were euthanized when moribund and samples were taken for histology, RNA and protein evaluation. The pelvic lymph nodes and the abdominal and thoracic cavities were observed for signs of metastasis and visible metastases were confirmed histologically.

MRI imaging. Mice were imaged with abdominal MRI biweekly by the Michigan Small Animal Imaging Resource (http://www.med.umich.edu/msair). Mice were anesthetized with 2% isoflurane–air mixture. Images were obtained with a 7.0T Varian MR scanner (183-mm horizontal bore; Varian, Palo Alto, CA, USA). A double-tuned volume radiofrequency coil was used to scan the abdominal region of the mice. Axial T_2-weighted images were acquired using a fast spin-echo sequence with the following parameters: repetition time/effective echo time, 4000/60 ms; echo spacing, 15 ms; number of echoes, 8; field of view 30 mm $\times$ 30 mm; matrix, 128 $\times$ 128; slice thickness, 1 mm; slice spacing, 0.25 mm; number of slices, 17 and number of scans, 4 (total scan time was approximately 4 min.).

Immunoblot. Previously frozen specimens were lysed on ice in radioimmunoprecipitation analysis buffer containing protease inhibitors. Membranes were probed using a 1 : 2000 dilution of rodent inhibitor of apoptosis protein (RIAP) rabbit polyclonal antibody (a gift from Peter Liston and Robert Korneluk), which recognizes mouse c-IAP1 and c-IAP2. Immunoblots were also probed for XIAP (goat polyclonal, R&D, cat no. AF8221, Minneapolis, MN, USA), caspase-3 (rabbit polyclonal, a gift from Guy Salvesen) and caspase-9 (mouse monoclonal, Stressgen, cat no. AAM-139, Ann Arbor, MI, USA). β-Actin antibody was purchased from Sigma (St Louis, MO, USA). The following HRP-conjugated secondary antibodies were used: sheep anti-mouse (Amersham, Piscataway, NJ, USA), donkey anti-rabbit (Amersham) and donkey anti-goat (Serotec, Raleigh, NC, USA). Densitometry was performed by NIH ImageJ software (http://rsb.info.nih.gov/ij/).

Quantitative RT-PCR. Tissue specimens were preserved in RNAlater (Ambion, Austin, TX, USA). RNA was extracted using an RNeasy kit (Qiagen, Valencia, CA, USA). cDNA was generated using RTScript reverse transcriptase and quantified using TaqMan gene expression assays (Applied Biosystems, Foster City, CA, USA) on an ABI 7500 qPCR instrument.

Histology. Hematoxylin and eosin-stained slides were prepared from paraffin-embedded formalin-fixed tissue by the University of Michigan Tissue core. Slides were examined in a blinded fashion by a certified genitourinary pathologist (KJW) and classified as phylloides, PIN, or carcinoma. Carcinoma specimens were graded as well, moderately or poorly differentiated. Liver and lung sections were similarly inspected. TUNEL staining was performed with the Apoptag kit (Chemicon, Temecula, CA, USA) by the University of Michigan Tissue core. Digital images of five independent fields were taken of each tumor at $\times$ 40 magnification. TUNEL-positive cells were counted manually, while total cell number was determined by ImageJ analysis. Quantification was recorded as the number of TUNEL-positive cells per 1000 cells. Mitotic and proliferative indices were calculated in an analogous manner, although images were visualized at $\times$ 100 to facilitate the identification of mitotic figures. Ki-67 staining was also performed by the University of Michigan Tissue core using a primary antibody from Dako (Carpinteria, CA, USA) and the MOM immunodetection kit from Vector Laboratories (Burlingame, CA, USA).

Statistical analysis. Statistical analysis for Kaplan–Meier plots was performed using a two-sided log-rank test. In addition, a one-sided log-rank test was used to determine whether the knockout mice had better outcomes than the wild-type mice. All other comparisons were performed using a two-tailed χ^2 test. Calculations were performed using the R statistical computation system (http://www.R-project.org). Values of $P<0.05$ were considered statistically significant.

Acknowledgements. We thank Drs. Peter Liston and Robert Korneluk for the generous gift of RIAP antibody, Dr. Guy Salvesen for his gift of caspase-3 antibody and Drs. Brian Ross and Brad Moffat for their assistance with MRI imaging. KO is a recipient of a Pre-doctoral Award funded through the Breast Cancer Research Program of the Department of Defense (W81XWH-06-1-0429). This study was supported by funding received from the Department of Defense

(W81XWH-04-1-0891) and the National Institutes of Health (5R01GM067827-03). Dr. Colin Duckett serves as a consultant to Aegera Therapeutics and is a member of their scientific advisory board. All other authors have no conflicting interests.

1. Hanahan D, Weinberg RA. The hallmarks of cancer. *Cell* 2000; **100**: 57–70.
2. Green DR, Evan GI. A matter of life and death. *Cancer Cell* 2002; **1**: 19–30.
3. Nunez G, Benedict MA, Hu Y, Inohara N. Caspases: the proteases of the apoptotic pathway. *Oncogene* 1998; **17**: 3237–3245.
4. Shiozaki EN, Shi Y. Caspases, IAPs and Smac/DIABLO: mechanisms from structural biology. *Trends Biochem Sci* 2004; **29**: 486–494.
5. Vaux DL, Silke J. IAPs, RINGs and ubiquitylation. *Nat Rev Mol Cell Biol* 2005; **6**: 287–297.
6. Deveraux QL, Takahashi R, Salvesen GS, Reed JC. X-linked IAP is a direct inhibitor of cell-death proteases. *Nature* 1997; **388**: 300–304.
7. LaCasse EC, Baird S, Korneluk RG, MacKenzie AE. The inhibitors of apoptosis (IAPs) and their emerging role in cancer. *Oncogene* 1998; **17**: 3247–3259.
8. Holcik M, Gibson H, Korneluk RG. XIAP: apoptotic brake and promising therapeutic target. *Apoptosis* 2001; **6**: 253–261.
9. Schimmer AD, Dalili S, Batey RA, Riedl SJ. Targeting XIAP for the treatment of malignancy. *Cell Death Differ* 2006; **13**: 179–188.
10. Jaffer S, Orta L, Sunkara S, Sabo E, Burstein DE. Immunohistochemical detection of antiapoptotic protein X-linked inhibitor of apoptosis in mammary carcinoma. *Hum Pathol* 2007; **38**: 864–870.
11. Kluger HM, McCarthy MM, Alvero AB, Sznol M, Ariyan S, Camp RL *et al.* The X-linked inhibitor of apoptosis protein (XIAP) is up-regulated in metastatic melanoma, and XIAP cleavage by phenoxodiol is associated with carboplatin sensitization. *J Transl Med* 2007; **5**: 6.
12. Krajewska M, Krajewski S, Banares S, Huang X, Turner B, Bubendorf L *et al.* Elevated expression of inhibitor of apoptosis proteins in prostate cancer. *Clin Cancer Res* 2003; **9**: 4914–4925.
13. Lopes RB, Gangeswaran R, McNeish IA, Wang Y, Lemoine NR. Expression of the IAP protein family is dysregulated in pancreatic cancer cells and is important for resistance to chemotherapy. *Int J Cancer* 2007; **120**: 2344–2352.
14. Mizutani Y, Nakanishi H, Li YN, Matsubara H, Yamamoto K, Sato N *et al.* Overexpression of XIAP expression in renal cell carcinoma predicts a worse prognosis. *Int J Oncol* 2007; **30**: 919–925.
15. Tamm I, Richter S, Oltersdorf D, Creutzig U, Harbott J, Scholz F *et al.* High expression levels of X-linked inhibitor of apoptosis protein and survivin correlate with poor overall survival in childhood *de novo* acute myeloid leukemia. *Clin Cancer Res* 2004; **10**: 3737–3744.
16. Tamm I, Kornblau SM, Segall H, Krajewski S, Welsh K, Kitada S *et al.* Expression and prognostic significance of IAP-family genes in human cancers and myeloid leukemias. *Clin Cancer Res* 2000; **6**: 1796–1803.
17. Berezovskaya O, Schimmer AD, Glinskii AB, Pinilla C, Hoffman RM, Reed JC *et al.* Increased expression of apoptosis inhibitor protein XIAP contributes to anoikis resistance of circulating human prostate cancer metastasis precursor cells. *Cancer Res* 2005; **65**: 2378–2386.
18. Holcik M, Yeh C, Korneluk RG, Chow T. Translational upregulation of X-linked inhibitor of apoptosis (XIAP) increases resistance to radiation induced cell death. *Oncogene* 2000; **19**: 4174–4177.
19. Liu Z, Li H, Derouet M, Filmus J, LaCasse EC, Korneluk RG *et al. ras* oncogene triggers up-regulation of cIAP2 and XIAP in intestinal epithelial cells: epidermal growth factor receptor-dependent and -independent mechanisms of *ras*-induced transformation. *J Biol Chem* 2005; **280**: 37383–37392.
20. Liu Z, Li H, Wu X, Yoo BH, Yan SR, Stadnyk AW *et al.* Detachment-induced upregulation of XIAP and cIAP2 delays anoikis of intestinal epithelial cells. *Oncogene* 2006; **25**: 7680–7690.
21. Ng CP, Bonavida B. X-linked inhibitor of apoptosis (XIAP) blocks Apo2 ligand/tumor necrosis factor-related apoptosis-inducing ligand-mediated apoptosis of prostate cancer cells in the presence of mitochondrial activation: sensitization by overexpression of second mitochondria-derived activator of caspase/direct IAP-binding protein with low pI (Smac/DIABLO). *Mol Cancer Ther* 2002; **1**: 1051–1058.
22. Nomura T, Mimata H, Takeuchi Y, Yamamoto H, Miyamoto E, Nomura Y. The X-linked inhibitor of apoptosis protein inhibits taxol-induced apoptosis in LNCaP cells. *Urol Res* 2003; **31**: 37–44.
23. Amantana A, London CA, Iversen PL, Devi GR. X-linked inhibitor of apoptosis protein inhibition induces apoptosis and enhances chemotherapy sensitivity in human prostate cancer cells. *Mol Cancer Ther* 2004; **3**: 699–707.
24. LaCasse EC, Cherton-Horvat GG, Hewitt KE, Jerome LJ, Morris SJ, Kandimalla ER *et al.* Preclinical characterization of AEG35156/GEM 640, a second-generation antisense oligonucleotide targeting X-linked inhibitor of apoptosis. *Clin Cancer Res* 2006; **12**: 5231–5241.
25. McManus DC, Lefebvre CA, Cherton-Horvat G, St-Jean M, Kandimalla ER, Agrawal S *et al.* Loss of XIAP protein expression by RNAi and antisense approaches sensitizes cancer cells to functionally diverse chemotherapeutics. *Oncogene* 2004; **23**: 8105–8117.
26. Ferreira CG, van der Valk P, Span SW, Ludwig I, Smit EF, Kruyt FA *et al.* Expression of X-linked inhibitor of apoptosis as a novel prognostic marker in radically resected non-small cell lung cancer patients. *Clin Cancer Res* 2001; **7**: 2468–2474.
27. Greenberg NM, DeMayo F, Finegold MJ, Medina D, Tilley WD, Aspinall JO *et al.* Prostate cancer in a transgenic mouse. *Proc Natl Acad Sci USA* 1995; **92**: 3439–3443.
28. Bilim V, Kasahara T, Hara N, Takahashi K, Tomita Y. Role of XIAP in the malignant phenotype of transitional cell cancer (TCC) and therapeutic activity of XIAP antisense oligonucleotides against multidrug-resistant TCC *in vitro*. *Int J Cancer* 2003; **103**: 29–37.
29. Eckelman BP, Salvesen GS. The human anti-apoptotic proteins cIAP1 and cIAP2 bind but do not inhibit caspases. *J Biol Chem* 2006; **281**: 3254–3260.
30. Harlin H, Reffey SB, Duckett CS, Lindsten T, Thompson CB. Characterization of XIAP-deficient mice. *Mol Cell Biol* 2001; **21**: 3604–3608.
31. Yang Y, Fang S, Jensen JP, Weissman AM, Ashwell JD. Ubiquitin protein ligase activity of IAPs and their degradation in proteasomes in response to apoptotic stimuli. *Science* 2000; **288**: 874–877.
32. Marienfeld C, Yamagiwa Y, Ueno Y, Chiasson V, Brooks L, Meng F *et al.* Translational regulation of XIAP expression and cell survival during hypoxia in human cholangiocarcinoma. *Gastroenterology* 2004; **127**: 1787–1797.
33. Cummins JM, Kohli M, Rago C, Kinzler KW, Vogelstein B, Bunz F. X-linked inhibitor of apoptosis protein (XIAP) is a nonredundant modulator of tumor necrosis factor-related apoptosis-inducing ligand (TRAIL)-mediated apoptosis in human cancer cells. *Cancer Res* 2004; **64**: 3006–3008.
34. Ravi R, Fuchs EJ, Jain A, Pham V, Yoshimura K, Prouser T *et al.* Resistance of cancers to immunologic cytotoxicity and adoptive immunotherapy via X-linked inhibitor of apoptosis protein expression and coexisting defects in mitochondrial death signaling. *Cancer Res* 2006; **66**: 1730–1739.
35. Arnt CR, Chiorean MV, Heldebrant MP, Gores GJ, Kaufmann SH. Synthetic Smac/DIABLO peptides enhance the effects of chemotherapeutic agents by binding XIAP and cIAP1 *in situ*. *J Biol Chem* 2002; **277**: 44236–44243.
36. Sasaki H, Sheng Y, Kotsuji F, Tsang BK. Down-regulation of X-linked inhibitor of apoptosis protein induces apoptosis in chemoresistant human ovarian cancer cells. *Cancer Res* 2000; **60**: 5659–5666.
37. Schimmer AD, Welsh K, Pinilla C, Wang Z, Krajewska M, Bonneau MJ *et al.* Small-molecule antagonists of apoptosis suppressor XIAP exhibit broad antitumor activity. *Cancer Cell* 2004; **5**: 25–35.
38. Bruckheimer EM, Brisbay S, Johnson DJ, Gingrich JR, Greenberg N, McDonnell TJ. Bcl-2 accelerates multistep prostate carcinogenesis *in vivo*. *Oncogene* 2000; **19**: 5251–5258.
39. Gupta S, Hastak K, Ahmad N, Lewin JS, Mukhtar H. Inhibition of prostate carcinogenesis in TRAMP mice by oral infusion of green tea polyphenols. *Proc Natl Acad Sci USA* 2001; **98**: 10350–10355.
40. Gupta S, Adhami VM, Subbarayan M, MacLennan GT, Lewin JS, Hafeli UO *et al.* Suppression of prostate carcinogenesis by dietary supplementation of celecoxib in transgenic adenocarcinoma of the mouse prostate model. *Cancer Res* 2004; **64**: 3334–3343.
41. Tenev T, Zachariou A, Wilson R, Ditzel M, Meier P. IAPs are functionally non-equivalent and regulate effector caspases through distinct mechanisms. *Nat Cell Biol* 2005; **7**: 70–77.
42. Yang L, Cao Z, Yan H, Wood WC. Coexistence of high levels of apoptotic signaling and inhibitor of apoptosis proteins in human tumor cells: implication for cancer specific therapy. *Cancer Res* 2003; **63**: 6815–6824.